



Universidad de Cantabria
**Instituto de Biomedicina y
Biotecnología de Cantabria (IBBTEC)**



TESIS DOCTORAL

**Analysis of the function of SP6 and SP8
transcription factors in the limb ectoderm**

**Análisis de la función de los factores de
transcripción SP6 y SP8 en el ectodermo
de la extremidad**

Directores de tesis

**María A. Ros Lasierra
Juan F. López Giménez**

Rocío Pérez Gómez

Septiembre 2018



UNIVERSIDAD DE CANTABRIA

**Instituto de Biomedicina y
Biotecnología de Cantabria
(IBBTEC)**



**Analysis of the function of SP6 and SP8 transcription
factors in the limb ectoderm**

**Análisis de la función de los factores de transcripción
SP6 y SP8 en el ectodermo de la extremidad**

TESIS DOCTORAL

presentada por:

ROCÍO PÉREZ GÓMEZ

**Licenciada en Biotecnología, para optar al grado de
Doctora en Biología molecular y Biomedicina
por la Universidad de Cantabria**

Santander, 2018

María A. Ros Lasierra, Profesora de Investigación del Instituto de Biomedicina y Biotecnología de Cantabria (CSIC-UC-SODERCAN) y

Juan F. López Giménez, c del Instituto de Parasitología y Biomedicina “López-Neyra”

como directores de la Tesis Doctoral titulada: “Analysis of the function of SP6 and SP8 transcription factors in the limb ectoderm”; “Análisis de la función de los factores de transcripción SP6 y SP8 en el ectodermo de la extremidad”

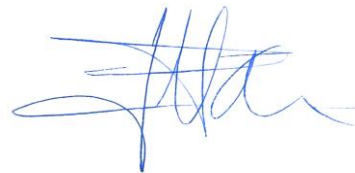
CERTIFICAN

Que dicho trabajo ha sido realizado por Doña **Rocío Pérez Gómez** y consideran que se encuentra terminado y reúne los requisitos para su presentación como memoria de doctorado por la interesada, al objeto de poder optar al grado de Doctor por la Universidad de Cantabria.



María A. Ros Lasierra

Directora y tutora de la tesis



Juan F. López Giménez

Director de la tesis

Santander a 19 de septiembre de 2018

A mis padres

INDEX

Page

ABBREVIATIONS and Acronyms

RESUMEN

1. INTRODUCTION	19
1.1 Limb development	23
1.2 Proximo-Distal limb outgrowth and patterning	27
1.3 Anterior-Posterior limb outgrowth	32
1.4 Dorso-Ventral limb patterning	36
1.5 Apical Ectodermal Ridge (AER)	39
1.5.1 AER induction.....	40
1.5.2 AER induction and DV axis.....	40
1.5.3 AER maturation.....	42
1.5.4 AER maintenance.....	43
1.5.5 AER regression	45
1.5.6 AER defects.....	45
1.6 SHFM.....	46
1.6.1 SP6 and SP8 and split hand/foot malformation	50
1.7 Specificity protein (SP) family	52
1.7.1 Phylogeny of SP family proteins.....	52
1.7.2 SP8 structure	54
1.7.3 SP6 and SP8 in the limb.....	55
2. AIM OF THE PRESENT THESIS	59
3. MATERIALS & METHODS	63
3.1 Sp8:3xFLAG knock-in mouse (Sp8-FL)	65
3.2 Mouse strains	66
3.3 Mouse Embryos	66
3.4 Genotyping.....	66
3.5 Skeletal preparations.....	67

3.6 Ectoderm-mesoderm separation	68
3.7 Cryostat sections	69
3.8 Paraffin embedding.....	69
3.9 RNA probes synthesis.....	69
3.10 Whole mount in situ hybridization (WMISH).....	70
3.11 In situ hybridization in paraffin sections	71
3.12 Immunofluorescence.....	71
3.12 Immunoblot.....	72
3.13 Cloning.....	73
3.14 Cell culture.....	74
3.15 BiFC and CoIP clones.....	74
3.16 Protein over-expression for anti SP8 antibody production	77
3.17 Bimolecular Fluorescent Complementation (BiFC)	78
3.18 Co-ImmunoPrecipitation (CoIP).....	79
3.19 ChIPmentation of SP8	80
3.20 ChIP-seq for Chromatin marks	82
3.21 RNA-seq	83
3.22 Transgenic mice for Lacz activity.....	83
3.23 Bioinformatic and statistical analysis	84
3.24 Additional Bioinformatic analysis	85
4. RESULTS	89
4.1 OBJECTIVE 1: Analysis of the SP8 regulatory network in the limb ectoderm... 91	
4.1.1 Genome-wide analysis of SP8-DNA binding sites in the developing limb bud ectoderm	91
4.1.2 SP8 expression and purification for antibody production.....	91
4.1.3 Generation of a 3XFLAG-tagged <i>Sp8</i> knock-in mice.....	94
4.1.4 Identification of the Genomic Regions Enriched in SP8 in the forelimb bud ectoderm by ChIPmentation.....	97
4.1.5 Analysis of SP8 putative regulatory elements and their associated genes... 103	
4.1.6 SP8-CRM Intersection with other tested or predicted enhancer collections 108	
4.1.7 RNAseq-based transcriptome comparison between WT and <i>Sp8</i> null limb bud ectoderm.....	111

4.1.8 Identification of SP8 Direct Targets in the Limb Bud Ectoderm.....	113
4.1.9 Physical interaction between SP8 and DLX5	115
4.1.10 Two modes of SP8 action.....	117
4.1.11 SP8 regulatory network in the limb ectoderm.....	119
4.1.12 Interactions between the SP8 GRN and the WNT/ β -CAT pathway	120
4.1.13 SP8 controls all major regulators of DV patterning.....	124
4.1.14 Sp autoregulation of gene expression.....	126
4.1.15 Evaluation of selected enhancer activity by mouse transgenesis.....	129
4.2 OBJECTIVE 2: Protein-Protein interactions	130
5. DISCUSSION	137
5.1 Characterization of the SP8 cistrome in vivo in the limb bud ectoderm	140
5.2 SP8 direct targets	141
5.3 DLX5 transcription factor is a SP8 cofactor.....	142
5.4 Interactions of the SP8 GRN with the WNT canonical pathway	144
5.5 The SP8 GRN and DV patterning.....	146
5.6 SHFM.....	147
6. CONCLUSIONS/ CONCLUSIONES	149
7. REFERENCES	157
8. AGRADECIMIENTOS	179
9. ANEX	183
9.1 SP8 bound regions	
9.2 Differentially expressed genes	
9.3 SP8 direct targets	

ABBREVIATIONS and Acronyms

AER	Apical Ectodermal Ridge
AP	Antero-Posterior
BCIP	5-Bromo-4-chloro-3-indolyl-phosphate
BiFC	Bimolecular Fluorescence Complementation
BMP	Bone Morphogenetic Protein
BSA	Bovine serum albumin
ChIP	Chromatin Immunoprecipitation
ChIPm	ChIPmentation
CoIP	Co-Immunoprecipitation
CRM	<i>Cis Regulatory Module</i>
DEG	Differentially Expressed Gene
DEPC	<i>Diethylpyrocarbonate</i>
Dlx	Distal-less homeobox
DMEM	Dulbecco's modified Eagle's medium
DNA	Deoxyribonucleic acid
DOX	Sodium deoxycholate
DTT	Dithiothreitol
DV	Dorso-Ventral
E	Embryonic day
<i>E. coli</i>	<i>Escherichia coli</i>
ECL	Enhanced chemiluminescence
EGTA	Egtazic acid
En1	Engrailed-1
FBS	Fetal Bovine Serum
FGF	Fibroblast Growth Factor
FL	Forelimb
FPKM	Fragments Per Kilobase of transcript per Million mapped reads
h	Hour
HEK	Human Embryonic Kidney
HH	Hamburger and Hamilton
HL	Hindlimb
HRP	Horseradish peroxidase
IHC	Immunohistochemistry
ISH	In situ hybridization
Kb	kilobase
KI	Knock In
KO	Knock Out
LB	Lysogeny <i>broth</i>
Lmx1b	LIM homeobox transcription factor 1 beta

M&M Materials and methods
Meis1 *Meis homeobox 1*
min Minute(s)
Msx Msh Homeobox
NBT Nitro blue tetrazolium
NP-40 Tergitol-type nonyl phenoxyethoxyethanol.
OHT hydroxy-tamoxifen
ON Over night
PBS Phosphate Buffered Saline
PCR Polymerase chain reaction
PD Proximo-Distal
PEI Polyethylenimine
PFA Paraformaldehyde
PIC Proteinase Inhibitor Cocktail
PK Proteinase K
PMSF Phenylmethylsulfonyl fluoride
RA Retinoic Acid
RE Restriction enzyme
RNA Ribonucleic acid
RNase Ribonuclease
Rspo R-spondin
RT Room temperature
SDS-PAGE Sodium dodecyl sulfate polyacrylamide gel electrophoresis
SHFM Split Hand/Split Foot Malformation
Shh Sonic hedgehog
Sp Specificity Protein
TBS-T Tris buffer saline Tween 20
TF Transcription Factor
TL Total lysate
Tp63 Tumor Protein 63
TSS Transcription Start Site
UV Ultra violet
ZF Zinc Finger

RESUMEN

RESUMEN

Una pregunta fundamental en biología es cómo un grupo de células aparentemente uniformes son capaces de diferenciarse y formar un órgano complejo y funcional en tres dimensiones. La extremidad de los vertebrados ha sido usada ampliamente en estudios genéticos y de desarrollo, ya que es un órgano no vital que puede ser fácilmente manipulado sin comprometer la supervivencia del embrión.

La formación de la extremidad comienza con la acumulación de células de la placa mesodérmica lateral, emergiendo inicialmente la extremidad como una protuberancia, el esbozo de la extremidad. Este esbozo está compuesto por una masa mesodérmica recubierta por una capa ectodérmica. Las interacciones entre los componentes del mesodermo y los componentes del ectodermo son las responsables de la correcta morfología y desarrollo de la extremidad. En la parte más distal del esbozo se produce un engrosamiento del ectodermo, formándose una estructura especializada llamada cresta ectodérmica apical (AER). Curiosamente la AER se forma en el límite DV y es uno de los principales centros señalizadores que controla el crecimiento a lo largo del eje PD a través de los FGFs. La correcta formación de patrón de la extremidad la llevan a cabo los centros señalizadores, que junto con la AER son la zona de actividad polarizadora (ZPA), controlando la formación del eje AP y el ectodermo no-AER, que controla la formación del patrón en el eje DV.

La importancia de la AER radica en la truncación de la extremidad cuando ésta es dañada o extirpada. Entender los mecanismos que dirigen la formación de la AER y su precisa y enigmática localización en el límite DV es de máximo interés. Su establecimiento está dirigido por complejas interacciones entre los componentes de 3 vías principales: BMP, WNT/ β -CANTENIN y FGFs, que actúan tanto en el ectodermo como entre el ectodermo y el mesodermo.

Previamente en el laboratorio se identificó que SP6 y SP8, dos factores de transcripción (TF) miembros de la familia Specificity Protein (SP) expresados en el ectodermo de la extremidad, son conjuntamente necesarios para la formación de la AER. SP6 y SP8 son factores redundantes dependientes de dosis y su pérdida conlleva a

diversas malformaciones que van desde una sindactilia, pasando por el síndrome de Split-Hand/Foot malformation (SHFM, síndrome de la mano hendida), truncación y finalmente amelia. El fenotipo de SHFM se produce cuando solo hay una copia de *Sp8* en ausencia de *Sp6* (*Sp6^{-/-}*; *Sp8^{+/-}*) y es un fenotipo reminiscente al que se observa en casos humanos. Esta malformación se caracteriza por presentar defectos en la AER, así como una alteración en el eje DV presentando extremidades bidorsales. La caracterización molecular de los dobles mutantes determinó la necesidad de SP6/8 en la inducción de *Fgf8* (marcador por excelencia de la AER) mediada por WNT/ β -CANTENIN, así como en la activación de *En1* (factor ventralizador), viéndose altamente reducido en los mutantes mientras que *Wnt7a* (factor dorsalizador) se encontró expresado no solo en la zona dorsal sino también en la ventral.

SP6 y SP8 son por tanto importantes factores que están operando en el ectodermo de la extremidad, tanto en el eje PD como en el DV. **El primer objetivo** de este trabajo es entender la compleja red reguladora de SP8 que opera en el ectodermo de la extremidad mediante la identificación de las dianas de SP8. Para ello, hemos combinado el perfil de unión de SP8 al genoma (ChIPmentación) y su perfil transcripcional (RNA-seq). Los genes diana directos de SP8 son definidos como aquellos genes que se encuentran diferencialmente expresados en ausencia de *Sp8* y están asociados a regiones del genoma unidas por SP8.

Ambos estudios se han realizado exclusivamente en los ectodermos de FL a E10.5, estadio en el que la AER presenta su máxima actividad, coincidiendo con el inicio del fenotipo de *Sp8*.

Para la ChIPmentación, debido a la ausencia de un anticuerpo anti-SP8 lo suficientemente específico, generamos un ratón *Sp8-FL*, que contiene el alelo *Sp8* tagueado con tres copias del epítipo FLAG. El perfil de unión de SP8 identificó 1,451 regiones. Paralelamente el perfil transcripcional de SP8 fue generado comparando a E10.5 ectodermos WT con ectodermos carentes de *Sp8*, identificando 892 genes diferencialmente expresados. La combinación de ambos conjuntos de datos reveló 184 genes diana de SP8, estando el 30% reprimidos y el 70% activados por SP8. Esta red de dianas directas de SP8 incluye todos los reguladores importantes en el modelado del ectodermo de la extremidad.

El análisis de estos genes reveló que SP8 actúa sobre los genes diana preferentemente desde sitios de unión situados distalmente (>5 kb desde el TSS). La búsqueda de motivos *de novo* identificó la caja GC conservada en la familia SP (SP1-like) cuando SP8 actúa preferencialmente como represor. Sin embargo, predominan motivos ricos en AT (DLX5-like) cuando SP8 funciona como activador. De acuerdo con ello, comprobamos mediante CoIP en células HEK-293 que SP8 se puede unir físicamente a DLX5. Nuestros resultados sugieren que SP8 controla la transcripción de *Fgf8* mediante la unión directa a cajas GC en su promotor, así como que las dianas de la vía de WNT dependientes de SP8 son probablemente mediadas por el control de la expresión de *Rspo2*. En relación con el eje DV, nuestros resultados indican que SP8 activa tanto a *En1* como a *Wnt7a* a través de enhancers putativos localizados distalmente. Podemos concluir que la actividad transcripcional de SP8 es compleja y puede funcionar directa o indirectamente para activar o reprimir genes diana dependiendo del contexto.

El segundo objetivo de este trabajo dada la redundancia de SP6 y SP8 es investigar su posible interacción a nivel de proteína. Mediante estudios de Complementación Fluorescente Bimolecular (BiFC) y Coimmunoprecipitación en células HEK-293 identificamos que SP6 y SP8 forman homo y heterodímeros, siendo el dominio de los dedos de zinc de SP8 esencial para esta interacción.

1. INTRODUCTION

1. INTRODUCTION

A fundamental question in biology is how a group of undifferentiated cells are able to differentiate and form a complex organ in three dimensions.

Several highly organized processes are involved in the embryonic development, which starts with a single cell, the zygote, and ends up with more than 200 different types of cells, forming part of the different tissues and organs that constitute an organism.

These processes include gastrulation, morphogenesis, growth, cell differentiation, cell migration and cell death. In the gastrulation, organized and drastic movements of cells will give rise to the formation of the three germ layers of the early embryo (ectoderm, mesoderm and endoderm). It follows the process of organogenesis, in which the cells interact and lead to the primordia of the main organs of the body. The ectoderm (outer layer) will give rise to the epidermis and the nervous system; the endoderm (inner layer) will form the digestive system and associated organs (liver, pancreas and lungs). The mesoderm (intermediate layer) will generate the heart, the gonads and the kidney, along with blood cells and vessels, bones, tendons and muscles.

The process of organogenesis implies pattern formation, a process in which the cells acquire positional information, originating differentiated cells organized in time and space forming the different parts of an organ. This positional information is established through signaling pathways mediated by signaling molecules (ligands) and their receptors. In embryonic development, a large part of signaling molecules can be grouped: the Wingless and Integration1 (WNT) family and their receptors (FRIZZLED); the family of fibroblast growth factors (FGFs) and their receptors (FGFRs); the superfamily of transforming growth factors- β (TGFs- β) and their receptors (TGFRs), the Delta-SERRATE family and its receptor NOTCH, and the family of HEDGEHOG and its receptor (PATCHED). Signal transduction of these ligands can be modulated by the specificity of their receptors, by the regulatory mechanisms of genomic expression and by secreted proteins, which could present binding affinity for ligands and interrupt their signaling.

The pattern formation is a process in which cells are sequentially specified, determined and then differentiated to form a morphological structure. A cell is specified to form a structure when it has received molecular information that allows it to develop to that structure autonomously even if it is isolated in a neutral environment. Specification is a reversible process. Cells are able to change their fate under the influence of new signals. Determination occurs after specification and is an irreversible process. A determined cell differentiates autonomously even if it receives new signals.

Animal models have been widely used for research based on the genetic and physiological similarities between the species. They have become an essential tool for studying the biological mechanisms conserved along evolution and also developmental processes that led to the appearance of different species. The possible generation of transgenic, knock-out and knock-in models have provided a wide and powerful window to study in detail specific molecular mechanisms and the diseases originated when these mechanisms malfunction. If the knowledge acquired by studying an animal model is to be translated to human, mouse is the model organism per excellence, because of the genetic and physiological similarities, simple breeding and the wide variety of genetical tools available. Along with mice, the chick embryo is one excellent model organism to study developmental biology. Fertilized chicken eggs are quite accessible and this model brings the opportunity of manipulating the embryo *in vivo*, allowing a continuous follow up in its development.

Within an organism, the limb is an accessible, non-vital organ that allows a variety of experimental manipulations without compromising the survival of the embryos. Therefore, the limb is an ideal organ to study the different mechanism orchestrating organogenesis, which can be extrapolated to other developmental processes.

1.1 Limb development

The presumptive limb territory is molecularly specified in chick at stage 13-14 of Hamburger and Hamilton (HH, (V. Hamburger, 1951)) although it only becomes visible at HH16 or at embryonic day 9.5 in mouse (E9.5). The limb bud derives from the somatopleural cells of the Lateral Plate Mesoderm (LPM) and consists of a central core of mesodermal cells surrounded by an ectodermal hull. At early stages, the somatopleure is an epithelial single cell layer and later on becomes mesenchymal and generates the limb primordium. Epithelial-to-Mesenchymal Transition (EMT) of the somatopleure was demonstrated to play a fundamental role in limb bud initiation (Gros and Tabin, 2014). Intense proliferation of somatopleural lateral plate cells will drive mesenchyme to expand outward. As limb bud grows, the pattern is laid down, with the structures nearest to the main body axis forming first and the most distal forming the last (Fig. 1).

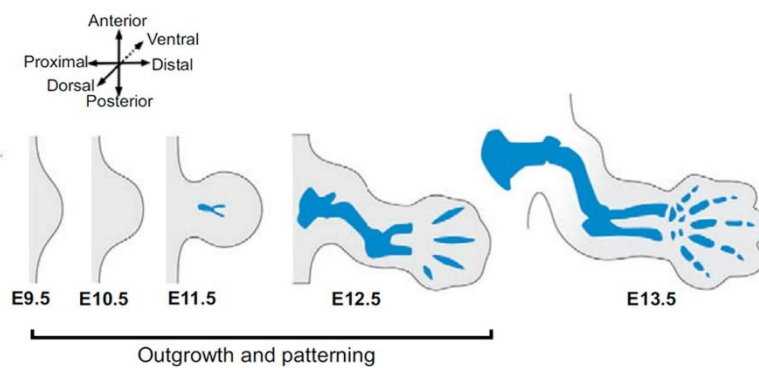


Figure 1. Schematic representations of mouse forelimb development from E9.5 to E13.5. Hindlimb bud, which development is E0.5 delayed in comparison with the forelimb, is not represented. Skeletal preparations are represented in blue, depicted as they appear when stained with Alcian Blue (to highlight mature cartilage). The three limb bud axes are also shown. Modified from Zuñiga (2015).

The limb bud grows along three main spatial axes: Proximo-Distal (PD, shoulder to fingertip), Antero-Posterior (AP, thumb to little finger) and Dorso-Ventral (DV, knuckle to palm). Each of these axes develops under the control of a specific signaling

center: the apical ectodermal ridge (AER), the zone of polarizing activity (ZPA) and the non-AER ectoderm, respectively (Fig. 2).

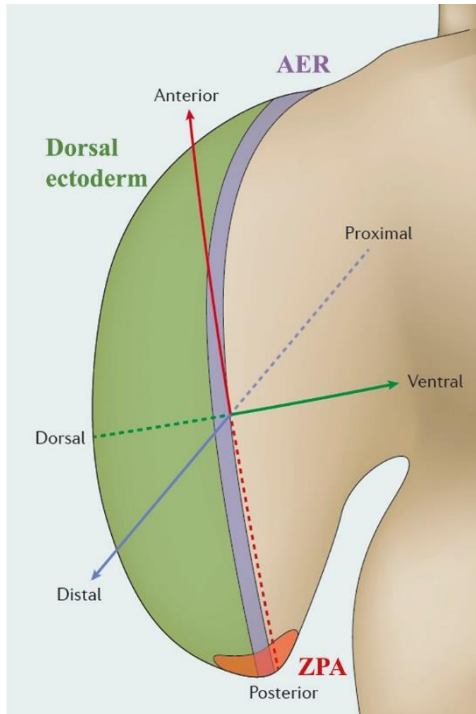


Figure 2. Overview of the three main signaling centers orchestrating limb development along the three different axes.

The proximal–distal axis is controlled by the apical ectodermal ridge (AER, purple color) signaling center. The anterior–posterior axis is directed by the zone of polarizing activity (ZPA, red color). The dorsal–ventral axis controlled by the non-AER ectoderm (green color). From Petit et al., 2017.

All signaling centers are necessary for the proper development of the limb, since they provide the growth factors necessary for limb growth and patterning. The AER is an ectodermal thickening at the most distal region of the limb bud with important signaling roles, mainly mediated by fibroblast growth factor (FGF) signals (Boulet et al., 2004; Mariani et al., 2008a; SAUNDERS, 1948; Sun et al., 2002a). The ZPA is a group of mesodermal cells localized at the posterior border of the limb bud, whose activity is mediated by Sonic Hedgehog (SHH) (Riddle et al., 1993; Saunders and Gasseling, 1968; Tickle, 1981; Tickle et al., 1975). In the non-AER ectoderm, the activation of *Engrailed1* (*En1*) in the ventral ectoderm and *Wingless-related MMTV integration site 7A* (*Wnt7a*) in the dorsal ectoderm, controls DV patterning (Altabef and Tickle, 2002; Parr and McMahon, 1995; Riddle et al., 1995; Vogel et al., 1995).

The tetrapod limb presents a basic design that includes three proximo-distal segments. The stylopod is the most proximal segment and contains a single skeletal element called the humerus in the forelimb (FL) and the femur in the hindlimb (HL). The intermediate segment corresponds to the zeugopod, containing the radius/tibia and

ulna/fibula (FL/HL). Finally, the autopod is the most distal segment and contains a set of elements subdivided into mesopodium (carpals/tarsals) and acropodium (metacarpals/metatarsals and phalanges) (Fig. 3).

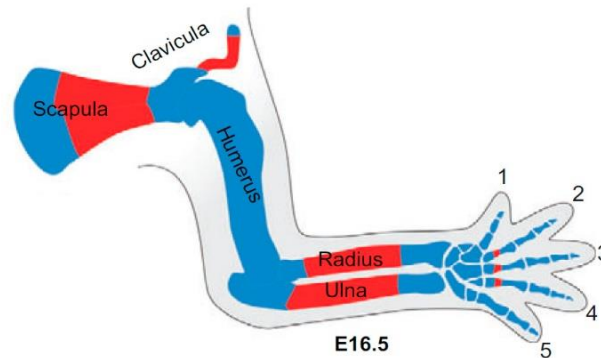


Figure 3. Schematic representations of all skeletal elements.

The figure corresponds to the morphological structure of E16.5 forelimb when all the elements are formed. Skeletal elements are depicted stained with Alcian Blue (to highlight mature cartilage) and Alizarin Red (to highlight mineralized bone). Bone identities are indicated, and digits are labelled 1 to 5 from anterior (thumb) to posterior (little finger). The proximal scapula (shoulder blade) and clavicle are located in the body. Modified from Zuñiga (2015).

Limbs are highly conserved structures in tetrapods, formed at a very precise location along the AP axis. The first morphological evidence of limb development is a bulge that emerges from either side of the embryo body wall at the appropriate levels (limb fields). The limb fields seem to be specified by expression of certain *Homeobox* (*Hox*) genes (Burke et al., 1995; Minguillon et al., 2012; Nishimoto et al., 2015). *Hox* genes encode transcription factors (TF) critical for the establishment of the basic body plan of bilaterian animals (Lewis, 1978). *Tbx5* and *Tbx4*, members of the T-BOX family of TFs, are downstream of *Hox* genes and are expressed in the prospective forelimb and hindlimb mesoderm respectively. In the forelimb presumptive field, antagonization of *Fgf8* expression through Retinoic Acid (RA) seems to be required for correct induction and positioning of *Tbx5* (Cunningham et al., 2013; Gibert, 2006; Zhao et al., 2009). In the hindlimb field, the homeodomain TF *Pitx1* and probably *Pitx2* (Marcil, 2003) along with *Hox* genes, determine its position mediated by *Tbx4* expression (Gibson-Brown et al., 1996; Logan et al., 1998; Logan and Tabin, 1999; Minguillon et al., 2005). However, more recently it was suggested that the TF *Islet1*, expressed in the same area

as *Pitx1*, is required for *Tbx4* expression and formation of the hindlimb bud (Kawakami et al., 2011; Narkis et al., 2012).

In tetrapods, *HoxA* and *HoxD* clusters, were coopted for the organization of limb morphology (Spitz et al., 2001; Zakany et al., 2007) being sequentially activated in time and space (Tarchini and Duboule, 2006). The correct morphology of the stylopod and zeugopod depends on the early phase of *Hoxd* expression (HOXD9 to HOXD11 highest transcription level) which relies on enhancers located telomeric to the cluster (T-DOM) while the proper patterning of the digits (HOXD10 to HOXD13 with HOXD13 higher level of expression) is governed by enhancers located centromeric to the cluster (C-DOM) (Andrey et al., 2013; Montavon et al., 2011; Montavon and Duboule, 2013).

Once the limb fields are specified, cells from the LPM maintain a highly proliferative state, leading to the limb bud formation. Limb outgrowth and patterning are highly regulated through a continuous molecular crosstalk between ectodermal and mesodermal components. Main signaling molecules of these Epitelial-Mesenchymal (E-M) interactions belong to several highly conserved families such as the FGF family, WNT family, and transforming growth factor- β (TFG- β) superfamily.

Initially, *Fgf10* is expressed in the LPM being restricted to the prospective limb mesoderm after *Wnt2b* activation (induced previously by *Tbx5*) in the forelimb, while in the hindlimb is through *Wnt8c* activation (induced by *Tbx4*) (Ohuchi et al., 1997).

Mesodermal *Fgf10* signals to the ectoderm through its receptor FGFR2b, activating *Fgf8* through *Wnt3* and SP6/8 TF in the ectoderm (Barrow et al., 2003; Haro et al., 2014; Kawakami et al., 2001; Kengaku et al., 1998; Soshnikova et al., 2003b). *Fgf8* in the AER signals back to the mesoderm through FGFR1 to maintain *Fgf10* expression, establishing a positive growth-promoting *Fgf10-Fgf8* feedback loop between the AER and the limb progenitors (Fig. 4). Moreover, the formation of a functional *Fgf* and *Wnt*-expressing AER depends on Bone Morphogenetic Proteins (BMPs), although the interaction of these two pathways remain elusive (Ahn et al., 2001a; Barrow et al., 2003; Benazet and Zeller, 2013; Bénazet and Zeller, 2009; Pajni-Underwood et al., 2007; Soshnikova et al., 2003b).

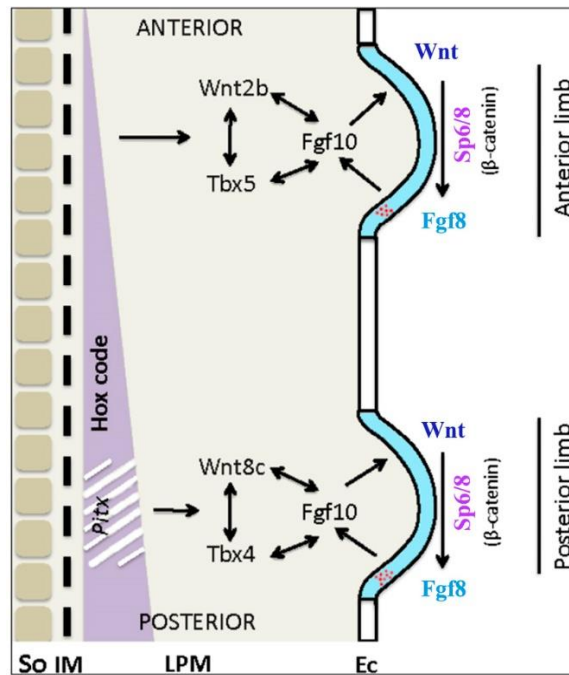


Figure 4. Limb initiation cascade.

A Hox code in the LPM act upstream of the TBX TFs and a WNT activity in the LPM. *Wnt2b* and *Wnt8c* in the FL and HL respectively, are required for the restriction of *Fgf10* expression in the prospective limb mesoderm. FGF10 signals to the surface ectoderm to induce *Wnt*, resulting in activation of *Fgf8* through *Sp6/8* in the limb ectoderm in a β -catenin dependent manner. Subsequently, FGF8 signals back to the mesoderm maintaining FGF10 expression. Positive regulatory loop between FGF10 in the mesoderm and FGF8 in the ectoderm is established. So, Somite; IM, Intermediate mesoderm; Ec, Ectoderm. Adapted from Kawakami et al., 2001.

1.2 Proximo-Distal limb outgrowth and patterning

The three morphological segments of the limb are progressively established in a PD sequence: the proximal stylopod (upper arm/thigh), the middle zeugopod (forearm/shin) and the distal autopod (hand/foot).

Stylopod and zeugopod are highly conserved structures across tetrapod species, meanwhile the autopod presents high evolutionary variability resulting in a handful of different adaptations to the environment. For example, the diversity in the number of digits across species (5 digits in mouse, 3 in the wing and 4 in leg of birds, or just one in the horse). Despite this morphological diversification, the development of the autopod across tetrapod animals share common mechanisms. Therefore, the autopod is an interesting model to investigate the development of patter formation in vertebrates.

Several FGF family members, *Fgf4*, *Fgf8*, *Fgf9* and *Fgf17*, exhibit a restricted pattern of expression in the AER (referred to as AER-Fgfs) (Martin, 1998; Tickle and Münsterberg, 2001). Among them, *Fgf8* is expressed at the highest level and in all AER cells during the whole period of AER activity, being therefore considered the best AER marker. The other AER-Fgfs, *Fgf4*, *Fgf9* and *Fgf1*, are subsequently activated in the posterior AER, and their expression expands in an anterior direction later during the development of the limb (Fernandez-Teran and Ros, 2008; Lewandoski et al., 2000; Mariani et al., 2008b). FGFs from the AER drive PD outgrowth and patterning via ERK/MAPK (Roux and Blenis, 2004) and AKT/PI3K pathway activation (Datta et al., 1999).

As stated before, *Fgf10* is expressed in the mesoderm and signals through FGFR2 in the overlaying ectoderm, activating WNT/ β -CATENIN signaling within the AER. Finally, with SP6/SP8 transcription *Fgf8* is up-regulated, which signals from the AER back to the mesoderm through FGFR1, to maintain *Fgf10* expression (Revest et al., 2001). This is a key event that initiates a crosstalk between the ectoderm and the mesoderm that drive limb outgrowth and patterning (Fernandez-Teran and Ros, 2008; Rodriguez-Leon et al., 2013).

Intense investigation has been carried out to unravel how the positional values along PD axis are specified. However, this is still an enigmatic problem, as no consensus model has been reached.

First evidence of how this pattern might work came up with microsurgical experiments from (Saunders, 1948) and (Summerbell et al., 1973) in which AER was removed at different stages. The earlier the AER removal, the most proximal the truncation of the limb was. This evidence led to the proposal of the first model to explain how the limb is specified: **Progress Zone Model** (PZM). This model postulates the existence of a defined-size region located at the most distal mesenchyme underlying the AER (of about 300 microns) called the “progress zone” (PZ). In this PZ, FGF signaling from the AER maintains the cells in an undifferentiated and proliferative state, where cells wait for acquirement of positional information of their future PD fate. Cells proliferate and limb outgrowths, being the cells of the PZ pushed from this area and then released from the influence of the AER, starting to differentiate. The more time the

cells spend in the PZ, the more distal specification they acquire. The model assumes that there is an intrinsic timer which provides cells the notion of the amount of time spent in the PZ, determining its PD positional identity. Therefore, cells first differentiate into the stylopod, then the zeugopod and finally the autopod. In this model time is an important factor, but the molecular nature of the internal 'clock' remained unsolved.

Experiments where a late chick bud AER is interchanged with an early one, and vice versa, show no alteration in the limb growth, indicating that the positional information of PD patterning depends on mesenchymal cells (Rubin and Saunders, 1972). Similar experiments where an old PZ was interchanged with a young one, and vice versa, lead to loss and duplication of limb elements (Summerbell and Lewis, 1975), respectively, reinforcing the prevalence of the PZM.

Conditional disruption of *Fgf8* and *Fgf4* in mouse with *Msx2-Cre* line allows the FL to receive an early and transient expression of both *Fgfs*, but they are removed before their induction in the HL. The phenotypes show the three elements in the FL, with hypoplasia in stylopod and autopod, and amelia in the HL (Sun et al., 2002b). These observed phenotypes in the FL did not stand with the PZM, which predicts the formation of proximal elements and the loss of the distal ones, being the **Early Specification Model** proposed (Dudley et al., 2002). This model postulates that at a very early stage, PD segments are specified, and as limb grows, they expand. Limb truncation phenotypes due to AER removal explained previously by PZM, could be explained through the increased apoptosis and the cessation of proliferation observed at the distal mesenchyme after AER removal (Rowe et al., 1982). However, no molecular markers could yet corroborate the model.

Experiments in chick wing buds proved that RA could be a potential candidate to control proximal fate, being repressed by the AER-FGFs. RA initially emanates from the LPM and then is restricted by the AER-Fgfs to the proximal limb domain. This analysis was done applying RA soaked beads in distal limb buds, where *Meis homeobox 1* (*Meis1*, the best proximal marker) was up-regulated and *Hoxa11* (the best zeugopod marker) and *Hoxd13* (the best autopod marker) were downregulated. It was proposed that FGF signaling was blocking RA and therefore inhibiting *Meis* expression (Mercader et al., 2000). To explain this, the **Two-signal model (TSM)** was proposed,

where two instructive opposing signals, one from the flank of the limb (RA) and the other from the AER (FGF), diffuse and specify PD axis. Proximal stylopod domain is under RA influence and distal autopod under FGF signal. Cellular interactions between proximal and distal domains (RA-FGF) might be responsible for specification of the zeugopod. Supporting this model, the triple conditional deletion of *Fgf8,4,9^{+/-}* resulted in the absence of the zeugopod in FLs and reduced stylopods and autopods in HLs. This is explained due to a decrease in distal signaling (Fgfs), allowing proximal signal to extend more distally, compromising autopod and zeugopod development (Mariani et al., 2008a). In addition, *Cyp26b1* KO mutants (Yashiro et al., 2004) and *Shh* KO mutants (Probst et al., 2011) also support this model. *Cyp26b1* is expressed in the distal region, induced by *Fgfs* and codes for a cytochrome P450 enzyme that processes RA. *Cyp26b1* mutants show an expansion of proximal limb identity (meromelia). *Shh* mutants show downregulation of *Cyp26b1*, being expression of proximal genes distally extended.

A modified version of this model has been proposed based on recombinant limbs experiments, postulating that early limb bud progenitors are specified as proximal by trunk signals but they lose this characteristic when exposed to distalizing FGF signaling (Cooper et al., 2011; Rosello-Diez et al., 2011). Although signaling environment seems to be essential for the specification of the main transition from stylopod to zeugopod, it is not enough to explain the zeugopod to autopod transition. It has been suggested that a low RA/FGF ratio, along with the time, allows *Hoxa13* expression (autopod marker; (Rosello-Diez et al., 2014). *Hoxa13* is key for autopod specification, as it suppress the zeugopod program when is expressed. The zeugopod would appear in the impasse frame of both stylopod and autopod patterning.

Although the specification of stylopod by proximal signals is well supported by RL, how the distal signals specify the zeugopod and the autopod remain elusive. In order to discriminate between intrinsic and signal-based timing mechanisms in the specification of the zeugopod and autopod segments, our group performed heterochronic grafting experiments (Saiz-Lopez et al., 2015). These heterochronic grafts consisted of transplants of GFP-expressing grafts (McGrew et al., 2004) from distal region of a stage 20HH limb to the distal region (under the AER) of a 24HH host. They demonstrated that once the limb progenitor cells are displaced, due to growth, from the

influence of the proximal signal (RA), they start an intrinsic developmental program under the permissive influence of the AER-FGFs.

These results allow the establishment of PD patterning, where RA from the trunk specifies the stylopod (Cooper et al., 2011; Rosello-Diez et al., 2011). Later on, this RA is processed by the *CYP26b1* enzyme, induced by FGFs, generating a RA-free domain in the distal mesenchyme where 5' *Hoxa/d* genes are expressed and AER-derived FGFs are maintained. They proposed that this event triggers an intrinsic cell cycle clock in the distal mesenchyme cells, activating a programme that first transit through an early phase of zeugopod specification, and then a second phase of autopod specification. This is based on cell adhesion properties and hence positional values intrinsically change over time, resulting in a spatial gradient of positional values along the PD axis (Nardi and Stocum, 1984; Wada and Ide, 1994). These findings are consistent with the classical PZ model, supporting the early idea that an intrinsic cell cycle clock (Lewis, 1975), sustained by AER signaling, is part of the timing mechanism that specifies the positional values of the zeugopod.

It could be concluded that stylopod–zeugopod transition is determined by environmental signaling meanwhile the zeugopod-autopod transition responds to a cell-autonomous timing mechanism that requires the AER permissive signaling environment (Fig. 5).

Finally, it is worth to mention that there is controversy on whether RA plays a role in PD patterning. It has been proposed that RA would be a teratogenic molecule whose function should be abolished for normal limb development. Mouse mutant *Rdh1^{trax/trax}* is a RA-deficient mouse, with stunted forelimbs but normal hindlimbs, both with maintenance of *Meis1* expression (Cunningham and Duester, 2015). This stands against an opposing diffusible gradient between RA and FGF, where RA specifies proximal fates. Alternatively, MEIS activity and the proximal program is a default state present before the limb appears and progressive distalization is achieved by the sole action of the distal FGFs signals, which would induce *Cyp26b1* responsible for RA degradation and therefore inhibiting *Meis1* expression. However, it has been argued that these mutants present a remaining RA activity responsible of limb outgrowth, and therefore a mutant lacking 100% RA would be necessary to take RA out of play.

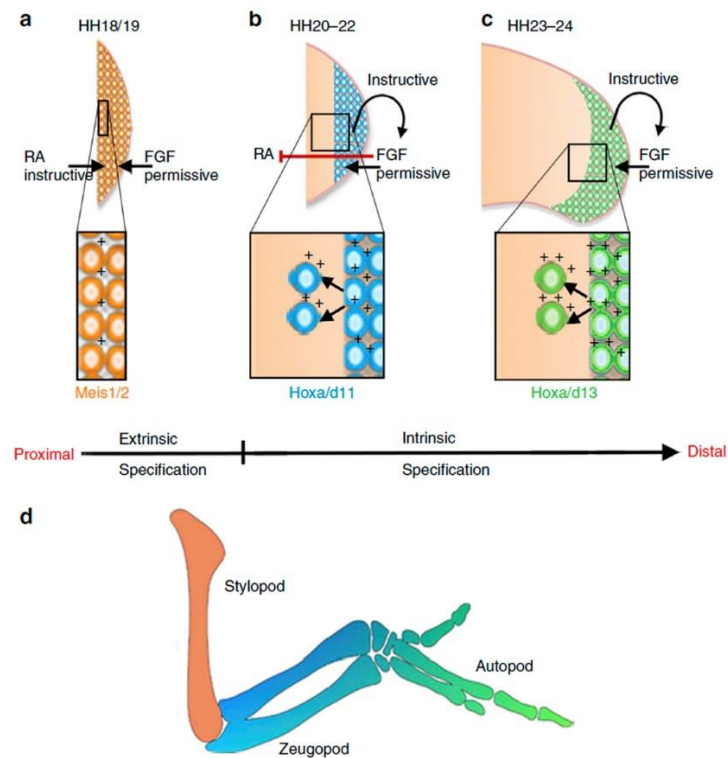


Figure 5. Proximo-distal patterning model.

This model takes as reference the chick wing. A) At early limb initiation stages (HH18/19) trunk-derived RA specifies the positional value of the stylopod (humerus, orange). **A-B)** AER-FGFs sustain the growth and induce the enzyme CYP26B1 that degrades RA (red-line) and consequently inhibits *Meis* expression. This creates a free RA domain at the distal mesenchyme of the bud which triggers the switch to intrinsic timing. **B-C)** Mesenchyme cells express 5'*Hoxa/d* genes and maintain AER-derived FGFs. Cell adhesion properties (greater cell adhesion shown by additional “+” symbols) result in a spatial gradient of positional values along the PD axis as cells are displaced from the distal mesenchyme by an intrinsic programme of proliferation. Therefore, at HH20–22 positional values of the zeugopod are specified (forewing, b, blue) and later (HH23–24) the autopod (wrist/digits, c, green). **D)** Skeletal specification shown by colors. From Saiz-Lopez et al., 2015.

1.3 Anterior-Posterior limb outgrowth

AP axis is the first axis specified in the limb and starts when HOX9 in FL (ISLET1 in HL) present in the flank, induces *Hand2* ('heart, autonomic nervous system and neural crest derivatives expressed transcript 2') in the posterior region of the presumptive limb (Itou et al., 2012; Xu and Wellik, 2011). The mutual antagonism of HAND2 and GLI3 ('glioblastoma') pre-patterned AP axis in the early limb bud. Both

TFs are initially expressed along the presumptive limb region, being later restricted to the anterior (*Gli3*) or to the posterior mesoderm (*Hand2*) (te Welscher et al., 2002). Indeed, GLI3 protein is processed into a short N-terminal form that acts as a strong transcriptional repressor, GLI3R (Wang et al., 2000). GLI3R interacts with two regulatory modules within the genomic landscape of *Hand2*, repressing HAND2 from the anterior mesoderm (Vokes et al., 2008). HAND2, expressed in the posterior mesoderm, is necessary for the activation of *Shh*, which mediates the activity of GLI3 protein. In SHH absence, GLI3 is processed to GLI3R. *Shh* is considered the main organizer of AP patterning and digit identity. *Shh* cis-regulatory region is known as the ZPA regulatory sequence (ZRS), located about 800 kb up-stream of *Shh*.

The Zone of Polarizing Activity (ZPA) is a group of mesodermal cells located at the posterior distal region of the limb bud mesoderm, identified and characterized by John Saunders. Grafting experiments of this posterior area from a donor to the anterior mesenchyme of a host produced a mirror image duplication of the posterior digits. (Saunders and Gasseling, 1968). This early experiment led L Wolpert (Wolpert, 1969) to propose the **Morphogen Gradient model**, which could explain that phenotype. This model assumes that a diffusible molecule coming from the ZPA is responsible for the AP polarity, establishing a gradient concentration along the axis responsible for the number and identity of the digits. Posterior digits would require the highest concentrations of the morphogen. Same phenotype was obtained when RA-beads were applied in the anterior border of the limb bud (Tickle et al., 1982). Later on, it was discovered that RA was promoting another ZPA, but it was SHH the morphogen required for ZPA activity (Riddle et al., 1993).

The application of beads with high concentrations of SHH in the anterior chick limb mesenchyme showed that the induction of extra digits was sequentially produced, being the anterior digits the first ones to be specified. With increasing time exposures, the anterior digits are promoted to posterior digits. This model was called **Promotion morphogen gradient model** (Yang et al., 1997). This model has into account not only the concentration of SHH but also the exposure time.

Genetic lineage tracing studies in mouse suggest that the specification of the digits depend on a SHH gradient, temporal and spatial, where mouse digit 1 does not

receive any SHH signaling, digit 2 just get SHH from producing cells, while ZPA descendants from part of digit 3 and digits 4 and 5 are exposed to autocrine SHH (Harfe et al., 2004). These results gave rise to the **Expansion-based temporal model**, where SHH activity is integrated over time (Harfe et al., 2004; Scherz et al., 2007).

Temporal conditional *Shh* KO show that the formation of digits was lost according to the time point *Shh* is arrested. Digit condensations show that the sequence of digit lost (d3, d5, d2 and d4) was inverse to the normal digit formation (d4, d2, d5 and d3). This suggest a **Biphasic model**, where SHH might act in two phases. In the first phase, early and transitory, SHH would be a morphogen specifying digit identities, while in the second phase, SHH would signal for long period of time to expand the progenitors, allowing the formation of the last digits (Zhu et al., 2008).

Based on chicken limb buds experiments the **Growth-morphogen model** was proposed, in which SHH integrates proliferation and specification of digits through the control of cell cycle regulators. Inhibition of *Shh* signaling by cyclopamine (SMO inhibitor), reduces the digital plate and posterior digits are lost. Blocking of proliferation applying Trichostatin A (TSA) results in SHH inhibition, with reduction of the limb size and loss of anterior digit specification, but when its effect is over, SHH is produced again. This implies that *Shh* is controlled by cell proliferation and expression of SHH after its inhibition is enough to specify posterior digit identity (Towers et al., 2008).

The observation that the phenotype of *Shh-Gli3* is polydactylous and similar to the *Gli3* mutant indicate that the main function of SHH is to avoid GLI3 cleavage to GLI3R. This make us switch from an intracellular AP gradient of SHH to an extracellular AP gradient of GLI3R.

The observation of the polydactylous phenotypes obtained after the progressive reduction in *Hoxa13* and *Hoxd11-Hoxd13* genes from the *Gli3*-null background, showed even more severe phenotype than the polydactylous *Gli3* KO, displaying also thinner and densely packed digits. This led to the proposal of a reaction diffusion model based in a **Turing type mechanism**, which assumes the interaction of an activator and inhibitor molecule, which will diffuse generating a wave stationary pattern in which the

wavelength is responsible for digit period, considering the digit/no digit pattern a consistent repetitive structure. The dose distal *Hoxd* genes and AER-FGFs would modulate the digit period wavelength (Sheth et al., 2012).

The nature of the two postulated activator and inhibitor Turing signals was further studied, where BMPS, SOX9 and WNT were identified as the key molecules of a substrate–depletion type model, termed the **BSW model** (Raspopovic et al., 2014). In the autopod, *Sox9* (earliest chondrogenic condensation marker) is positively regulated by BMPs and highlights the positions of the future digits. BMP ligands expressed in the interdigital mesenchyme signal to SOX9 positive progenitors. On the other hand, WNT inhibits SOX9 expression in the interdigit, finally resulting in the digit primordia. The interactions of BMPS, SOX9 and WNT modulated by HOX and FGFs would explain the digit/no-digit patterning.

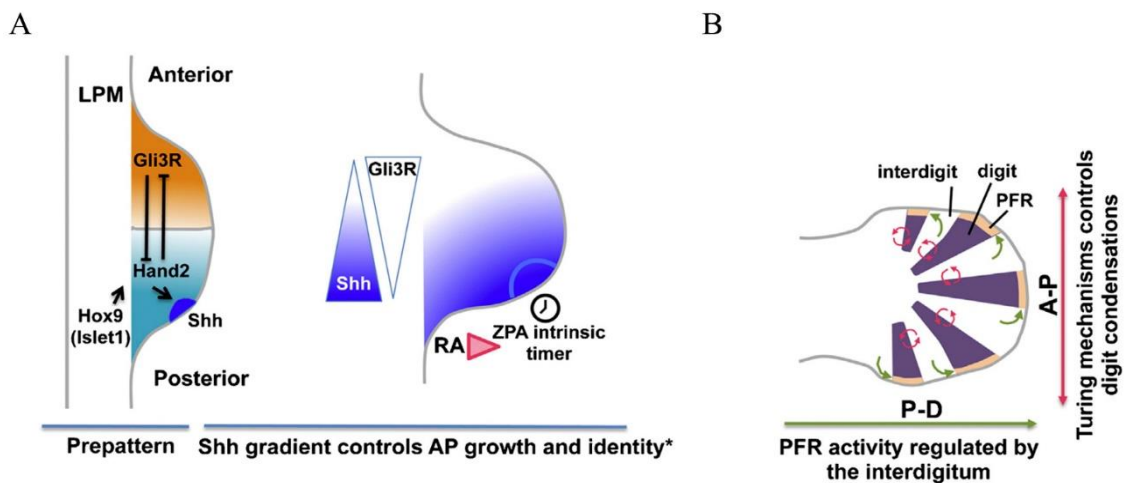


Figure 6. Antero-posterior patterning model.

A) AP pre-patterning occurs in the early limb bud when *Hox9* genes in the LPM (or *Islet1* in the case of the HL) induce *Hand2*, which is restricted to the posterior region by GLI3R. HAND2 then induces *Shh* in the ZPA establishing a SHH gradient along the AP axis which determines AP growth and identity. Moreover, SHH expression duration depends on an intrinsic timer (represented by a clock). **B)** At later stages, a Turing's reaction-diffusion mechanism specifies digit and interdigital regions generating the AP pattern of digit condensations. The number of condensations would depend on the size of the handplate. The number of phalanges in each digit is determined by the PFR activity, whose duration depends on signals from the immediate posterior interdigital region. Each interdigital region controls PFR activity to establish phalange number in each digit. From Delgado and Torres 2016.

After the digit/interdigit pattern is established, digital rays continue the formation of the corresponding phalanges. Phalanges are sequentially derived from a crescent-shaped area at the tip of the digits, the **Phalange Forming Region (PFR)**, where progenitors, with a unique BMP signature, proliferate under AER influence (Suzuki et al., 2008). Phalanges and interzones are coordinately specified in the PFR under signaling balance between *GLI3* and *5'Hoxd* at the posterior interdigital space (Huang et al., 2016) (Fig. 6B).

1.4 Dorso-Ventral limb patterning

The morphology of the limb reflects the DV asymmetries. In mouse limbs, hair is present in the dorsal surface of the autopod and nails are developed at the dorsal tips of the digits. Ventrally, footpads and eccrine glands are present. In addition, internal DV asymmetry is evident for example in the specific organization and morphologies of extensor and flexor muscles and tendons.

When DV polarity of the limb is specified is not precisely determined yet. Several Surgical manipulation experiments in chick have proved that DV polarity is established before the limb bud emerges (Altabef et al., 1997; Altabef and Tickle, 2002; Kimmel et al., 2000; Michaud et al., 1997). Two different phases can be established. In the earliest phase, the mesoderm is the responsible of imparting the DV polarity to the ectoderm. In the second phase, when the ectoderm has acquired the polarity information, imposes the DV polarity to the mesoderm (Geduspan and MacCabe, 1989; Kieny et al., 1971; Saunders and Reuss, 1974).

Kieny et al., (Kieny et al., 1971) performed the experiments in which DV inversion of the presumptive limb mesoderm grafted under the flank ectoderm, resulted in no difference of DV limb pattern in comparison with ipsilateral, non-manipulated ones.

However, similar grafts performed by Saunders and Reus (1994) resulted in limbs with inverted polarity. This led to the idea that DV polarity remains in the mesoderm.

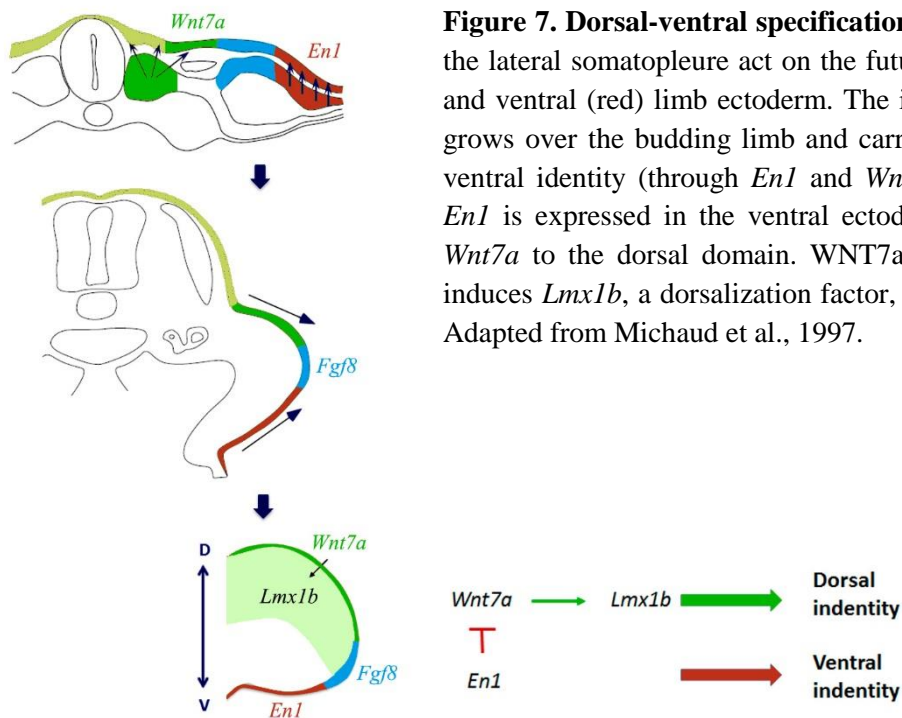
Further experiments in chick were performed by Michaud et al., (1997). The positioning of the limb prospective field between two rows of somite or the insertion of a barrier between the prospective limb field and the lateral somatopleure, led to the formation of bi-dorsal limbs. This confirmed the hypothesis that signals emanating from the somitic mesoderm and the LPM were responsible for the DV polarity of the limb between stage 13 and 15HH. These results demonstrated that the dorsal limb bud ectoderm originates from the ectoderm overlying the somite and the intermediate mesoderm and the ventral limb bud ectoderm comes from the ectoderm overlying the somatopleural mesoderm. Nevertheless, the molecular mechanisms that mediate the signals from the mesoderm at early stages are not clear. BMPs in ventral LPM and NOGGIN in the somatic mesoderm could be the responsible for the polarization of the dorsal and ventral ectoderm respectively (Ahn et al., 2001a; Michaud et al., 1997).

At later stages, Geduspan and MacCabe (Geduspan and MacCabe, 1989) performed surgical experiments in chick where 180° rotation of the ectoderm after 16HH lead to inversion of DV polarity of the limb, while inversion of the ectoderm before this stage did not perturb normal DV polarity. Therefore, DV polarity is established before the limb bud emerges (HH16).

All this evidence suggests that before the limb bud emerges (16HH), the mesoderm imparts DV information to the ectoderm, and then this information is transferred to the surrounding ectoderm (non-AER ectoderm) that will ultimately lead DV polarity.

The dorsal ectoderm expresses *Wnt7a*, a WNT family member that imparts polarity to the underlying limb mesoderm by triggering the expression of *LIM homeobox transcription factor 1 beta (Lmx1b)*, a LIM homeodomain TF that is ultimately responsible for limb dorsalization (Chen et al., 1998; Parr and McMahon, 1995; Riddle et al., 1995; Vogel et al., 1995). In the ventral ectoderm, BMP signaling, through *BMPR1A* activates *En1*, a homeodomain TF (Pizette et al., 2001), that inhibits *Wnt7a*, restricting its expression to the dorsal ectoderm (Cygan et al., 1997; Loomis et al., 1996) (Fig. 7). At the same time, BMP signaling is positioned downstream, or in parallel to the WNT-B-CATENIN signaling (Barrow et al., 2003; Soshnikova et al., 2003b).

Genetically engineered mouse models with loss of function of *Wnt7a* and of *En1* have been instrumental for understanding their role in DV patterning. Null mutants for *Wnt7a* present a double ventral limb phenotype (Parr and McMahon, 1995) while null mutants for *En1* resulted in dorsal transformation of the ventral region (Loomis et al., 1996). Mice lacking functional *Lmx1b*, as *Wnt7a* null mutants, develop a ventral-ventral limb phenotype, whereas ectopic ventral expression of *Lmx1b* leads to a dorsal-dorsal limb phenotype (Chen et al., 1998; Cygan et al., 1997; Vogel et al., 1995). The phenotype of double *En1/Wnt7a* mutant is double ventral, similarly to *Wnt7a* mutant, which would indicate that the main role of *En1* in the DV polarity is to impair the expression of *Wnt7a* in the dorsal ectoderm (Cygan et al., 1997; Loomis et al., 1998, 1996; Parr and McMahon, 1995).



Further experiments with double *Sp6^{-/-};Sp8^{CreERT2/CreERT2}* mutants revealed that DV pattern establishment is not established in the absence of SP6 and SP8, developing this double mutant double dorsal limb buds. There was absence of *En1* expression in the ventral limb ectoderm followed by ectopic expression of *Wnt7a* extending all over the

limb ventral ectoderm. Results also show that *Bmp4* was expressed in the ectoderm and mesoderm of this mutant, not being enough for *En1* induction in the ventral ectoderm.

1.5 Apical Ectodermal Ridge (AER)

The AER has morphological identity. It is a strip of pseudostratified columnar epithelium in chick and polystratified epithelium in mouse. Is worth mentioning that the human AER structure is more similar that of the mouse. The AER is a highly dynamic structure that constantly undergoes morphogenetic changes. Genetic cell lineage experiments in mouse show there is no evidence of AER descendent cells at birth, suggesting that the AER is a transitory structure (Guo et al., 2003). Three main phases can be distinguished during AER life span: the first phase (pre-AER) or specification of the AER precursor cells, a middle phase where a mature AER is formed and stablished, and a final phase where AER flattens and regresses (Fig. 8).

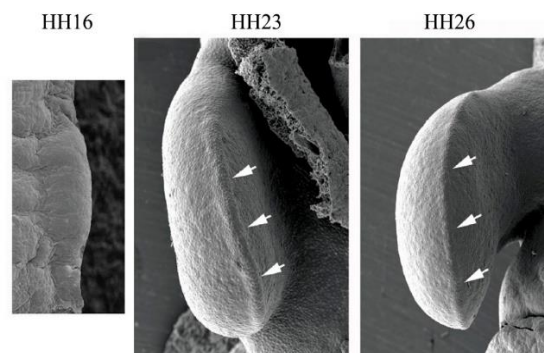


Figure 8. AER morphology at its initiation, maturation and regression.

Microphotograph of scanning microscopy showing the early stage of an anlage wing bud of a stage 16 HH (dorsal view), and the wing bud at stage 23HH and 26HH (distal view). The prominence of the AER is seen in both wings, being more bulging at stage 23HH than a stage 26HH. Adapted from Fernández-Terán and Ros (2008).

1.5.1 AER induction

The induction of the AER is governed by complex interactions between FGF, WNT/ β -CATENIN and BMP signaling pathways that take place within the ectoderm and between the ectoderm and mesoderm of the prospective limb bud.

Specification of AER precursor cells (termed pre-AER cells) occurs in a wide territory over the presumptive limb bud (which in mouse occupies the ventral ectoderm). Initially, by E9, *Fgf8* expression is patched in the ventral ectodermal region and soon becomes uniform (Kimmel et al., 2000; Loomis et al., 1998) (Fig. 9). Pre-AER cells are those cells expressing *Fgf8* before AER becomes morphologically distinguishable (Bell et al., 1998; Loomis et al., 1998). *Fgf10* in the LPM signals through to the ectoderm to activate *Wnt3*, and through SP6/8 TF, activate *Fgf8*. *Fgf8* signals back to the mesoderm to maintain *Fgf10* expression, maintaining a positive feedback loop (Ouchi 1997; Kawakami 2001). As will be later mentioned in more detail, BMP signaling plays a critical role in AER induction (Ahn et al., 2001a; Barrow et al., 2003; Pajni-Underwood et al., 2007; Pizette et al., 2001; Soshnikova et al., 2003a).

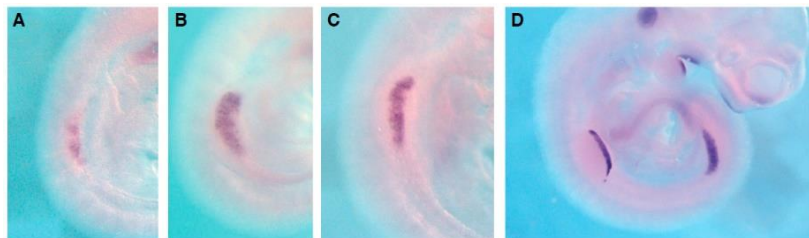


Figure 9. *Fgf8* expression in mouse pre-AER and AER cells.

A) Emerging limb bud (E9) showed *Fgf8* expression in a patched pattern in the ventral ectoderm, marking the precursors of the AER. **B,C)** *Fgf8* transcripts occupy a broader territory **D)** and progressively become confined to the mature AER. From Fernández-Teran and Ros (2008).

1.5.2 AER induction and DV axis

The fact that the PD signaling center, the AER, is localized at the distal tip of the limb bud, at the interface between the dorsal and ventral ectoderm lead to hypothesize that the patterning of these axis are under common regulatory mechanisms.

A very first connection between the AER induction and the DV specification of the ectoderm was proposed with the study of several mutants (chick limbless and wingless, and mouse legless), which showed defective in both DV patterning and AER induction or maintenance (Bell et al., 1998; Grieshammer et al., 1996; Ohuchi et al., 1997; Ros et al., 1996). *Limbleless* mutants are characterized by absence of *Fgf8* in the ectoderm (which would lead to lack AER), as well as *En1* in the ventral ectoderm (leading to bi-dorsal limb buds). Similarly, double mutants of *Msh Homeobox (Msx)1;Msx2* showed proper AER induction and maintenance except in the anterior border, where the DV boundary fails to form (Lallemand, 2005).

In 2001 Ahn et al., and Pizette et al., demonstrated that DV and AER induction are linked by a common signal, BMP (Bone Morphogenic Protein), which is expressed in the ventral ectoderm. The experiments of gain and loss of BMP function showed that BMP is necessary not only for AER induction and maintenance but also for DV patterning through the activation of *En1* in the ventral ectoderm (Ahn et al., 2001a; Barrow et al., 2003; Pizette et al., 2001; Soshnikova et al., 2003b) (Fig. 10). Loss of BMP signaling in the ventral limb ectoderm shows defects in DV patterning (bi-dorsal limbs) and also in AER formation Pizette 2001 (Ahn et al., 2001). Manipulation of BMP signaling lead to disruptions in the endogenous AER, resulting in absent or highly truncated limbs, probably because BMP signaling alteration results in ectopic *Fgf8* expression. Downstream of *Bmp*, *Msx* genes are co-expressed at the ventral ectoderm, probably regulating the AER induction. Therefore, it was proposed that BMP signal bifurcates at the level of EN1 and MSX to mediate differentially DV patterning and AER induction, respectively (Pizette et al., 2001).

The epistatic relationships between the BMP and the WNT signaling pathways in AER induction and DV patterning remain controversial (Barrow et al., 2003; Soshnikova et al., 2003b). The implication of canonical WNT signaling in the AER was studied by the conditional removal of β -catenin prior to AER induction (Soshnikova et al., 2003b). This resulted in a limbless phenotype, with failure in AER induction along with absence of *Fgf8*, *Bmp2* and *Bmp4*, as well as DV patterning defects with no *En1* and an increased *Wnt7a* expression. These defects were very similar to the *Bmpr1A* mutant. Compound mutants carrying LOF of *Bmpr1A* and GOF mutation in β -

Introduction

CATENIN in the limb ectoderm were performed (Soshnikova et al., 2003b). Surprisingly, β -CATENIN was capable of rescuing the *Bmpr1A* AER defective phenotype, recovering *Bmp4* and *Fgf8* expression, but not *En1*, maintaining the DV defects. This suggested that WNT signaling is downstream BMP signaling in the AER induction, but in parallel or upstream in DV pattern establishment (Soshnikova et al., 2003b). However, interactions between these pathways are highly complex since *Bmp2*, *Bmp4* and *Bmp7* are also induced by WNT/ β -CATENIN signaling, establishing a positive reinforcing feedback loop between both pathways (Barrow et al., 2003; Soshnikova et al., 2003b).

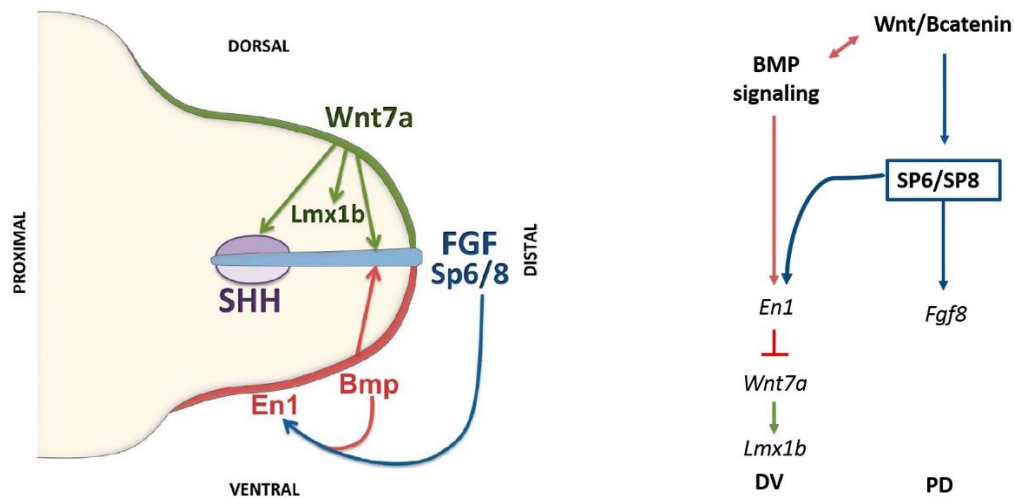


Figure 10. Dorso-ventral patterning in the limb bud ectoderm regulates AER positioning. Cooperation between SP6/8 and BMPs induces *En1* in the ventral ectoderm (blue and red arrows), and interaction between dorsal ectodermal *Wnt7a* (green arrow) and ventral ectodermal *En1* (red arrow) ensures AER positioning. WNT7A from the dorsal ectoderm activates *Lmx1b* and contributes to Shh activation in the mesenchyme (green arrows). Modified from Delgado and Torres (2016).

1.5.3 AER maturation

After AER specification, ectodermal morphogenetic movements compact AER cells on the DV tip of the bud. This results in a linear and compacted AER of polystratified epithelium of 3-4 cell layers at the DV boundary of the bud at E10.5-11, in mice (Loomis et al., 1998; Wanek et al., 1989). This process is called AER

maturation and is under the control of multiple factors. It is known that in the absence of *En1*, there is ventral expansion of the anterior half of the AER, giving rise to bifurcated or additional AERs (Loomis et al., 1998).

Several components of the WNT pathway have been shown to be involved in AER maturation, such as *Dickkopf1 (DKK1)*, a negative regulator of WNT signaling. DKK null mutant present a *doubleridge* phenotype which has been associated with enhanced canonical WTN signaling (Adamska et al., 2004, 2003; Mukhopadhyay et al., 2001).

Another important factor needed for AER maturation is SP8. In the *Sp8* mutant, pre-AER cells are induced, but ventral ectodermal cells do not compact (Bell et al., 2003; Treichel et al., 2003). In addition, *Sp6* (previously known as *Ephiprofin*) was found to be required for AER maturation. The *Sp6* mutant presents an abnormally broad and flat AER, sometimes protruding into the mesoderm. In some cases, it presents a *doubleridge* phenotype (Talamillo et al., 2010).

1.5.4 AER maintenance

Once the AER is induced, it requires of continuous signals from the mesoderm for its maintenance. There are two important feedback loops, one is positive inputs of WNT and FGF10 from the ectoderm and mesoderm respectively, another one is the blocking of negative effect of BMP signaling through GREM1, a member of the DAN family of BMP antagonist.

As stated before, FGF10 signaling from the mesoderm induces *Fgf8* in the limb ectoderm through the WNT/ β -CATENIN signaling (Barrow et al., 2003; De Moerloose et al., 2000; Gorivodsky and Lonai, 2003; Lu et al., 2008; Min et al., 1998; Sekine et al., 1999; Soshnikova et al., 2003a; Xu et al., 2013). Removal of any component of this interaction once the AER is established resulted in AER regression, indicating its continuous requirement also for AER maintenance (Lu et al., 2008).

BMP signaling is necessary for AER induction, but after that, BMP acts negatively on FGFs from the AER, perturbing maturation and maintenance of the AER, triggering an early regression. In this phase, a regulatory loop between FGFs from the

AER and SHH from the ZPA through *Gremlin1* (*Grem1*) is responsible for blocking BMP signaling. *Grem1* is activated by SHH from the ZPA, antagonizing BMPs and allowing the proper AER maturation and maintenance (Gañan et al., 1996; Khokha et al., 2003; Michos et al., 2004; Pizette and Niswander, 1999; Zúñiga et al., 1999). Subsequently, FGF maintains *Shh* expression in the ZPA establishing the regulatory feedback loop (Laufer et al., 1994; Niswander et al., 1993).

The combination of mouse molecular genetics with mathematical modeling of Benazet and coworkers (Benazet et al., 2009) have unraveled the existence of two feedback loops that coordinate AP patterning: a fast BMP4-GREM1 module and a slower SHH-GREM1-FGF module, regulating BMP levels through GREM1. The involvement of an additional feedback loop that converge in the BMP induction was proposed by Bastida et al., (Bastida et al., 2009), in which BMP is subjected to an auto-regulatory loop. Both studies agree that the level of BMP signaling is key in the crosstalk between the major signaling pathways operating in the posterior limb bud.

Curiously, experiments of cell lineage tracing those cells expressing SHH and its descendants are unable to express GREM1, and this refractoriness is crucial in the eventual termination of the SHH-FGF loop (Scherz et al., 2004). Alternatively, it was also proposed that high levels of FGF inhibits *Grem1* expression. Thus, as the limb bud grows and the FGF expression level in the AER becomes higher, the gap between these two domains becomes bigger allowing the inhibitory function of BMP on the AER (Verheyden and Sun, 2008).

The breakdown of the epithelial-mesenchyme feedback loop and loss of AER is considered to terminate limb bud outgrowth at the end of the patterning phase. However, a recent study (Pickering et al., 2018) in which grafting distal mesenchyme cells from late stage chick wing buds to the epithelial environment of younger wing buds, show that wing bud outgrowth at the end of the patterning phase terminates intrinsically in the distal mesenchyme in the presence of E-M signaling. Their data provide evidence that BMP signaling forms an autoregulatory circuit, controlling the cell cycle timer in the mesenchyme, which will extrinsically maintain the AER and permissively allows the timer to run (Pickering et al., 2018).

1.5.5 AER regression

By E11, the AER reaches its highest height and begins to regress. BMP signaling becomes detrimental for FGF expression in the AER and the regression starts. Regression of the AER starts first over the interdigital spaces, where the level of BMP signaling is higher, and it last over the digits until the last phalanges are laid down (Bastida et al., 2004; Guo et al., 2003; Pajni-Underwood et al., 2007).

1.5.6 AER defects

Abnormal AER morphologies due to defects in AER development include hyperplastic, hypoplastic, immature and misaligned AERs.

Hyperplastic AERs are thicker than normal and is probably because of accumulation of greater number of cells. It has been observed an elevated AER morphology in cases of decreased BMP signaling, where there is overexpression of NOGGIN (BMP antagonist) or loss of *Bmp4* in the mesoderm (Bastida et al., 2004; Pizette and Niswander, 1999; Selever et al., 2004). As we already stated, BMP signaling is required for AER induction and DV patterning, but after BMP is detrimental for AER through AER-FGF inhibition and controls AER regression. Upregulation of BMP signaling leads to premature AER regression and its reduction results in hyperplastic AER. In addition, modification in the NOTCH pathway also leads to hyperplastic AER. Both, *Notch1* and *Jagged2* are expressed in the AER and their conditional removal results in a DV expansion of the AER that protrudes into the mesoderm (Francis et al., 2005; Jiang et al., 1998; Pan et al., 2005; Sidow et al., 1997). This is due to reduced apoptosis in the AER, where NOTCH signaling is involved in the control of cell number probably through an apoptotic mechanism (Francis et al., 2005).

Defects in the maturation process lead to flat and broad AERs, which can also be considered as hyperplastic AERs. *En1* and *Dkk1* mutants present a “Double ridge” morphology where there is a thickening in the DV domain of *Fgf8*, outlined by two borders that might lead to two stripes of *Fgf8* (Loomis et al., 1998; Mukhopadhyay et al., 2001). These two parallel ridges could independently promote digit outgrowth or partial distal digit duplications. *Dkk1* is a negative regulator of the WNT signaling, and

the *doubleridge* phenotype has been associated with an upregulation of the WNT signaling.

Hypoplastic AERs are thinner than normal and interestingly, the Split-Hand/Foot human Malformation (SHFM), also known as ectrodactyly, is due to this AER morphology.

1.6 SHFM

SHFM is a congenital limb defect affecting predominantly the central rays of hands and/or feet. Failure in maintaining the medial region of the AER, that lacks *Fgf8* expression, affects the formation of the autopod (Sifakis et al., 2001; Temtamy and McKusick, 1978).

SHFM has an estimated prevalence of 1 per 8,500–25,000 births, which represents 8–17% of congenital limb deficiencies (Elliott et al., 2005, 2006; Elliott and Evans, 2006). It can appear as an isolated trait (non-syndromic SHFM) or in association with other limb manifestations (syndromic SHFM), such as tibia or femur aplasia, is called SHFM with long bone deficiency (SHFLD).

In human at least 7 loci have been associated to this SHFM syndrome, including SHFM1–6 and SHFLD3 (Table 1).

Regarding familiar cases, it is commonly inherited in an autosomic dominant fashion (SHFM1, SHFM3, SHFM4, and SHFM5), with incomplete penetrance and variable expressivity (Scherer et al., 1994), being SHFM2 X-linked, and SHFM6 transmitted in an autosomal recessive fashion (Faiyaz-Ul-Haque et al., 2005). Intragenic mutations have been identified in different genes (*DLX5*, *DLX6*, *ZAK*, *TP63*, and *WNT10B*) (Aziz et al., 2014; Ianakiev et al., 2000; Khan et al., 2012; Lango Allen et al., 2014; Shamseldin et al., 2012; Simonazzi et al., 2012; Spielmann et al., 2016; Ugur and Tolun, 2008; Ullah et al., 2016; Wang et al., 2014).

Table 1. SHFM Classification in humans

Locus	ONIM	Chromosomal location	Molecular mechanism	Causative gene	Inheritance
SHFM1	183600	7q21.2-q21.3	Mutation Deletion/duplication	<i>Dlx5 and Dlx6</i>	AR and AD AD
SHFM2	313350	Xq26	Unkown	Suspected <i>Fgf13</i> and <i>Tondu</i>	XL
SHFM3	608071	10q24.32	Duplications	<i>Dactylin, Btrc,</i> <i>Poll, Fgf8, Lbx1,</i> <i>Fbxw4</i>	AD
SHFM4	605289	3q27	Mutation	<i>Tp63</i>	AD
SHFM5	606708	2q31	Deletions	<i>Dlx1,2, Hoxd</i> <i>Cluster and/or</i> <i>Evx2</i>	AD
SHFM6	225300	12q13.12	Homozygous mutation	<i>Wnt10b</i>	AR
	616826	19p13.11	Micro deletions	<i>Eps15l1</i>	AR
SPD1	186000	2q31.1	Mutation	<i>Zak</i>	AR
SHFM- HH2	147950	8p11.23	Mutation	<i>Fgfr1</i>	AR
SHFLD1	119100	1q42.2-q43	Unknown	<i>Unknown</i>	AD
SHFLD2	610685	6q14.1	Unknown	<i>Unknown</i>	AD
SHFLD3	612576	17p13.3-p13.1	Microduplications	<i>Bhlha9</i>	AD

Hypogonadotropic hypogonadism 2 with or without anosmia (HH)
Synpolydactyly 1 (SPD1)

SHFM1 is caused by chromosomal rearrangements of the 7q21.3-q22.1 region, which encompass several genes involved in limb development, *Dss1* and *distalless*-relates homeogenes *Dlx5* and *Dlx6* (Crackower, 1996; Duijf et al., 2003; Shamseldin et al., 2012; Ullah et al., 2017; Wang et al., 2014) (Table 2).

Introduction

Table 2. Human reported SHFM1

Mutation			
Nonsense (DLX5)	c.115G>T	SHFM	(Sowińska-Seidler et al., 2014)
Missense (DLX5)	c.533A>C	SHFM with palmar dorsalization	(Shamseldin et al., (2012); Wang et al., (2014)
Missense (DLX5)	c.558G>T	SHFM	(Wang et al., 2014)
Missense (DLX5)	c.576C>G	RHS, SHFM	(Wang et al., 2014)
Small insertion (DLX5)	c.482_485dupACCT	SHFM	(Ullah et al., 2016)
Missense (DLX6)	c.632T>A	SHFM	(Ullah et al., 2017)
Chromosomal rearrangements			
DLX5, DLX6, and >50 others genes	8.478-Mb deletion	SHFM	(Vera-Carbonell et al., 2012)
DLX5, DLX6, and DSS1	0.9 – 1.8-Mb deletion	SHFM with Mondini dysplasia	(Wieland et al., 2004)
DLX5 and DLX6	719-kb duplication	SHFM	(Velinov et al., 2012)

In mouse, double *Dlx5;Dlx6* KO resembles the ectrodactylous phenotype characteristic of SHFM (Conte et al., 2016; Merlo et al., 2002; Robledo et al., 2002) confirming the implication of the human orthologs DLX5 and DLX6 in this pathology. *Fgf8*, best AER marker, is a target of DLX5 and DLX6 shown to be downregulated, along with *Dlx2*, in these mutants. The polarization of the AER is regulated by *Wnt5a*, another target of DLX, also downregulated in *Dlx5;Dlx6* KO (Conte et al., 2016). In *Dlx5;Dlx6* KO, (Restelli et al., 2014) suggested an essential loop for AER stratification, where DLX5, p63, Pin1 and FGF8 participate to at same time and location.

SHFM2 was reported to be X-linked inheritance of the trait, which mapped the SHFM2 locus to Xq26.3 (Faiyaz-Ul-Haque et al., 2005, 1993). Although no gene has been associated, there are two potential candidate genes located in this region, *Fgf13* and *Tondu* (Vaudin et al., 1999).

SHFM3 maps to chromosome 10q24 and the causative rearrangement involves a submicroscopic tandem duplication spanning a region of 325–570 kb (de Mollerat et al., 2003; Dimitrov et al., 2010; Xiang et al., 2017). Genes located within the duplicated region include DACTYLIN (SFHM3), BTRC, POLL, FGF8 and LBX1. Interestingly, this genomic region contains AER-specific enhancers, many of them embedded in the FBXW4 gene, which drive expression all along the AP extension of the AER, likely affecting *Fgf8* expression. Therefore, SHFM type III is likely the result of *Fgf8* misregulation (Marinić et al., 2013).

SHFM4 mapped to 3q27 region and is directly associated with mutations in *Tp63* (also known as *P63*) gene (Alves et al., 2015; Ianakiev et al., 2000; van Bokhoven et al., 2001).

Disruption analyses in mice revealed that *Tp63* is required for AER formation. Interestingly, in mice lacking *Tp63* the AER fails to stratify and the expression of *Dlx* genes is downregulated, positioning *p63* upstream of the *Dlx* for proper AER development (Lo Iacono et al., 2008b).

SHFM5 is associated with deletions of chromosome 2q31, region encompassing the entire HOXD gene cluster (HOXD1-HOXD13) which has been described in patients with SHFM, including monodactily and probably *Dlx1,2* regions (Boles et al., 1995; Del Campo et al., 1999; Ramer et al., 1990). However, Goodman et al. have suggested that SHFM5 is associated with the deletions in the 5 Mb interval centromeric to EVX2 gene, which is located upstream of the HOXD cluster (Goodman, 2002).

SHFM6 maps to chromosome 12q13, were cases of autosomal recessive SHFM resulted from a spectrum of homozygous mutations in WNT10B (Aziz et al., 2014; Blattner et al., 2010; Kantaputra et al., 2018; Khan et al., 2012; Ugur and Tolun, 2008; Ullah et al., 2018). It is reported that WNT10B acts upstream of FGFs, establishing the AER (Crackower et al., 1998; Kengaku et al., 1998).

SHFLD3 maps the 17p13.3 chromosomal duplication, including the *Bhlha9* gene, which has been associated with the distinct entity, inherited as an autosomal dominant trait (Armour et al., 2011; Fusco et al., 2017; Klopocki et al., 2012; Nagata et al., 2014).

Recently Umair et al., (2018) reported a homozygous variant in the *Eps15l1* gene located on chromosome 19p13.11 caused isolated SHFM. Also, mutations in *FGFR1* has been reported to be underlying mechanism responsible for the syndromic SHFM along with Congenital hypogonadotropic hypogonadism (CHH) (Ohtaka et al., 2017; Villanueva et al., 2015).

Mutations in *TP63*, *DLX5*, *DLX6*, *EPS15L1*, *FGF8*, *FGFR1*, and *WNT10B* were associated with SHFM, being undistinguishable the clinical features from each mutation (Merlo et al., 2002; Shamseldin et al., 2012; Ullah et al., 2017; Wang et al., 2014). This implies that they might be playing roles in the same underlying regulatory pathway. *TP63*, *DLX5*, *DLX6*, *FGF8*, *FGFR1*, and *WNT10B* are found to be co-expressed in the AER cells of the developing mouse limb (Lo Iacono et al., 2008a), probably downregulating *FGF8* in the medial portion of AER, which lead to SHFM (Conte et al., 2016; Lewandoski et al., 2000).

It is appreciated the involvement of the *TP63* network within some types of SHFM. *TP63*, responsible for SHFM4, is an upstream regulator of *Dlx* genes, responsible for SMFM1 (*DLX5/6*). As mentioned above, SHFM3 is caused by duplications of the *Fgf8* regulatory landscape. Therefore, it seems likely that SHFM 1, 3 and 4 are due to defects in the *TP63* network directing *Fgf8* expression.

1.6.1 SP6 and SP8 and split hand/foot malformation

Phenotypes of *Sp6^{-/-};Sp8^{+/-}* mutants are identical, including the DV component, to those reported in a human mutation in *DLX5* (Shamseldin et al., 2012) (Fig. 11). Since similar phenotypes are frequently caused by disruption of different components of a regulatory network. Haro et al., (2014) considered the possibility that *Sp6* and *Sp8* genes might be part of the *TP63* network.

Furthermore, the SP6/8-dependent SHFM is most similar, including the bidorsal finger tips, to a novel form of non-syndromic autosomal recessive human SHFM caused by a missense mutation in a highly conserved residue of the homeobox domain of *Dlx5* (Shamseldin et al., 2012). This similarity raises the appealing hypothesis that *Dlx5* is an upstream regulator of *Sp6* and/or *Sp8* also supported by the relatively normal expression of *Tp63*, *Dlx5* and *Dlx6* in the double *Sp6;Sp8* mutant (Haro et al., 2014). On the other hand, a cooperative function between *Dlx* and *Sp* genes has been reported in several contexts including the fly appendage and the planarian prototypic eye (Franch-Marro, 2006; Lapan and Reddien, 2011). An alternative hypothesis is that DLX and SP are needed in a synergistic but not linear pathway for *Fgf8* activation.



Figure 11. SHFM1 phenotype in human and mouse model.

Similarity in phenotypes between the human *Dlx5*-SHFM (Shamseldin et al., 2012) and the *Sp*-SHFM mice model Haro et al., 2014. Note the similarities between the human and mouse model, where even the bidorsal distal tips in *Sp6^{-/-};Sp8^{+/-}* are present. Adapted from Haro et al., 2014 and Shamseldin et al., 2012.

1.7 Specificity protein (SP) family

Specificity protein (SP) family of TF members are a large and wide-spread family of deoxyribonucleic acid (DNA) binding proteins which play an important role in transcriptional regulation. Nine SP genes have been identified in mammals. They share three highly conserved Cys2-His2-type Zinc Fingers (ZF).

1.7.1 Phylogeny of SP family proteins

Phylogenetic sequence analysis tried to track the origin of SP family, concluding that all SP factors fall into three monophyletic clades. One clade contains SP1, SP2, SP3 and SP4 of the vertebrate species and a single SP representative of each of the invertebrate species, the SP1-4 clade. The second clade contains SP5 of the vertebrate species and a single SP representative of each of the invertebrate. It was denominated the SP5/BTD clade, as includes the well-known *Btd* from *D. melanogaster*. The third clade contains SP6, SP7, SP8, and SP9 of all vertebrate species and again a single SP representative of each of the invertebrates, the SP6-9 clade. Therefore, *CG5669* gene in *Drosophila* is the homolog of *Sp1-4* in vertebrates, *Btd* gene would have the *Sp5* homolog in vertebrates and *D-Sp1* homolog would be *Sp6-9* in vertebrates. These three clades were also supported by protein domain structure, gene expression, and chromosomal location (Schaeper et al., 2010) (Fig. 12).

This distribution where in invertebrates there is just one SP protein is in each clade suggests that a set of three *Sp*-family genes (*Sp1-4*, *Sp5/ btd* and *Sp6-9* gene), is the ancestral state in the Metazoa. Genomic analysis in mouse revealed a pair distribution of *Sps* along the chromosomes in opposite directions: *Sp1-Sp7*, *Sp2-Sp6*, *Sp3-Sp9* and *Sp4-Sp8*, whereas *Sp5*, located at 3257 kb from *Sp3*, is not linked to other *Sp* gene (Kadonaga et al., 1987; Kawakami, 2004). Therefore, due to the whole genome duplications in vertebrates, it is likely that a single primordial gene underwent a tandem duplication event and produced progenitor genes for the *Sp1-Sp4* subfamily and *Sp6-Sp9* subfamily (Kawakami, 2004; Schaeper et al., 2010). *Sp5* was proposed to be the evolutionary link between the SP and another Zn finger factor family, *Kruppel-like factor* (KLF) family (Ravasi et al., 2003; Treichel et al., 2003).

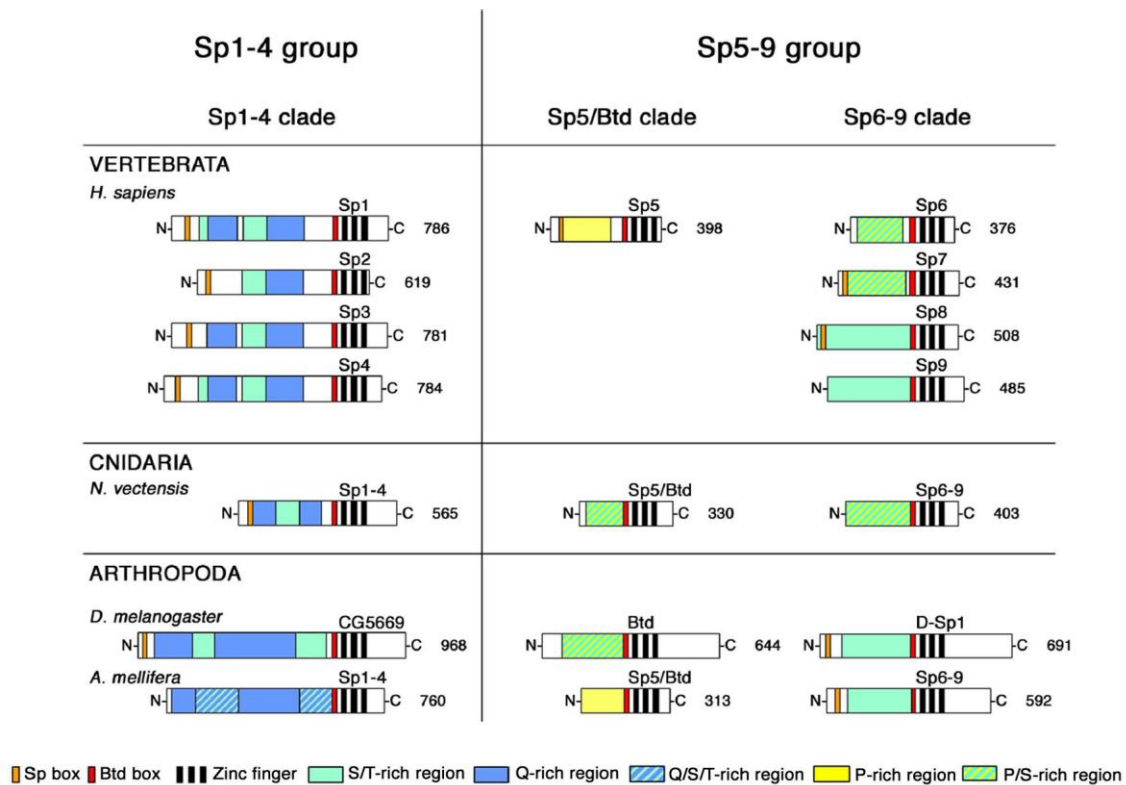


Figure 12. Protein domain structure of selected SP-family species.

SP family proteins of different species, *H.sapiens* (vertebrata), *N.vectensis* (cnidaria), and *D. melanogaster* and *A. mellifera* (Arthropoda). The proteins are arranged into columns according to the clades obtained in the phylogenetic sequence analysis (SP1-4 clade, SP5/Btd clade, SP6-9 clade). All proteins are oriented with their amino-terminus (N) to the left, and the carboxy-terminus (C) to the right. The length of each protein (if more than one isoform, the longest one is represented) is given next to the C-terminus (number of amino acids). Structural domains are highlighted and represented in the legend. Modified from Schaeper et al., 2010.

Beside the Zinc Finger domains, this family of proteins also present a highly conserved Buttonhead (BTD) box CXCPXC (where X could be any amino acid), prior to the zinc fingers. In addition, all the members of the family contain a SP box in their N-terminus, with the exception of SP6 (Runko and Sagerström, 2003; Xiao et al., 2002), and its role has been related to proteolytic cleavage or transcriptional activity (Murata et al., 1994). N-terminal regions are generally less conserved, but in general, are enriched for certain amino acid residues. The proteins of the SP1-4 clade are characterized by a bipartite glutamine (Q)-rich region, described as a transactivation domain which is divided by a serine/threonine (S/T)-rich region. The S/ T-rich regions are required for

proteasome-dependent degradation. The structure of the SP1-4 group is clearly different from the SP proteins of the SP5/BTD and SP6-9 clades. These latter two clades contain shorter proteins and are more similar to each other than each is to the SP1-4 group. Due to higher similarities, SP5/BTD and SP6-9 clades were grouped together: SP5-9/BTD group. The N-terminal end of these proteins contains only a single long region enriched for serine and/or proline. These more variable N-terminal regions encode a variety of transactivation/repression domains, some of which have been well characterized in mammalian model systems (McConnell and Yang, 2010; Suske et al., 2005).

The expression patterns in arthropod and vertebrate members within each clade are very similar. *Sp1-4* genes are highly ubiquitous meanwhile *Sp5/btd* and *Sp6-9* genes display more complex expression patterns predominantly present in the nervous system, limbs and segments. These proteins have been shown to be necessary for the correct development of the embryo, where removal of several members of the family have been reported to be lethal, including SP1 and SP3 (Marin et al., 1997) or died in the perinatal period as in the case of SP7 and SP8 mutants (Bell et al., 2003; Nakashima et al., 2002; Treichel et al., 2003). SP5-9 have previously been shown to have distinct expression patterns during embryogenesis but only SP6 and SP8 are expressed in the forming and mature murine AER.

1.7.2 SP8 structure

SP8 has two isoforms, the long SP8L (504aa) and the short, SP8S (486aa) one. *Sp8* has 3 exons, starting SP8L at the end of the first one, and continuing in the third one. The short isoform starts with the first methionine in the third exon.

Typically, SP-family members contain an amino-terminal hydrophobic domain called the SP-motif with the consensus sequence PLAMLLA. SP8L in vertebrata consensus sequence for SP-motif is TPLAMLAATCNKI, being the methionine residue the start of translation of SP8S mentioned above. Both isoforms differ in 18aa at the N-terminal domain, where the SP-motif is located.

SP8S is the isoform which has been proved to have an important function during development. SP8S, hereafter, SP8 contains the partial sequence of the SP-box at the N-

terminal domain. This N-terminal region is a low complexity region characterized by enriched domains: Ser-rich (11-104aa), Ala-rich (68-116aa) and Gly-rich (132-149aa). The highly conserved Button-head box (BTD) with the consensus sequence CxCP(N/Y)C is located previous the three conserved zinc-fingers (332-337aa). These zinc-fingers are located towards the COOH terminus (ZF1: 358-380; ZF2: 388-410; ZF3: 418-438aa) and are involved in binding DNA and proteins in a sequence specific manner (Milona et al., 2004; Treichel et al., 2003) (Fig. 13).

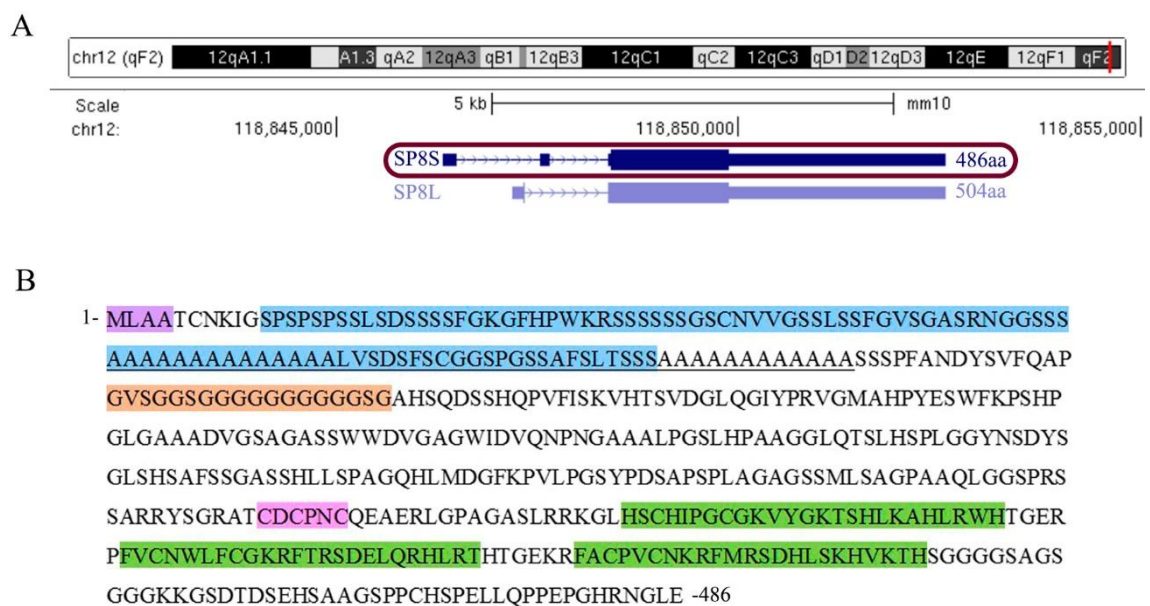


Figure 13. Mouse SP8 sequence features.

A) UCSC screenshot with the two *Sp8* isoforms (short and long isoform). Surrounded, the isoform that has been shown to be important in limb development. **B)** Amino acid sequence of mSP8 (486aa) with the features highlighted: incomplete SP-box (purple), Ser-rich region (blue), Ala-rich (underlined), Gly-rich (orange), BTD-box (pink) and the zinc fingers (green).

1.7.3 SP6 and SP8 in the limb

Sp6 is expressed in the limb ectoderm (Fig. 14), in the matrix of hair follicles and in proliferating dental epithelium during early tooth development (Hertveldt et al., 2008; Nakamura et al., 2004). SP8, besides limb ectoderm (Fig. 14), is present within

the central nervous system during organogenesis, in the telencephalon, midbrain–hindbrain boundary, spinal cord, otic vesicles, and nasal placodes (Treichel et al., 2003).

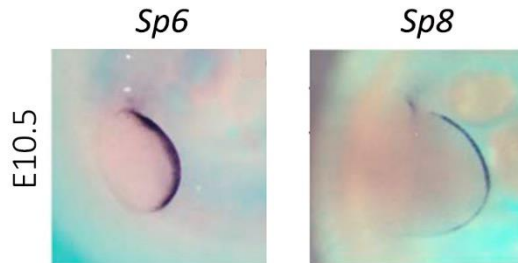


Figure 14. WMISH of *Sp6* and *Sp8* at E10.5 showing expression at the AER. Modified from Haro et al., 2014.

Sp6 KO shows normal external morphology and defects in the limbs, presenting mesoaxial syndactyly in FL and synostosis in HL, along with bidorsal digital tips (Talamillo et al., 2010). The phenotype of *Sp8* KO is more severe, presenting exencephaly (at forebrain and acerebellar hindbrain level), spina bifida, loss of nasal and palate structures, absence of tail and severely truncated FL and HL (Bell et al., 2003; Treichel et al., 2003).

Both, SP6 and SP8 are required for AER formation (Haro et al., 2014; Talamillo et al., 2010). Of these two factors SP8 makes a greater contribution than SP6, presumably due to a higher level of expression (Haro et al., 2014). To determine the redundancy of these two genes, double *Sp6;Sp8* null mutants were generated.

As the dose of *Sp6;Sp8* (hereafter *Sps*) is progressively reduced, the limb morphology goes from a mild syndactyly, to SHFM, to oligodactyly, to truncation and finally to amelia (Fig. 15). Most interestingly, these malformations are associated with a DV phenotype of bidorsal limb buds and digital tips.

As stated previously, the most striking and constant phenotypic feature in human and animal models of SHFM is the phenotypic variability. This spectrum of morphologies ranges from the mildest cases of soft tissue syndactyly to the most severe cases in which all digits are lost and, remarkably, the two ends of this phenotypic spectrum can occur in the same individual. This confirms that syndactyly, SHFM, oligodactyly and amelia can have a common genetic origin (Haro et al., 2014; O. Schatz

et al., 2014) and reflects how the genotype-phenotype relationships are based on complex networks and molecular interactions that may be subject to some variability.

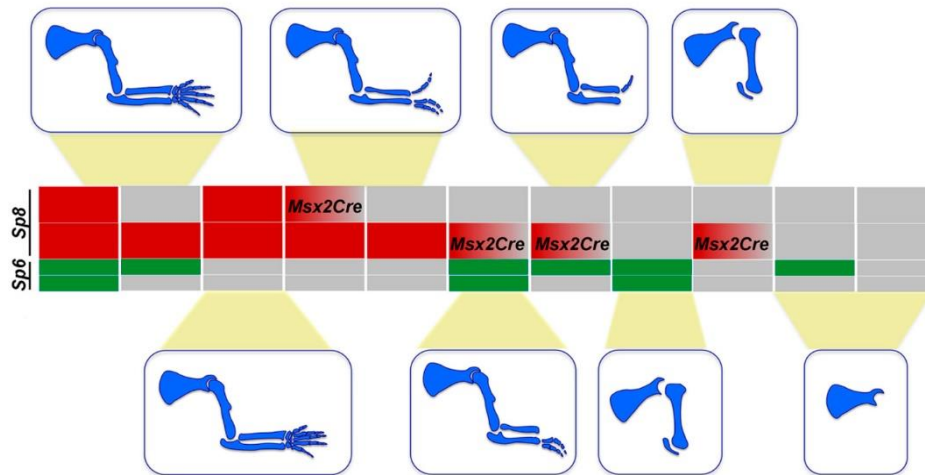


Figure 15. *Sp6/Sp8* gene dose correlation with the severity of the limb phenotype.

Sp6 alleles are depicted with green boxes and *Sp8* alleles with red ones. Null alleles are represented in grey. Note that boxes with a red to grey graduation represent conditional removal with the *Msx2Cre* allele. Modified from Haro et al., 2014.

To unravel the cause of this phenotypic variability, the AER formation was studied in the double mutant *Sp6;Sp8* allelic series (Haro et al., 2014). Animal models helped determine that the cause of the SHFM is a failure to maintain the AER preferentially in its central region (Crackower et al., 1998; Elliott et al., 2005; Graham et al., 1994; Seto et al., 1997). Using *Sp6;Sp8* model of SHFM, it was found that *Fgf8* activation occurs in a faint and irregular manner in correlation with the dose of *Sp6* suggesting a cell-autonomous effect of the mutation. The gene product obtained from one allele of *Sp8*, in the absence of *Sp6* alleles, seems to be on the threshold required for *Fgf8* induction but only reaching the threshold in some cells, probably due to normal biologic variation. For unknown reasons this initial defect always results to the loss of *Fgf8* in the central AER with a variable extension to the anterior border. The posterior AER segment is the one more resistant to *Sp6* dose reduction. The extent and time of onset of the AER defect correlates with the severity of the phenotype (Haro et al., 2014).

The previous observations suggest that SPs are direct transcriptional activators of *Fgf8*, downstream of WNT/ β -CATENIN signaling, and that they mediate *En1* activation, downstream of BMP signaling, through the interaction/cooperation with SMAD proteins (Haro et al., 2014). Thus, SP6 and SP8 are important nodes in the GRN operating in the limb ectoderm at a crossroad between PD and DV patterning (Haro et al., 2014).

The *Wnt-Sp8-Fgf8* genetic pathway seems to be a conserved cassette employed in the formation of appendages and possibly in other contexts (Lin et al., 2013). However, conflicting reports have been published on the SP8-FGF8 relationships in the telencephalon (Borello et al., 2014; Griesel, 2006; Sahara et al., 2007a) suggesting that SP8 transcriptional activity is complex and may work directly or indirectly to activate or repress target genes depending on the context. The role of SPs in *En1* induction and interaction with the Bmp signaling pathway has not been explored. Given that SP6 and SP8 are necessary for *Fgf8* and *En1* activation, to understand the complexity of the GRNs operating in the limb ectoderm it is necessary to identify the downstream targets of these two factors.

2. AIM OF THE PRESENT THESIS

2. AIM OF THE PRESENT THESIS

Objective 1:

SP6 and SP8 are important factors operating in the limb ectoderm at a crossroad between proximo-distal and dorso-ventral patterning. The aim of the present thesis is to understand the complexity of the SP8 dependent regulatory networks operating in the limb ectoderm. Therefore, combination of genome-wide ChIP-seq and RNA-seq analyses were performed for the identification of SP8 target genes.

Objective 2:

SP6 and SP8 are functionally equivalent and work in concert during limb development. The aim of the present thesis is to investigate their possible protein-protein interactions by Co-Immunoprecipitation and Bimolecular Fluorescent Complementation essays in HEK293 cells.

3. MATERIALS & METHODS

3. MATERIALS AND METHODS

3.1 Sp8:3xFLAG knock-in mouse (Sp8-FL)

The *Sp8:3xFLAG* knock-in mouse (*Sp8-FL*) was generated by Cyagen Biosciences Inc. The tagging strategy was based in a strategy already proven successfully in the limb, targeting *Gli3R* and *Hand2* (Vokes et al., 2008) (Osterwalder et al., 2014a). Three copies of the FLAG epitope (DYKDHDGDYKDHDIDYKDDDDK) were inserted in frame at the C-terminal domain of SP8 (Fig. 16).

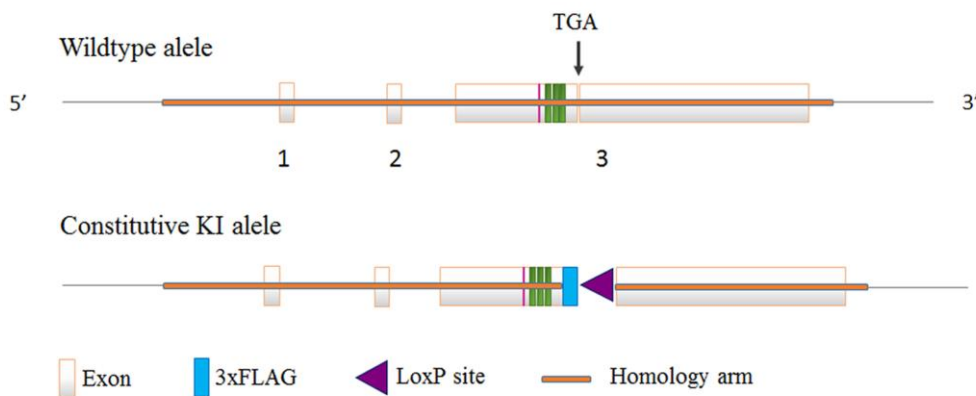


Figure 16. 3xFLAG-SP8 KI generation. Scheme of the generation of the *Sp8-FL* allele by homologous recombination (homology arms in orange). Three copies of the epitope FLAG (blue) were introduced at the C-terminal domain of *Sp8*, before the STOP codon TGA (middle of the third exon). Numbers 1, 2, 3 indicate *Sp8* exons (white).

Mouse genomic fragments containing homology arms (HAs) were amplified from a BAC clone by using high fidelity Taq and were sequentially assembled into a targeting vector together with recombination sites and selection markers. After confirming correctly targeted ES clones via Southern Blotting, some clones were selected for blastocyst microinjection, followed by chimera production. Founders were confirmed by PCR screening. In the end, 8 mice were confirmed as transgenics, 4 pups from clone 1D10 and 4 pups from clone 1C7 were identified positive by PCR screening for region 1.

3.2 Mouse strains

The *Sp8-FL*, *Sp8^{CreERT2}*, and *Sp6*, mouse lines were used in this study. All animal procedures were conducted accordingly to the EU regulations and 3R principles and reviewed and approved by the Bioethics Committee of the University of Cantabria. All mice were maintained in a C57BL6 genetic background and genotyped based on (Haro et al., 2014) (*Sp6*, *Sp8^{CreERT2}*) or recommended by Cyagen Biosciences Inc (*Sp8-FL*).

The generation of the *Sp8-FL* is described above. Briefly, it consists of the addition of three copies of the epitope FLAG at the C-terminus of the endogenous *Sp8*.

The *Sp8^{CreERT2}* line bears a tamoxifen inducible *Cre* in substitution of the *Sp8* gene (Treichel et al., 2003). This line expresses the CreERT2 recombinase in the *Sp8* locus and is the loss of function of *Sp8*. The *CreERT2* is a modification of the *Cre* that contains a G400V/M543A/L544A triple mutation in the Estrogen Receptor ligand-binding domain (ER-LBD) that makes it more sensitive to 4-hydroxy-tamoxifen (OHT) than the mutant ER-LBD with a single G521R substitution.

The *Sp6* line is characterized by the absence of the second exon of the *Sp6* gene that encodes the entire coding sequence (CDS) of *Sp6* (Nakamura et al., 2004).

3.3 Mouse Embryos

Embryonic day (E)0.5 was assigned to the noon of the day the vaginal plug was detected. Embryos were harvested at the desired developmental stage by cesarean section of pregnant mice, dissected in Phosphate buffered saline (PBS) and fixed overnight (ON) in 4% PFA.

3.4 Genotyping

Mutant mice and embryos were genotyped by collecting tail biopsies and yolk sac respectively. DNA extraction was done with an alkaline lysis (25 mM NaOH, 0.2

mM disodium EDTA) at 95°C for 1h, followed by its neutralization (40 mM Tris-HCl) (Truett et al., 2000).

Genotype was performed following standard PCR protocols, varying the annealing temperature according to the melting temperature (T_m) of the primers used. The PCR was performed with 1 μ l of the extracted DNA, primer final concentration at 700 nM, and Supreme NZYTaQ II 2x MasterMix (MB35903) in a total volume of 13 μ l. PCR products were run in a 1-1.5% agarose gel containing Sybr® Safe for DNA staining and visualized in the Gel-Doc under ultraviolet light and the use of the Quantity–One software (Bio-Rad). Finally, the molecular weight of the products was determined with the use of Gene Ruler DNA Ladder (Thermo Scientific). The set of primers used to genotype each mouse strain is specified below and it is indicated into 5' to 3' orientation.

Sp8-FL

Fwd	ACCTGAGCAAGCACGTGAAGAC	WT: 257 bp
Rev	GGAAAGAACGCACAGCTAGCC	MUT: 436 bp

Sp8^{CreERT2}

WT-Fwd	CAAGCACGTGAAGACACACAGT	WT: 323 bp
MUT-Fwd	GAAGTCTCTGGAAGAGAAGGACCAT	MUT: 702 bp
Common-Rev	TGTGTGCTACTTACTGTCCACATCC	

Sp6

WT-Fwd	GCTGGAAACCGTGAAGGAAAGG	WT : 331 bp
MUT-Fwd	GCTTCCTCGTGCTTTACGGTATC	MUT: 729 bp
Common-Rev	GGTTAGGGGTCATAAGGGATAGG	

3.5 Skeletal preparations

Newborn mice were collected and dissected in PBS. Newborns were un-skinned, eviscerated and fixed in 95% EtOH ON. For cartilage staining, 95% EtOH was replaced by Alcian Blue Staining solution (80% EtOH, 20% glacial acetic acid and 0.3 mg/ml Alcian Blue) for the next 24-72 hours. Excess of staining solution was removed through

successive changes in 95% EtOH until the traces of Alcian Blue disappeared. The tissue was cleared by potassium hydroxide (1% KOH) for 3-4 hours until the bones became visible. For bone staining, 1% KOH was replaced by Alizarin Red staining solution (0.05 mg/ml Alizarin Red in 1% KOH) for 20 hours in darkness approximately. When bones acquired the desired Alizarin Red staining, tissue was cleared for approximately 24 hours in 20% glycerin (in 1% KOH) and dehydrated in successive changes of 70% EtOH : glycerin : H₂O (1:2:7, 3:3:4, 4:4:2 and 5:5:0), every 24 hours.

3.6 Ectoderm-mesoderm separation

E10.5 forelimbs were dissected in cold PBS and digested in 0.25% trypsin (HyClone™ Trypsin Protease, SV30037.01) with soft agitation on ice for approximately 20 min. Then, to inhibit trypsin activity but avoid the serum response, the limb buds were quickly rinsed in 10% FBS and transferred to cold PBS where the separation of the ectoderm from the mesoderm was done with fine forceps (Fig. 17). Ectoderms were collected together when no genotyping was needed or individually if needed.

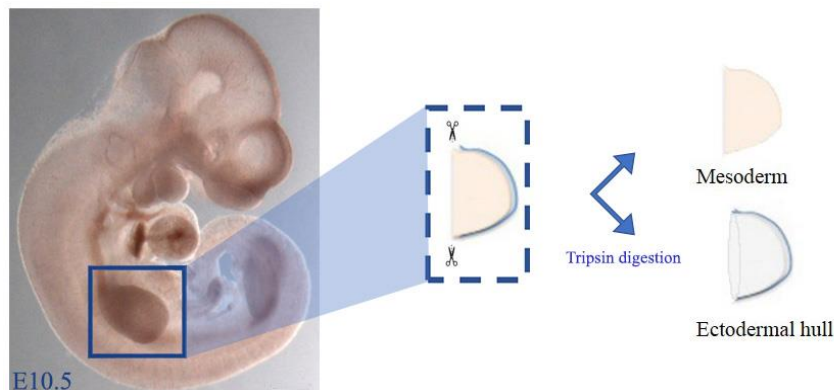


Figure 17. Schematic representation of the isolation of the limb bud ectoderm. Forelimbs were dissected from E10.5 embryos and incubated in trypsin for 20 min on ice. Then transfer to PBS were the ectoderm was completely separated from the mesoderm with fine forceps.

3.7 Cryostat sections

Embryos were fixed (4% PFA, 0.5% tritonx100) and then incubated in raising concentrations of sucrose in PBS until 30% sucrose. Finally, the limbs were embedded in OCT (Tissue-Tek), oriented as desired and stored at -80°C, until sectioned. Sections were cut at 7-15 µm thickness at -20°C in a cryostat Microm HM550 (Thermo Scientific), transferred to siliconized slides (SuperFrostPlus), and stored at -20°C until needed.

3.8 Paraffin embedding

After fixation in 4% PFA, embryos were washed in PBS and dehydrated in increasing concentrations of ethanol until absolute ethanol. Then embryos were cleared twice with xylene (time depending on stage and size of the sample) before being embedded in paraffin (SIGMA P-3558) at 60°C for at least 1h. A Leica RM2125RT microtome was used to perform 7-10 µm sections placed on siliconized slides (SuperFrostPlus).

3.9 RNA probes synthesis

When the probe of interest was within a vector, following standard procedures, plasmid DNA was transformed in *E.Coli* DH5α competent cells, plated in LB agar with antibiotic, and culture at 37°C ON. Next day, one colony was selected for inoculation in LB with antibiotic and incubated at 37°C ON in a shaker. High Pure Plasmid Isolation Kit (Roche) was used for plasmid purification. To synthesize an anti-sense transcript, specific restriction endonucleases were used to linearize the plasmids and digestion was performed following standard protocols.

Finally, the transcription of the probes was generated by in vitro transcription reaction in the presence of digoxigenin labeled nucleotides, following standard protocols and using diethylpyrocarbonate (DEPC) treated water to inhibit ribonucleases (RNases).

3.10 Whole mount in situ hybridization (WMISH)

Embryos were fixed in 4% PFA in PBS at 4°C ON. The next day, they were washed in PBS, PBS-Tween (PBT- 0.1% Tween in PBS) and dehydrated in increasing concentrations of MetOH (25-50-75-100%) in PBT before their storage at -20°C until needed. For WISH, embryos were rehydrated in decreasing concentrations of MetOH, washed in PBT and then bleached with 6% H₂O₂ for 1h. Embryos were rinsed in PBT and digested with proteinase K (PK, 10 µg/ml) in PK buffer (50 mM Tris-HCl pH 7.4, 5 mM EDTA), adjusting the digestion time to the stage of the embryo for mesodermal expressed genes. To examine ectodermal expressions, 5 min of PK (5 µg/ml) was used. Embryos were washed in PBT and post-fixed in 0.2% glutaraldehyde + 4% PFA before immersion in hybridization buffer (50% formamide, 5x SSC, 2% blocking powder, 0.1% Triton X-100, 0.1% CHAPS, 1 mg/ml tRNA, 50 µg/ml Heparin pH 4.5, 500 mM EDTA pH 8) at 65°C ON.

The following day, the samples were frozen at -20°C for at least 6 hours. After that, the hybridization buffer was replaced with new buffer containing the desired probe and incubated at 65°C ON. The next day, several post-hybridization washes were done to get rid of unspecific binding: three washes of 2x SSC + 0.1% CHAPS (1M NaCl, 100 mM Sodium Citrate, 0.1% Chaps) of 30 min each at 65°C, followed by three washes of 0.2x SSC + 0.1% CHAPS (10 mM NaCl, 1 mM Sodium Citrate, 0.1% Chaps) for 70 min total at 65°C. Then, two washes of KTBT buffer (50 mM Tris-HCl pH 7.4, 150 mM NaCl, 10 mM KCl, 1% Triton X-100) were done for 10 min at RT. Samples were blocked in 20% sheep serum (in KTBT) for 2 h at RT prior incubation with anti-Digoxigenin-Alkaline Phosphatase antibody (anti-dig-AP) diluted (1:2,000) in blocking solution at 4°C ON. After this, several washes were performed with KTBT at RT.

Finally, detection of alkaline phosphatase activity was performed by incubating the embryos in darkness in NTMT buffer (100 mM Tris-HCl pH 9.5, 50 mM MgCl₂, 100 mM NaCl, 1% Triton X-100), with NBT (3 µg/ml) and BCIP (2.3 µg/ml). Once signal level was clear and robust, reaction was stop with several washes in KTBT and fixed in 4% PFA for analysis.

3.11 In situ hybridization in paraffin sections

A similar method to the above described for WMISH was followed in sections. Briefly, after dewaxing and rehydration, the samples were permeabilized by incubation in PK (10 µg/ml) for 7 min 30 sec. Then, samples were fixed in 4% PFA and washed with PBS, followed by an acetylating step (0.1 M triethanol-amine, 0.066 mM Acetic Anhydride) of 10 min to reduce background. The sections were incubated in hybridization buffer containing the desired antisense ribonucleic acid (RNA) probe, at 65°C ON in a humid chamber.

Next day, post-hybridization washes (at 65 °C) were performed to remove unspecific binding. Slides were washed 30 min in 1x SSC/ 50% Formamide, 20 min in 2x SSC and two additional 20 min washes in 0.2x SSC. Finally, three washes (5 min, RT) in MABT pH 7.5 (150 mM NaCl, 100 mM Maleic Acid, 0.04% Tween) were performed before incubation with blocking solution (20% sheep serum in MABT) for 1 hour, at RT. After that, sections were incubated ON with the antibody α -DIG-AP (1:2500) at 4°C in a humid chamber.

The following day, and after 3 washes in MABT (5 min, RT), the signal was revealed with NTM/NBT (3 µl/ml)/BCIP(2.3 µl/ml). When the desired signal level was obtained, the slides were rinsed in PBS for 5 min and fixed in 4% PFA ON. Dehydration and mounting followed routinary procedures.

The probes used in this study were: Dlx5/6, En1, Fgf8, Fzf1, Msx1, Rspo2, Sp6, Wnt10b, Wnt5a and Wnt7a.

3.12 Immunofluorescence

Immunoassays were performed in cryostat sections. Sections were permeabilized in PBT at 4°C and blocked in 10% goat serum with 2% Bovine serum albumin (BSA) in PBS during 1h. The incubation in the primary antibodies was ON at 4°C and fluorescent-coupled secondary antibodies were usually incubated for 1 hour at RT.

The primary antibodies used were: 1) mouse monoclonal anti FLAG M2 (1:500; Sigma F1804), 2) goat polyclonal anti Sp8-C18 (1:400; Sc-104661), 3) mouse monoclonal anti b-catenin (1:100; BD610154) and 4) rabbit polyclonal anti laminin (1:200; Ab11575).

Secondary antibodies were: 1) Alexa 488-conjugated anti-goat IgG secondary antibody (1:500, Invitrogen), 2) Alexa 488-conjugated anti-mouse IgG secondary antibody (1:500, Invitrogen) and 3) Atto 594-conjugated anti-rabbit IgG secondary antibody (1:500, Rockland).

Sections were mounted with DAPI-Vectashield and analyzed with Leica Laser Scanning Confocal TCS-SP5 with a 63x 1.4 NA objective. Cells were excited sequentially with 405nm, 488nm and 532nm laser lines and emission captured between 498-525nm (Alexa488) and 604-650nm (Atto594). Images were processed with ImageJ software (Rasband, W.S., ImageJ, U. S. National Institutes of Health, Bethesda, Maryland, USA, <http://imagej.nih.gov/ij/>, 1997-2016).

3.12 Immunoblot

For immunoblot (western blot), cells and tissue were washed and dissected respectively with cold PBS. Whole protein extraction was performed with ice-cold RIPA buffer [50 mM Tris-HCl pH 7.5, 150 mM NaCl, 1% NP-40, 1% DOX, 0.1% SDS, 1 mM EDTA, Protease Inhibitor Cocktail (PICS), 1 mM Phenylmethanesulfonyl fluoride (PMSF)] and quantified with Bradford (BioRad protein assay) procedures. Then, protein extracts were mixed with *Laemmli* (2x SDS gel-loading buffer: 100 mM Tris-HCl pH 6.8, 8% β -mercaptoethanol, 4% SDS, 20% glycerol, and 0.1% bromophenol blue) for cells and tissue, respectively, and denaturalized at 95°C for 5 min. Electrophoresis was carried out on 8-12% (v/v) SDS-Polyacrylamide Gel Electrophoresis (SDS-PAGE). Precision Plus Protein Standards (Bio-Rad) and/or NZYColour Protein Marker II (NZY) were used as markers for determination of the molecular weight (MW). Proteins were transferred on to nitrocellulose filters (Amersham Biosciences) and then blocked in TBS-T (20 mM Tris pH 7.5, 500 mM

NaCl, 0.1% Tween-20) and 4% BSA for 1 hour. Incubation with primary antibodies (1:1,000) diluted in 4% BSA in TBS-T was carried out at 4°C ON.

Proteins were visualized with HRP (horseradish peroxidase)-conjugated anti-goat (NB7379), anti-rabbit (Sc 2004) or anti-mouse (#170-5047) secondary antibodies diluted (1:10,000, 1 h, RT), followed by ECL detection.

- Blue Coomassie and Ponceau Red staining

To visualize the amount of protein run in each lane (complementary to Bradford test), acrylamide gels were stained after the transfer with Coomassie Blue (0.1% Coomassie Blue in 50% methanol, 10% acetic acid). Transfer efficiency was also checked with Ponceau Red (0.1% Ponceau Red in 1% acetic acid) staining.

3.13 Cloning

PCR to amplify the genes of interest was carried out using Phusion High-Fidelity DNA Polymerase (Thermo Scientific). The PCR product was purified with MinElute PCR purifying Kit, (Qiagen) or loaded in an agarose gel for its purification with GenJet Gel Extraction Kit, (ThermoFisher) when needed. The PCR product was ligated into pcDNA3 (ratio 3:1 DNA:vector) at 20°C ON. Ligation was dialyzed to get rid of extra salts and then transformed into *Dh5 α* (*E. coli*) competent cells following standard procedures. Cells were plated in Luria-Bertani (LB) agar with appropriate antibiotics (100 μ g/ml of ampicillin and/or 25 μ g/ml of kanamycin) at 37°C ON. In general, screening of 8 individual colonies was done. Each of them was picked from the plate and then inoculated in LB broth with antibiotic. Incubation was carried out in a shaker at 37°C 6 h - ON. Minipreps were done with High PCR template preparation Kit (Roche) and then double digestion with specific restriction enzymes (RE) were used for corroboration of the PCR product incorporation within the plasmid. One positive clone was chosen for sequencing (STAB VIDA) and future analysis.

3.14 Cell culture

HEK-293 cells were cultured in DMEM (#41965-039) medium supplemented with 10% FBS (#26140-087) and Penicillin/Streptomycin (#15140-122).

Transfection

HEK-293 cells were plated the day before and transfected at around 70% confluence. Plasmid DNA was diluted in serum-free DMEM (volume of media was 10% of final volume in culture vessel). Next, PEI (#23966) was added (3:1 ratio of PEI: DNA) and mixed properly. Then, it was incubated 10-15 min at RT. Medium of cells was changed to fresh DMEM/10% FBS medium and DNA/PEI mixture was added to cells. Transfected cells were harvested at 48 hours post-transfection.

**If needed, 6 to 12 hours before cell-harvest, DMEM/10% FBS medium of cells was changed to serum-free DMEM.

3.15 BiFC and CoIP clones

To check the interaction by CoIP and BiFC, different combinations of epitopes and fusion proteins were cloned along with the genes of interest (Fig. 18).

SP6 (376aa), SP8 (486aa), $\Delta(1-126)$ SP8, $\Delta(1-241)$ SP8, $\Delta(1-331)$ SP8, $\Delta(353-487)$ SP8 and $\Delta(440-487)$ SP8 proteins tagged N-terminally with FLAG or MYC epitopes were generated by PCR with the appropriate RE to be fused to YFP (1-240aa), YN [$\Delta(73-240)$ YFP] and YC [$\Delta(173-240)$ YFP] to the C-terminus.

Myc-Dlx5 and FLAG-Dlx5 clones were kindly provided by (Hojo et al., 2016).

The primers used were:

Name		Primer sequence (5'-3')
SP6-FLAG	Fwd	cccaagcttATGGACTACAAGGACGACGATGATAAGCTAA CCGCTGTCTGTGGCTCT
	Rev	cggggtaccTCAGTTGGAGGACGCCGAGCT
SP6-MYC	Fwd	cccaagcttATGGAGCAGAACTCATCTCTGAAGAGGATC TGCTAACCGCTGTCTGTGGCTCT
	Rev	cggggtaccGTTGGAGGACGCCGAGCTGCC
SP8-FL	Fwd	cccaagcttATGCTTGCTGCTACCTGTAATAAGATC
	Rev	cggggtaccCTCCAGGCCGTTGCGGTGGCC
Δ(1-126)SP8	Fwd	cccaagcttATGGAGCAGAACTCATCTCTGAAGAGGATC TGGTGTTCAGGCTCCGGGCGTC
	Rev	cggggtaccCTCCAGGCCGTTGCGGTGGCC
Δ(1-241)SP8	Fwd	cccaagcttATGGAGCAGAACTCATCTCTGAAGAGGATC TGACGTCGCTGCATTCACCGCTG
	Rev	cggggtaccCTCCAGGCCGTTGCGGTGGCC
Δ(1-331)SP8	Fwd	cccaagcttATGGAGCAGAACTCATCTCTGAAGAGGATC TGTGCGACTGCCCAACTGCCAG
	Rev	cggggtaccCTCCAGGCCGTTGCGGTGGCC
Δ(353-487)SP8	Fwd	cccaagcttATGGAGCAGAACTCATCTCTGAAGAGGATC TGCTTGCTGCTACCTGTAATAAG
	Rev	cggggtaccTTTGCGACGCAGGCTC
Δ(440-487)SP8	Fwd	cccaagcttATGGAGCAGAACTCATCTCTGAAGAGGATC TGCTTGCTGCTACCTGTAATAAG
	Rev	cggggtaccACCACTGTGTGTCTTCACGTG

RE (lower case); FLAG (blue); MYC (purple); gene sequence (black)

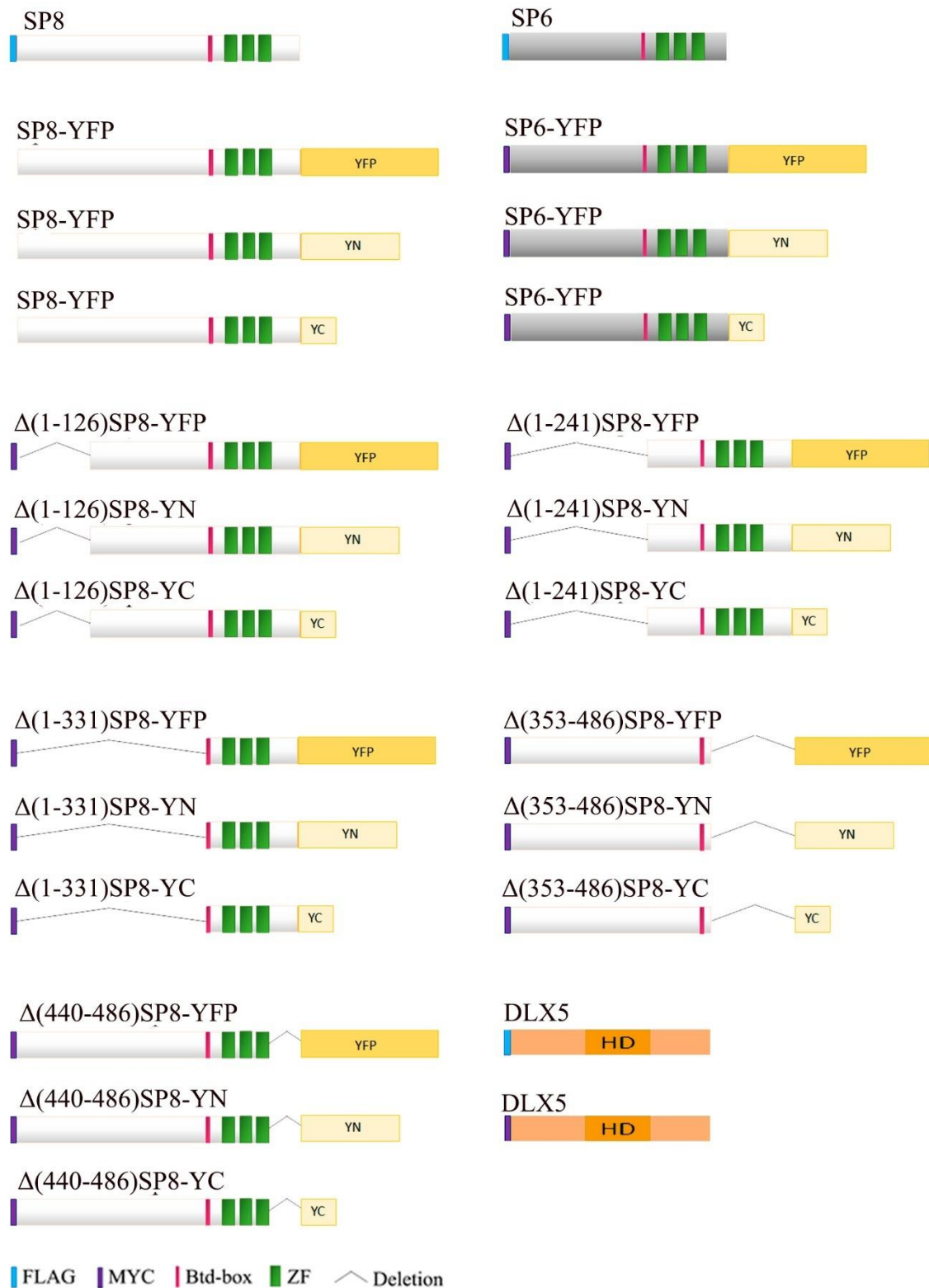


Figure 18. Constructs generated for BiFC and CoIP assays. Each construct is represented with its name on top. *Sp8* (white), *Sp6* (grey,) Btd box (pink), ZFs (green), deleted regions (\frown), *Dlx5* (orange), Homeodomain (dark orange), FLAG epitope (blue), MYC epitope (purple), *YFP* (yellow), *YN* and *YC* (soft yellow).

3.16 Protein over-expression for anti SP8 antibody production

To overexpress and purify SP8 we used the pET-28a-c(+) vector (Novagen #69864-3). We amplified the mouse *Sp8* by PCR and cloned it with NdeI and BamHI REs, downstream the N-terminal His-tag of the pET-28a (His-SP8), with the following primers (5' to 3' orientation):

SP8-(Ab) Fwd gggaattccatagATGCTTGCTGCTACCTGTAATAAG
 Rev cgcgatccTCACTCCAGGCCGTTGCGGTG

REs (lower case); gene sequence (upper case)

His-SP8 contained in the Bacteria were grown in LB liquid medium (10 g/l tryptone, 5 g/l yeast extract, 10 g/l NaCl) at 37°C to an optical density of 0.4-0.6 at 600 nm. Then, 1 ml was taken as a control and isopropyl-2-D-thio-galactopyranoside (IPTG) was added to a final concentration of 0.4 mM. The cells were grown for 2 h at 37°C with kanamycin (25 µg/ml).

The Lac operon is repressed by the LacI, which is always expressed unless the substrate is available and binds to it, inactivating it. *E. coli* C41 strain was used for the overexpression of the His-SP8, starting the transcription at optical density of 0.4-0.6 with isopropyl-2-D-thio-galactopyranoside (IPTG) 0.4 mM. IPTG is a molecular mimic of a lactose metabolite that triggers transcription of the lac operon.

Bacterial pellet was frozen at -80°C to help disruption of cells. When needed, the pellet was thaw and was resuspend properly with Lysis buffer (50 Mm Tris-HCl pH 7.5, 150 mM NaCl, 10 µg/ml Leupetine, 6.5 ng/ml Aprotinine, 100 µg/ml PMSF). Cell disruption was carried on in French press and fluid was collected on ice. Centrifugation at 40,000 rpm, 4°C, 30 min was performed to collect proteins in supernatant (sample is taken as positive control). For the purification of His-SP8 tagged, two different columns were tried individually or in combination. Sample of flow through is collected as negative control. On one hand, proteins were loaded onto Ni column (5 ml) and eluted in a linear gradient of imidazole. On the other hand, proteins were applied to a HiTrap

SP-Sepharose (5 ml) column (Amer-sham, GE) and eluted in a linear gradient of NaCl. Fractions were pooled and run into 12% SDS-PAGE for the verification.

3.17 Bimolecular Fluorescent Complementation (BiFC)

YFP is a fluorescent protein but when YFP is divided in two moieties [amino (YN; residues 1-172) and carboxy (YC; residues 173-240)], they cannot emit fluorescence. These moieties can re-associate and yield functional YFP if brought into close proximity by the interaction between the proteins they are fused to (Fig. 19) (Hu et al., 2002). The estimation is that fluorescence complementation could occur when YN and YC are fused at positions that are separated by an average distance of greater than 100 Å, as long as there is sufficient flexibility to allow association of the fragments (Hu et al., 2002).

YFP-full length was used as a positive control of the transfection as well as for the localization of each protein. Moieties YN and YC fused to the proteins are not fluorescent and were used as negative control when transfected individually.

Microscope cover Glasses (Ø 18 mm) were washed in 100% EtOH, placed into T6-well plates and treated with PolyLisine (P6407, Sigma). HEK-293 cells were plated and next day cells were transfected with each individual fused protein (for positive and negative controls, e.g. SP6-YFP; SP6-YN; and SP6-YC) and co-transfected with the proteins of interest, each one with a complementary YFP moiety (e.g. SP6-YN + SP6-YC) to prove the homo or heterodimerization.

After 48h of transfection, cells were treated with Hoechst33342 (Invitrogen) (1:1000) for 10 min before the analysis to stain nuclei. Each experiment was performed in triplicate. Cells were washed with Leibovitz's medium (# 21083027, ThermoFisher) and the interaction analyzed with Leica Laser Scanning Confocal TCS-SP5 with a 63x 1.4 NA objective. Cells were excited sequentially with 405 nm and 514 nm laser lines and emission captured between 420-480 nm (Hoechst) and 525-600 nm (YFP). Images were processed with ImageJ software (Rasband, W.S., ImageJ, U. S. National Institutes of Health, Bethesda, Maryland, USA, <http://imagej.nih.gov/ij/>, 1997-2016).

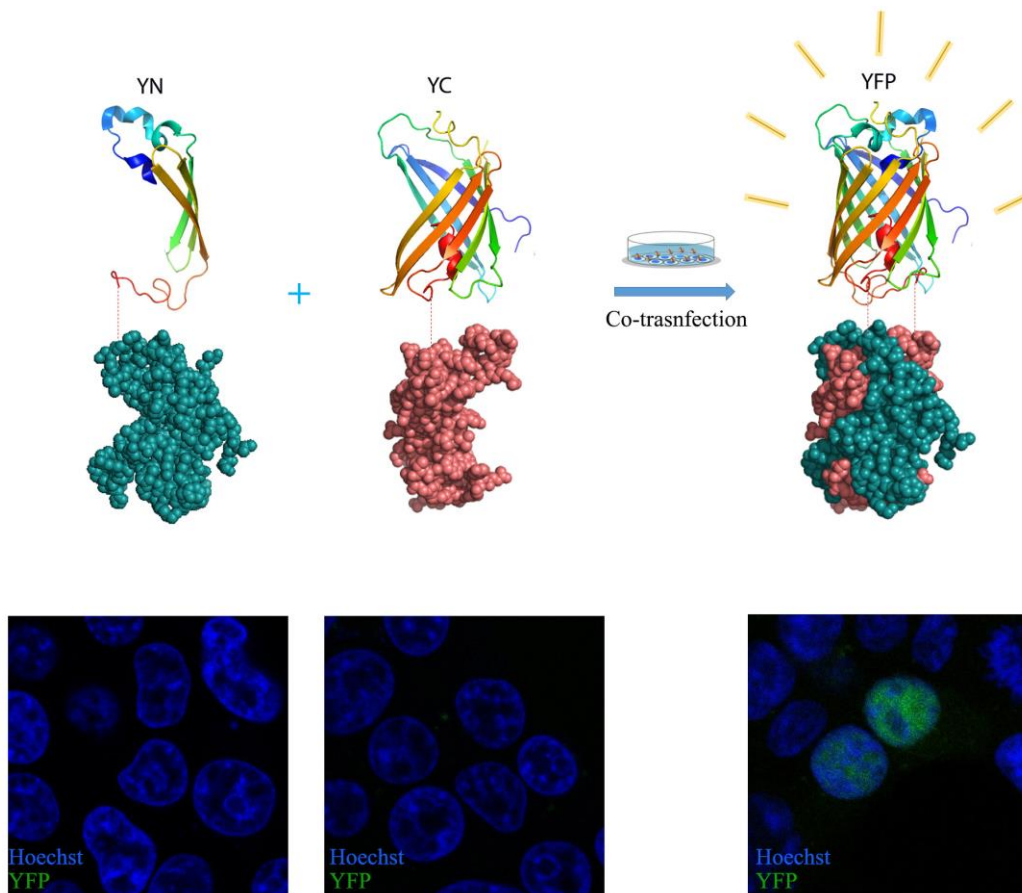


Figure 19. Schematic representation of BiFC technique. On the top left, YFP moieties (YN and YC) were fused (represented with a dashed line) to the proteins of interest: protein 1 (green) and protein 2 (pink). These fusion proteins were co-transfected into HEK-293 cells. If protein 1 and 2 interact, the YN and YC reconstitute a functional YFP (top right panel). Bottom row: No fluorescence is observed when Protein1-YN or Protein2-YC are individually transfected. Fluorescence is only observed upon transfection of both proteins if they interact. [Hoechst (blue) stains the nuclei and in green is shown the fluorescence of the resulting interaction].

3.18 Co-ImmunoPrecipitation (CoIP)

HEK-293 cells were co-transfected with the desired plasmids using PEI. Total amount of DNA transfected was 10 μ g in P100 plates. Cells were lysed in a soft buffer lysis (20 mM Hepes (pH 7.5), 10 mM EGTA pH 8, 40 mM Glycerol-phosphate, 1% NP-40, 2.5 mM $MgCl_2$, 2 mM orthovanadate, 1 mM DTT, 1x PICS, 1 mM PMSF) in order not to disrupt protein interactions. From the total lysate, 5% was stored at $-20^\circ C$ to be used as positive control. To the remaining protein extract, 1 μ g of the desired antibody (i.e. FLAG-M2) was added for 1 h at $4^\circ C$. In parallel, un-transfected cells

were used as negative control C(-), following the same procedure (or if specified, same protein extract was used when no antibody was used to precipitate). Following steps were carried in both samples. 10 μ l of Dynabeads™ Protein G (Thermo Fisher Scientific, 10004D) were washed twice in cold PBS and then added to the lysate and incubated ON at 4°C with rotation. Beads were magnetized (therefore the complex bead-Ab-protein), and eluate was discarded. Beads were washed twice in ice-cold buffer (1% NP-40) by completely solving the beads every time and were resuspended in laemmli along with 5% inputs thaw. Samples were vortex properly, and then incubated 5 min at 95°C. Beads were magnetized and just eluate was loaded in the SDS-PAGE for western blot analysis.

3.19 ChIPmentation of SP8

ChIPmentation protocol was based on (Schmidl et al., 2015) with some modifications from A. Rada-Iglesias's lab. Due to the lower amount of input material needed with this protocol, 50 ectoderms *Sp8^{FLAG/FLAG}* were used for each TF ChIPmentation replicate.

Crosslinking

Ectoderms were collected and crosslinked with 1% formaldehyde for 10min. The reaction was quenched by adding glycine to a final concentration of 0.125 M for 5 min. Ectoderms were pelleted (900 g, 5 min, 4°C), discarding the supernatant and then rinsed once in cold PBS (1x PICS + 1mM PMSF). Again, supernatant was discarded, and cell pellet was frozen in dry ice and stored at -80°C until use.

Sonication

The desired number of ectoderms were joined in a single tube and sonicated together in the sonication buffer (10 mM Tris-HCl pH 8, 0.25% SDS, 2 mM EDTA, inhibitors). The sonication was carried out (pulse for 20 seconds ON and 30 seconds OFF, 25 cycles) in the bioruptor-UCD300 to obtain most fragments in the range of 500

bp. Sonication efficiency was evaluated by 1.5% agarose gel electrophoresis. Then, lysate was diluted 1:0.5 with Equilibration Buffer (30 mM Tris-HCl pH 8, 700 mM NaCl, 5% Triton X-100, 0.5% DOX, 3 mM EDTA, inhibitors). Samples were centrifuged at 13,200 rpm, 4°C for 10 min to pellet insoluble material and the remaining soluble chromatin was transferred to a new tube (0.2 ml tube). 1% of the material was collected (in a 0.2 ml tube) for input and stored at -20°C.

Next, 1 µg of anti-FLAG M2 (Sigma F1804) was added to the soluble chromatin and it was incubated on a rotator overnight at 4°C. Simultaneously, 10 µl of Dynabeads™ Protein G (Thermo Fisher Scientific, 10004D) were washed twice with 0.1% BSA and then incubated in 0.1% BSA on a rotator overnight at 4°C to block beads.

ChIPmentation

Beads were transferred to tubes with chromatin and incubated for 4 h at 4°C rotating. Then, beads were washed twice in ice-cold RIPA-LS (10 mM Tris-HCl, pH 8; 140 mM NaCl; 1 mM EDTA; 0,1% SDS; 0,1% Na-Deoxycholate; 1% Triton X-100, inhibitors), RIPA-HS (10 mM Tris-HCl pH 8; 500 mM NaCl; 2 mM EDTA; 0,1% SDS; 0,1% Na-Deoxycholate; 0,1% Triton X-100, inhibitors) and RIPA-LiCl (10 mM Tris-HCl pH 8; 1 mM EDTA; 250 mM LiCl; 0,5% NP-40; 0,1% Na-Deoxycholate, inhibitors). Finally, beads were resuspended in 10 mM Tris-HCl pH 8.

Beads and thaw input were resuspended in 25µl of the tagmentation reaction (12 µl 2xTagmentation Buffer, 1 µl Tagmentation DNA Enzyme and 12 µl Nuclease free water) and incubated at 37°C for 10 min. To inactivate Tn5 transposase, RIPA-LS was added just to the ChIPmentation reaction, incubating 5 min on ice. Beads were then washed twice in RIPA-LS and TE (10 mM Tris-HCl pH 8, 1 mM EDTA). Finally, Elution Buffer (10 mM Tris-HCl pH 8, 300 mM NaCl, 0.4% SDS, 5 mM EDTA) with 0.2 mg/ml of PK (#EO0491) was added to the beads and the input.

Elution

Beads and input were incubated for 1 h at 55°C and for 6 – 10 h at 65°C for de-crosslinkage. Beads were magnetized, and supernatant is transferred to a new tube. A second elution was performed (Elution Buffer + PK for 1 h at 55°C) to assure all chromatin was collected. First and second elute were combined. Purification of the input and combined sample was performed with the Qiagen MinElute Kit by eluting in 2 x 10 µl EB.

Finally, the library was normally prepared by amplification with the Nextera sequencing primers for 12 - 14 cycles.

3.20 ChIP-seq for Chromatin marks

A similar method to the above described for ChIPmentation was done. Chromatin Immunoprecipitation (ChIP) protocol was based on (Rehimi et al., 2017). Total of 65 ectoderms of E10.5 were joined together for histone marks.

Basically, crosslinking was done with 1% formaldehyde (15 min, RT). Pellet was resuspend in Lysis Buffer (10 mM Tris- HCl pH 8.0, 100 mM NaCl, 1 mM EDTA, 0.5 mM EGTA, 0.1% Na-Deoxycholate, 0.5% N-lauroylsarcosine, inhibitors) and sonicated with BioRuptor Sonicator (25% amplitude, pulse for 20 seconds ON and 30 seconds OFF, 31 cycles). Lysate was transferred and Triton X-100 was added to final concentration of 1% (10% lysate taken for input and kept at -20°C). 1 µg of antibody [H3K27ac (ab4729) and H3K4me2 (39141)] was added to sonicated chromatin and incubated at 4°C ON. Next day dynabeads were incubated with antibody bound chromatin for 4 hours. Then, bound beads were washed four times with cold RIPA Wash Buffer (50 mM Hepes, 500 mM LiCl, 1 mM EDTA, 1% NP-40, 0.7% Na-Deoxycholate, inhibitors) and once with TE + 50 mM NaCl. Elution Buffer (50 mM Tris- HCl pH 8.0, 10 mM EDTA, 1% SDS, inhibitors) was added to the beads and incubated 15 min at 65°C at 600 rpm. Beads were spin down for 1 min at 1,600g, RT. Elution buffer was added (3V) to input, and both ChIP and input were incubated at 65°C ON to reverse crosslinks. TE buffer and RNase A (0.2 mg/ml) were added and incubated at 37°C for 2 hours to digest RNA. Then, PK (0.2 mg/ml) was added at 55°C

for 2 hours to digest protein. DNA fragments were conventionally purified with Phenol-Chloroform.

3.21 RNA-seq

Ectoderms from E10.5 wild-type and homozygous *Sp8-KO* (*Sp8-Cre-ERT2* line) embryos were individually collected. Experiment was done in triplicates and each replicate contained 2x ectoderms (forelimbs) of a single embryo. RNA was extracted with RNeasy-Plus Micro Kit (Qiagen).

Due to low amount of input material, pre-amplification using the Ovation RNaseq System V2 was performed. Total RNA was used for first strand cDNA synthesis, using both poly(T) and random primers, followed by second strand synthesis and isothermal strand-displacement amplification. For library preparation, the Illumina Nextera XT DNA sample preparation protocol was used, with 1 ng cDNA input. After validation (Agilent 2200 TapeStation) and quantification (Invitrogen Qubit System) all six transcriptome libraries were pooled. The pool was quantified using the Peqlab KAPA Library Quantification Kit and the Applied Biosystems 7900HT Sequence Detection and pooled on one lane of an Illumina HiSeq4000sequencing instrument with a 2x75 bp paired-end read length.

3.22 Transgenic mice for Lacz activity

To examine the activity of some putative enhancers such as *En1*(-19,543) or the *Rspo2* (+217,676), we used a vector carrying the β -globin minimal promoter and the LacZ coding sequence (pSK- LacZ). This vector was kindly provided by Denis Duboule lab.

The genomic region containing the regulatory elements of *En1* (mm10, chromosome 1:120,621,403-120,622,419) and *Rspo2* (mm10, chromosome 15:43,388,035-43,389,518) were PCR-amplified using specific primers containing XhoI RE and cloned into the pSK-LacZ vector.

Name		Primer sequence (5'-3')
<i>En1</i> (-19,543)	Fwd	ccgctcgagTAGGAAAGTATGGCCGGCAG
	Rev	ccgctcgagCCATACCCCTGAGCAGAACA
<i>Rspo2</i> (+217,676)	Fwd	ccgctcgagTGGGTTCTCACACTTGCACA
	Rev	ccgctcgagTTGTGTCCCCTGATCTTGGC

REs (lower case); gene sequence (upper case)

In both cases, the insert carrying the enhancer, β -globin minimal promoter, and LacZ coding sequence will be excised from the vector backbone by digestion with ApaI–XbaI. The fragment will be gel-purified and injected into fertilized oocytes.

3.23 Bioinformatic and statistical analysis

RNA-seq

To analyze the data, high-throughput next-generation sequencing analysis pipeline (Wagle et al., 2015) was used. Basic read quality check was performed using FastQC (Babraham Bioinformatics) and read statistics were obtained with SAMtools. Reads were mapped to the mouse reference assembly (GRCm38), using TopHat2 (Kim et al., 2013). Read count means, fold-change (FC) and values were calculated with DEseq2 (Anders and Huber, 2010) and gene expression for the individual samples was calculated with Cufflinks (Trapnell et al., 2010) as Fragments Per Kilobase of transcript per Million mapped reads (FPKMs), using in both cases genomic annotation from the Ensembl database. Differentially expressed genes (DEG) were obtained considering only genes with an Ensembl ID and an official Gene Symbol applying the following criteria:

For *Sp8* wild-type Vs *Sp8* KO:

- Up-regulated in *Sp8* KO: p-value<0.01, FC>1.5, FPKM in *Sp8* KO sample>0.1.
- Down-regulated in *Sp8* KO: p-value<0.01, FC<1.5, FPKM in wild-type sample>0.1

ChIP-seq and ChIPmentation

ChIPmentation (and ChIP-seq) sequencing reads were mapped to the mouse genome (mm10 assembly) using Burrows-Wheeler Aligner (BWA) (Li and Durbin, 2009). Duplicate reads were filtered, and only unique reads were considered. The resulting Binary Alignment/Map (BAM) files were then analyzed with MACS2 (Zhang et al., 2008) using the following settings to identify genomic regions significantly enriched in the investigated proteins in comparison to the total genomic input DNA: q value 0.1; Fold change >3.

3.24 Additional Bioinformatic analysis

PhastCons

Average vertebrate PhastCons score profiles around the center of enhancer sequences were generated with the Conservation Plot tool from the Cistrome Analysis pipeline (<http://cistrome.dfci.harvard.edu/ap/root>) (Liu et al., 2011).

Correlation coefficients

Pearson Correlation coefficients of the two SP8 ChIPmentation biological replicates were performed with the bamCorrelate tool from deepTools (bins mode and a bin size of 10 kb across the whole mouse genome) (Ramírez et al., 2014).

Heatmaps

To generate heatmaps, BAM files were normalized as RPGC (reads per genome coverage) and then used to visualize scores associated with genomic regions using deepTools (Ramírez et al., 2014). We obtained the following information:

- Enrichment profile of Histone marks (H3K27ac and H3K4me2) around SP8 peaks.
- Enrichment profile of ChIPm-replicate 1 around ChIPm-replicate 2 peaks, vice versa.

GREAT

Genomic regions enrichment of annotations tool (GREAT 3.0.0; <http://great.stanford.edu/public/html/>) (McLean et al., 2010) was used for association of SP8-CRM. GREAT currently supports three different parametrized association rules to define gene regulatory domains (Fig. 20).

Associating genomic regions with genes

GREAT calculates statistics by associating genomic regions with nearby genes and applying the gene annotations to the regions. Association is a two step process. First, every gene is assigned a regulatory domain. Then, each genomic region is associated with all genes whose regulatory domain it overlaps.

Basal plus extension

Proximal: kb upstream, kb downstream, plus Distal: up to kb

Gene regulatory domain definition: Each gene is assigned a basal regulatory domain of a minimum distance upstream and downstream of the TSS (regardless of other nearby genes). The gene regulatory domain is extended in both directions to the nearest gene's basal domain but no more than the maximum extension in one direction.

Two nearest genes

within kb

Gene regulatory domain definition: Each gene is assigned a regulatory domain that extends in both directions to the nearest gene's TSS but no more than the maximum extension in one direction.

Single nearest gene

within kb

Gene regulatory domain definition: Each gene is assigned a regulatory domain that extends in both directions to the midpoint between the gene's TSS and the nearest gene's TSS but no more than the maximum extension in one direction.

Gene Transcription Start Site (TSS)

Include curated regulatory domains [What are curated regulatory domains?](#)

Figure 20. GREAT settings. Optional settings given by the tool. Note that Basal Plus extension and Single nearest gene association rules were used for our analysis with default parameters.

The “Basal Plus Extension Association Rule” was used with default parameters (basal domain that extends 5 kb upstream and 1 kb downstream from the TSS) up to 1Mb, for the gene ontology association categories (e.g. Biological Process, Mouse Genome Informatics expression or Mouse Phenotype). The “Single Nearest Gene Association Rule” (up to 1 Mb) was used to look at the distribution of the SP8-CRM.

DAVID

Direct target genes of SP8 (up or down regulated in Sp8 KO with a SP8-CRM) were functionally annotated using the Database for Annotation, Visualization and Integrated Discovery (DAVID) (Huang et al., 2007) (version 6.8, <https://david.ncifcrf.gov/summary.jsp>). GOTERM-BP-FAT categories (summarized version of Biological Processes Ontology) using DAVID default settings (count = 2, EASE-score < 0.1) were considered.

MEME-ChIP

Motif discovery analyses of SP8-ChIPmentation were performed using the online tool MEME-ChIP (Version 5.0.1, <http://meme-suite.org/tools/meme-chip>) as described by (Ma et al., 2014). Input sequences were centered within summit regions of recovered intervals and MEME will find motifs that are between 6 and 20 bp wide with an E-value cut-off of >0.5 for the discovery of enriched motifs.

MatInspector

For the prediction of potential TFBS, we used the MatInspector (MI) tool provided by *Genomatrix* software suite (Munich, Germany) (Cartharius et al., 2005). FASTA sequences of SP8-CRM were loaded into MI tool, being scanned for matches to a library based on position weight matrices (PWM), identifying putative binding sites (matrix similarity scores not less than 0.75/optimized).

Publicly available datasets used in this study

The data for comparison were converted to the mouse build mm10 using the UCSC LiftOver tool when needed. Common regions were obtained creating an intersection between Vista and SP8-ChIPmentation regions with the UCSC Table-Browser tool.

Materials and methods

The datasets used in our analysis were β -CATENIN ChIP-seq (GEO: GSE43597) (Zhang et al., 2013), DLX5 ChIP-seq (GEO: GSE76187) (Hojo et al., 2016), Topologically Associated Domains (GEO: GSE35156) (Dixon et al., 2012) and Capture C (GEO: GSE84795) (Andrey et al., 2017).

The Limb-Enhancer Genie (LEG)

We run the analysis type “Scan for Top” with the combined model, finding the overlap of the input regions, SP8-CRM, with the top 10,000 predicted limb-enhancers <https://leg.lbl.gov/> (Monti et al., 2017).

Vista Enhancer Browser

Human (hg19) and mouse (mm9) enhancers in the database (2,892 elements, <https://enhancer.lbl.gov/>) were downloaded. The data for comparison were converted to the mouse build mm10 using the UCSC LiftOver tool. Common regions were obtained creating an intersection between Vista and SP8-ChIPmentation regions with the UCSC Table-Browser tool.

We divided the VISTA sequences (total = 2,892) in various groups: negative (negative enhancer activity, n =1,318), positive (positive enhancer activity, n =1,574), and limb (positive enhancer activity in limb, n =337). Then, overlaps percentage of SP8-CRM with the previous groups of VISTA sequences were calculated.

A representative embryo figure showing LacZ activity of some selected regions was downloaded from VISTA Enhancer Browser.

4. RESULTS

4. RESULTS

4.1 **OBJECTIVE 1**: Analysis of the SP8 regulatory network in the limb ectoderm

4.1.1 Genome-wide analysis of SP8-DNA binding sites in the developing limb bud ectoderm

To understand the complexity of the SP8 dependent regulatory networks operating in the limb ectoderm, it is necessary to identify its downstream targets. To this end we have combined genome-wide binding profiling and transcriptional profiling to identify SP8 direct targets defined as the set of genes that are differentially expressed in the absence of *Sp8* and that have nearby SP8 binding sites.

To detect SP8 binding sites in the genome, we decided to use ChIP-seq [chromatin immunoprecipitation (ChIP) combined with high-throughput sequencing]. This technique, as ChIP, requires an effective, specific, and high-quality antibody. Since no anti-SP8 antibody had been validated for ChIP, we assayed several commercial anti-SP8 antibodies (Santa Cruz C-18 (sc-104661) and H-50 (sc-98511)) but only the anti SP8 C-18 showed specificity in immunofluorescence and Western Blots but not for ChIP in whole embryo assays. Therefore, initially we decided to generate a ChIP grade anti-SP8 antibody.

4.1.2 SP8 expression and purification for antibody production

To generate a SP8 specific and ChIP grade antibody we contacted the Protein Tools Unit at the National Center for Biotechnology (<http://www.cnb.csic.es/index.php/en/servicios/384-herramientas-proteicas.html>; CNB, Madrid) to immunize mice with the full length SP8-Histidine (His) tagged protein overexpressed in *E. coli* and with two synthetic antigenic peptides not previously employed in commercial antibodies (aa 51-64; LSSFVSGASRNGG and aa 151-164; HSQDSSHQPVFISK) identified with Predict protein open and Bepipred Linear Epitope Prediction.

To overexpress and purify SP8 we used the pET-28a-c(+) vector (Novagen #69864-3) which carries a N-terminal His-Tag®/thrombin/T7-Tag® and an additional C-terminal histidine-Tag sequence. We amplified the mouse *Sp8* by PCR (see M&M) and subcloned it with NdeI and BamHI REs, downstream of the N-terminal His-tag of the pET-28a (His-SP8). His-tagged proteins can be easily purified because the string of histidine residues binds to several types of immobilized metal ions (including nickel).

For the overexpression of His-SP8, the pET-28a-c(+) vector contains a T promoter, the *lac* repressor (*lacI*) and the *lac* operon, which allows the controlled transcription of the sequence cloned downstream. This specific control depends upon de availability of the substrate lactose (or an analog such as isopropyl-2-D-thiogalactopyranoside (IPTG)) to the *E. coli*. Proper induction of the protein was tested by sodium dodecyl sulfate polyacrylamide gel electrophoresis (SDS-PAGE), comparing the expression before and after the induction, at different concentrations and times. A concentration of IPTG of 0.4 μ M and 2 hours of incubation was the selected condition. His-SP8 corresponded with a band of 50 kDa of the used marker (Fig. 21A, arrow). Solubility of His-SP8 before purification steps was also examined comparing the presence of the protein in pellet, protein lysate and control (protein expression before induction) in SDS-PAGE. SP8 was shown to be soluble as it was present in the protein lysate (supernatant) and not in the pellet (Fig. 21B, arrow).

Isolation of His-SP8 was performed based on the nickel-histidine affinity by High Performance Liquid Chromatography (HPLC) through Nickel column. The His-SP8 should be retained within the nickel-column, and then eluted with increasing concentrations of imidazole, which competes with the His for the binding to the nickel. All eluate fractions were collected, and some of them were evaluated for the His-SP8 presence by SDS-PAGE. Unfortunately, we were unable to recover His-SP8 with this method (Fig. 21C).

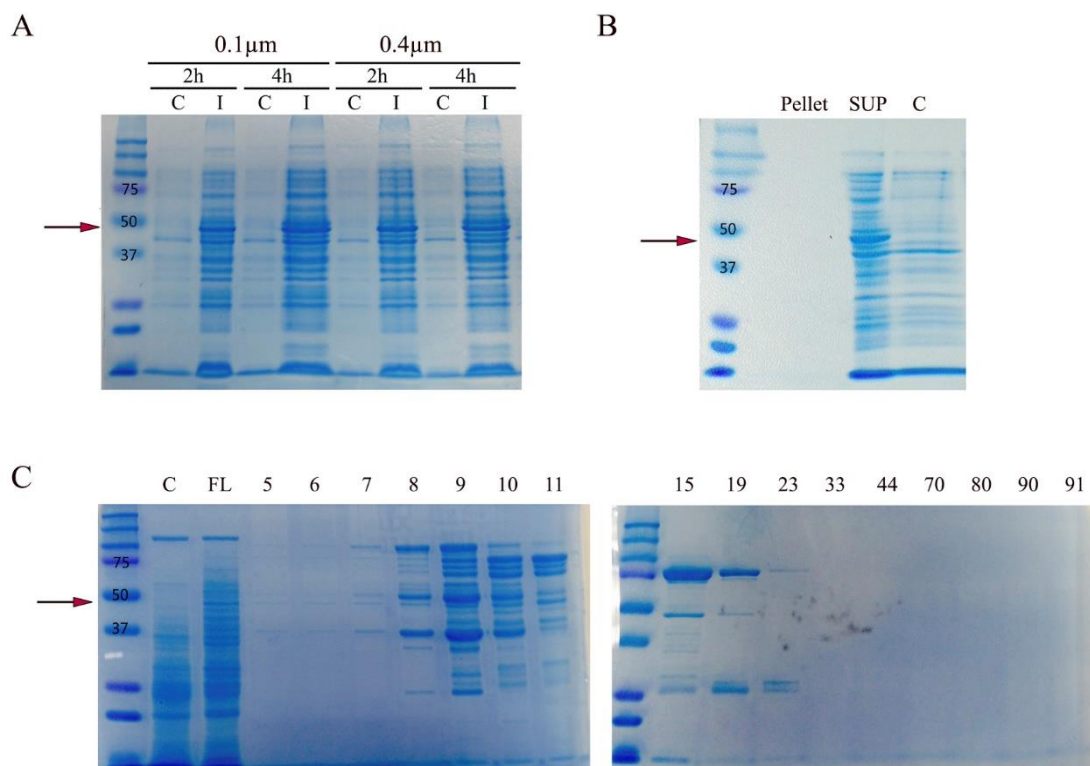


Figure 21 SP8 expression and purification. **A)** Comparison between control (C) samples (before adding IPTG) and induced (I) samples (after IPTG addition) at 2 and 4 hours after induction and at IPTG concentrations of 0.1 and 0.4 μM . The induction with 0.4 μM of IPTG for 2h was the selected condition because the His-SP8 band appeared clearer. Red arrow shows predicted size for SP8. **B)** Solubility test showing Pellet debris, Supernatant (SUP) and control (C) lanes for comparison. The hypothesized band for His-SP8 is found in the supernatant lane but not in Pellet, showing the solubility of SP8. **C)** Different eluted fractions collected and tested for His-SP8 specific elution through HPLC with nickel column. Flow-through (FL); Eluted samples (#) were collected each 90sec in an increasing concentration of Imidazole. The hypothesized SP8-His band is not recovered. All panels show SDS-PAGE stained with Blue Coomassie for the visualization of all proteins.

Therefore, we used a pH gradient to isolate SP8 based on its isoelectric point (pI). At pH values below the pI, peptides carry a net positive charge. If a voltage is applied to a complex peptide mixture in a pH gradient, peptides will migrate to the pH at which they were neutrally charged. Considering that SP8 has an isoelectric point of 9.10, HiTrap SP-Sepharose High Performance (SPHP) columns were used, which were strong cation exchangers. Separation was based on the reversible interaction between a charged molecule and an oppositely charged chromatography medium. Elution was performed by a continuous gradient in ionic strength, using NaCl. All eluate fractions were collected, and some of them were evaluated for the His-SP8 presence by SDS-PAGE. However, we could not successfully isolate the His-SP8 (data not shown).

The difficulty in purifying SP8 protein for immunization made us consider the alternative strategy of generating an epitope-tagged *Sp8* allele.

4.1.3 Generation of a 3XFLAG-tagged *Sp8* knock-in mice

We decided to generate a knock-in (KI) mouse in which the endogenous *Sp8* gene was tagged with three copies of the FLAG (FL) epitope appended at its C-terminus (*Sp8:FL*; see M&M). This strategy has been widely used in ChIP-seq studies (Osterwalder et al., 2014b), (Yu et al., 2009), (Vokes et al., 2008). Using homologous recombination, the desired FL-epitope was incorporated in frame at the C-terminal domain of *Sp8*, generating the *Sp8^{FL}* allele. This strategy was carried out in mouse embryonic stem cells (ES) by Cyagen Biosciences Inc.

Mice homozygous for the *Sp8^{FL}* allele were viable and fertile and showed no obvious phenotype. Skeletal preparations (alcian blue/alizarin red staining) of newborns showed no difference between wild-type (WT), heterozygous (*Sp8^{FL/+}*) and homozygous (*Sp8^{FL/FL}*) specimens (Fig. 22A) indicating that the tagged protein was fully functional. In Western blots, the anti-FLAG (M2, Sigma F1804) antibody detected a specific band around 50 KDa that corresponded to SP8-FL (Fig. 22B). Forelimbs and hindlimbs of E10.5 wild-type, heterozygous and homozygous *Sp8^{FL}* embryos were examined and no specific band was detected in WT tissue, which was used as a negative control of the antibody.

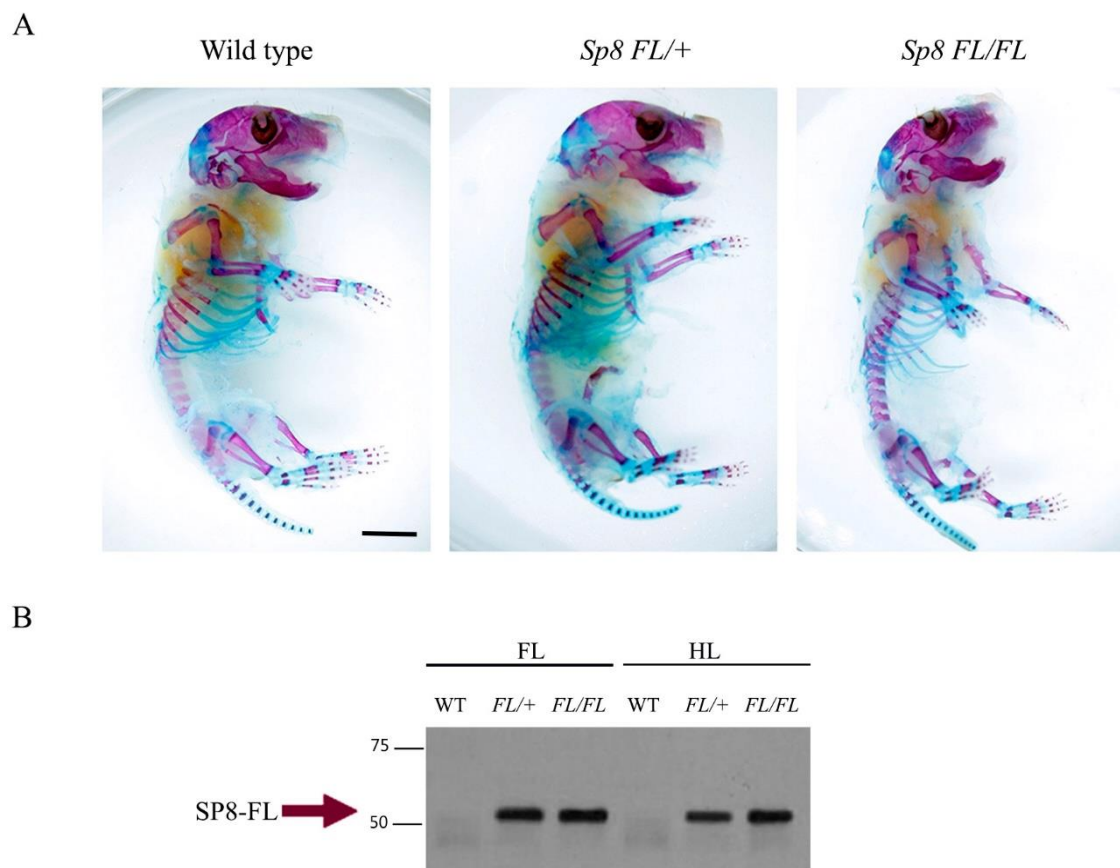


Figure 22. 3xFLAG-tagged *Sp8* (*Sp8*^{FL}) knock-in mice. **A) Skeletal preparations of newborn mice failed to detect any difference between wild-type, *Sp8*^{FL/+}, and *Sp8*^{FL/FL} specimens. **B**) Western blot anti FLAG showing SP8-FL (arrowhead) expression in FL and HL in *Sp8*^{FL/+} and *Sp8*^{FL/FL} but not wild-type E10.5 embryos. Scale bar: 1 cm.**

The distribution of SP8-FL protein was examined by immunofluorescence in cryostat sections of E10.5 *Sp8*^{FL/FL} and WT embryos using the M2 anti FLAG (Fig. 23A) and the C-18 anti SP8 (Sc-104661; Fig. 23B) antibodies, respectively. As expected, the expression pattern of SP8-FL (M2 immunofluorescence) was identical to that of the endogenous SP8 (C-18 immunofluorescence). In the limb bud, the expression was restricted to the ectoderm with higher levels in the apical ectodermal ridge (AER). To help delimiting the ectoderm, we also analyzed the distribution of Laminin (Abcam, Ab11575) and of β -catenin (CTNNb; Biosciences BD610154). Laminin is an ectodermal marker present in the basement membrane that underlies the epithelium and β catenin is a component of the adherent junctions (Fig. 23A).

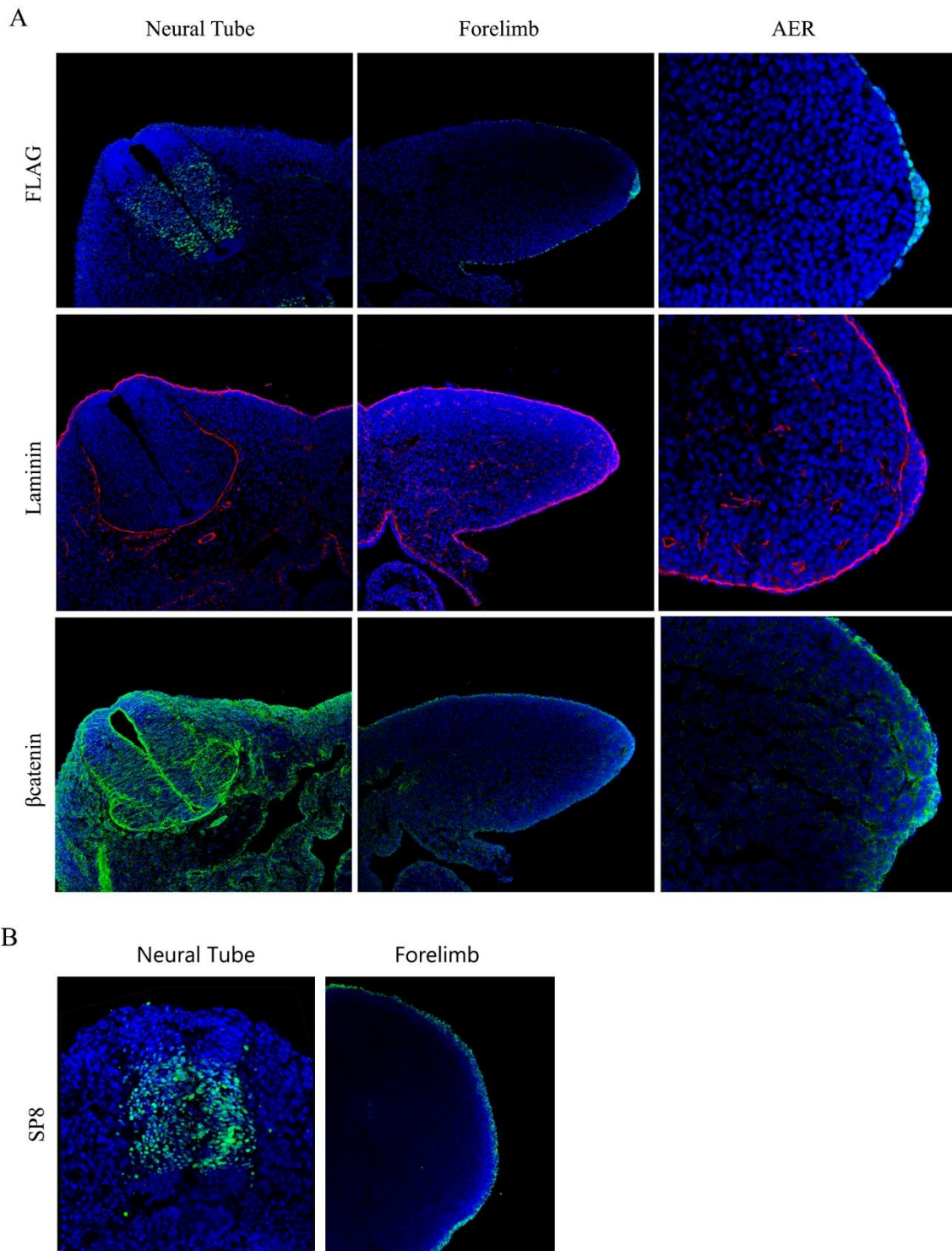


Figure 23. 3xFLAG-tagged *Sp8* knock-in mice (*SP8-FL*). **A**) Immunofluorescence in cryostat transverse sections of a *Sp8*^{FL/FL} E10.5 embryo with anti-FLAG, Laminin and β -catenin as indicated on the left. Note expression in the neural tube and limb bud ectoderm mainly concentrating in the apical ectodermal ridge (AER). **B**) Immunofluorescence with anti SP8-C18 antibody in cryostat sections of a wild-type E10.5 embryo showing similar distribution of the endogenous protein.

Therefore, the *Sp8^{FL}* KI model we have generated provides a useful tool for the specific detection of SP8 using anti-FLAG specific antibodies. Our aim is to use this model in ChIP-seq experiments in order to identify SP8 binding sites in vivo.

4.1.4 Identification of the Genomic Regions Enriched in SP8 in the forelimb bud ectoderm by ChIPmentation

To assess the genomic target sites occupied by SP8 in the limb, we performed ChIP-seq analysis using the M2 antibody against FLAG in E10.5 forelimb ectoderms of homozygous *Sp8^{FL}* embryos. Since SP8 is exclusively expressed in the ectoderm during limb development, to reduce background and unspecific binding, only the limb bud ectoderm was used for the analysis. For this purpose, the forelimb buds of *Sp8^{FL/FL}* embryos were dissected, incubated briefly in trypsin and then the ectoderm isolated from the mesoderm (see M&M).

We focused on the developmental stage E10.5, which corresponds to a fully matured AER and the stage of the onset of the *Sp8* null phenotype (Bell et al., 2003; Fernandez-Teran and Ros, 2008; Treichel et al., 2003). In a pilot experiment we isolated WT E10.5 limb bud ectoderms, dissociated them to single cell level and estimated the number of cells per each ectodermal hull that roughly was 15,000. About 2.5×10^6 cells (164 ectodermal hulls of *Sp8^{FL/FL}*) were used for each of the two ChIP replicates.

Final DNA samples were prepared according to Illumina protocol for library preparation and sequenced with a 1x50-bp protocol on a HiSeq 4000 sequencer (Illumina) at the Cologne Center for Genomics (CCG, University of Cologne) (see M&M for details). The data sets were analyzed using model-based analysis for ChIP-seq (MACS) based peak calling. However, the ChIP-seq with the anti-FLAG antibody did not enrich for SP8 binding peaks in the E10.5 limb bud ectoderm samples versus the input control (without FLAG antibody immunoprecipitation) suggesting that we had not effectively immunoprecipitated the chromatin regions bound by SP8. We concluded that the failure was probably due to insufficient amount of input material and decided to change our strategy.

To reduce the size of the samples, and therefore the number of embryos needed, we tried the ChIPmentation procedure that is based on tagmentation and has proven highly efficient for low input samples. ChIPmentation is a ChIP-seq that incorporates a step of tagmentation (incubation with Tn5 transposase for library preparation). This tagmentation introduces sequencing compatible adapters directly on the complex bead-bound chromatin, which reduce time, cost, and input requirements (Schmidl et al., 2015). ChIPmentation was performed with 50 ectodermal hulls (approx. 7.5×10^5 cells) using anti-FLAG antibody. Final DNA samples were prepared according to Illumina as for ChIP-seq (see M&M for details). ChIPmentation profiles were generated with MACS in comparison with the input and resulted in the identification of 1,451 genomic regions considered as bound by SP8.

The quality and specificity of the ChIPmentation peaks was supported by the following observations. First, using PhastCons (Liu et al., 2011) we estimated the conservation score based on multiple vertebrate alignment. The analysis of the SP8 associated regions showed a high conservation among different vertebrate species (Fig. 24A).

Second, the specificity of the SP8 DNA bound regions was verified and highlighted by the significant overrepresentation of expected binding motifs. SP family members share three highly conserved zinc-finger domains in their carboxy-terminus and all of the SP family members were thought to share the same DNA recognition site, with the consensus sequence 5'-GGGCGG-3', the GC box (Suske, 1999). To double check the expected binding motif for SP8 we used a “DNA binding site predictor for Cys2His2 Zinc Finger Proteins” (<http://zf.princeton.edu/logoMain.php>) (Fig. 24B). In order to determine the preferential motifs of SP8, *de novo* motif discovery was performed with MEME-ChIP (Machanick and Bailey, 2011). This tool performs motif analysis of large DNA datasets and was used to identify the most representative motifs found in our ChIPmentation dataset. It performs motif discovery, enrichment, visualization, binding affinity analysis and motif identification. As expected, the most highly over-represented motif found in the analysis was a GC-rich motif (E-value 5.9×10^{-209}), corresponding to the SP1 motif (Fig. 24C). Surprisingly, the second enriched motif was an AT-rich motif (E-value 5×10^{-140}), described as the preferential motif for

SP7 to indirectly bind the DNA through DLX5 (Hojo et al., 2016). SP7, one of the members of the SP family, was recently reported to bind DNA indirectly through AT-rich motifs instead of the canonical GC box. This AT-rich motif contains a putative homeodomain-response element (Fig. 24C). The third enriched motif found in the analysis was a CA-rich motif which corresponded to an already reported motif for RREB1 (binds to RAS-responsive elements (RREs) of gene promoters) and ZN502 (Zinc finger protein 502) (E-value $3.7e-81$) (Fig. 24C).

Because functional TF binding sites tend to occur within cis-regulatory elements enriched in certain histone marks, we also wanted to compare the SP8-DNA association profile with that of histone marks typical of active cis-regulatory elements. Therefore, to define the chromatin state of SP8 binding regions, we generated by ChIP-seq profiles of Histone 3 (H3) lysine (K) 27 acetylation (H3K27ac) and H3K4 dimethylation (H3K4me2) in E10.5 limb bud ectoderm. H3K4me2 is typically enriched at promoters and enhancers found in either primed or active states, while H3K27ac is exclusively found in active promoters and enhancers. When the genomic regions associated to H3K4me2 and H3K27ac were sorted by SP8 bound regions a considerable enrichment in both marks was evident (Fig. 24D). Interestingly, the regions decorated with H3K4me2 and H3K27ac were positioned around the SP8 peak centers. The analysis showed that SP8 occupies genomic sites that have high levels of primed enhancer marks. In our further analysis, distal SP8-CRM will be considered putative enhancers (primed or active)

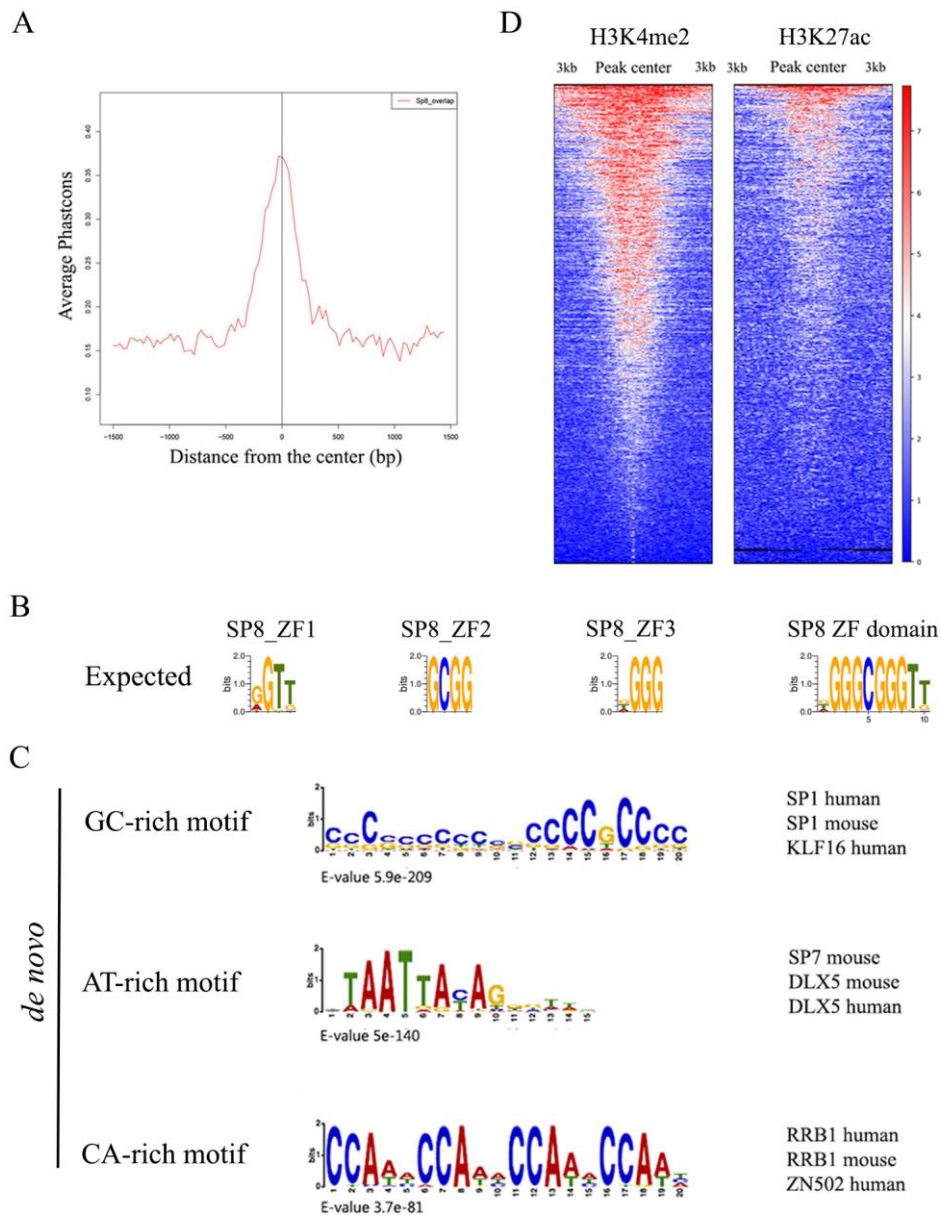


Figure 24. Genome-wide analysis of SP8-DNA association profiles in the limb bud ectoderm. **A)** Average vertebrate PhastCons score profiles around the center of SP8-Cis Regulatory Modules (CRM) showing evolutionary conservation. **B)** On top the predicted motif for each SP8 ZF obtained with DNA Sequence Logo generator. **C)** *De novo* motif discovery analysis of the SP8-CRM with MEME-ChIP reveals the three most enriched binding motifs. The known binding motifs that best match each of the novo identified motifs are shown to the right. **D)** Heatmaps of chromatin regulatory marks (H3K27ac, H3K4me2) around the SP8-CRM (+3 kb and -3 kb from the peak center).

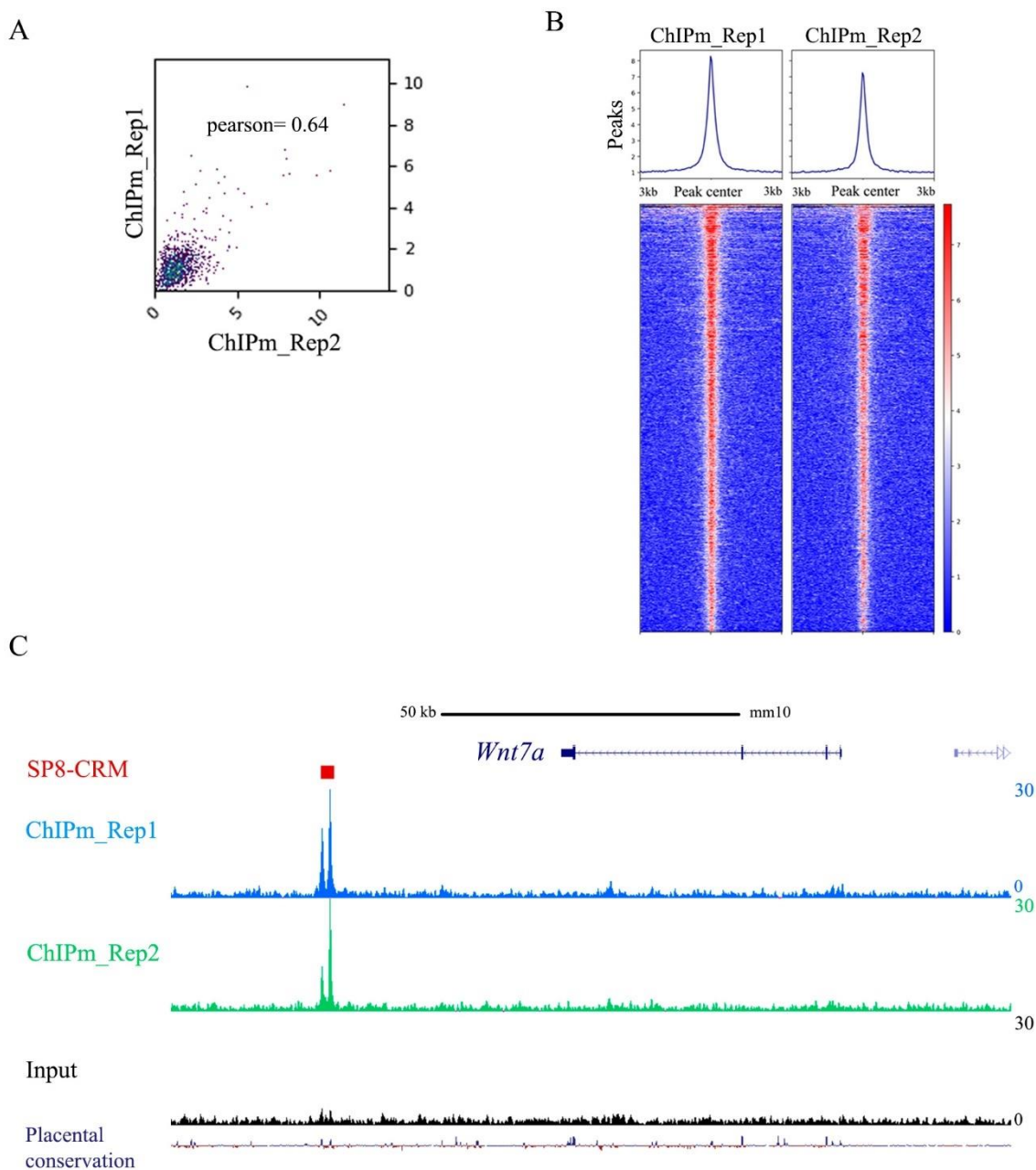


Figure 25. ChIPmentation replicate validation. **A)** Pearson Correlation Plot showing the similarity between ChIPmentation replicates. **B)** Heatmap of each replicate showing the overlapping of SP8-CRM. **C)** UCSC genome browser view of SP8-ChIPmentation and ChIPmentation input profiles around the *Wnt7a* landscape locus. A SP8-CRM associated to *Wnt7a* is seen in both replicates. Replicate 1 (blue), replicate 2 (green), input track (black) and base-wise conservation by phylop (Consv) are shown.

Finally, to validate the analysis a second ChIPmentation replicate was performed. Although a lesser number of SP8 binding regions (1,004 regions) were identified, the intersection of the two biological replicates identified 558 common peaks was highly significant ($p < e^{-222}$). Moreover, the similarity between both replicates was further highlighted by the high correlation of ChIPmentation signals across the union of SP8 binding sites identified in both ChIPmentation experiments. The correspondence between both replicates was assessed by the Pearson's correlation coefficient comparing genome-wide binding sites (10 kb bins) between both replicates that gave a value of 0.64 (Fig. 25A). The similarity of both ChIPmentation experiments can be further appreciate using heatmaps plots in which the signals of both SP8-ChIPmentaton replicates are shown around the union of identified SP8 peaks. Moreover, heatmaps displaying peak signals of one replicate around the peak center summit (3 kb) of the other showed an extensive overlap between both replicates (Fig. 25B). Therefore, according to all these criteria, the consistency between replicates is high. An example of the highly reproducibility between the two biological replicates was illustrated by the genome browser representation of SP8 ChIPmentation profiles at the *Wnt7a* locus, an essential marker of the dorsal ectoderm and direct target of SP8 (Fig. 25C and see below).

In summary, the evolutionary conservation, enrichment of expected specific motifs, decoration with histone marks characteristics of active/primed regulatory regions and reproducibility between biological replicates demonstrate that the SP8 ChIPmentation dataset is a valuable resource for the study the SP8 dependent regulatory network in the limb bud ectoderm.

4.1.5 Analysis of SP8 putative regulatory elements and their associated genes

Having shown the consistency between the two biological replicates, because of its higher signal to noise ratio, we only used the dataset of the first biological ChIPmentation sample (1,451 genomic regions) for further analyses. SP8 bound regions will be referred to as SP8 Cis Regulatory Modules (CRM).

We first analyzed the SP8 CRM with the Genomic Regions Enrichment Annotations Tool (GREAT; (Mclean et al., 2010), an in silico tool that enables the functional annotation of non-coding regulatory elements. GREAT first step is to associate a given chromosomal coordinate to a gene, based on the association rule and settings of choice (see M&M). After this association, GREAT assigns biological functions to genomic regions providing insights into the biological significance of cis-regulatory data sets of interest. Using the Single Nearest Gene Association Rule up to 1 Mb (see M&M), we first analyzed the distribution of the distance of SP8-CRM to the nearest transcription start site (TSS) (Fig. 26A). This distribution showed that the percentage of peaks in regions proximal to promoters (defined as regions ± 5 kb from the known TSS) was similar (48% vs and 52%) to that in distal regions (more than 5 kb distant from the TSS, considered putative enhancers) (Fig. 26A). This indicates that SP8 can similarly execute its regulatory function in two different genomic contexts, promoters and distal cis-regulatory elements.

GREAT analysis was used as the tool to functionally annotate the SP8 bound genes with the Basal Plus Extension Association Rule, up to 1Mb (see M&M). Canonical and no-canonical WNT receptor signaling pathways were the predominant biological processes associated with putative genes regulated by SP8, as well as different developmental and morphogenetic processes, primarily associated with the kidney and neural tube. This information was consistent with the role SP8 plays in the limb ectoderm (Bell et al., 2003; Haro et al., 2014; Treichel et al., 2003), which was the predominant tissue detected in MGI Expression together with very early embryo development (Fig. 26B). The analysis of the most representative mouse phenotypes associated with the SP8-CRM revealed spina bifida and craniofacial malformations within the top 10 most representative phenotypes. These two traits are characteristics of the *Sp8KO* phenotype.

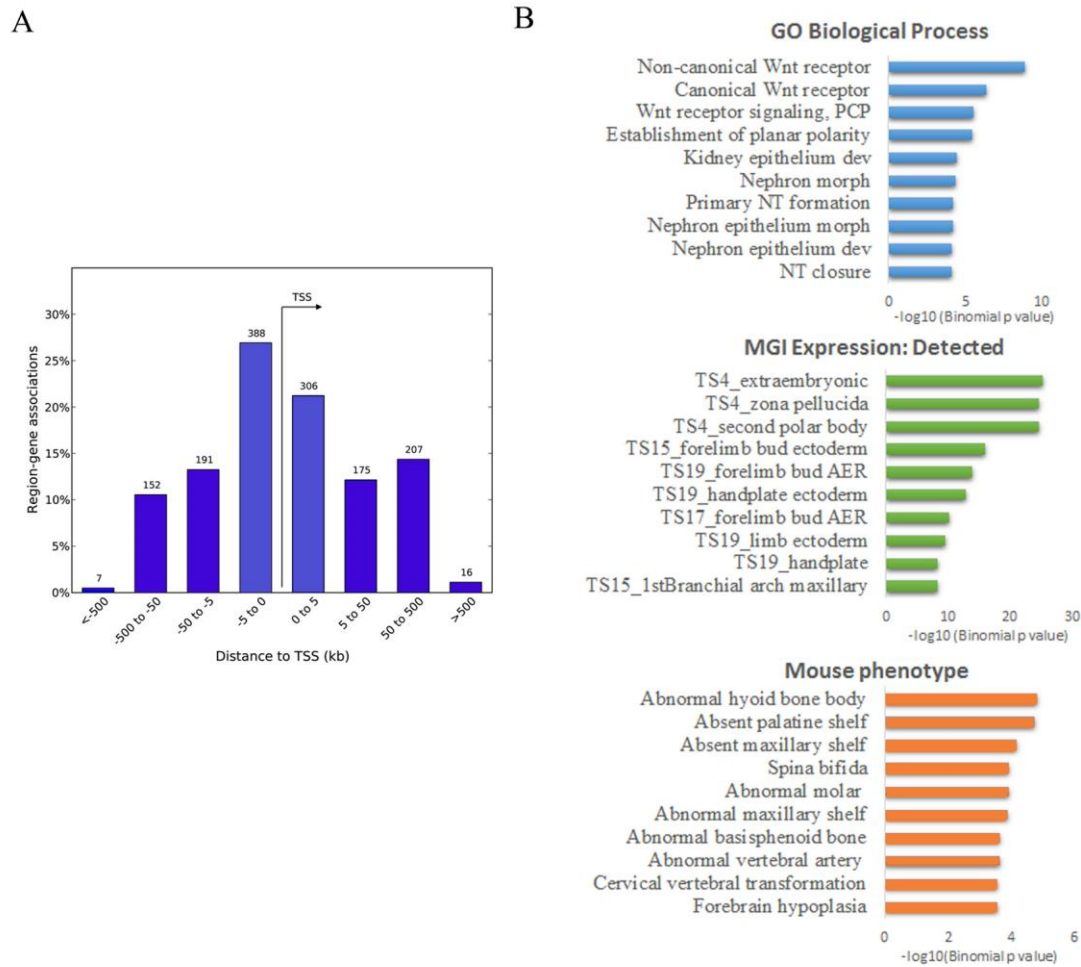


Figure 26. Genome-wide analysis of SP8-CRM association with GREAT. **A)** Distribution of the distance of SP8-CRM to the nearest TSS with the “Single Nearest Gene Association Rule” (up to 1 Mb). **B)** Functional annotation of SP8 was performed with the “Basal Plus Extension Rule” (using default parameters: 5 kb upstream and 1 kb downstream of the TSS, up to 1 Mb). To illustrate the gene categories with which SP8 was preferentially associated, ten of the twenty most overrepresented terms belonging to three major gene ontologies are shown: Gene Ontology (GO) Biological Process (blue), Mouse Genome Informatics (MGI) Expression: detected (green), and Mouse Phenotype (orange).

This suggests that some of the SP8 binding sites and/or SP8 target genes might be shared between different embryonic tissues in which SP8 is expressed.

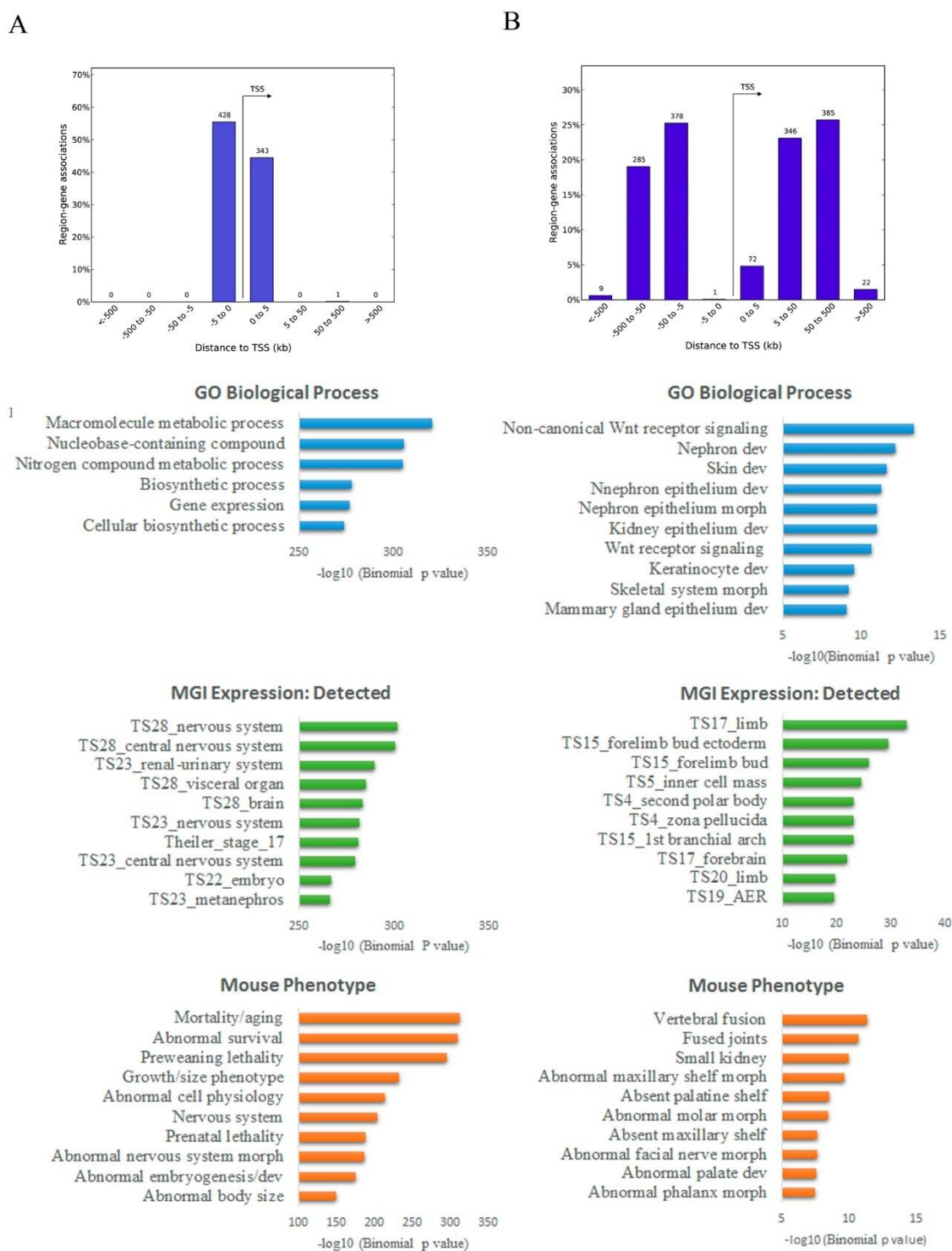


Figure 27. Proximal and distal SP8 ontologies. **A)** Proximal associated genes. **B)** Distal associated genes. GREAT analysis with the “Basal Plus Extension Association Rule” (default parameters). On top the distance distribution of each set of genes and below the functional annotation. Ten of the twenty most overrepresented terms belonging to three major gene ontologies are shown: Gene Ontology (GO) Biological Process (blue), Mouse Genome Informatics (MGI) Expression: detected (green), and Mouse Phenotype (red).

To determine possible differences in the expression and functions of genes assigned to SP8-CRM depending on whether binding occurs into proximal promoters or distal regulatory regions, the analysis was repeated separately in proximal versus distal peaks (Fig. 27). We found that promoter located binding sites were predominantly associated with general functions and processes (e.g. regulation of macromolecule metabolic process) and with embryonic renal and nervous MGI expression (Fig. 27A). Mouse phenotypes associated within this set of genes highlighted mortality and abnormal physiology and embryogenesis, as well as abnormal growth. Interestingly, distal binding sites were mainly associated with the canonical and non-canonical WNT signaling pathways and kidney and renal epithelium development, , and importantly, expression during mouse embryogenesis was preferentially observed in the early embryo and early limb bud (Fig. 27B). Abnormal vertebral, joint and craniofacial morphologies were within the top mouse associated phenotypes.

To examine if SP8 recognizes a different DNA binding sequence when it binds to proximal versus more distant regulatory sites, *de novo* motif discovery was performed independently in proximal versus distal peaks. The analysis showed that the GC-rich motif (SP1-like) was the predominant motif in proximal elements (E-value 1.2e-224) (Fig. 27A) while the AT-rich motif (DLX) was the most prevalent (E-value 1.1e-192) in distal ones (Fig. 27B). This indicates that SP8 is more likely to interact with SP1-like binding sites in proximal promoters than in distal CRM in which it is most likely to interact with a DLX binding site possibly through association with DLX5.

The signal density of H3K4me2 and H3K27ac marks was also separately analyzed in proximal and distal SP8-CRM separately. We observed that the vast majority of the proximal SP8-CRM overlapped with H3K4me2 regions and a considerable proportion with H3K27ac marks. Although the overlapping with H3K4me2 marks was also intense in distal regions, they showed a modest decoration with H3K27ac marks (Fig. 28). This is consistent with the presence of putative primed/active promoters and enhancers in the SP8 bound regions. This indicates that while the SP8 bound promoters are frequently active, the bound distal CRMs can

represent putative primed enhancers that might switch to a fully active state at later developmental stages.

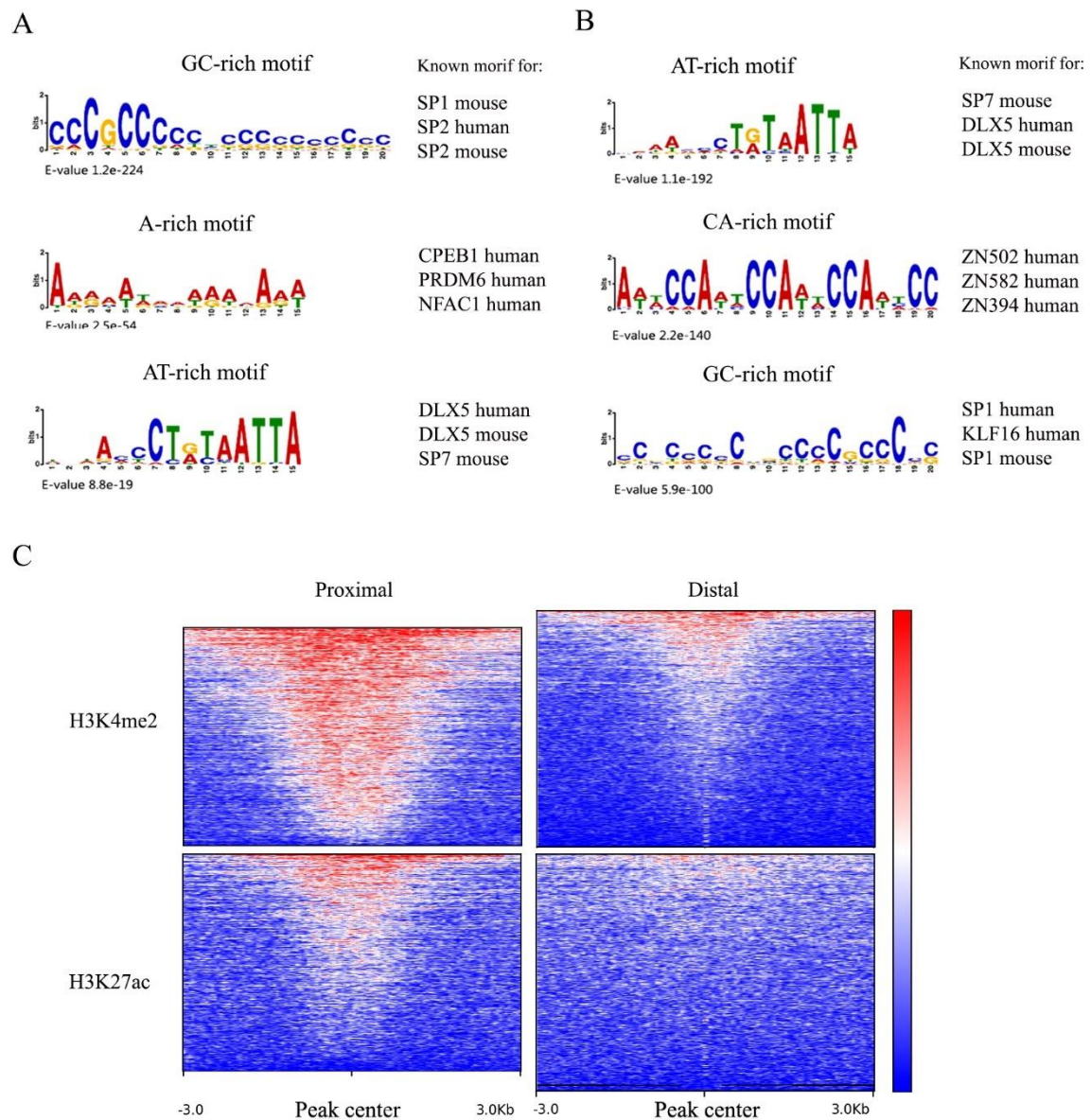


Figure 28. Proximal and distal SP8 features. A-B) Motif enrichment of proximal and distal SP8 associated regions respectively. MEME-ChIP tool was used to obtain the three most representative binding motifs found the novo. On the right of each binding motif, the association with already described ones. C) Histone-modification density at SP8 binding sites. The signal density of H3K4me2 and H3K27Ac is shown around the peak center of proximal and distal SP8 binding regions.

In summary, the analysis of SP8 bound regions showed similar distribution between proximal and distal regions when one gene per region was associated. *De novo* motif discovery predicts SP1-like and DLX binding sites as the SP8 primary genomic interaction sites. Interestingly, the separate analysis of proximal versus distal regions identified that SP8 binding to proximal regions was preferentially direct (through SP1-like motifs) while binding to distal regions preferentially occurred through interaction with DLX5 (DLX motifs). SP8 bound promoters coupled to genes associated with general cellular processes while SP8 bound distal putative enhancers associated with genes with specific embryonic and limb development functions.

4.1.6 SP8-CRM Intersection with other tested or predicted enhancer collections

As a first attempt to test the hypothesis that SP8 could be regulating active enhancers, we compared the SP8-CRM identified by ChIPmentation with the experimentally validated enhancers in the VISTA Enhancer Browser repository (<https://enhancer.lbl.gov>). This browser contains thousands of genomic regions that have been experimentally tested for tissue specific enhancer activity by transient mouse transgenic assays at E11.5. Tested putative enhancers were identified based on loci bound by p300 or on their conservation between human and no mammalian vertebrates across long and extremely long evolutionary distances or based on their ultra-conservation. Both, human (hg19) and mouse (mm9) enhancers in the Vista Enhancer database (2,892 elements) were downloaded and converted to mm10 for their comparison with our SP8 CRM. There were 19 common regions, of which 9 showed positive LacZ activity and 6 of these in the limb (Fig 29A).

The enrichment in limb activity (31%; 6 out of 19) of the common enhancers highlighted the limb specificity of the SP8 ChIPmentation, as this was a much higher percentage than if considered all the vista-enhancers tested (11,6%: 337 out of 2,892 with limb activity) (Fig 29B).

The 6 common regions with functional activity in the limb were associated with *Msx1*, *Gnpda1-Ndfip1*, *Kirrel*, *Scube1*, *Zfp395*, *2610019F03Rik* (Fig. 29C).

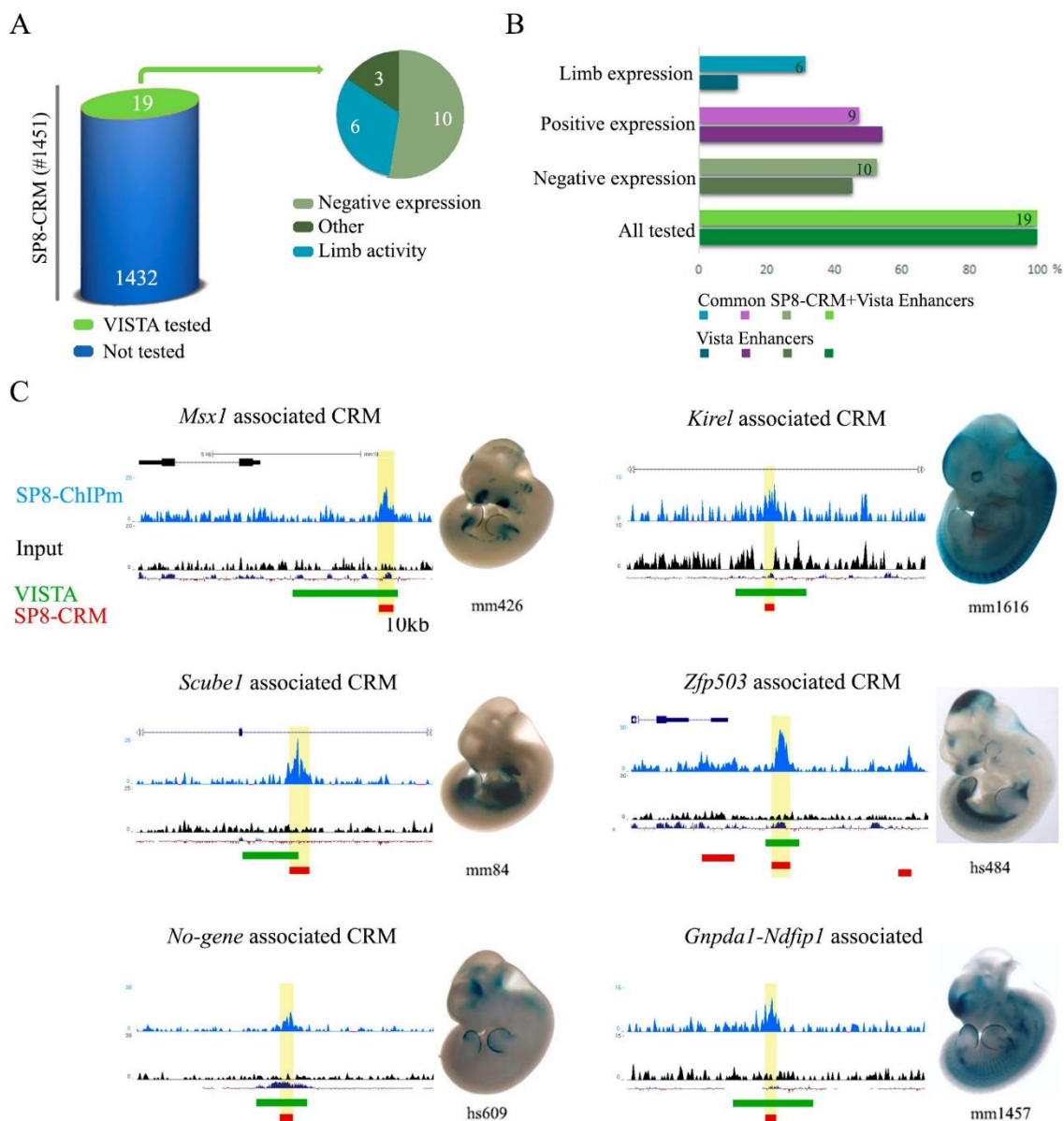


Figure 29. SP8-CRMs common to VISTA enhancer browser putative enhancers (PE). **A)** SP8-CRM found in common with tested human and mouse PE from VISTA enhancer browser (19, green). From those 19, 10 showed negative LacZ activity (soft green), 6 showed limb expression (blue) and 3 of them no-limb detected expression (dark green). **B)** Percentage of VISTA enhancer browser PEs (darker colors) and common SP8-CRMs with VISTA enhancer browser (lighter colors) comparison. 100% considered for All tested VISTA enhancers (2,892), and all common SP8-CRMs (19). From bottom to top bars: All regions – negative LacZ activity – positive LacZ activity – limb LacZ activity. **C)** UCSC screenshots showing –10 kb of genomic DNA with the SP8 ChIPmentation track (replicate 1, blue), input track (black), the base-wise conservation by phyloP (Consv), the corresponding VISTA element (green) and the SP8-CRM (red). The enhancer activity at E11.5 (LacZ reporter, VISTA Enhancer Browser, database; Visel et al., 2007) is shown on the right.

Results

Of these only, *Msx1* was an activated SP8 direct target gene (see below) confirming that the genomic region bound by SP8 and associated with *Msx1* was a bona-fide enhancer capable of directing transcription in the limb ectoderm recapitulating the *Msx1* pattern. *Kirrel* is expressed in kidney podocytes, *Scube1* is expressed in platelets and endothelial cells and may play an important role in vascular biology. *Gnpda1*-*Ndfip1* and *Zfp395* have not been characterized in the context of embryonic development.

We also matched our SP8 peaks with the list of 1,237 putative enhancers identified by promoter-Capture-C data as linked to the promoters of 446 selected genes relevant to limb development (Andrey et al., 2017). Promoter-Capture-C identifies regions of physical interactions with the selected promoters that were then considered as putative enhancers. Of these 1,237 putative enhancers, 54 overlapped with SP8 bound regions (4.3% of Capture-C identified promoters and 3.7% of SP8-CRM). When considering SP8 direct target genes, only 4 regions overlapped (1.6% of SP8 direct targets). Of these 4 genes, *Dnajc1*, *Hoxb1* and *Hoxc9* only the latter has reportedly ectodermal expression.

Finally, we also compared the set of SP8 CRM with the Limb-Enhancer Genie (LEG) collection of predicted enhancers active in the developing limbs (Monti et al., 2017). This collection is easily accessible and can be directly and systematically queried through a user-friendly interface. It derives from the combination of published limb-specific datasets and clusters of evolutionarily conserved TF binding sites. We found that about 10% of the distal SP8 CRM (83/831 regions) overlapped with these predicted enhancers.

Table 3. SP8-CRM comparison with Enhancer collections

Predicted enhancer collections		Intersection with SP8 CRM
VISTA	2,892 elements	1.31% of SP8 CRM (19/1451)
Capture-C	1,237 elements	3.7% of SP8 CRM (54/1451)
LEG		10% of distal SP8 CRM (83/831)

Several reasons may have contributed to the low overlapping between SP8 occupied enhancers and the VISTA and promoter-Capture-C and LEG element sets. Among them, the different tissue used to extract the information, as we specifically used in the limb ectoderm, while the other enhancers collections were identified in whole limb buds, what may result in a dilution of the signal from specific subset of cells such as the ectoderm.

4.1.7 RNAseq-based transcriptome comparison between WT and *Sp8* null limb bud ectoderm

To understand the developmental program controlled by SP8 in the limb ectoderm, we generated and compared the expression profiles of wild-type versus *Sp8* deficient (*Sp8KO*) limb bud ectoderm.

We used a robust RNA-seq protocol for low-abundance RNA (requirement of 500 pg of total RNA) that permitted the use of only two forelimb ectoderms for each replicate. The samples were obtained from E10.5 WT and *Sp8KO* embryos from the same litter. Three replicates per condition were analyzed using multiplexed RNA-Seq library preparation strategy and with a 2x75bp paired-end read length on an HiSeq4000 platform (Illumina) at the CCG, University of Cologne (See M&M for details).

Differentially expressed genes (DEG) were obtained through DEseq2 (Anders and Huber, 2010), considering only genes with an Ensembl ID, an official Gene Symbol and applying the following criteria: $p < 0.01$, fold change ≥ 1.5 and FPKM ≥ 0.1 (see M&M). A total of 892 DEG that were common in the three replicates were identified. These 892 DEG contained both direct and indirect SP8 transcriptional target genes of which 519 were downregulated and 373 upregulated in the *Sp8KO* (Fig 30). All genes known to be affected by the loss of *Sp8* were included in the set of DEG (such as *Fgf8*, *Dlx5*, *Rspo2*, *En1* or *Wnt7a* among others).

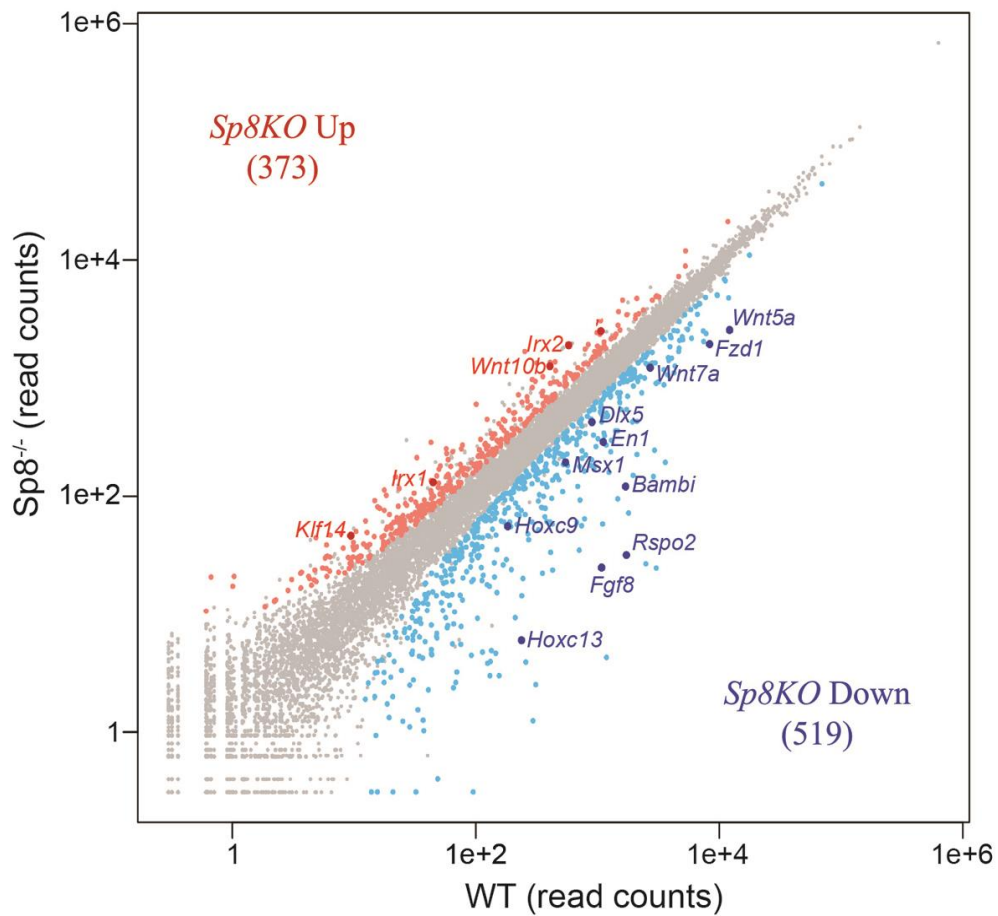


Figure 30. Whole transcriptome data of WT versus *Sp8* null E10.5 limb bud ectoderm. Mouse genes were plotted according to the average normalized RNA-seq read counts in WT and *Sp8*^{-/-}. Each gene is represented by a dot. Genes considered as significantly up and downregulated in *Sp8*^{-/-} are shown in red and blue, respectively. Some relevant genes that are also direct targets of SP8 are indicated.

4.1.8 Identification of SP8 Direct Targets in the Limb Bud Ectoderm

In order to determine the SP8 direct target genes, we combined the RNA-seq and ChIPmentation datasets. We identified 184 DEGs bound by SP8 that were, therefore, considered SP8 direct target genes. Of them, 55 genes were repressed (up regulated in *Sp8* KO) ($p=3e-4$) and 129 activated (downregulated in *Sp8* KO) ($p=4.3e-26$) by SP8 (Fig. 31A) indicating that SP8 mainly functions as an activator in the limb ectoderm. GREAT analysis with Single Nearest Gene Association Rule (up to 1 Mb) of each set of associated regions showed a predominant distal distribution of both repressed (75%) and activated (73%) SP8 direct targets (Fig. 31B) indicating that SP8 predominantly regulates its direct target genes through distal putative enhancers.

De novo motif discovery in each dataset (repressed and activated) of SP8 direct targets gave interesting results (Fig. 31C-D). SP1-like motifs were similarly enriched in repressed and activated SP8 direct targets (E-values of $5.2e-13$ and $1.2e-13$, respectively) but, in addition, the DLX motif was the top scoring motif (E-values of $9.5e-38$) in the set of activated SP8 target genes. This result indicates that the SP8 activator function likely depends on interaction with DLX-TFs (Fig. 31C-D).

To elucidate the function of these 184 SP8 direct targets, both sets of SP8 target genes (repressed and activated) were functionally annotated using GREAT. GO-terms for renal development were significantly enriched in the set of genes repressed by SP8 (Fig. 31E) while epithelial and embryonic GO-terms showed the highest enrichment in the set of genes activated by SP8 (Fig. 31F).

Taken together the data indicate that SP8 preferentially controls its target genes through distally located binding regions (putative primed enhancers), disregarding whether it acts as an activator or as a repressor. Most interestingly, the data also indicate that the activator function of SP8 is preferentially mediated by physical interaction with DLX5 through DLX-motifs, particularly in the limb bud. These data suggest that when it binds to promoters, SP8 binding might be more redundant or less essential.

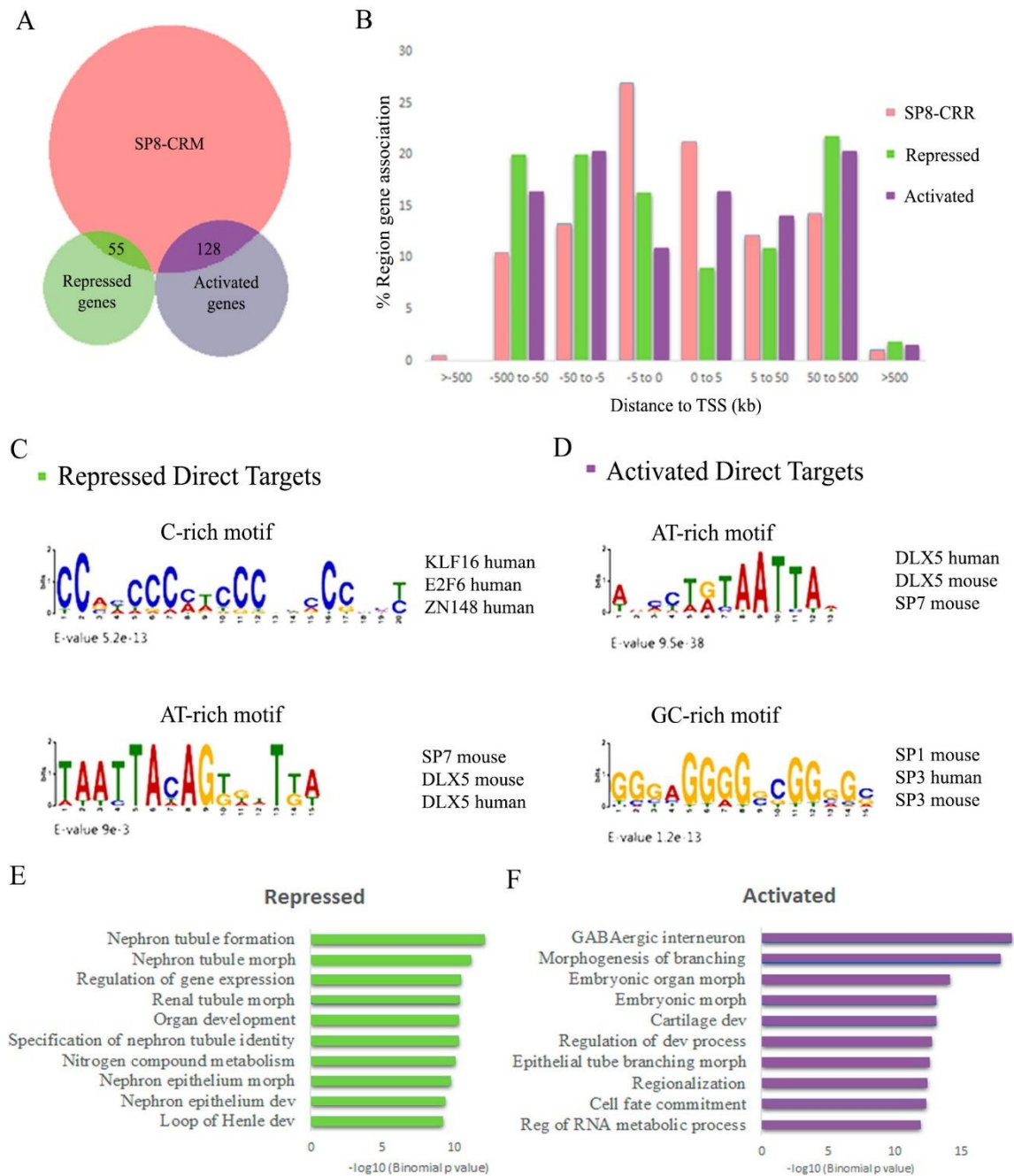


Figure 31. SP8 direct targets. **A)** Venn diagram showing the overlap between up (purple) and down (green) regulated genes in *Sp8* KO with genes bound by SP8 (pink) datasets. The intersection shows the SP8 direct target genes. **B)** Distribution comparison of percentage gene-association genes in SP8-CRM (“all” 1,442 genes, pink bar), directly activated (128 down-reg genes, green bar) and repressed (55 up-reg genes, purple bar) by SP8. **C)** Most representative motifs found with MEME-ChIP tool in repressed SP8-direct targets. **D)** and in activated SP8-direct targets. **E-F)** GO Biological Process of SP8 direct target genes showing ten out of the twenty most overrepresented. **E)** repressed direct targets (green); **F)** activated direct targets (purple).

4.1.9 Physical interaction between SP8 and DLX5

Our results raised the interesting possibility that SP8 has more affinity for DLX5 than for the DNA and that it engages distal putative enhancers of activated target genes through interaction with DLX5.

Dlx5 is a member of the DLX family of homeobox containing genes that are the mammalian homologs of the *Drosophila Distal-less (Dll)*. *Dlx5*, together with *Dlx6*, *Dlx2* and *Dlx3* are expressed in the developing limbs, including the apical ectodermal ridge (AER) (Robledo et al., 2002). *Dlx5* is also essential for chondrocyte and osteoblast differentiation under the transcriptional control of BMP signaling. DLX TFs function by binding the 5-TAATTA-3 consensus sequence in the DNA through their homeodomain.

DLX5 has been shown to mediate SP7 promoter activity in bone development (Hojo et al., 2016). SP7 diverges from other family members as it engages its targets as a DLX co-factor (Hojo et al., 2016). Specific amino acid differences in the SP7 zinc finger domain, not shared by SP8, are responsible for this divergent mode of action. However, the fact that *de novo* motif analysis in the SP8 ChIPmentation dataset unexpectedly identified the AT-rich SP7-DLX5 binding site as primarily enriched motif, raised the possibility that SP8 also functions as a DLX5 co-factor. This is also supported by the overlapping expression patterns of both TFs in the limb bud ectoderm and by the similarities in the loss of function phenotypes (Lo Iacono et al. 2008; Robledo et al., 2002). Indeed, diseases associated with DLX5 include Split-Hand/Foot Malformation1 (SHFM1) with sensorineural hearing loss (SHFM1D; OMIM 220600; Shamseldin et al. (2012) and Split-Hand/Foot Malformation1 (SHFM1; OMIM 186300; Wang et al. (2014)) a phenotype that is similar to that reported in *Sp6^{-/-};Sp8^{+/-}* compound mutants (Haro et al., 2014).

To examine a possible interaction between SP8 and DLX5, we performed Co-Immunoprecipitation (CoIP) assays. FLAG-SP8 and MYC-DLX5 (see M&M) were co-transfected in vitro in HEK-293 cells, SP8 immunoprecipitated with anti-FLAG M2 antibody and DLX5 detected in WB with anti-MYC antibody, demonstrating that these two TFs physically interact (Fig 32A). In addition, to determine if the ZF domain of

Results

SP8 was the region necessary to accomplish this interaction, as it has been shown for SP7 (Hojo et al., 2016), a truncated version of SP8, $\Delta(353-487)$ SP8, that lacks the ZF domain was used for the CoIP assays. Co-transfection of FLAG-DLX5 and MYC- $\Delta(353-487)$ SP8 showed no interaction indicating that the ZF region of SP8 was essential for this protein-protein interaction (Fig. 32B). This result is consistent with SP8 indirectly binding enhancers by partnership with DLX5. Because several members of the DLX family are expressed in the limb ectoderm (Robledo et al., 2002) and it is known that they are functionally equivalent, SP8 could potentially interact with any of them. We also note here that all *Dlx* genes are direct targets of SP8 adding an additional level of complexity to their cooperatively modulation of gene expression.

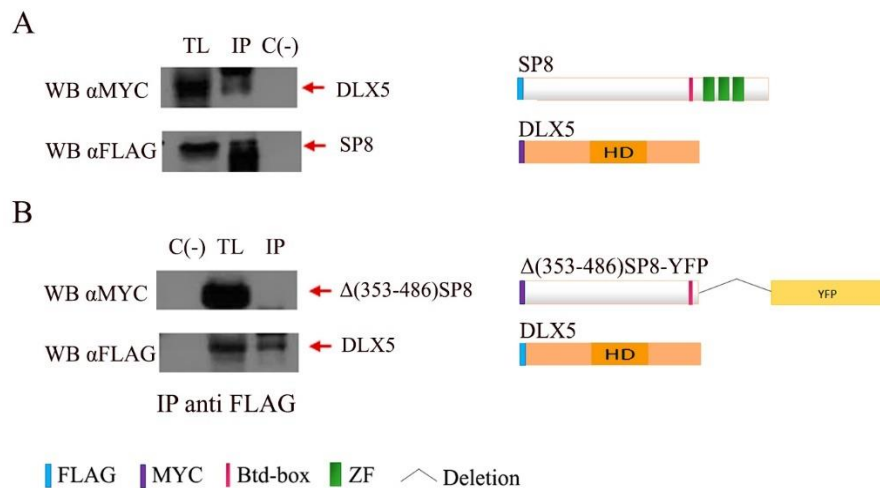


Figure 32. Interaction of SP8 and DLX5 by CoIP. A) SP8 and DLX5 CoIP. **B)** $\Delta(353-487)$ SP8 and DLX5 CoIP. On the left, CoIP showing the interaction of the co-transfected proteins. Schematic representation of the co-transfected constructs is shown on the right. Co-transfected but not immunoprecipitated cells were used as negative control. Anti-FLAG antibody is used for Immunoprecipitation and anti MYC for WB detection of the interaction. Anti-FLAG was also used in WB to prove successful IP.

4.1.10 Two modes of SP8 action

Our data provide strong evidence for a dual mode of SP8 action: directly binding to the consensus GC-box sequence (SP1-like motif) and indirectly engaging to DLX binding sites through the association with DLX5. The second mode of action requires the presence of DLX5 or other family member, therefore being operative only in the cells that express both TFs.

We next asked which mode of action was SP8 using in each of its direct targets. To answer this question, the interacting regions were categorized according to the presence of DLX and SP binding sites into four groups (Fig. 33): 1) target genes with only SP1-like binding sites (about 33% of activated and 34% of repressed), 2) target genes with only DLX binding sites (about 31% of activated and 15% of repressed), 3) target genes with both types of binding sites (about 27% of activated and 30% of repressed) and 4) target genes whose assigned enhancers have none of these binding sites (about 8% of activated and 19% of repressed). Interestingly, this later group of SP8 target genes, which does not contain SP1-like or DLX binding sites in their associated CRMs, strongly suggest that SP8 also acts through other interactors.

Table 4. SP1 and DLX binding sites within SP8 direct targets

SP8 direct targets (# regions)	Only SP1 % (# regions)	Only DLX % (# regions)	Both SP1+DLX % (# regions)	None % (# regions)
Activated (171)	33.33% (57)	30.99% (53)	27.48% (47)	7.60% (14)
Repressed (69)	34.78% (24)	14.49% (10)	30.43% (21)	18.84% (14)

Thus, this analysis shows that SP8 does not require DLX interaction to regulate about one third of its direct targets but that the interaction with DLX is absolutely indispensable to regulate another subset (30.99% activated and 14.49% repressed).

To further explore the interaction between SP8 and DLX, we searched for similarity in target genes by comparing our SP8-ChIPmentation dataset with a similar one for DLX5. Unfortunately, the only DLX5 ChIP-seq peak dataset available is the one generated in the MC3T3E1 osteoblast cell line (Hojo et al., 2016). Of the 24,365 DLX5 binding regions identified in MC3T3E1 cells, 258 overlapped with SP8-CRM (1% of DLX5 binding regions and 17.2% SP8 CRM). Even though the biological relevance of this comparison is rather limited due to the developmental distance between samples, still the amount of SP8 peaks shared with DLX5 peaks was considerable if compared with overlapping with other TFs (i.e. β -CATENIN).

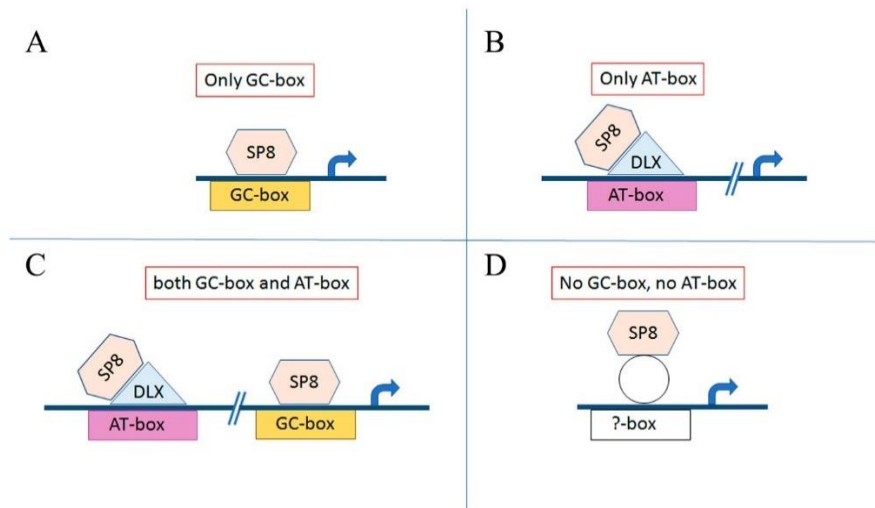


Figure 33. Schematic representation of SP8 modes of action. A) Target genes with only SP1-like binding sites. **B)** Target genes with only DLX binding sites. **C)** Target genes with both types of binding sites. **D)** Target genes whose assigned enhancers do not contain SP1-like or DLX binding sites.

4.1.11 SP8 regulatory network in the limb ectoderm

Of the 184 identified SP8 target genes, the set of genes activated by SP8 included many well-known patterning regulators of limb development, including all the genes (*Fgf8*, *Sp6*, *En1*, *Msx1*, *Msx2*, *Wnt7a*, *Rspo2* and several *Dlx*) that we and others have previously shown to be regulated by SP8 (Bell et al., 1998; Haro et al., 2014; Treichel et al., 2003). The set of genes repressed by SP8 also included some very well-known limb patterning genes such as *Sox9*, *Wnt10b* and *Tfap2b*, that had not been previously identified as regulated by SP8. Interestingly, the dataset of SP8 target genes also gave some surprising results. For example, *Wnt7a*, a gene considered to be negatively regulated by SP8, was identified as a gene activated by SP8. WNT7a is a marker of the dorsal ectoderm and a determinant of dorsal identity as it induces *Lmx1b* in the subjacent mesoderm which in turn is responsible for the dorsal morphology. Based on the observation that the early limb bud that forms in *Sp6;Sp8* double mutants as well as the digit tips of the *Sp6;Sp8* were bidorsal (Haro et al., 2014), SP8 was considered to repress *Wnt7a* transcription either directly or indirectly through EN1 a result that is not confirmed by our current results.

Therefore, to understand the regulatory function of SP8, a fraction of genes, selected accordingly to their relevance in limb development, were subject to further analysis including their loci landscape and *in situ* hybridization to assess how the quantitative changes in expression profile corresponded with spatial changes in expression pattern. The genes analyzed were classified according to their connection with the WNT/ β -CATENIN pathway controlling PD patterning (*Fgf8*, *Rspo2*, *Fzd1*, *Wnt5a*), with DV patterning (*En1*, *Wnt7a*), with SHFM (*Wnt10b*), and with their SP autoregulation (*Sp6*, *Dlx*).

4.1.12 Interactions between the SP8 GRN and the WNT/ β -CAT pathway

In the limb bud ectoderm, SP6 and SP8 have been shown to act downstream of WNT/ β -CATENIN signaling in the activation of *Fgf8*, the marker and principal signaling factor emanating from the AER. In addition, both canonical WNT signaling and SP8 function are required not only for induction of the AER but also for its maintenance (Barrow et al., 2003; Haro et al., 2014). The WNT/ β CAT-SP8-FGF8 is a highly conserved cassette repeatedly used in different contexts (Lin et al., 2013) but that is not a simple lineal pathway (Barrow et al., 2003; Haro et al., 2014).

Accordingly, *Fgf8* and *Fgf4* were identified as SP8 direct targets. Our bioinformatic analysis, paid special scrutiny on a region that contains a coherent integrated regulatory ensemble for *Fgf8* (Marinić et al., 2013) and also in the *Fgf8* proximal promoter (Sahara et al., 2007b). Nearly 50 *Fgf8*-regulatory modules have been identified in a 220 kb region centromeric to the gene, many of them embedded in the FBXW4 gene (Marinić et al., 2013). Although several of these enhancers show overlapping AER activity, our analysis showed no SP8 overlap in this intricate *Fgf8*-regulatory region. The SP8 peak assigned to *Fgf8* is located in the gene promoter (-326 bp) and is full of SP1-like binding sites (Fig. 34). *Fgf8* is never activated in double *Sp6;Sp8* mutants and is only initially transitory expressed in the *Sp8* mutant. We have suggested that this initial activation depends on the presence of *Sp6* that requires *Sp8* for maintenance of expression (Haro et al., 2014). Thus, SP8 regulation of *Fgf8* occurs at the promoter by binding to the consensus GC and without apparent interaction with DLX.

To assess which part of the WNT regulatory pathway depends on SP8, we first investigated the presence of components of the WNT pathway among the SP8 direct targets. The GREAT analysis identified the following components of the WNT signaling pathway (P00057): *Ankrd6*, *En1*, *Fzd1*, *Kremen1*, *Myc*, *Mycn*, *Plcb1*, *Plcb4*, *Tle4*, *Wnt5a* and *Wnt7a*.

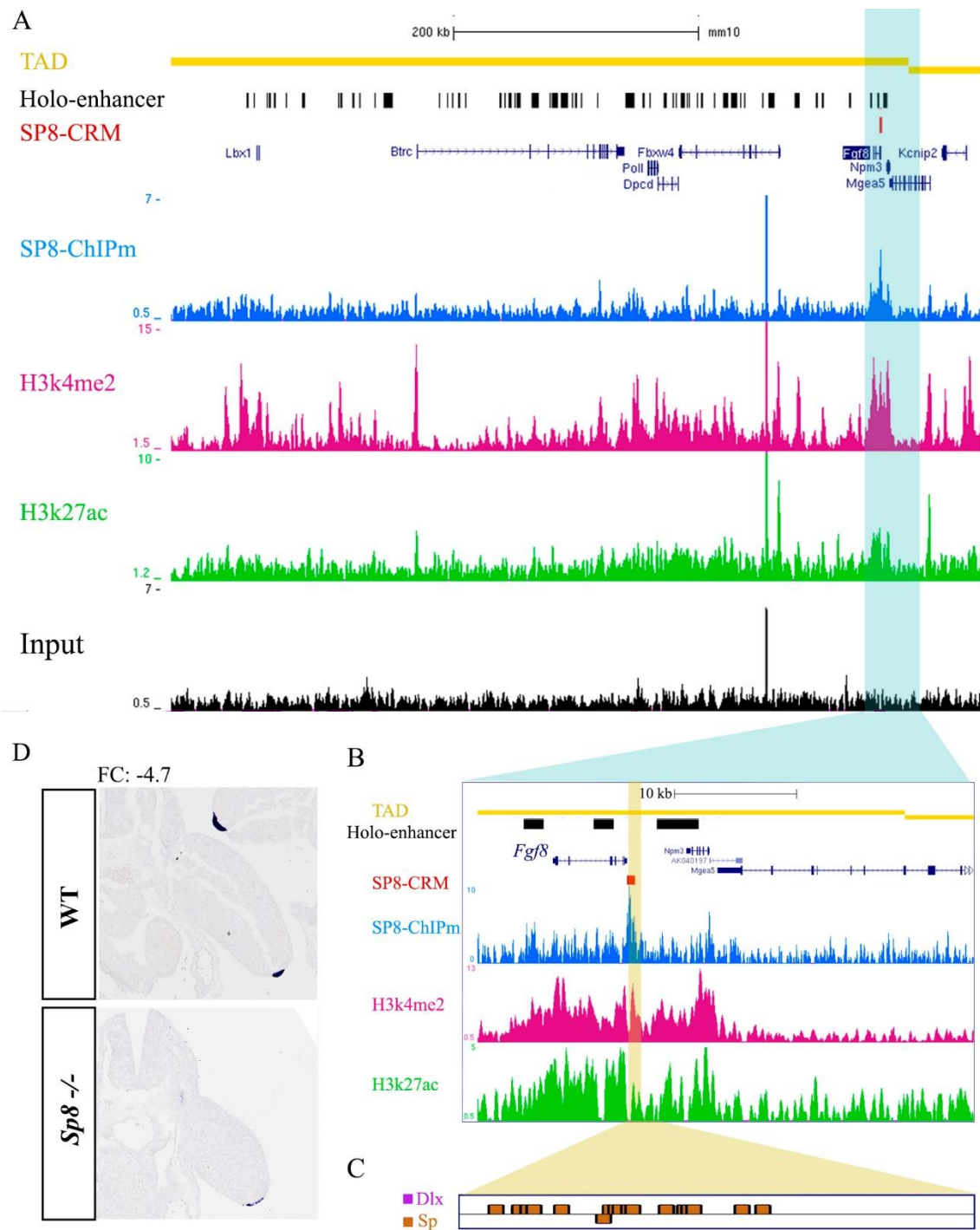


Figure 34. UCSC genome browser view of the *Fgf8* regulatory landscape and *Fgf8* expression in *Sp8* null embryos. **A) Yellow lines indicate the TAD in ES cells as in Dixon et al. (Dixon et al., 2012). Black boxes indicate the holo-enhancer described in Marinic et al. (Marinic et al., 2008). SP8-CRM and ChIPm track for SP8 are shown in red and blue on the top and the input on the bottom (black). The H3k4me2 and H3k27ac profiles are also shown in pink and green respectively. **B**) *Fgf8* landscape zoom in (blue shadow). **C**) SP8-CRM zoom in the DLX (purple) and SP1 (orange) putative binding motifs found with the Mat Inspector tool within the region. **D**) Expression of *Fgf8* in E10.5 forelimbs of WT and *Sp8*^{-/-} embryos by ISH. Fold change obtained in the RNA-seq indicated below.**

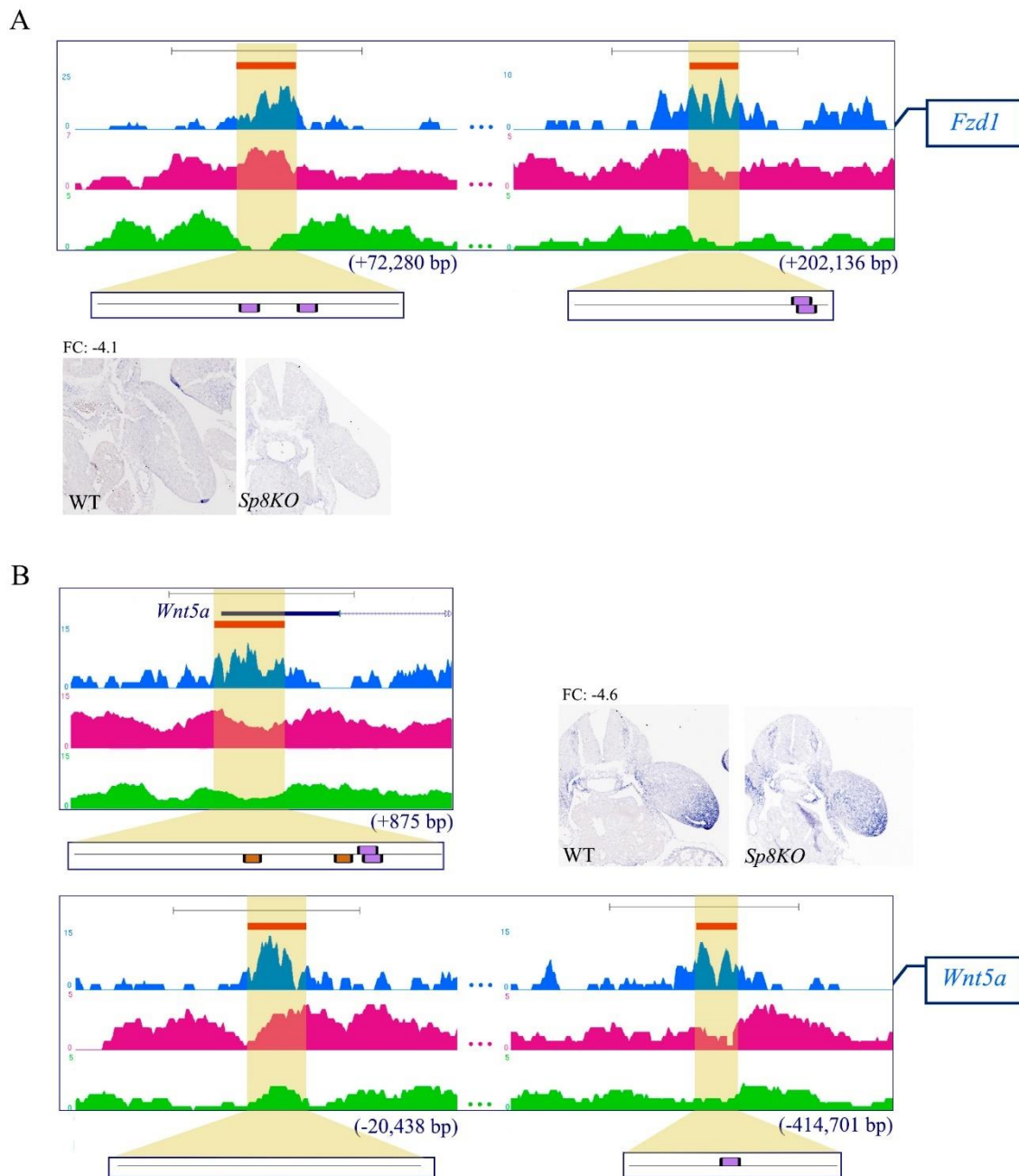


Figure 35. UCSC genome browser view of the *Fzd1* and *Wnt5a* regulatory landscape and their expression in *Sp8* null embryos. A) *Fzd1* B) *Wnt5a*. Representation of the two SP8-CRM associated to *Fzd1* and the three SP8-CRM for *Wnt5a*. Scale bar: 1 kb. Profiles of SP8 ChIPmentation (blue), H3k4me2 (pink) and H3k27ac (green) are shown. Below, SP8-CRM zoom in for the visualization of the DLX (purple) and SP1 (orange) putative binding motifs found with the Mat Inspector tool within the region. Expression of A) *Fzd1* and B) *Wnt5a* in E10.5 forelimbs of WT and *Sp8*^{-/-} embryos by ISH. Fold change obtained in the RNA-seq indicated above.

Fzd1 expression was not detected in the AER of *Sp8* LOF mutants by in situ hybridization (Fig. 35A) indicating that SP8 is required for expression of this gene. Two SP8-CRM were assigned to *Fzd1* and both of them contained DLX but not SP1-like sites.

Similarly, *Wnt5a* expression was not detected in the *Sp8*-null limb bud ectoderm, although it may be difficult to appreciate due to the expression in the distal mesoderm. *Wnt5a* activates both the canonical and the planar cell polarity WNT dependent pathways. Three SP8 peaks were assigned to *Wnt5a*, one within the gene first exon and two in distal enhancers (Fig. 35B). Two of these peaks contain DLX binding sites, what explains the low levels of *Wnt5a* in *Dlx5;6 DKO* limbs (Conte et al., 2016).

We also compared the genome-wide binding profile of SP8 with that of β -CATENIN in mouse embryonic cells that identified 9,885 peaks (Zhang et al., 2013). The intersection of both datasets revealed that 88 regions associated to 120 genes (6% of SP8 and 0.89% of β -CATENIN bound regions) were bound by both factors. When considering the set of SP8 direct target genes, only 10 regions were shared between SP8 and β -CATENIN chromatin complexes. These were assigned to 8 genes: *Tfcp2l1*, *Creb3l1*, *Tbx3*, *Dusp4*, *Kremen1*, *Sp8*, *Arhgap8* and *Pim1*. We note that one of these genes is *Sp8*. Thus, multiple lines of evidence point to SP8 mediating of only a fraction of WNT/ β -CATENIN target genes.

Within the WNT/ β -CATENIN pathway, four R-SPONDINS ligands (RSPO1-4) act as enhancers of WNT signaling by binding to their receptors LGR4, LGR5 and LGR6 to recruit the RNF43 and ZNRF3 E3 ligases and prevent degradation of the FRIZZLED (FZD) receptors (Huang et al., 2007; Kazanskaya et al., 2004; Nam et al., 2007).

Because it has been well established that during limb-development *Rspo2* is expressed in the limb ectoderm under the control of SP8 (Bell et al., 2008, 2003), we were surprised by the fact that *Rspo2* was not identified as a SP8 direct target. Actually, RNA-seq revealed *Rspo2* as one of the most down regulated gene in *Sp8KO* (fold change -36.2). However, the inspection of the *Rspo2* landscape exposed a peak located 217,676 bp upstream its TSS (-217,676) that we assigned as the putative SP8-CRM for

Results

Rspo2 (Fig. 36). This peak contains three DLX binding sites and none for SP1 indicating that SP8 requires DLX5 for *Rspo2* control. Interestingly, the SP8 peak assigned to *Rspo2* is also present in LEG.

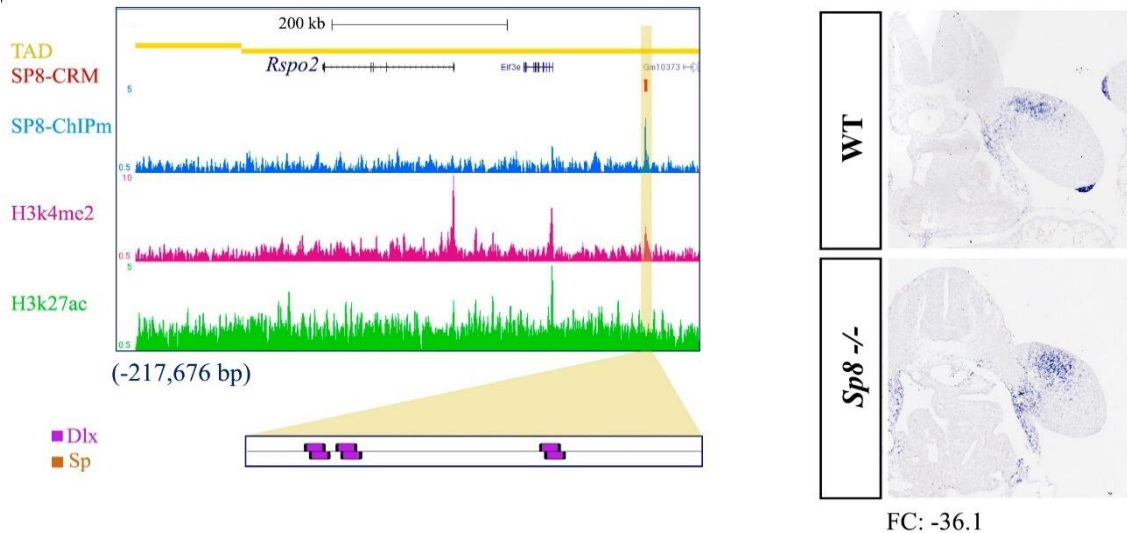


Figure 36. UCSC genome browser view of the *Rspo2* regulatory landscape and *Rspo2* expression in *Sp8* null embryos. Same tracks as in Fig. 34 are shown. SP8-CRM zoom in for the visualization of the DLX (purple) and SP1 (orange) putative binding motifs found with the Mat Inspector tool within the region. C) Expression of *Rspo2* in E10.5 forelimbs of WT and *Sp8*^{-/-} embryos by ISH. Fold change obtained in the RNA-seq indicated below.

In summary, some important components of the WNT signaling pathway such as *Fzd1* and *Wnt5a* are direct targets of SP8, it is likely that a considerable part of the SP8-dependent WNT pathway components are mediated by *Rspo2* expression rather than by SP8 itself.

4.1.13 SP8 controls all major regulators of DV patterning

Patterning in the dorso-ventral axis depends on the non-AER ectoderm. The ventral ectoderm expresses *En1*, which controls ventral patterning by restricting *Wnt7a* expression to the dorsal ectoderm. LOF of *Sp6;Sp8*, either partial or complete, bear bidorsal phenotypes (Bell et al., 2003; Haro et al., 2014; Talamillo et al., 2010). Thus, the digital tips of *Sp6* and *Sp6;Sp8* mutants display bidorsal traits such as double nails.

Similarly, the initial limb buds that form in *Sp6;Sp8* double mutants express *Wnt7a* throughout the ectodermal cover while *En1* is not detected. This finding led us to propose that *En1* required SP8 for activation in the limb ectoderm. Accordingly, *En1* was identified as a direct target of SP8 in the limb ectoderm (fold change -2.27) and was assigned a 288 bp SP8-CRM located 19,543 bp downstream of its TSS (+19,543). This enhancer contains two DLX binding sites and one SP1 binding site (Fig. 37A).

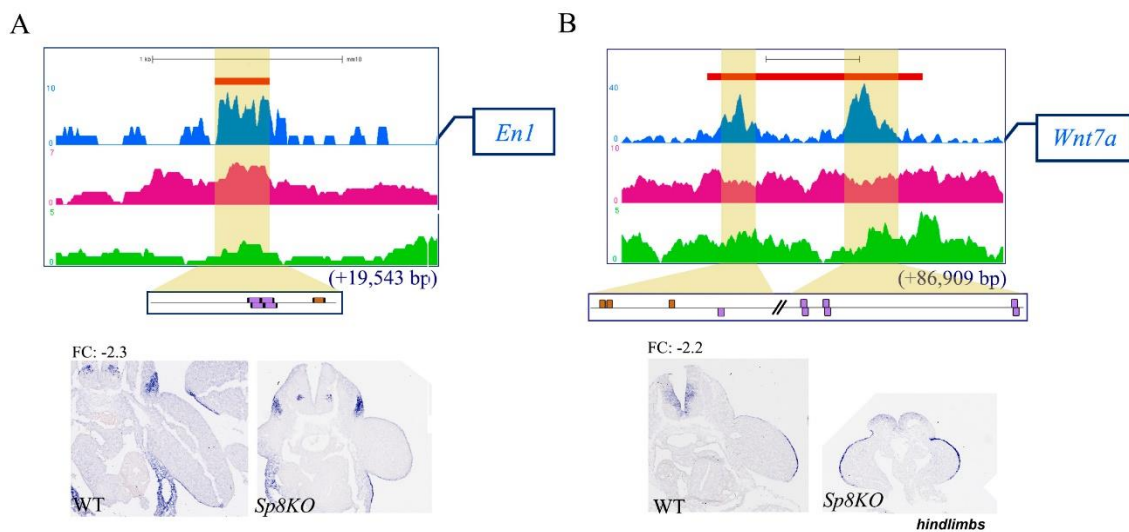


Figure 37. UCSC genome browser view of the *En1* and *Wnt7a* regulatory landscape and their expression in *Sp8* null embryos. A) *En1* B) *Wnt7a*. Same tracks as in Fig. 34 are shown. Below, SP8-CRM zoom in for the visualization of the DLX (purple) and SP1 (orange) putative binding motifs found with the Mat Inspector tool within the region. Expression of A) *En1* and B) *Wnt7a*, in E10.5 forelimbs of WT and *Sp8*^{-/-} embryos by ISH. Fold change obtained in the RNA-seq indicated above.

As previously mentioned, the analysis of *Sp6/8* mutants led to the conclusion that *Sp8* negatively regulated *Wnt7a* transcription either directly or indirectly through EN1. Most interestingly, our current results revealed that *Wnt7a* is activated by SP8 as its expression level is reduced in the *Sp8* mutant (fold change -2.2) despite an expanded domain. SP8 controls *Wnt7a* expression through a CRM located downstream of the gene (+86,909 bp), which can be subdivided in two peaks, one contains three SP and one DLX binding sites, and the other containing three DLX binding sites (Fig. 37B).

4.1.14 Sp autoregulation of gene expression

We also found that SP8 targets putative enhancers of *Sp6* and of itself indicating cross and autoregulation. *Sp6* has already been proposed to be regulated by SP8 as its expression decays in the *Sp8* mutant (Haro et al., 2014). The CRM associated with *Sp6* locates in the promoter (+3,419 bp) and only contains SP1-like sites (Fig. 38A). Therefore, any member of the SP family could be acting on them. Besides *Sp8* and *Sp6*, *Sp9* is another family member expressed in the ectoderm, but the expression level is very low and during a limited period of time (Kawakami, 2004). The function of *Sp9* seems to be negligible, as it has no limb phenotype and shows no function in the absence of *Sp6/8* (Haro et al., 2014). Other family members such as *Sp1* and *Sp3* are considered to have ubiquitous expression, and therefore could potentially contribute to the activation and maintenance of SP8 expression in the limb ectoderm.

Four members of the *Dlx* gene family (*Dlx1*, *Dlx2*, *Dlx4* and *Dlx6*) were identified as SP8 direct targets. However, given that the 6 family members are distributed in pairs on the same chromosomes as the *Hox* cluster, and that the paired *Dlx* genes are in an inverted configuration and separated by a short intergenic region, we took a closer look at their loci landscape (Fig. 38B-D). Four SP8-CRM were identified in the *Dlx1/Dlx2* locus (Fig. 38B), all of them assigned to *Dlx1* and located upstream its TSS (-4,477, -8,008, -13199, -15,316 bp). Three of these CRM were also assigned to *Dlx2* (+10,633, +5,442 and +3,325 bp). The single SP8-CRM identified in the *Dlx3/Dlx4* locus located upstream of *Dlx4* (-64,693 bp) and downstream *Dlx3* was assigned just to *Dlx4*, although we considered that this CRM could be regulating both distally (Fig. 38C). The same situation was observed in the *Dlx5/Dlx6* locus, where a SP8-CRM located upstream of *Dlx6* (-265,482 bp) and downstream of *Dlx5* was just assigned to *Dlx6*. The *Dlx1/Dlx2* and *Dlx3/Dlx4* regions were full of SP-like motifs while the *Dlx5/Dlx6* CRM contained two DLX binding sites. This analysis is compatible with SP8 regulating the transcription of all *Dlx* family members. The ISH analysis showed that *Dlx5* and *Dlx6*, normally expressed in the AER, were clearly downregulated (fold change -1.9) in absence of SP8 (Fig. 38D).

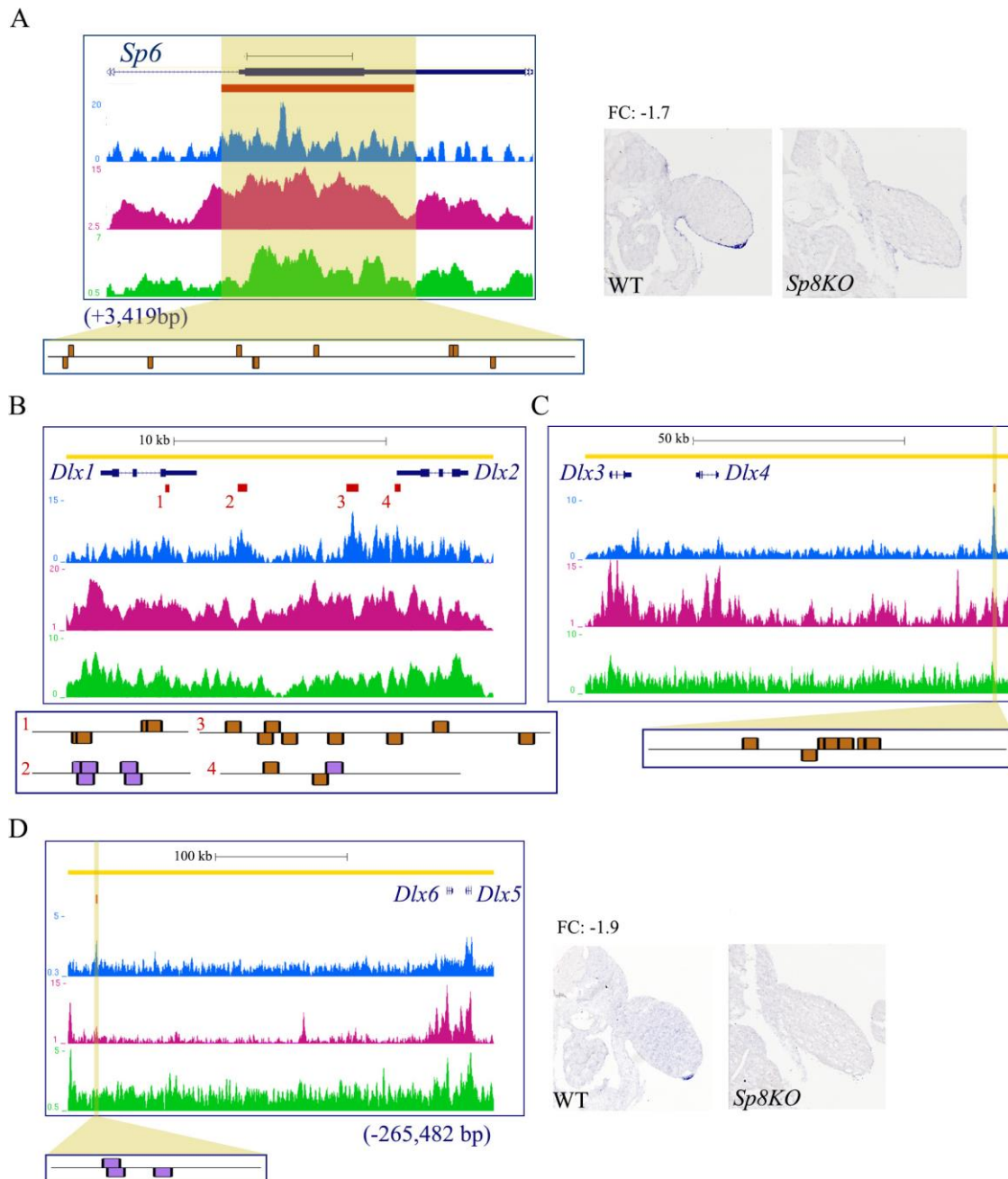


Figure 38. UCSC genome browser view of the *Sp6* and *Dlxs* regulatory landscape and their expression in *Sp8* null embryos. A) *Sp6* B) *Dlx1,2* C) *Dlx3,4* D) *Dlx5,6*. Same tracks as in Fig. 34 are shown. Below, SP8-CRM zoom in for the visualization of the DLX (purple) and SP1 (orange) putative binding motifs found with the Mat Inspector tool within the region. Expression of A) *Sp6* and D) *Dlx5/6* in E10.5 forelimbs of WT and *Sp8*^{-/-} embryos by ISH. Fold change obtained in the RNA-seq indicated above.

In summary, this analysis identifies the network of SP8 target genes that include the major regulators of PD and DV patterning in the limb ectoderm confirming SP8 as an essential node in the limb bud ectoderm.

SHFM and *Wnt10b*

Our results revealed that *Wnt10b* is a direct target of SP8. Different homozygous mutations in the genomic region of *Wnt10b* were found in patients with SHFM6 (MIM 225300). Two missense mutations (p.Arg332Trp; p.Thr329Arg) were reported (Khan et al., 2012, Ugur and Tolun, 2008) in familiar cases, which could potentially change WNT10B structure affecting its interaction with other proteins. Duplications and deletions were also found. A 4 bp homozygous duplication in exon 4 (c.458_461dupAGCA) would lead to a frameshift in the protein, resulting in a premature TAA termination (Blattner et al., 2010). In addition, two mutations were identified by Aziz et al., (2014) in two different families. First, a 4 bp deletion (c.1165_1168delAAGT) which results in the incorporation of 36 illegitimate amino acids and a new termination (p.Lys388Glufs*36) creating a conformational shift which might affect FZD8 binding. Second, a 7 bp duplication (c.300_306dupAGGGCGG) created a premature stop codon (TGA) probably affecting the function of the protein. Recently, Kantaputra et al., (2018) identified a deletion of 3 bp predicted to cause a single amino acid deletion (p.Asn232del) disrupting protein structure.

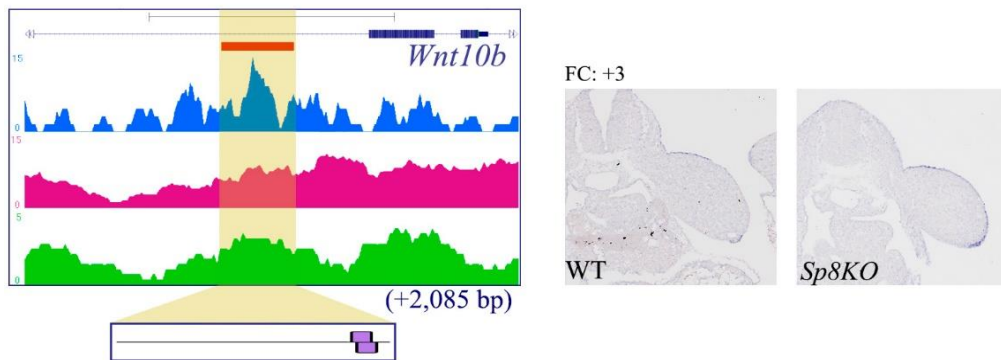


Figure 39. UCSC genome browser view of the *Wnt10b* regulatory landscape and *Wnt10b* expression in *Sp8* null embryos. Same tracks as in Fig. 34 are shown. Below, SP8-CRM zoom in for the visualization of the DLX (purple) and SP1 (orange) putative binding motifs found with the Mat Inspector tool within the region. Expression of *Wnt10b* in E10.5 forelimbs of WT and *Sp8*^{-/-} embryos by ISH. Fold change obtained in the RNA-seq indicated above.

In the absence of normal WNT10B expression, SHFM phenotype develops. Unexpectedly, our results revealed that *Wnt10b* is repressed by SP8 as its expression level was increased in the *Sp8* mutant (fold change +3) along the dorsal ectoderm and AER (Fig. 39). The SP8 CRM associated to *Wnt10b* is located 2,085 bp downstream its TSS, and this region contains one DLX binding site.

4.1.15 Evaluation of selected enhancer activity by mouse transgenesis

The *En1* and the *Rspo2* putative enhancers were selected for functional testing in mouse transgenesis (Fig. 40). The SP8-bound region was extended considering the conservation across species and associated histone marks. The SP8 regulatory region associated with *En1* was 288 bp size and was located 19,543 bp downstream from the *En1* TSS (chr1:120,621,817-120,622,105). The region was extended to 1017 bp (Fig. 38A). The SP8 regulatory region associated with *Rspo2* was 466 bp size and was located 217,676 bp upstream from *Rspo2* TSS (chr15:43,388,494-43,388,960). The region was extended to 1484 bp (Fig. 38B). These two enhancers were cloned upstream of B-globin promoter, which drives LacZ reporter activity in the pSK-LacZ vector. The reporter construct was linearized for pronuclear injection at the Servicio de Transgenesis del Centro Nacional de Biotecnología (CNB, Madrid). Injected embryos will be harvested at the E10.5 for LacZ staining.

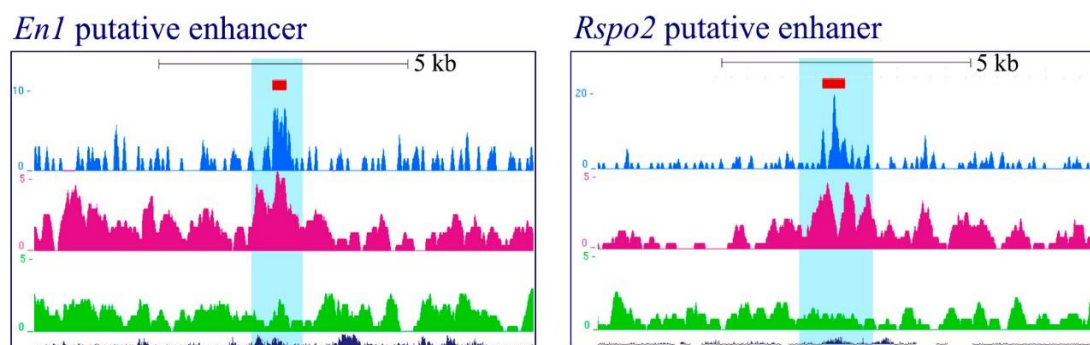


Figure 40. LacZ transgenesis. SP8-CRM associated with *En1* (red, 288 bp size) was extended to 1,017bp (left panel) and SP8-CRM associated with *Rspo2* (red, 466 bp size) was extended to 1,484bp (right panel). Amplified regions shown by a vertical blue shaded bar. Selected regions are highly conserved across vertebrate species. SP8-ChIPmentation, H3k4me2 and H3k27ac profiles are shown (blue, pink and green, respectively).

4.2 OBJECTIVE 2: Protein-Protein interactions

To further understand the functional redundancy between SP6 and SP8 we have also investigated their possible protein-protein interactions by CoIP and by Bimolecular Fluorescence Complementation (BiFC). The BiFC has the advantage that besides demonstrating interaction, it also permits the subcellular localization of this interaction.

For this, *Sp6* and *Sp8* were tagged with the MYC or FLAG epitope to the N-terminus by conventional PCR (see M&M). In addition, the C-terminus of these tagged proteins was fused in frame with the Yellow Fluorescent Protein (YFP) and with each of two non-fluorescent amino (YN; residues 1-172) and carboxy (YC; residues 173-240) moieties of the YFP. Fusion constructs were subcloned into the pcDNA3 expression vector for transient expression in HEK-293 cells (see M&M). The FLAG and MYC epitopes were used for the CoIP experiments following standard procedures, and the YFP and its moieties for the BiFC experiments.

SP6 and SP8 fused to the full-length YFP showed the expected nuclear localization of a TF and were used as positive controls of the transfections for the BiFC assays (Fig. 41A-B). The two YFP fragments, YN and YC, are not fluorescent by themselves, but they can re-associate and yield functional YFP, if brought in close proximity by the interaction between the proteins they are fused to. This is the rationale of the BiFC technique that has been probed very useful in the study of interactions among many different structural classes of TFs. Proteins fused to the moieties of the YFP (YN or YC) gave no signal when individually transfected and were used as negative control when individually transfected (data not shown).

Protein pairs comprised of *Sp8* and *Sp6*, and pairs of the same *Sp* fused with complementary YFP moieties were simultaneously transfected to assay for hetero and homodimerization. As mentioned, SP6-YFP and SP8-YFP showed nuclear localization (Fig. 41A-B). BiFC experiments co-transfecting SP8-YN + SP8-YC and SP6-YN + SP6-YC showed nuclear complementation indicating that both SP6 and SP8 can homodimerize (Fig. 41C-D). Similarly, co-transfection of SP8-YN + SP6-YC showed nuclear complementation indicating that SP6 and SP8 heterodimerize (Fig. 41E).

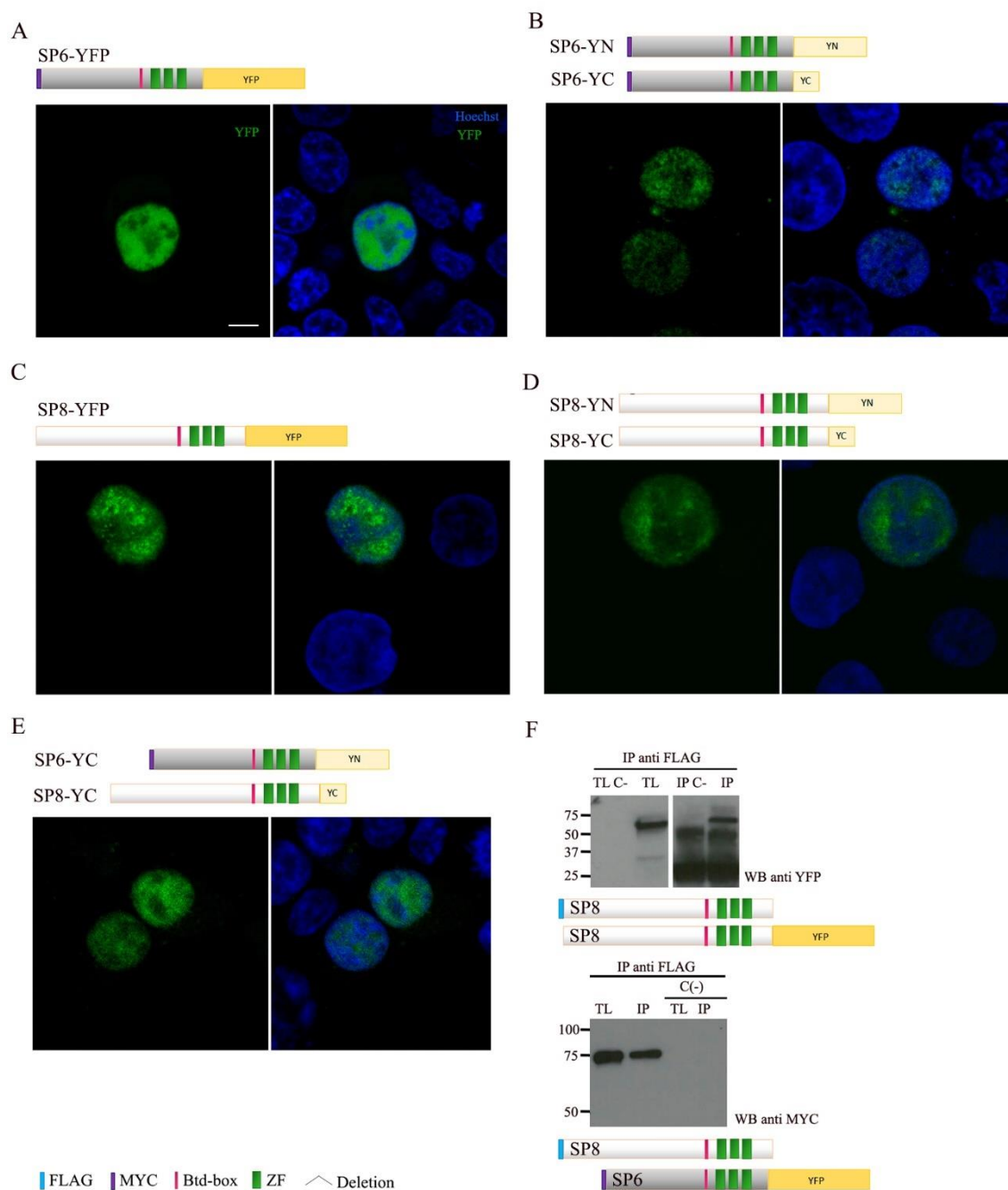


Figure 41. SP6- SP8 homo and heterodimerization. Representation of the constructs transfected above of each panel. **A)** Localization of SP8. **B)** BiFC of co-transfected SP6-YN and SP6-YC. **C-D)** Idem for SP8. **E)** BiFC of the co-transfected SP8-YN and SP6-YC. **F)** CoIP for homodimerization of SP8 (top) and heterodimerization of SP6-SP8 (bottom). Below each WB are shown the clones used. Hoechst (blue) stains the nuclei and YFP (green) shows the resulting protein interaction. On each experiment is shown YFP channel (first column), and Hoechst + YFP channels (second column). Scale bar: 10 μ m. FLAG antibody is used for immunoprecipitation and YFP and MYC for WB detection. TL (Total Lysate), C- (Negative control), IP (Immunoprecipitation).

Homodimerization of SP8 and heterodimerization with SP6 was also confirmed by CoIP (Fig. 41F).

To find out which region of the protein was mediating these interactions, 5 different truncations of the SP8 were generated (see M&M). First, construct $\Delta(1-126)$ SP8 lacks the N-terminal region that is a low complexity region enriched in Ser-Ala-rich. Second construct, $\Delta(1-241)$ SP8, bears a bigger truncation of the N-terminal region that in addition includes the Gly-rich region. Third, $\Delta(1-331)$ SP8 construct lacks the low complexity region, until the BTD-box (332-337 aa). The fourth truncated form, $\Delta(353-487)$ SP8, lacks the ZF domain (358-438 aa) and C-terminal region. Finally, $\Delta(440-487)$ SP8 lacks just the C-terminal region located 3' to the ZF domain, maintaining the remaining protein. Note that all the truncations contain the BTD-box.

Each SP8 truncation was N-terminal tagged with MYC and fused at the C-terminal to the YFP, YN or YC generating then 3 constructs for each truncated form. Truncation forms fused to the YFP permitted the analysis of their subcellular localization (Fig. 42-43, A-B). BiFC assays for SP8 homodimerization using the designed truncated forms showed that the ZF domain of the protein was the responsible for its interaction. Positive BiFC signal was observed when the $\Delta(1-126)$ SP8, $\Delta(1-241)$ SP8 and $\Delta(1-331)$ SP8 truncated forms were transfected but not when the $\Delta(353-487)$ SP8 construct was used (Fig 42, 43) indicating that the ZF domain was responsible for the homodimerization of SP8.

SP8 full-length (FLAG-SP8) was co-transfected with each SP8-truncation (MYC-tagged and YFP fused) for CoIP assays. Anti-FLAG antibody was used for immunoprecipitation and anti-MYC antibody for western blots with TLs loaded as positive controls in the same order as the IP products (Fig. 44A). This confirmed the BiFC results and the requirement of the ZF domain for the SP8-SP8 protein interaction. In addition, to rule out a possible function of the more C-terminus region to the ZF domain in SP8 homodimerization, an additional truncation ($\Delta(440-487)$ SP8) was designed which lacked the C-terminal domain of SP8 but kept the ZF domain (Fig. 44B). The CoIP assay with this $\Delta(353-487)$ SP8 isoform was negative, indicating that the ZF domain was specifically responsible for SP8 homodimerization and not the rest of the C-terminal region of SP8. BiFC assays were also used to investigate the SP8

protein domain involved in heterodimerization with SP6. To this end, pairs of the SP6-full-length and each of the different SP8 truncations were co-transfected. Interestingly, all these protein pairs showed fluorescence, although the fluorescence intensity was lower when the ZF domain was absent (Fig. 42E-F and 43E-F). This result suggests that, in addition to the ZF domain, SP6 and SP8 may interact through other domains.

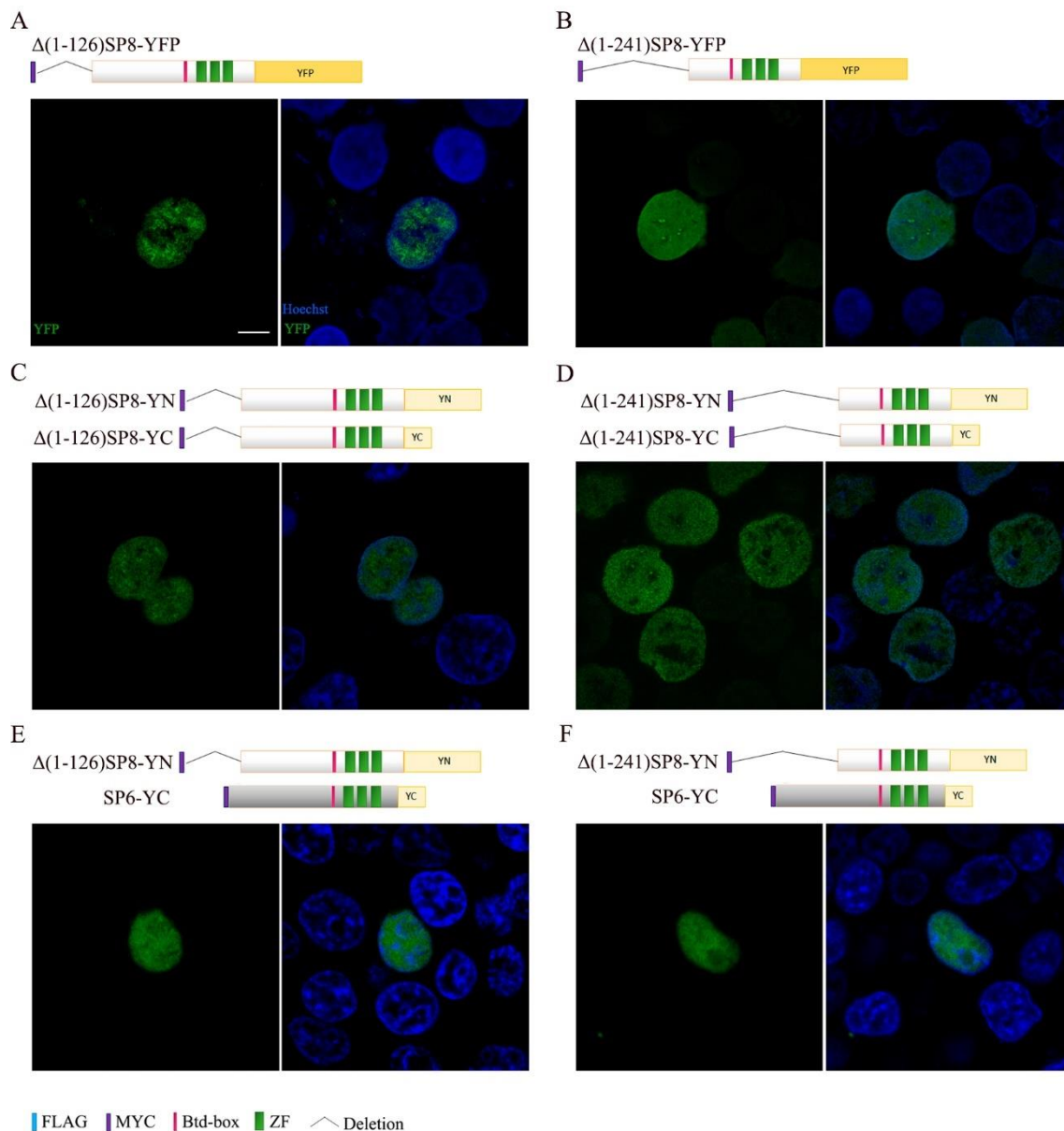


Figure 42. Interactions of $\Delta(1-126)$ SP8 and $\Delta(1-241)$ SP8 deletions by BiFC. First row, fused protein with YFP showing its localization. Second row, homodimerization of SP8-deletion and third row heterodimerization of the SP8 deletion with the SP6 (full-length). **A, C, E)** $\Delta(1-126)$ SP8 deletion. **B, E, F)** $\Delta(1-241)$ SP8 deletion. Scale bar: 10 μ m.

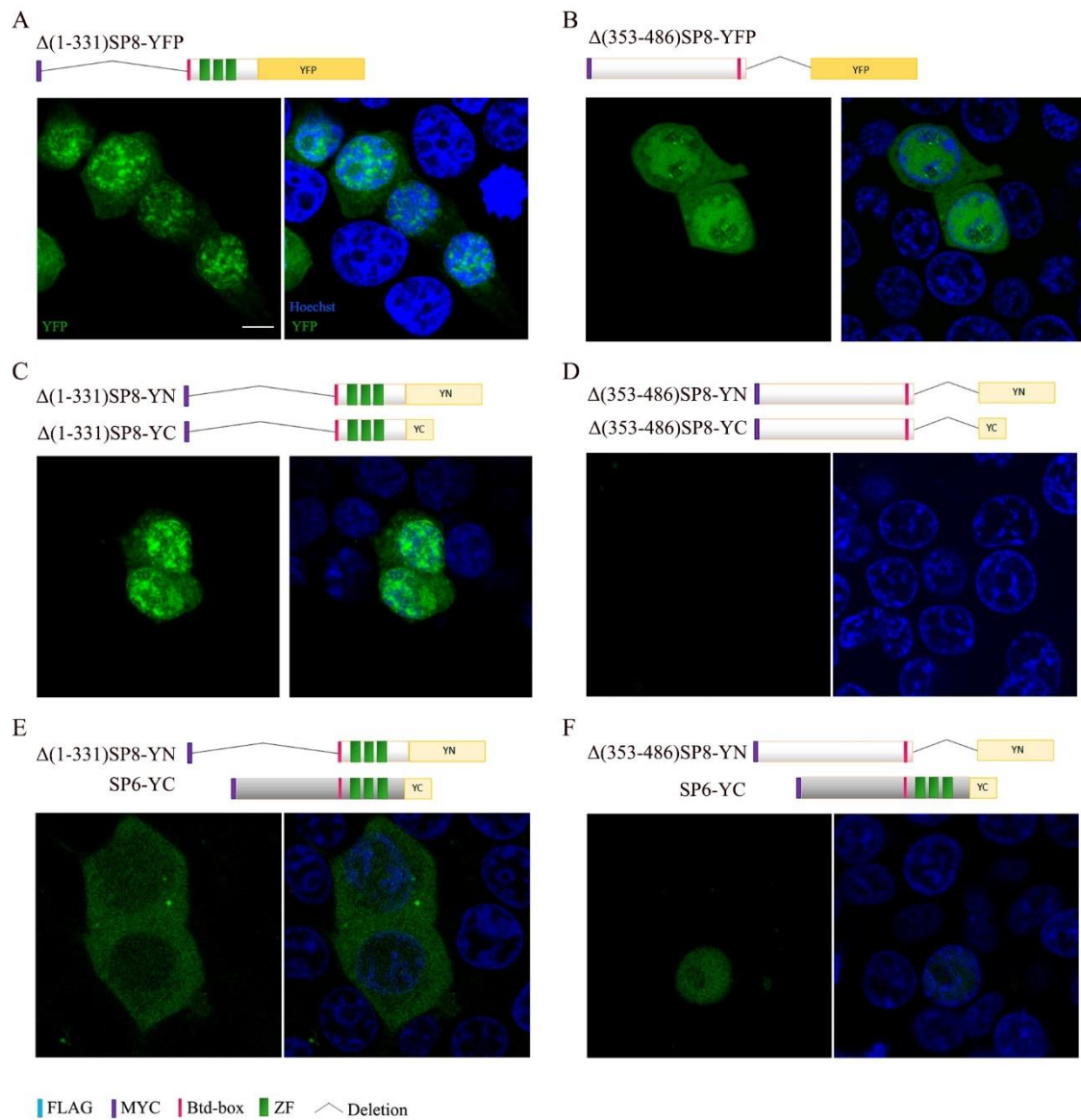


Figure 43. Interactions of $\Delta(1-331)SP8$ and $\Delta(353-487)SP8$ deletions by BiFC. First row, fused SP8-deletion with YFP showing its localization. Second row, homodimerization of SP8-deletion and third row heterodimerization of the SP8 deletion with the SP6 (full-length). **A, C, E**) $\Delta(1-331)SP8$ deletion. **B, E, F**) $\Delta(353-487)SP8$ deletion. Scale bar: 10 μ m.

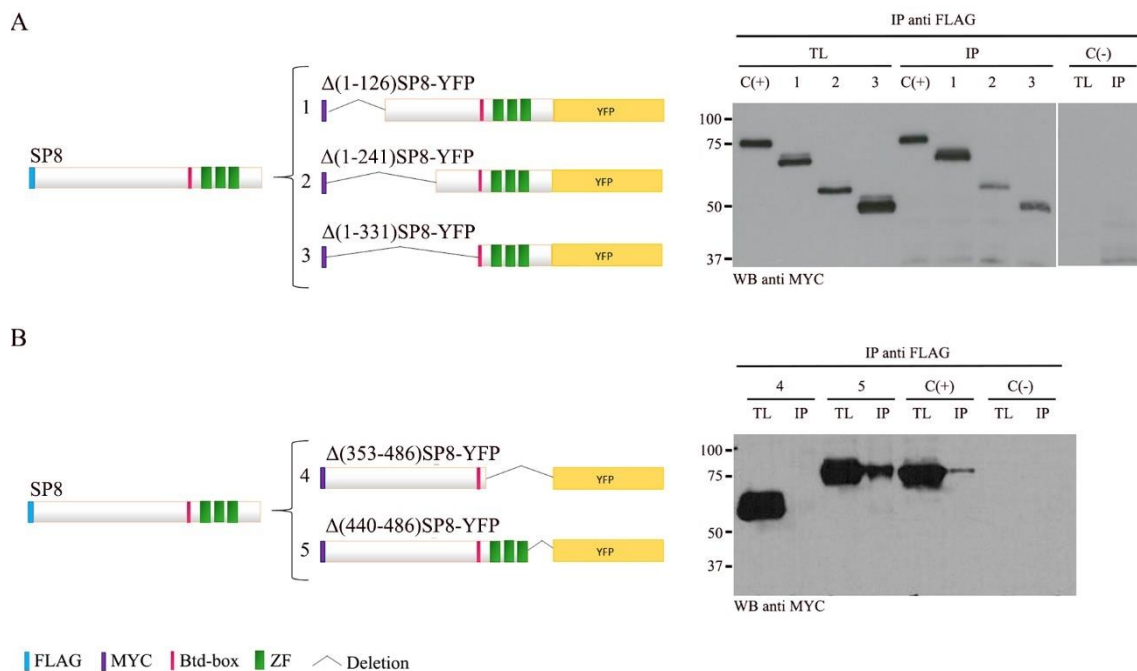


Figure 44. Interaction of SP8 deletions by CoIP. CoIP for homodimerization of SP8-deletions. SP8 full-length (with FLAG epitope) was co-transfected with each SP8-deletion (with MYC epitope). On the right the scheme of the clones co-transfected in each blot. Note that each deletion : $\Delta(1-126)$ SP8, $\Delta(1-241)$ SP8, $\Delta(1-331)$ SP8, $\Delta(353-487)$ SP8 and $\Delta(440-487)$ SP8 was numbered from 1 to 5, respectively for the WB panel. **A)** $\Delta(1-126)$ SP8, $\Delta(1-241)$ SP8 and $\Delta(1-331)$ SP8 deletions. **B)** $\Delta(353-487)$ SP8 and $\Delta(440-487)$ SP8 deletions. Immunoprecipitation was done with anti-FLAG and WB detection with anti MYC antibodies. TL (Total Lysate), C+ (positive control), C- (negative control), IP (Immunoprecipitation).

The subcellular localization of the different SP8 truncations merits some consideration. SP8 localized to the nucleus, as well as the two first truncations, $\Delta(1-126)$ SP8 and $\Delta(1-241)$ SP8 (Fig. 42A-B). However, $\Delta(1-331)$ SP8 and $\Delta(353-487)$ SP8 besides nuclear localization, were also detected in the cytoplasm (Fig. 43A-B). The BiFC signal of $\Delta(1-331)$ SP8 homodimerization was also found in nucleus and cytoplasm (Fig. 43C). Surprisingly, the BiFC signal produced by co-transfection of SP6 full-length and $\Delta(1-331)$ SP8 showed a predominant cytoplasmic localization.

This could be explained by a disruption in a Nuclear Localization Signal (NLS) when truncating SP8. SP1 has no classical NLS (Ito et al., 2010) but its three zinc finger domains were reported to play a NLS role, being transported to the nucleus in an importin-dependent manner. The SP5 NLS has been identified between the ZF and btd-

Results

box (Kennedy et al., 2016). We checked for putative NLS in silico, but predicted NLS varied according to the algorithm used (Fig. 44). Putative NLS obtained with the SeqNLS algorithm developed by (Lin and Hu, 2013) gives a region in between BTD-box and ZF domain (341-353aa), in accordance with the SP5-NLS. However, all SP8 truncations conserved this region. cNLS mapper tool predicts 3 putative NLS for SP8 (373-400; 408-437; 408-440) being these regions within the ZF domain, which could explain the cytoplasmic localization for $\Delta(353-487)$ SP8, but not for $\Delta(1-331)$ SP8.

```
MLAATCNKIGSPSPSSLDSSSSFGKGFHPWKRSSSSSSGSCNVVGSLSLSSFGVSGAS
RNGGSSSAAAAAAAAAAAAAAAAALVDSFSCGGSPGSSAFSLTSSSAAAAAAAAAAAAAS
SSPFANDYSVFPQPGVSGGSGGGGGGGGGGSGAHSQDSSHQPVFISKVHTSVDGLQG
IYPRVGMHPYESWFKPSHPGLGAAADVGSAGASSWWDVVGAGWIDVQNPNGAAAL
PGSLHPAAGGLQTSLSPLGGYNSDYSGLSHSAFSSGASSHLLSPAGQHLMDFKPV
PGSYPDSAPSLAGAGSSMLSAGPAAQLGGSPRSSARRYSGRATCDPCNCQEAERLGP
AGASLRRKGLHSCHIPGCGKVYGKTSHLKAHLRWHTGERPFVCNWLFCGKRFTR
SDELQRHLRTHTGEKRFACPVCNKRFMRSDHLSKHVKTHSGGGGSAGSGGGKKG
SDTDEHSAAGSPPCHSPELLQPPEPGHRNGLE
```

BTD-box	Zinc Finger
	cNLS mapper prediction
	SeqNLS prediction

Figure 44. Nuclear Localization Signal prediction in the amino acid sequence of SP8 (486aa). Highlighted NLS prediction with the cNLS mapper (yellow) and seqNLS (blue), Btd box (red) and the three ZF in bold.

To summarize, we showed that SP6/SP8 form homo and heterodimers, being the ZF domain essential for SP8 homodimerization.

5. DISCUSSION

5. DISCUSSION

In amniotes, the limbs derive from limb buds formed by the accumulation of proliferating limb progenitor cells under the surface ectoderm (Gros and Tabin, 2014). These multipotent progenitors are specified by a battery of TFs (Takeuchi, 2003) and characterized by the expression of Fibroblast Growth Factor 10 (FGF10), which is responsible of inducing *Fgf8* in the surface ectoderm generating the apical ectodermal ridge (AER). The AER is a crucial signaling center for limb outgrowth and patterning (Fernandez-Teran and Ros, 2008). Understanding the mechanisms that lead to the formation of the AER and its precise and enigmatic position at the dorso-ventral (DV) boundary is of maximum interest not only for development but also for regeneration and evolution studies. Even though important regulators have been identified, the gene regulatory networks (GRN) in which they are embedded are not completely known. These GRN are dynamic and complex and may operate only within the mesoderm, only within the ectoderm or across compartments.

Our group has previously shown that SP6 and SP8, two members of the SP family of TFs expressed in the limb ectoderm, are together absolutely necessary for AER induction (Haro et al., 2014; Talamillo et al., 2010). *Sp6* and *Sp8* are functionally equivalent and their conjoint removal leads to tetra-amelia. Most interestingly, the progressively reduction of the *Sp6;Sp8* gene dosage produces progressively more severe limb morphologies that go from a mild syndactyly, to SHFM, to oligodactyly, to truncation and finally to amelia (see figure 15). In addition, these malformations associate DV patterning defects (see figure 11).

The molecular characterization of the limbs of the *Sp6;Sp8* allelic series led us to propose that SP6 and SP8 are direct transcriptional activators of *Fgf8*, downstream of WNT/ β -CATENIN signaling, and that they mediate *En1* activation, downstream of or in parallel to BMP signaling (Haro et al., 2014). Our study clearly exposed that SP6/8 formed an important node in the gene regulatory networks operating in the limb ectoderm at a crossroad between PD and DV patterning (see figure 10).

Here, to extent our knowledge of how SP6 and SP8 play this essential role, we have carried out a genome-wide CHIP-seq approach complemented with a RNAseq-

based approach to explore the direct transcriptional activity of SP8 specifically in the limb bud ectoderm. In addition, we have used Co-immunoprecipitation and Bimolecular Fluorescent Complementation assays to evaluate some of its protein-protein interaction.

Previously to our study very little information was available on the regulatory elements bound by SP8 during development. Indeed, this was practically limited to in vitro assays showing SP8 binding to a *Fgf8* promoter sequence containing SP1-like binding sites (Sahara et al., 2007b) and to a more recent study of SP8 binding to the *Ccnd1* locus (Borello et al., 2018). However, a genome-wide study of the SP8-DNA associations in limb development was missing.

5.1 Characterization of the SP8 cisome in vivo in the limb bud ectoderm

Due to the lack of ChIP grade commercial anti-SP8 antibodies and the difficulties that we experienced in purifying the protein, we generated a 3xFLAG epitope-tagged *Sp8* allele. *Sp8^{FL}* homozygous were viable and fertile and phenotypically indistinguishable from wild type. The use of an anti-FLAG specific antibody permitted the easy detection of SP8 protein that showed a normal pattern of expression. We have used the *Sp8^{FL}* mouse model to identify the genomic regions enriched in SP8 binding complexes in the early forelimb ectoderm in vivo by ChIPmentation.

Several criteria, including evolutionary conservation, overrepresentation of expected specific binding sites, chromatin state and reproducibility between biological replicates proved the high quality of the ChIPmentation dataset establishing the *Sp8^{FL}* mouse model as a very useful tool for studying SP8 in its natural state. It permits experiments of immunoprecipitation, western blot and immunohistochemistry without the need for specialized antibodies using anti-FLAG specific antibodies. This model can be used to identify the SP8 chromatin in other developmental contexts besides the limb bud ectoderm such as the neural tube, in which SP8 plays a relevant function (Bell et al., 2003; Treichel et al., 2003).

The bioinformatic analysis of the set of SP8 bound regions showed that SP8 occupied genomic sites were equally distributed between promoters and distal cis-regulatory elements (GREAT, single nearest gene).

The overlapping with histone marks indicated SP8 targets regions with high levels of marks typical of active promoter and primed enhancers. The majority of distal CRM seem to only have H3K4me2 and not H3K27ac, indicating an overrepresented primed state instead of active. The fact that many CRM are putative primed and not active enhancers could be due to different possibilities. It is possible that those CRM are active in only a small part of the ectoderm (e.g AER) and therefore the decoration of H3K27ac is too diluted. Another plausible explanation is that at E10.5 enhancers present a primed state, which will turn into an active state at later stages. This would require further analysis.

When using the basal plus extension rule, SP8 occupied genomic sites were preferentially found in distal primed enhancers, associated with the canonical and non-canonical WNT pathway and early embryo and limb development. In contrast, SP8-bound promoters coupled with more general cellular processes. All these results nicely fit with previously known or suspected SP8 activities in limb development.

De novo motif discovery uncovered that SP8 is more likely to interact with a GC box in proximal promoters and through AT-rich motif (DLX-like) in distal CRM, possibly through association with DLX5. It should be noted that, the comparison of the set of SP8 distal CRM with other published enhancer datasets gave a very low overlapping. This fact was expected having into account that the SP8 ChIP-seq was generated from a very specific and minority cell population, as is the limb ectoderm in the limb bud.

5.2 SP8 direct targets

To distinguish functional from non-functional binding we correlated the SP8 chromatin binding profile with genes differentially expressed upon knockout of SP8. With this purpose, the expression profile of the limb ectoderm of wild-type and *Sp8*-null embryos were generated and compared to identify differentially expressed genes that were considered to contain both direct and indirect SP8 transcriptional target genes. Out of the 892 DEG, 519 were downregulated and 373 upregulated in the *Sp8KO*. Binding of SP8 in a gene locus was considered functionally relevant if this gene was

differentially expressed upon knockout of *Sp8*. This strategy defined 184 SP8 direct targets of which 129 were activated by SP8 reflecting a certain predominance of the SP8 transcriptional activation function versus its transcriptional repression.

As expected, the set of 184 identified SP8 target genes contained all genes previously known to be regulated by SP8, including *Fgf8*, *En1*, *Wnt7a*, *Sp6*, *Msx1*, *Msx2* and *Dlx* genes, among others. The majority of these limb relevant genes are activated by SP8.

5.3 DLX5 transcription factor is a SP8 cofactor

Our data reveal the complex mode of SP8 DNA interaction: directly binding to the consensus GC-box sequence and indirectly engaging through association with other TFs. We also provide strong evidence of DLX5 and other family members being important associated factors during limb development.

All SP family members were thought to share the same DNA recognition site, the GC box (Suske., 1999), but recently SP7 has been shown to use a distinct mode of action. SP7 is the only member of the SP family that does not bind the consensus GC-rich motif but binds DNA through DLX5 interaction (Hojo et al., 2016). Interestingly, *de novo* motif discovery in SP8-bound genomic regions, besides the expected overrepresentation of the consensus GC-rich motif, also exposed the DLX5 AT-rich motif as the second top scored motif. Moreover, the DLX motif was the top scoring motif when only SP8 direct targets were considered. These results made us to consider the possibility that SP8 could also use the SP7 mode of DNA-binding, a hypothesis that was reinforced by the demonstration by CoIP that SP8 can bind DLX5. Similarly to SP7, we also show that SP8 binds DLX through its ZF domain.

During development, *Dlx* genes are expressed in craniofacial primordia, basal telencephalon and diencephalon, and in the limb bud and genital tubercle (Robledo et al., 2002). In the limb bud ectoderm, the domains of expression of *Sp6/8* and several *Dlx* genes overlap permitting the interaction between these two TFs. DLX proteins bind DNA through their homeodomain and their transcriptional activity may be modulated

by other TFs such as MSX1/2 (Satokata and Maas, 1994) in craniofacial development and SP7 in bone development (Hojo et al., 2016).

SP7 distinct mode of action is due to the presence of three variant amino acid residues in the ZF domain that impair the interaction with the GC-box while favoring DLX binding (Hojo et al., 2016). Despite our results strongly indicate that SP8 interacts with DLX for gene regulation, SP8 does not present the SP7 variants allowing the conclusion that these amino acid variants are not required for DLX5 binding but rather act in impairing GC box recognition. Overall, our results are compatible with SP8 being able to interact through its ZF domain with the GC box as well as with DLX proteins. Because the ZF domain is the domain needed for these two types of interactions, it seems likely that the presence of DLX5 or other family members “sequester” SP8 therefore potentiating DLX5 mediated targets while attenuating direct binding dependent targets. In addition, to test the biological relevance of *Sp8* and *Dlx5* on reporter gene activity, we plan to perform in vitro reporter essays using AT-rich motif constructs. Moreover, to corroborate that SP8 binds AT-rich motifs using DLX5 as a cofactor, an electrophoretic mobility shift assay is an appealing idea.

To weight the importance of DLX in SP8-dependent regulation, we categorized SP8 target genes according to the presence of SP1-like and DLX binding sites in four groups: target genes with only SP1-like binding motifs, target genes with only DLX binding motifs, target genes with both types of binding motifs, and target genes with none of these binding motifs. This showed that approximately one third of the SP8-direct targets were absolutely dependent on DLX interaction, as only DLX sites were present in their associated CRMs. Analysis of *Sp;Dlx* compound mutants will be particularly interesting in this respect.

An additional level of regulation between *Sp8* and *Dlx* genes is given by the fact that all *Dlx* genes are very likely SP8 activated direct targets and these are controlled through CRM containing mainly SP1-like binding sites. It is worth nothing here the high degree of functional conservation of all these interactions between vertebrates and flies. In *Drosophila*, both *Btd* and *Sp1* (the homologues of *Sp5* and *Sp8* respectively) are involved in leg development with *Sp1* playing a much more important role acting as a leg selector gene upstream of *Dll* (Estella et al., 2003; Estella and Mann, 2010).

Most interesting was the presence of a small percentage of target genes that did not show SP1-like or DLX binding motifs indicating that SP8 must have additional interactors. SP1 and other family members associate with coregulatory proteins in a cell context-dependent manner reflecting the complexity of SP mode of action. In addition, SP1, the first mammalian TF characterized and the best-known member of the SP family, and other SP family members forms homo and heterodimers (Pascal and Tjian, 1991). In this regard, we show here by CoIP and BiFC that SP6 and SP8 form dimers and heterodimers and that this interaction is also mediated by the ZF domain. The functional relevance of SP6 and SP8 homo and heterodimers remain to be investigated.

Thus, SP interaction between family members in the limb bud ectoderm or with different cofactors such as DLX proteins, may significantly impact SP8 regulation. Such protein-protein interactions may result in sequestering one or both proteins. If the hypothesis of inhibition by sequestering is correct, then some of the defect observed in *Sp6*, *Sp8* or *Dlx* mutants might be due to improper or excessive activation of target genes of the TFs that remain.

5.4 Interactions of the SP8 GRN with the WNT canonical pathway

It is well-known that WNT/ β -CATENIN signaling is absolutely required in the limb ectoderm for *Fgf8* activation (Barrow et al., 2003; Soshnikova et al., 2003b) and that this function is mediated by SP6/8 (Haro et al., 2014). The WNT-SP8-FGF8 genetic pathway is a conserved cassette employed not only in the formation of the limb but also in other contexts such as the genital tubercle (Lin et al., 2013).

Recently, it has been shown that, besides activating some of the WNT/ β -CAT direct targets, SP5/8 are also capable of binding chromatin-bound TCF/LEF to facilitate recruitment of β -CATENIN and activate a subset of WNT target genes (Kennedy et al., 2016). Accordingly, in the limb bud ectoderm SP8 targets enhancers of components of the WNT pathway including *Fzd1*, *Wnt5a* and *Rspo2* to potentiate WNT signaling. Particularly important is the regulation of RSPO2, a secreted agonist of the canonical WNT/ β -CATENIN signaling pathway. RSPO2 binds to the G-protein-coupled receptors LGR4, LGR5 and LGR6 to recruit the RNF43 and ZNRF3 E3 ligases and prevent

degradation of the FRIZZLED (FZD) receptors (Lau et al., 2014). Surprisingly, it has recently been shown that RSPO2 and RSPO3 can block RNF43 and ZNRF3 function independently of LGR4/5/6 genes (Lebensohn and Rohatgi, 2018; Szenker-Ravi et al., 2018).

GO analysis of SP8-CRM showed the WNT pathway as one of the most representative, but this enrichment was attenuated when only considering SP8 direct targets. We interpreted this result as SP8 mediating transactivation of WNT/B-CATENIN target genes through the modulation of R-SPON2. *Rspo2*^{-/-} mutant mice present limb truncations (Aoki et al., 2008; Nam et al., 2007) that are exacerbated upon the additional removal of *Rspo3*, demonstrating functional redundancy of these genes (Neufeld et al., 2012). DV patterning defects have also been reported in *Rspo2* mutants (Aoki et al., 2008).

A major target of WNT signaling in the limb bud ectoderm is *Fgf8*, the marker of the AER and absolutely necessary for limb development. Our bioinformatic analysis, paid special scrutiny on a region that contains a coherent integrated regulatory ensemble for *Fgf8* (Marinić et al., 2013) and also in the *Fgf8* proximal promoter (Sahara et al., 2007b) where the *in silico* analysis shows abundant SP1-like binding sites and where we were expecting to find multiple SP8 binding regions. Nearly 50 *Fgf8*-regulatory modules have been identified in a 220 kb region centromeric to the gene, many of them embedded in the *FBXW4* gene (Marinić et al., 2013). Several of these enhancers show overlapping AER activity. SHFM3 (OMIM 246560), a condition that may associate micrognathia and hearing disorders (de Mollerat et al., 2003; Dimitrov et al., 2010), is caused by duplications of this genomic region that modify the genomic architecture and results in altered *Fgf8* expression.

However, our analysis showed no SP8 binding in this intricate *Fgf8*-regulatory region comprising multiple genes, but only in the promoter region indicating that SP8 controls *Fgf8* expression by directly binding to its promoter. The mouse *Fgf8* promoter is considered to span about 700 bp upstream the transcriptional start site. Its proximal region is highly conserved in mammals and the entire region is decorated by promoter-associated histone marks in *Fgf8*-expressing tissues (Shen et al., 2012). This region contains several putative SP1-like sites and it has been previously shown that SP8

recognizes and binds to these sites activating the *Fgf8* expression (Sahara et al., 2007b). Thus, SP8 controls *Fgf8* expression through direct binding to GC boxes in its promoter. It is very likely that SP6 and at later stages SP9 also participate in the modulation of *Fgf8* expression.

5.5 The SP8 GRN and DV patterning

The anatomy of the limb is clearly polarized in the DV axis. In the skeleton these asymmetries are absolutely required for normal function. On the surface, DV asymmetries are also obvious, hair and nails are dorsal structures while footpads and eccrine glands are ventral.

By the time the limb bud emerges, the pre-limb ectoderm is patterned in specific domains of gene expression. The prospective ventral ectoderm expresses *En1*, which functions to restrict *Wnt7a* expression to the dorsal ectoderm. During normal development the AER always forms at the interface between the *Wnt7a* and *En1* domains reflecting a tight link between AER formation and DV patterning. Based on the analysis of the *limbless* and *En1* mutants and on misexpression experiments in chick, it was hypothesized that a DV boundary was a prerequisite for AER formation (Ros et al., 1996). This view was further supported by the observation that the ectopic juxtaposition of dorsal and ventral limb ectoderm induced the formation of ectopic AERs (Laufer et al., 1997; Tanaka et al., 1997). However, there are several examples of normal AERs forming in the absence of a DV boundary, such as in the *eudiplopodia* and double *Wnt7a;En1* mutants (reviewed in Fernandez-Teran and Ros., 2008).

It was latter shown that WNT and BMP signaling played a key role both in DV patterning and AER induction (Ahn et al., 2001b; Barrow et al., 2003; Pizette et al., 2001; Soshnikova et al., 2003b). The interaction between these signaling pathways is complex and not completely understood. BMP signaling works upstream of WNT/ β -CAT to induce *Fgf8* while it works downstream or in parallel to induce *En1* in the ventral ectoderm. More recently we showed that SP6 and SP8 were essential TFs mediating both WNT and BMP signaling in the induction of *Fgf8* and *En1* respectively (Haro et al., 2014). Here we provide new evidence on how SP8 accomplishes this

function. We show that SP8 activates both *Wnt7a* and *En1* from distally located enhancers (type of binding sites) revealing an unexpected complexity in the regulation of the DV patterning.

A major question to understand is how the three compartments are established in the pre-limb bud ectoderm and how SP8, that initially is expressed throughout the whole ectoderm but progressively confined to the AER can participate in the generation of these defined compartments of expression.

5.6 SHFM

The double *Sp6;Sp8* mutant that retains a functional copy of *Sp8* (*Sp6^{-/-};Sp8^{+/-}*) consistently display SHFM and is, therefore, an excellent animal model to investigate the etiology of this malformation. As explained in the Introduction, the SHFM is a highly variable malformation of the hand and/or foot characterized by the loss or deformity of the central rays that leads to a central cleft and the subsequent split appearance. SHFM is also termed ectrodactyly and cleft hand (Duijf et al., 2003; Elliott and Evans, 2006; Gurrieri and Everman, 2013). In humans, the non-syndromic SHFM is a genetically heterogeneous and rare congenital malformation. It has an incidence of 1 per 8,500–25,000 live born infants representing 8-17 % of all limb malformations (Elliott et al., 2005, 2006; Elliott and Evans, 2006).

A striking and constant feature of SHFM is the phenotypic variability. The spectrum of morphologies ranges from the mildest cases of soft tissue syndactyly to the most severe cases in which all digits are lost and, remarkably, the two ends of this phenotypic spectrum can occur in the same individual. This proves that syndactyly, SHFM, oligodactyly and amelia can have a common genetic origin (Omri Schatz et al., 2014) and reflects how the genotype-phenotype relationships are based on complex networks and molecular interactions that may be subject to some variability. Remarkably, the limb phenotypes of *Sp6;Sp8* double mutants reproduce the whole spectrum of SHFM limb morphologies, therefore being an excellent animal model to unravel the molecular and cellular mechanisms involved in the generation of this malformation.

Despite the genetic heterogeneity in SHFM, a convergence towards the TP63 network can be clearly appreciated. TP63, responsible for SHFM4, is an upstream regulator of *Dlx* genes, responsible for types 1 (DLX5/6) and probably type 5 (DLX1/2) (Kouwenhoven et al., 2010; Lo Iacono et al., 2008b). SHFM3 is caused by duplications of the *Fgf8* regulatory landscape, a region in which TP63 and DLX binding sites are abundant (preliminary in silico analysis). Therefore, it seems likely that SHFM types 1, 3, 4 and 5 are due to defects in the TP63 network regulating *Fgf8* expression.

Since similar phenotypes are frequently caused by disruption of different components of a regulatory network, it seems likely that SP6/8 participate in the TP63 network. Our study uncovers an unexpected level of complexity given the fact that part of SP8 function is mediated by DLX-binding and that SP8 is a transcriptional regulator of all *Dlx* genes.

Also unexpected was the link with the SHFM6 found in our analysis. SHFM6 has been linked to mutations in the *Wnt10b* coding region, leading to an early STOP codon and/or changing the conformation of the resulting protein. In our analysis *Wnt10b* is a repressed direct target of SP8. One possible explanation is that the mutant versions of the protein represent a gain of function in the ectoderm. In this case, the SHFM phenotype of *Sp8* mutants could be mediated, at least partially, by WNT10B. In any case, if SP8 and WNT10B are in the same signaling pathway their interaction seems complex and requires further evaluation.

The implication of *Sp* genes in human SHFM has not been reported to date. However, the underlying cause remains elusive in a large number of cases and it is likely that there are more genetic loci than those so far identified. Here we present good evidence for a possible participation of SP8 in SHFM1 and SHFM5 through the modulation of the expression and function of *Dlx* genes and in SHFM6 through the modulation of *Wnt10b* expression.

6. CONCLUSIONS/ CONCLUSIONES

6. CONCLUSIONS

1. We have generated a 3xFLAG epitope-tagged *Sp8* allele (*Sp8^{FL}*) that is functionally normal. This model was successfully used to identify the genomic regions enriched in SP8 and can be used to identify the SP8 chromatin profile in other developmental contexts in which SP8 plays a relevant function.
2. Our study provides a genome-wide map of SP8 bound regions in the limb bud ectoderm improving our understanding of SP8 function.
3. SP8 bound regions are equally distributed between proximal and distal regions, when one gene per region was associated. *De novo* motif discovery predicted SP1-like GC-box and DLX5 AT-rich motif binding sites as the SP8 primary genomic interaction sites supporting a dual mode of SP8 function: direct binding to GC regions and indirect binding through DLX5 interaction.
4. Separate analysis of proximal versus distal regions revealed that SP8 binding to proximal regions was preferentially direct (through SP1-like motifs) while binding to distal regions preferentially occurred through interaction with DLX5 (DLX5 motifs). SP8 bound promoters coupled to genes associated with general cellular processes while SP8 bound distal enhancers associated with genes with specific embryonic and limb development functions.
5. We have generated by RNA-seq the expression profile of the limb bud ectoderm in wild type and *Sp8* mutants and identified the 892 genes differentially expressed.
6. By combining the ChIPmentation dataset and the set of genes differentially expressed in the absence of *Sp8*, we identified 184 direct targets in the ectoderm. Of these 129 were activated and 55 repressed by SP8.

Conclusions

7. SP1-like motifs were similarly enriched in repressed and activated SP8 direct targets while the DLX5 motif was the top scoring motif specifically in the set of activated SP8 target. This last set of genes is enriched in limb development terms and include all the genes known to be regulated by SP8.
8. Co-Immunoprecipitation using HEK-293 cells demonstrated that SP8 and DLX5 can physically interact. The ZF domain of SP8 is essential for this interaction.
9. The network of SP8 target genes included all major regulators of PD and DV patterning in the limb ectoderm.
10. SP8 controls *Fgf8* transcription through direct binding to GC boxes in its promoter.
11. SP8-dependent WNT pathway targets are likely mediated by the control of *Rspo2* expression.
12. The SP8-dependent GRNs operating in the limb ectoderm are particularly complex. SP8 activates both *En1* and *Wnt7a* through distal located enhancers. Sp8 transcriptional activity may work directly or indirectly to activate or repress target genes depending on the context.
13. SP8 and SP6 form homo and heterodimers. The ZF domain of SP8 is essential for this interaction.
14. We provide useful information for the interpretation of genetic studies assessing human congenital malformations.

6. CONCLUSIONES

1. Hemos generado un ratón que contiene el alelo *Sp8* tagueado con el epítipo 3xFLAG, siendo funcionalmente normal. Este modelo se ha utilizado para identificar las regiones genómicas enriquecidas en SP8 y puede ser usado para identificar el perfil de cromatina en otros contextos de desarrollo en los que SP8 juegue un papel relevante.
2. Hemos generado un dataset de la ChIPmentación de SP8 de alta calidad que es una fuente muy relevante para el estudio de la red reguladora dependiente de SP8 en el ectodermo de la extremidad.
3. Las regiones unidas por SP8 están igualmente distribuidas entre las regiones proximales y distales, cuando está asociado un gen por región. El descubrimiento de motivos *de novo* predijo el motivo de SP1, caja GC, y el de DLX5, motivo rico en AT, como principales sitios de unión de SP8 a regiones del genoma, avalando el modo de función dual de SP8: uniéndose directamente a regiones GC e indirectamente a través de la interacción con DLX5.
4. Un análisis independiente separando las regiones distales de las proximales reveló que la unión de SP8 a regiones proximales es preferentemente directa (a través de motivos SP1-like), mientras que la unión a regiones distales ocurre preferentemente a través de la interacción con DLX5 (motivos DLX). La unión de SP8 a los promotores de genes está asociada con procesos celulares generales, mientras que cuando SP8 se une distalmente a enhancers, los genes asociados tienen funciones específicas de desarrollo embrionario y de la extremidad.
5. Hemos generado por RNA-seq el perfil de expresión del ectodermo de la extremidad en wild type y en mutantes de *Sp8*, identificando 892 genes diferencialmente expresados.

6. Combinando el dataset de la ChIPmentación con el conjunto de los genes diferencialmente expresados en ausencia de *Sp8*, hemos identificado 184 targets directos en el ectodermo. De estos, 129 fueron activados y 55 reprimidos por SP8.
7. Los motivos de SP1-like fueron similarmente encontrados en los targets directos reprimidos y activados de SP8, mientras que el motivo de DLX5 fue el motivo con más alto score en el conjunto de targets directos activados por SP8. Este último conjunto de genes está enriquecido en términos del desarrollo de la extremidad e incluye todos los genes conocidos que están regulados por SP8.
8. Mediante Co-Inmunoprecipitación en células HEK-293 demostramos que SP8 y DLX5 pueden interactuar físicamente. El dominio de los dedos de zinc de SP8 es esencial para esta interacción.
9. La red de targets directos de SP8 incluye todos los reguladores importantes en el modelado del ectodermo de la extremidad.
10. SP8 controla la transcripción de *Fgf8* mediante la unión directa a cajas GC en su promotor.
11. Los targets de la vía de WNT dependientes de SP8 están mediados probablemente por el control de la expresión de *Rspo2*.
12. Las redes reguladoras de genes dependientes de SP8 que operan en el ectodermo de la extremidad son particularmente complejas. SP8 activa tanto a *En1* como a *Wnt7a* a través de enhancers localizados distalmente. La actividad transcripcional de SP8 puede funcionar directa o indirectamente para activar o reprimir genes diana dependiendo del contexto.
13. SP6 y SP8 forman homo y heterodímeros. El dominio de los dedos de zinc de SP8 es esencial para esta interacción.

14. Proporcionamos información de utilidad para la interpretación de los estudios genéticos que evalúan malformaciones congénitas humanas.

7. REFERENCES

8. REFERENCES

- Adamska, M., MacDonald, B.T., Meisler, M.H.,** 2003. Doubleridge, a mouse mutant with defective compaction of the apical ectodermal ridge and normal dorsal-ventral patterning of the limb. *Dev. Biol.* 255, 350–62.
- Adamska, M., MacDonald, B.T., Sarmast, Z.H., Oliver, E.R., Meisler, M.H.,** 2004. En1 and Wnt7a interact with Dkk1 during limb development in the mouse. *Dev. Biol.* 272, 134–144. doi:10.1016/j.ydbio.2004.04.026
- Ahn, K., Mishina, Y., Hanks, M.C., Behringer, R.R., Crenshaw, E.B.,** 2001. BMPR-IA signaling is required for the formation of the apical ectodermal ridge and dorsal-ventral patterning of the limb. *Development* 128, 4449–4461.
- Altabef, M., Clarke, J.D., Tickle, C.,** 1997. Dorso-ventral ectodermal compartments and origin of apical ectodermal ridge in developing chick limb. *Development* 124, 4547–4556.
- Altabef, M., Tickle, C.,** 2002. Initiation of dorso-ventral axis during chick limb development 116, 19–27.
- Alves, L.U., Pardon, E., Otto, P.A., Célia, R., Netto, M.,** 2015. A novel c . 1037C > G (p . Ala346Gly) mutation in TP63 as cause of the ectrodactyly-ectodermal dysplasia and cleft lip / palate (EEC) syndrome 41, 37–41.
- Anders, S., Huber, W.,** 2010. Differential expression analysis for sequence count data. *Genome Biol.* 11, R106.
- Andrey, G., Montavon, T., Mascrez, B., Gonzalez, F., Noordermeer, D., Leleu, M., Trono, D., Spitz, F., Duboule, D.,** 2013. A Switch Between Topological Domains Underlies HoxD Genes Collinearity in Mouse Limbs. *Science* (80-.). 340, 1234167–1234167. doi:10.1126/science.1234167
- Andrey, G., Schöpflin, R., Jerković, I., Heinrich, V., Ibrahim, D.M., Paliou, C., Hochradel, M., Timmermann, B., Haas, S., Vingron, M., Mundlos, S.,** 2017. Characterization of hundreds of regulatory landscapes in developing limbs reveals two regimes of chromatin folding. *Genome Res.* 27, 223–233. doi:10.1101/gr.213066.116
- Aoki, M., Kiyonari, H., Nakamura, H., Okamoto, H.,** 2008. R-spondin2 expression in the apical ectodermal ridge is essential for outgrowth and patterning in mouse limb development. *Dev. Growth Differ.* 50, 85–95. doi:10.1111/j.1440-169X.2007.00978.x
- Armour, C.M., Bulman, D.E., Jarinova, O., Rogers, R.C., Clarkson, K.B., DuPont, B.R., Dwivedi, A., Bartel, F.O., McDonell, L., Schwartz, C.E., Boycott, K.M., Everman, D.B., Graham, G.E.,** 2011. 17p13.3 microduplications are associated with split-hand/foot malformation and long-bone deficiency (SHFLD). *Eur. J. Hum. Genet.* 19, 1144–1151. doi:10.1038/ejhg.2011.97
- Aziz, A., Irfanullah, Khan, S., Zimri, F.K., Muhammad, N., Rashid, S., Ahmad, W.,** 2014. Novel homozygous mutations in the WNT10B gene underlying autosomal recessive split hand/foot malformation in three consanguineous families. *Gene* 534, 265–271. doi:10.1016/j.gene.2013.10.047
- Barrow, J.R., Thomas, K.R., Boussadia-zahui, O., Moore, R., Kemler, R., Capecchi, M.R., McMahon, A.P.,** 2003. ectodermal Wnt3 beta cantenin signaling is required for the establishment and maintenance of the apical ectodermal ridge. *Mol. Cell. Biol.* 394–409.

doi:10.1101/gad.1044903.ing

- Bastida, M.F., Delgado, M.D., Wang, B., Fallon, J.F., Fernandez-Teran, M., Ros, M.A.,** 2004. Levels of Gli3 repressor correlate with Bmp4 expression and apoptosis during limb development. *Dev. Dyn.* 231, 148–160. doi:10.1002/dvdy.20121
- Bastida, M.F., Sheth, R., Ros, M.A.,** 2009. A BMP-Shh negative-feedback loop restricts Shh expression during limb development. *Development* 136, 3779–89. doi:10.1242/dev.036418
- Bell, S.M., Schreiner, C.M., Scott, W.J.,** 1998. The loss of ventral ectoderm identity correlates with the inability to form an AER in the legless hindlimb bud. *Mech. Dev.* 74, 41–50. doi:10.1016/S0925-4773(98)00065-3
- Bell, S.M., Schreiner, C.M., Waclaw, R.R., Campbell, K., Potter, S.S., Scott, W.J.,** 2003. Sp8 is crucial for limb outgrowth and neuropore closure. *Proc. Natl. Acad. Sci. U. S. A.* 100, 12195–12200.
- Bell, S.M., Schreiner, C.M., Wert, S.E., Mucenski, M.L., Scott, W.J., Whitsett, J. a.,** 2008. R-spondin 2 is required for normal laryngeal-tracheal, lung and limb morphogenesis. *Development* 135, 1049–1058. doi:10.1242/dev.013359
- Benazet, J.D., Zeller, R.,** 2013. Dual requirement of ectodermal Smad4 during AER formation and termination of feedback signaling in mouse limb buds. *Genesis* 51, 660–666. doi:10.1002/dvg.22412
- Bénazet, J.D., Zeller, R.,** 2009. Vertebrate limb development: moving from classical morphogen gradients to an integrated 4-dimensional patterning system. *Cold Spring Harb. Perspect. Biol.* 1, 1–14. doi:10.1101/cshperspect.a001339
- Blattner, A., Huber, A.R., Röthlisberger, B.,** 2010. Homozygous nonsense mutation in WNT10B and sporadic split-hand/foot malformation (SHFM) with autosomal recessive inheritance. *Am. J. Med. Genet. A* 152A, 2053–6. doi:10.1002/ajmg.a.33504
- Boles, R.G., Pober, B.R., Gibson, L.H., Willis, C.R., McGrath, J., Roberts, D.J., Yang-Feng, T.L.,** 1995. Deletion of chromosome 2q24-q31 causes characteristic digital anomalies: Case report and review. *Am. J. Med. Genet.* 55, 155–160. doi:10.1002/ajmg.1320550204
- Borello, U., Berarducci, B., Delahaye, E., Price, D.J., Dehay, C.,** 2018. SP8 transcriptional regulation of Cyclin D1 during mouse early corticogenesis. *Front. Neurosci.* 12, 1–14. doi:10.3389/fnins.2018.00119
- Borello, U., Madhavan, M., Vilinsky, I., Faedo, a., Pierani, a., Rubenstein, J., Campbell, K.,** 2014. Sp8 and COUP-TF1 Reciprocally Regulate Patterning and Fgf Signaling in Cortical Progenitors. *Cereb. Cortex* 24, 1409–1421. doi:10.1093/cercor/bhs412
- Boulet, A.M., Moon, A.M., Arenkiel, B.R., Capecchi, M.R.,** 2004. The roles of Fgf4 and Fgf8 in limb bud initiation and outgrowth. *Dev. Biol.* 273, 361–372. doi:10.1016/j.ydbio.2004.06.012
- Burke, A.C., Nelson, C.E., Morgan, B.A., Tabin, C.,** 1995. Hox genes and the evolution of vertebrate axial morphology. *Development* 121, 333–346. doi:7768176
- Cartharius, K., Frech, K., Grote, K., Klocke, B., Haltmeier, M., Klingenhoff, a., Frisch, M., Bayerlein, M., Werner, T.,** 2005. MatInspector and beyond: Promoter analysis based on transcription factor binding sites. *Bioinformatics* 21, 2933–2942.

doi:10.1093/bioinformatics/bti473

- Chen, H., Lun, Y., Ovchinnikov, D., Kokubo, H., Oberg, K.C., Pepicelli, C. V., Can, L., Lee, B., Johnson, R.L.,** 1998. Limb and kidney defects in *Lmx1b* mutant mice suggest an involvement of LMX1B in human nail patella syndrome. *Nat. Genet.* 19, 51–55. doi:10.1038/ng0598-51
- Conte, D., Garaffo, G., Lo Iacono, N., Mantero, S., Piccolo, S., Cordenonsi, M., Perez-Morga, D., Orecchia, V., Poli, V., Merlo, G.R.,** 2016. The apical ectodermal ridge of the mouse model of ectrodactyly *Dlx5;Dlx6*^{-/-} shows altered stratification and cell polarity, which are restored by exogenous *Wnt5a* ligand. *Hum. Mol. Genet.* 25. doi:10.1093/hmg/ddv514
- Cooper, K.L., Hu, J.K.-H., ten Berge, D., Fernández-Terán, M.A., Ros, M.Á., Tabin, C.J.,** 2011. Initiation of proximal-distal patterning in the vertebrate limb by signals and growth. *Science* (80-.). 332, 1083–1086. doi:10.1126/science.1199499
- Crackower, M.,** 1996. Characterization of the split hand/split foot malformation locus SHFM1 at 7q21.3-q22.1 and analysis of a candidate gene for its expression during limb development. *Hum. Mol. Genet.* 5, 571–579. doi:10.1093/hmg/5.5.571
- Crackower, M. a, Motoyama, J., Tsui, L.C.,** 1998. Defect in the maintenance of the apical ectodermal ridge in the Dactylaplasia mouse. *Dev. Biol.* 201, 78–89. doi:10.1006/dbio.1998.8938
- Cunningham, T.J., Duester, G.,** 2015. Mechanisms of retinoic acid signalling and its roles in organ and limb development. *Nat. Rev. Mol. Cell Biol.* 16, 110–123. doi:10.1038/nrm3932
- Cunningham, T.J., Zhao, X., Sandell, L.L., Evans, S.M., Trainor, P.A., Duester, G.,** 2013. Antagonism between Retinoic Acid and Fibroblast Growth Factor Signaling during Limb Development. *Cell Rep.* 3, 1503–1511. doi:10.1016/j.celrep.2013.03.036
- Cygan, J. a, Johnson, R.L., McMahon, a P.,** 1997. Novel regulatory interactions revealed by studies of murine limb pattern in *Wnt-7a* and *En-1* mutants. *Development* 124, 5021–5032.
- Datta, S.R., Brunet, A., Greenberg, M.E.,** 1999. Cellular survival: A play in three akts. *Genes Dev.* 13, 2905–2927. doi:10.1101/gad.13.22.2905
- De Moerloze, L., Spencer-Dene, B., Revest, J., Hajihosseini, M., Rosewell, I. And Dickson, C.** 2000. An important role for the IIIb isoform of fibroblast growth factor receptor 2 (FGFR2) in mesenchymal-epithelial signalling during mouse organogenesis. *Dev.* 127, 483-492.
- de Mollerat, X.J., Gurrieri, F., Morgan, C.T., Sangiorgi, E., Everman, D.B., Gaspari, P., Amiel, J., Bamshad, M.J., Lyle, R., Blouin, J.-L., Allanson, J.E., Le Marec, B., Wilson, M., Braverman, N.E., Radhakrishna, U., Delozier-Blanchet, C., Abbott, A., Elghouzzi, V., Antonarakis, S., Stevenson, R.E., Munnich, A., Neri, G., Schwartz, C.E.,** 2003. A genomic rearrangement resulting in a tandem duplication is associated with split hand-split foot malformation 3 (SHFM3) at 10q24. *Hum. Mol. Genet.* 12, 1959–71.
- Del Campo, M., Jones, M.C., Veraksa, A.N., Curry, C.J., Jones, K.L., Mascarello, J.T., Ali-Kahn-Catts, Z., Drumheller, T., McGinnis, W.,** 1999. Monodactylous Limbs and Abnormal Genitalia Are Associated with Hemizygoty for the Human 2q31 Region That Includes the HOXD Cluster. *Am. J. Hum. Genet.* 65, 104–110. doi:10.1086/302467

- Dimitrov, B.I., de Ravel, T., Van Driessche, J., de Die-Smulders, C., Toutain, A., Vermeesch, J.R., Fryns, J.P., Devriendt, K., Debeer, P., 2010.** Distal limb deficiencies, micrognathia syndrome, and syndromic forms of split hand foot malformation (SHFM) are caused by chromosome 10q genomic rearrangements. *J. Med. Genet.* 47, 103–111. doi:10.1136/jmg.2008.065888
- Dixon, J.R., Selvaraj, S., Yue, F., Kim, A., Li, Y., Shen, Y., Hu, M., Liu, J.S., Ren, B., 2012.** Topological domains in mammalian genomes identified by analysis of chromatin interactions. *Nature* 485, 376–380. doi:10.1038/nature11082
- Dudley, A.T., Ros, M. a, Tabin, C.J., 2002.** A re-examination of proximodistal patterning during vertebrate limb development. *Nature* 418, 539–544. doi:10.1038/nature00945
- Duijf, P.H.G., van Bokhoven, H., Brunner, H.G., 2003.** Pathogenesis of split-hand/split-foot malformation. *Hum. Mol. Genet.* 12 Spec No 1, R51-60.
- Elliott, a M., Evans, J. a, Chudley, a E., 2005.** Split hand foot malformation (SHFM). *Clin. Genet.* 68, 501–5. doi:10.1111/j.1399-0004.2005.00530.x
- Elliott, A.M., Evans, J.A., 2006.** Genotype-phenotype correlations in mapped split hand foot malformation (SHFM) patients. *Am J Med Genet A* 140, 1419–1427. doi:10.1002/ajmg.a.31244
- Elliott, A.M., Reed, M.H., Chudley, A.E., Chodirker, B.N., Evans, J.A., 2006.** Clinical and epidemiological findings in patients with central ray deficiency: Split hand foot malformation (SHFM) in Manitoba, Canada. *Am. J. Med. Genet. Part A* 140, 1428–1439. doi:10.1002/ajmg.a.31245
- Estella, C., Mann, R.S., 2010.** Non-redundant selector and growth-promoting functions of two sister genes, buttonhead and Sp1, in *Drosophila* leg development. *PLoS Genet.* 6, e1001001. doi:10.1371/journal.pgen.1001001
- Estella, C., Rieckhof, G., Calleja, M., Morata, G., 2003.** The role of buttonhead and Sp1 in the development of the ventral imaginal discs of *Drosophila*. *Development* 130, 5929–5941. doi:10.1242/dev.00832
- Faiyaz-Ul-Haque, M., Uhlhaas, S., Knapp, M., Schiller, H., Friedl, W., Ahmad, M., Propping, P., 1993.** Mapping of the gene for X-chromosomal split-hand / split-foot anomaly to Xq26-q26.1. *Hum Genet* 91, 17–9.
- Faiyaz-Ul-Haque, M., Zaidi, S.H.E., King, L.M., Haque, S., Patel, M., Ahmad, M., Siddique, T., Ahmad, W., Tsui, L.C., Cohn, D.H., 2005.** Fine mapping of the X-linked split-hand/split-foot malformation (SHFM2) locus to a 5.1-Mb region on Xq26.3 and analysis of candidate genes. *Clin. Genet.* 67, 93–97. doi:10.1111/j.1399-0004.2004.00369.x
- Fernandez-Teran, M., Ros, M. a., 2008.** The Apical Ectodermal Ridge: morphological aspects and signaling pathways. *Int. J. Dev. Biol.* 52, 857–871. doi:10.1387/ijdb.072416mf
- Franch-Marro, X., 2006.** Association of tracheal placodes with leg primordia in *Drosophila* and implications for the origin of insect tracheal systems. *Development* 133, 785–790. doi:10.1242/dev.02260
- Francis, J.C., Radtke, F., Logan, M.P.O., 2005.** Notch1 signals through Jagged2 to regulate apoptosis in the apical ectodermal ridge of the developing limb bud. *Dev. Dyn.* 234, 1006–1015. doi:10.1002/dvdy.20590

- Fusco, C., Nittis, A.P. De, Alfaiz, A., Pellico, M.T., Augello, B., Malerba, N., Zelante, L., Reymond, A., Merla, G.,** 2017. A New Split Hand / Foot Malformation with Long Bone De fi cency Familial Case 98–102.
- Gañan, Y., Macias, D., Duterque-Coquillaud, M., Ros, M.A., Hurle, J.M.,** 1996. Role of TGF beta s and BMPs as signals controlling the position of the digits and the areas of interdigital cell death in the developing chick limb autopod. *Development* 122, 2349–57.
- Geduspan, J.S., MacCabe, J.A.,** 1989. Transfer of dorsoventral information from mesoderm to ectoderm at the onset of limb development. *Anat. Rec.* 224, 79–87. doi:10.1002/ar.1092240110
- Gibert, Y.,** 2006. Induction and pre patterning of the zebrafish pectoral fin bud requires axial retinoic acid signaling. *Development* 133, 2649–2659. doi:10.1242/dev.02438
- Gibson-Brown, J.J., Agulnik, S.I., Chapman, D.L., Alexiou, M., Garvey, N., Silver, L.M., Papaioannou, V.E.,** 1996. Evidence of a role for T-box genes in the evolution of limb morphogenesis and the specification of forelimb/hindlimb identity. *Mech. Dev.* 56, 93–101.
- Goodman, F.R.,** 2002. Limb malformations and the humanHOX genes. *Am. J. Med. Genet.* 112, 256–265. doi:10.1002/ajmg.10776
- Gorivodsky, M., Lonai, P.,** 2003. Novel roles of Fgfr2 in AER differentiation and positioning of the dorsoventral limb interface. *Development* 130, 5471–9. doi:10.1242/dev.00795
- Graham, A., Francis-West, P., Brickell, P., Lumsden, A.,** 1994. The signalling molecule BMP4 mediates apoptosis in the rhombencephalic neural crest. *Nature* 372, 684–6. doi:10.1038/372684a0
- Griesel, G.,** 2006. Sp8 controls the anteroposterior patterning at the midbrain-hindbrain border. *Development* 133, 1779–1787. doi:10.1242/dev.02326
- Grieshammer, U., Minowada, G., Pisenti, J.M., Abbott, U.K., Martin, G.R.,** 1996. The chick limbless mutation causes abnormalities in limb bud dorsal-ventral patterning: implications for the mechanism of apical ridge formation. *Development* 122, 3851–61.
- Gros, J., Tabin, C.,** 2014. Vertebrate Limb Bud Formation Is Initiated by Localized Epithelial-to-Mesenchymal Transition. *Science* (80-.). 343, 1253–1256. doi:10.1126/science.1248228
- Guo, Q., Loomis, C., Joyner, A.L.,** 2003. Fate map of mouse ventral limb ectoderm and the apical ectodermal ridge. *Dev. Biol.* 264, 166–178. doi:10.1016/j.ydbio.2003.08.012
- Gurrieri, F., Everman, D.B.,** 2013. Clinical, genetic, and molecular aspects of split-hand/foot malformation: An update. *Am. J. Med. Genet. Part A* 161, 2860–2872. doi:10.1002/ajmg.a.36239
- Harfe, B.D., Scherz, P.J., Nissim, S., Tian, H., McMahon, A.P., Tabin, C.J.,** 2004. Evidence for an expansion-based temporal Shh gradient in specifying vertebrate digit identities. *Cell* 118, 517–528. doi:10.1016/j.cell.2004.07.024
- Haro, E., Delgado, I., Junco, M., Yamada, Y., Mansouri, A., Oberg, K.C., Ros, M.A.,** 2014. Sp6 and Sp8 Transcription Factors Control AER Formation and Dorsal-Ventral Patterning in Limb Development. *PLoS Genet.* doi:10.1371/journal.pgen.1004468
- Hertveldt, V., Louryan, S., Van Reeth, T., Drèze, P., Van Vooren, P., Szpirer, J., Szpirer, C.,** 2008. The development of several organs and appendages is impaired in mice lacking

- Sp6. *Dev. Dyn.* 237, 883–892. doi:10.1002/dvdy.21355
- Hojo, H., Ohba, S., He, X., Lai, L.P., McMahon, A.P.**, 2016. Sp7/Osterix Is Restricted to Bone-Forming Vertebrates where It Acts as a Dlx Co-factor in Osteoblast Specification. *Dev. Cell* 37, 238–253. doi:10.1016/j.devcel.2016.04.002
- Hu, C.D., Chinenov, Y., Kerppola, T.K.**, 2002. Visualization of interactions among bZIP and Rel family proteins in living cells using bimolecular fluorescence complementation. *Mol. Cell*. doi:10.1016/S1097-2765(02)00496-3
- Huang, B.L., Trofka, A., Furusawa, A., Norrie, J.L., Rabinowitz, A.H., Vokes, S.A., Taketo, M.M., Zakany, J., Mackem, S.**, 2016. An interdigit signalling centre instructs coordinate phalanx-joint formation governed by 5'Hoxd-Gli3 antagonism. *Nat. Commun.* 7, 1–10. doi:10.1038/ncomms12903
- Huang, D.W., Sherman, B.T., Tan, Q., Kir, J., Liu, D., Bryant, D., Guo, Y., Stephens, R., Baseler, M.W., Lane, H.C., Lempicki, R.A.**, 2007. DAVID Bioinformatics Resources: Expanded annotation database and novel algorithms to better extract biology from large gene lists. *Nucleic Acids Res.* 35. doi:10.1093/nar/gkm415
- Ianakiev, P., Kilpatrick, M.W., Toudjarska, I., Basel, D., Beighton, P., Tsipouras, P.**, 2000. Split-hand/split-foot malformation is caused by mutations in the p63 gene on 3q27. *Am. J. Hum. Genet.* 67, 59–66. doi:10.1086/302972
- Ito, T., Kitamura, H., Uwatoko, C., Azumano, M., Itoh, K., Kuwahara, J.**, 2010. Interaction of Sp1 zinc finger with transport factor in the nuclear localization of transcription factor Sp1. *Biochem. Biophys. Res. Commun.* 403, 161–166. doi:10.1016/j.bbrc.2010.10.036
- Itou, J., Kawakami, H., Quach, T., Osterwalder, M., Evans, S.M., Zeller, R., Kawakami, Y.**, 2012. Islet1 regulates establishment of the posterior hindlimb field upstream of the Hand2-Shh morphoregulatory gene network in mouse embryos. *Development* 139, 1620–1629. doi:10.1242/dev.073056
- Jiang, R., Lan, Y., Chapman, H.D., Shawber, C., Norton, C.R., Serreze, D. V., Weinmaster, G., Gridley, T.**, 1998. Defects in limb, craniofacial, and thymic development in Jagged2 mutant mice. *Genes Dev.* 12, 1046–57.
- Kadonaga, J.T., Carner, K.R., Masiarz, F.R., Tjian, R.**, 1987. Isolation of cDNA encoding transcription factor Sp1 and functional analysis of the DNA binding domain. *Cell* 51, 1079–90.
- Kantaputra, P.N., Kapoor, S., Verma, P., Intachai, W., Ketudat Cairns, J.R.**, 2018. Split hand-foot malformation and a novel WNT10B mutation. *Eur. J. Med. Genet.* 61, 372–375. doi:10.1016/j.ejmg.2018.02.001
- Kawakami, Y.**, 2004. Sp8 and Sp9, two closely related buttonhead-like transcription factors, regulate Fgf8 expression and limb outgrowth in vertebrate embryos. *Development* 131, 4763–4774. doi:10.1242/dev.01331
- Kawakami, Y., Capdevila, J., Büscher, D., Itoh, T., Esteban, C.R., Belmonte, J.C.I.**, 2001. WNT signals control FGF-dependent limb initiation and AER induction in the chick embryo. *Cell* 104, 891–900. doi:10.1016/S0092-8674(01)00285-9
- Kawakami, Y., Marti, M., Kawakami, H., Itou, J., Quach, T., Johnson, A., Sahara, S., O'Leary, D.D.M., Nakagawa, Y., Lewandoski, M., Pfaff, S., Evans, S.M., Izpisua Belmonte, J.C.**, 2011. Islet1-mediated activation of the β -catenin pathway is necessary for hindlimb initiation in mice. *Development* 138, 4465–73. doi:10.1242/dev.065359

- Kazanskaya, O., Glinka, A., del Barco Barrantes, I., Stannek, P., Niehrs, C., Wu, W., 2004.** R-Spondin2 is a secreted activator of Wnt/ β -catenin signaling and is required for *Xenopus* myogenesis. *Dev. Cell* 7, 525–534. doi:10.1016/j.devcel.2004.07.019
- Kengaku, M., Capdevila, J., Rodriguez-Esteban, C., De La Peña, J., Johnson, R.L., Izpisua Belmonte, J.C., Tabin, C.J., 1998.** Distinct WNT pathways regulating AER formation and dorsoventral polarity in the chick limb bud. *Science* 280, 1274–7.
- Kennedy, M.W., Chalamalasetty, R.B., Thomas, S., Garriock, R.J., Jailwala, P., Yamaguchi, T.P., 2016.** Sp5 and Sp8 recruit β -catenin and Tcf1-Lef1 to select enhancers to activate Wnt target gene transcription. *Proc. Natl. Acad. Sci.* 201519994. doi:10.1073/pnas.1519994113
- Khan, S., Basit, S., Zimri, F.K., Ali, N., Ali, G., Ansar, M., Ahmad, W., 2012.** A novel homozygous missense mutation in WNT10B in familial split-hand/foot malformation. *Clin. Genet.* 82, 48–55. doi:10.1111/j.1399-0004.2011.01698.x
- Khokha, M.K., Hsu, D., Brunet, L.J., Dionne, M.S., Harland, R.M., 2003.** Gremlin is the BMP antagonist required for maintenance of Shh and Fgf signals during limb patterning. *Nat. Genet.* 34, 303–307. doi:10.1038/ng1178
- Kieny, M., Mauger, A., Thevenet, A., 1971.** [Influence of the axial nervous system on the morphogenesis of the limbs in the chick embryo]. *C. R. Acad. Sci. Hebd. Seances Acad. Sci. D.* 272, 121–4.
- Kim, D., Perte, G., Trapnell, C., Pimentel, H., Kelley, R., Salzberg, S.L., 2013.** TopHat2: accurate alignment of transcriptomes in the presence of insertions, deletions and gene fusions. *Genome Biol.* 14, R36. doi:10.1186/gb-2013-14-4-r36
- Kimmel, R.A., Turnbull, D.H., Blanquet, V., Wurst, W., Loomis, C.A., Joyner, A.L., 2000.** Two lineage boundaries coordinate vertebrate apical ectodermal ridge formation. *Genes Dev.* 14, 1377–1389. doi:10.1101/gad.14.11.1377
- Klopocki, E., Lohan, S., Doelken, S.C., Stricker, S., Ockeloen, C.W., Soares Thiele de Aguiar, R., Lezirovitz, K., Mingroni Netto, R.C., Jamsheer, A., Shah, H., Kurth, I., Habenicht, R., Warman, M., Devriendt, K., Kordaß, U., Hempel, M., Rajab, A., Mäkitie, O., Naveed, M., Radhakrishna, U., Antonarakis, S.E., Horn, D., Mundlos, S., 2012.** Duplications of *BHLHA9* are associated with ectrodactyly and tibia hemimelia inherited in non-Mendelian fashion. *J. Med. Genet.* 49, 119–125. doi:10.1136/jmedgenet-2011-100409
- Kouwenhoven, E.N., van Heeringen, S.J., Tena, J.J., Oti, M., Dutilh, B.E., Alonso, M.E., de la Calle-Mustienes, E., Smeenk, L., Rinne, T., Parsaulian, L., Bolat, E., Jurgelenaite, R., Huynen, M. a., Hoischen, A., Veltman, J. a., Brunner, H.G., Roscioli, T., Oates, E., Wilson, M., Manzanares, M., Gómez-Skarmeta, J.L., Stunnenberg, H.G., Lohrum, M., van Bokhoven, H., Zhou, H., 2010.** Genome-Wide Profiling of p63 DNA-Binding Sites Identifies an Element that Regulates Gene Expression during Limb Development in the 7q21 SHFM1 Locus. *PLoS Genet.* 6, e1001065. doi:10.1371/journal.pgen.1001065
- Lallemant, Y., 2005.** Analysis of *Msx1*; *Msx2* double mutants reveals multiple roles for *Msx* genes in limb development. *Development* 132, 3003–3014. doi:10.1242/dev.01877
- Lango Allen, H., Caswell, R., Xie, W., Xu, X., Wragg, C., Turnpenny, P.D., Turner, C.L.S., Weedon, M.N., Ellard, S., 2014.** Next generation sequencing of chromosomal rearrangements in patients with split-hand/split-foot malformation provides evidence for

- DYNCH11* exonic enhancers of *DLX5/6* expression in humans. *J. Med. Genet.* 51, 264–267. doi:10.1136/jmedgenet-2013-102142
- Lapan, S.W., Reddien, P.W.**, 2011. *dlx* and *sp6-9* Control Optic Cup Regeneration in a Prototypic Eye. *PLoS Genet.* 7, e1002226. doi:10.1371/journal.pgen.1002226
- Lau, W. De, Peng, W.C., Gros, P., Clevers, H.**, 2014. The R-spondin / *Lgr5* / *Rnf43* module : regulator of Wnt signal strength 305–316. doi:10.1101/gad.235473.113.of
- Laufer, E., Dahn, R., Orozco, O.E., Yeo, C.Y., Pisenti, J., Henrique, D., Abbott, U.K., Fallon, J.F., Tabin, C.**, 1997. Expression of Radical fringe in limb-bud ectoderm regulates apical ectodermal ridge formation. *Nature.* doi:10.1038/386366a0
- Laufer, E., Nelson, C.E., Johnson, R.L., Morgan, B.A., Tabin, C.**, 1994. Sonic hedgehog and *Fgf-4* act through a signaling cascade and feedback loop to integrate growth and patterning of the developing limb bud. *Cell* 79, 993–1003.
- Lebensohn, A.M., Rohatgi, R.**, 2018. R-spondins can potentiate WNT signaling without LGRs. *Elife* 7, 1–18. doi:10.7554/eLife.33126
- Lewandoski, M., Sun, X., Martin, G.R.**, 2000. *Fgf8* signalling from the AER is essential for normal limb development. *Nat. Genet.* 26, 460–463. doi:10.1038/82609
- Lewis, E.**, 1978. A gene complex controlling segmentation in *Drosophila*. *Nature* 277, 565–570. doi:10.1038/276565a0
- Lewis, J.H.**, 1975. Fate maps and the pattern of cell division: a calculation for the chick wing-bud. *J. Embryol. Exp. Morphol.* 33, 419–34.
- Lin, C., Yin, Y., Bell, S.M., Veith, G.M., Chen, H., Huh, S.-H., Ornitz, D.M., Ma, L.**, 2013. Delineating a Conserved Genetic Cassette Promoting Outgrowth of Body Appendages. *PLoS Genet.* 9, e1003231. doi:10.1371/journal.pgen.1003231
- Lin, J., Hu, J.**, 2013. SeqNLS: nuclear localization signal prediction based on frequent pattern mining and linear motif scoring. *PLoS One* 8, e76864. doi:10.1371/journal.pone.0076864
- Liu, T., Ortiz, J.A., Taing, L., Meyer, C.A., Lee, B., Zhang, Y., Shin, H., Wong, S.S., Ma, J., Lei, Y., Pape, U.J., Poidinger, M., Chen, Y., Yeung, K., Brown, M., Turpaz, Y., Liu, X.S.**, 2011. Cistrome: An integrative platform for transcriptional regulation studies. *Genome Biol.* 12, 1–10. doi:10.1186/gb-2011-12-8-r83
- Lo Iacono, N., Mantero, S., Chiarelli, A., Garcia, E., Mills, A.A., Morasso, M.I., Costanzo, A., Levi, G., Guerrini, L., Merlo, G.R.**, 2008. Regulation of *Dlx5* and *Dlx6* gene expression by *p63* is involved in EEC and SHFM congenital limb defects. *Development* 135, 1377–1388. doi:10.1242/dev.011759
- Logan, M., Simon, H.G., Tabin, C.**, 1998. Differential regulation of T-box and homeobox transcription factors suggests roles in controlling chick limb-type identity. *Development* 125, 2825–35.
- Logan, M., Tabin, C.J.**, 1999. Role of *Pitx1* upstream of *Tbx4* in specification of hindlimb identity. *Science* 283, 1736–9.
- Loomis, C. a, Kimmel, R. a, Tong, C.X., Michaud, J., Joyner, a L.**, 1998. Analysis of the genetic pathway leading to formation of ectopic apical ectodermal ridges in mouse *Engrailed-1* mutant limbs. *Development* 125, 1137–48.
- Loomis, C.A., Harris, E., Michaud, J., Wurst, W., Hanks, M., Joyner, A.L.**, 1996. The

- mouse Engrailed-1 gene and ventral limb patterning. *Nature* 382, 360–3. doi:10.1038/382360a0
- Lu, P., Yu, Y., Perdue, Y., Werb, Z.,** 2008. The apical ectodermal ridge is a timer for generating distal limb progenitors. *Development* 135, 1395–1405. doi:10.1242/dev.018945
- Ma, W., Noble, W.S., Bailey, T.L.,** 2014. Motif-based analysis of large nucleotide data sets using MEME-ChIP. *Nat Protoc* 9, 1428–1450. doi:10.1038/nprot.2014.083.Motif-based
- Machanick, P., Bailey, T.L.,** 2011. MEME-ChIP: Motif analysis of large DNA datasets. *Bioinformatics* 27, 1696–1697. doi:10.1093/bioinformatics/btr189
- Marcil, A.,** 2003. Pitx1 and Pitx2 are required for development of hindlimb buds. *Development* 130, 45–55. doi:10.1242/dev.00192
- Mariani, F. V., Ahn, C.P., Martin, G.R.,** 2008. Genetic evidence that FGFs have an instructive role in limb proximal–distal patterning. *Nature* 453, 401–405. doi:10.1038/nature06876
- Marin, M., Karis, A., Visser, P., Grosveld, F., Philipsen, S.,** 1997. Transcription factor Sp1 is essential for early embryonic development but dispensable for cell growth and differentiation. *Cell* 89, 619–28.
- Marinić, M., Aktas, T., Ruf, S., Spitz, F.,** 2013. An Integrated Holo-Enhancer Unit Defines Tissue and Gene Specificity of the Fgf8 Regulatory Landscape. *Dev. Cell* 24, 530–542. doi:10.1016/j.devcel.2013.01.025
- Martin, G.R.,** 1998. The roles of FGFs in the early development of vertebrate limbs. *Genes Dev.* 12, 1571–1586. doi:10.1101/gad.12.11.1571
- McConnell, B.B., Yang, V.W.,** 2010. Mammalian Krüppel-Like Factors in Health and Diseases. *Physiol. Rev.* 90, 1337–1381. doi:10.1152/physrev.00058.2009
- McGrew, M.J., Sherman, A., Ellard, F.M., Lillico, S.G., Gilhooley, H.J., Kingsman, A.J., Mitrophanous, K.A., Sang, H.,** 2004. Efficient production of germline transgenic chickens using lentiviral vectors. *EMBO Rep.* 5, 728–33. doi:10.1038/sj.embor.7400171
- Mclean, C.Y., Bristor, D., Hiller, M., Clarke, S.L., Schaar, B.T., Wenger, A.M., Bejerano, G.,** 2010. GREAT improves functional interpretation of cis-regulatory regions 28, 495–501. doi:10.1038/nbt.1630.GREAT
- Mercader, N., Leonardo, E., Piedra, M.E., Martínez-A, C., Ros, M. a, Torres, M.,** 2000. Opposing RA and FGF signals control proximodistal vertebrate limb development through regulation of Meis genes. *Development* 127, 3961–3970. doi:Opposing RA and FGF signals control proximodistal vertebrate limb development through regulation of Meis genes
- Merlo, G.R., Paleari, L., Mantero, S., Genova, F., Beverdam, A., Palmisano, G.L., Barbieri, O., Levi, G.,** 2002. Mouse model of split hand/foot malformation type I. *Genesis* 33, 97–101. doi:10.1002/gene.10098
- Michaud, J.L., Lapointe, F., Le Douarin, N.M.,** 1997. The dorsoventral polarity of the presumptive limb is determined by signals produced by the somites and by the lateral somatopleure. *Development* 124, 1453–63.
- Michos, O., Panman, L., Vintersten, K., Beier, K., Zeller, R., Zuniga, A.,** 2004. Gremlin-mediated BMP antagonism induces the epithelial-mesenchymal feedback signaling controlling metanephric kidney and limb organogenesis. *Development* 131, 3401–3410.

- doi:10.1242/dev.01251
- Milona, M., Gough, J.E., Edgar, A.J.**, 2004. Genomic structure and cloning of two transcript isoforms of human Sp8. *BMC Genomics* 5, 86. doi:10.1186/1471-2164-5-86
- Min, H., Danilenko, D.M., Scully, S.A., Bolon, B., Ring, B.D., Tarpley, J.E., DeRose, M., Simonet, W.S.**, 1998. Fgf-10 is required for both limb and lung development and exhibits striking functional similarity to *Drosophila* branchless. *Genes Dev.* 12, 3156–3161. doi:10.1101/gad.12.20.3156
- Minguillon, C., Del Buono, J., Logan, M.P.**, 2005. Tbx5 and Tbx4 Are Not Sufficient to Determine Limb-Specific Morphologies but Have Common Roles in Initiating Limb Outgrowth. *Dev. Cell* 8, 75–84. doi:10.1016/j.devcel.2004.11.013
- Minguillon, C., Nishimoto, S., Wood, S., Vendrell, E., Gibson-Brown, J.J., Logan, M.P.O.**, 2012. Hox genes regulate the onset of Tbx5 expression in the forelimb. *Development* 139, 3180–3188. doi:10.1242/dev.084814
- Montavon, T., Duboule, D.**, 2013. Chromatin organization and global regulation of Hox gene clusters. *Philos. Trans. R. Soc. B Biol. Sci.* 368, 20120367–20120367. doi:10.1098/rstb.2012.0367
- Montavon, T., Soshnikova, N., Mascrez, B., Joye, E., Thevenet, L., Splinter, E., De Laat, W., Spitz, F., Duboule, D.**, 2011. A regulatory archipelago controls hox genes transcription in digits. *Cell* 147, 1132–1145. doi:10.1016/j.cell.2011.10.023
- Monti, R., Barozzi, I., Osterwalder, M., Lee, E., Kato, M., Garvin, T.H., Plajzer-Frick, I., Pickle, C.S., Akiyama, J.A., Afzal, V., Beerenwinkel, N., Dickel, D.E., Visel, A., Pennacchio, L.A.**, 2017. Limb-Enhancer Genie: An accessible resource of accurate enhancer predictions in the developing limb. *PLoS Comput. Biol.* 13, e1005720. doi:10.1371/journal.pcbi.1005720
- Mukhopadhyay, M., Shtrom, S., Rodriguez-Esteban, C., Chen, L., Tsukui, T., Gomer, L., D'Orlando, D.W., Glinka, A., Grinberg, A., Huang, S.P., Niehrs, C., Izpisua Belmonte, J.C., Westphal, H.**, 2001. Dickkopf1 is required for embryonic head induction and limb morphogenesis in the mouse. *Dev. Cell* 1, 423–34.
- Murata, Y., Kim, H.G., Rogers, K.T., Udvadia, A.J., Horowitz, J.M.**, 1994. Negative regulation of Sp1 trans-activation is correlated with the binding of cellular proteins to the amino terminus of the Sp1 trans-activation domain. *J. Biol. Chem.* 269, 20674–81.
- Nagata, E., Kano, H., Kato, F., Yamaguchi, R., Nakashima, S., Takayama, S., Kosaki, R., Tonoki, H., Mizuno, S., Watanabe, S., Yoshiura, K.-I., Kosho, T., Hasegawa, T., Kimizuka, M., Suzuki, A., Shimizu, K., Ohashi, H., Haga, N., Numabe, H., Horii, E., Nagai, T., Yoshihashi, H., Nishimura, G., Toda, T., Takada, S., Yokoyama, S., Asahara, H., Sano, S., Fukami, M., Ikegawa, S., Ogata, T.**, 2014. Japanese founder duplications/triplications involving BHLHA9 are associated with split-hand/foot malformation with or without long bone deficiency and Gollop-Wolfgang complex. *Orphanet J. Rare Dis.* 9, 125. doi:10.1186/s13023-014-0125-5
- Nakamura, T., Unda, F., De-Vega, S., Vilaxa, A., Fukumoto, S., Yamada, K.M., Yamada, Y.**, 2004. The Krüppel-like Factor Epiprofin Is Expressed by Epithelium of Developing Teeth, Hair Follicles, and Limb Buds and Promotes Cell Proliferation. *J. Biol. Chem.* 279, 626–634. doi:10.1074/jbc.M307502200
- Nakashima, K., Zhou, X., Kunkel, G., Zhang, Z., Deng, J.M., Behringer, R.R., de**

- Crombrughe, B.**, 2002. The novel zinc finger-containing transcription factor osterix is required for osteoblast differentiation and bone formation. *Cell* 108, 17–29.
- Nam, J.S., Park, E., Turcotte, T.J., Palencia, S., Zhan, X., Lee, J., Yun, K., Funk, W.D., Yoon, J.K.**, 2007. Mouse R-spondin2 is required for apical ectodermal ridge maintenance in the hindlimb. *Dev. Biol.* 311, 124–135. doi:10.1016/j.ydbio.2007.08.023
- Nardi, J.B., Stocum, D.L.**, 1984. Surface properties of regenerating limb cells: Evidence for gradation along the proximodistal axis. *Differentiation* 25, 27–31. doi:10.1111/j.1432-0436.1984.tb01334.x
- Narkis, G., Tzchori, I., Cohen, T., Holtz, A., Wier, E., Westphal, H.**, 2012. Isl1 and Ldb co-regulators of transcription are essential early determinants of mouse limb development. *Dev. Dyn.* 241, 787–91. doi:10.1002/dvdy.23761
- Neufeld, S., Rosin, J.M., Ambasta, A., Hui, K., Shaneman, V., Crowder, R., Vickerman, L., Cobb, J.**, 2012. A conditional allele of *Rspo3* reveals redundant function of R-spondins during mouse limb development. *Genesis* 50, 741–749. doi:10.1002/dvg.22040
- Nishimoto, S., Wilde, S.M., Wood, S., Logan, M.P.O.**, 2015. RA Acts in a Coherent Feed-Forward Mechanism with *Tbx5* to Control Limb Bud Induction and Initiation. *Cell Rep.* 12, 879–891. doi:10.1016/j.celrep.2015.06.068
- Niswander, L., Tickle, C., Vogel, A., Booth, I., Martin, G.R.**, 1993. FGF-4 replaces the apical ectodermal ridge and directs outgrowth and patterning of the limb. *Cell* 75, 579–587. doi:10.1016/0092-8674(93)90391-3
- Ohtaka, K., Fujisawa, Y., Takada, F., Hasegawa, Y., Miyoshi, T., Hasegawa, T., Miyoshi, H., Kameda, H., Kurokawa-Seo, M., Fukami, M., Ogata, T.**, 2017. *FGFR1* Analyses in Four Patients with Hypogonadotropic Hypogonadism with Split-Hand/Foot Malformation: Implications for the Promoter Region. *Hum. Mutat.* 38, 503–506. doi:10.1002/humu.23178
- Ohuchi, H., Nakagawa, T., Yamamoto, a, Araga, a, Ohata, T., Ishimaru, Y., Yoshioka, H., Kuwana, T., Nohno, T., Yamasaki, M., Itoh, N., Noji, S.**, 1997. The mesenchymal factor, FGF10, initiates and maintains the outgrowth of the chick limb bud through interaction with FGF8, an apical ectodermal factor. *Development* 124, 2235–2244.
- Osterwalder, M., Speziale, D., Shoukry, M., Mohan, R., Ivanek, R., Kohler, M., Beisel, C., Wen, X., Scales, S.J., Christoffels, V.M., Visel, A., Lopez-Rios, J., Zeller, R.**, 2014. HAND2 targets define a network of transcriptional regulators that compartmentalize the early limb bud mesenchyme. *Dev. Cell* 31, 345–57. doi:10.1016/j.devcel.2014.09.018
- Pajni-Underwood, S., Wilson, C.P., Elder, C., Mishina, Y., Lewandoski, M.**, 2007. BMP signals control limb bud interdigital programmed cell death by regulating FGF signaling. *Development* 134, 2359–2368. doi:10.1242/dev.001677
- Pan, Y., Liu, Z., Shen, J., Kopan, R.**, 2005. Notch1 and 2 cooperate in limb ectoderm to receive an early Jagged2 signal regulating interdigital apoptosis. *Dev. Biol.* 286, 472–482. doi:10.1016/j.ydbio.2005.08.037
- Parr, B.A., McMahon, A.P.**, 1995. Dorsalizing signal Wnt-7a required for normal polarity of D-V and A-P axes of mouse limb. *Nature* 374, 350–3. doi:10.1038/374350a0
- Pascal, E., Tjian, R.**, 1991. Different activation domains of Sp1 govern formation of multimers and mediate transcriptional synergism. *Genes Dev.* 5, 1646–56.

- Pickering, J., Chinnaiya, K., Rich, C.A., Saiz-lopez, P., Maria, A.,** 2018. An intrinsic cell cycle timer terminates limb bud outgrowth 1–27. doi:10.7554/eLife.37429
- Pizette, S., Abate-Shen, C., Niswander, L.,** 2001. BMP controls proximodistal outgrowth, via induction of the apical ectodermal ridge, and dorsoventral patterning in the vertebrate limb. *Development* 128, 4463–4474.
- Pizette, S., Niswander, L.,** 1999. BMPs negatively regulate structure and function of the limb apical ectodermal ridge. *Development* 126, 883–894. doi:10.1126/science.276.5314.955
- Probst, S., Kraemer, C., Demougin, P., Sheth, R., Martin, G.R., Shiratori, H., Hamada, H., Iber, D., Zeller, R., Zuniga, A.,** 2011. SHH propagates distal limb bud development by enhancing CYP26B1-mediated retinoic acid clearance via AER-FGF signalling. *Development* 138, 1913–1923. doi:10.1242/dev.063966
- Ramer, J.C., Mowrey, P.N., Robins, D.B., Ligato, S., Towfighi, J., Ladda, R.L.,** 1990. Five children with del (2)(q31q33) and one individual with dup (2)(q31q33) from a single family: Review of brain, cardiac, and limb malformations. *Am. J. Med. Genet.* 37, 392–400. doi:10.1002/ajmg.1320370320
- Ramírez, F., Dündar, F., Diehl, S., Grüning, B.A., Manke, T.,** 2014. deepTools: a flexible platform for exploring deep-sequencing data. *Nucleic Acids Res.* 42, W187–W191. doi:10.1093/nar/gku365
- Raspopovic, J., Marcon, L., Russo, L., Sharpe, J.,** 2014. Digit patterning is controlled by a Bmp-Sox9-Wnt Turing network modulated by morphogen gradients. *Science* (80-.). doi:10.1126/science.1252960
- Ravasi, T., Huber, T., Zavolan, M., Forrest, A., Gaasterland, T., Grimmond, S., Arakawa, T., Carninci, P., Kawai, J., Hayashizaki, Y.,** 2003. Systematic characterization of the zinc-finger-containing proteins in the mouse transcriptome. *Genome Res.* 13, 1430–1442. doi:10.1101/gr.949803
- Rehimi, R., Bartusel, M., Solinas, F., Altmüller, J., Rada-Iglesias, A.,** 2017. Chromatin Immunoprecipitation (ChIP) Protocol for Low-abundance Embryonic Samples. *J. Vis. Exp.* 1–13. doi:10.3791/56186
- Restelli, M., Lopardo, T., Lo Iacono, N., Garaffo, G., Conte, D., Rustighi, A., Napoli, M., Del Sal, G., Perez-Morga, D., Costanzo, A., Merlo, G.R., Guerrini, L.,** 2014. DLX5, FGF8 and the Pin1 isomerase control Np63 protein stability during limb development: a regulatory loop at the basis of the SHFM and EEC congenital malformations. *Hum. Mol. Genet.* 23, 3830–3842. doi:10.1093/hmg/ddu096
- Revest, J.-M., Spencer-Dene, B., Kerr, K., De Moerlooze, L., Rosewell, I., Dickson, C.,** 2001. Fibroblast Growth Factor Receptor 2-IIIb Acts Upstream of Shh and Fgf4 and Is Required for Limb Bud Maintenance but Not for the Induction of Fgf8, Fgf10, Msx1, or Bmp4. *Dev. Biol.* 231, 47–62. doi:10.1006/dbio.2000.0144
- Riddle, R.D., Ensini, M., Nelson, C., Tsuchida, T., Jessell, T.M., Tabin, C.,** 1995. Induction of the LIM homeobox gene *Lmx1* by WNT6a establishes dorsoventral pattern in the vertebrate limb. *Cell* 83, 631–640. doi:10.1016/0092-8674(95)90103-5
- Riddle, R.D., Johnson, R.L., Laufer, E., Tabin, C.,** 1993. Sonic hedgehog mediates the polarizing activity of the ZPA. *Cell* 75, 1401–16.
- Robledo, R.F., Rajan, L., Li, X., Lufkin, T.,** 2002. The *Dlx5* and *Dlx6* homeobox genes are essential for craniofacial, axial, and appendicular skeletal development. *Genes Dev.* 16,

- 1089–1101. doi:10.1101/gad.988402
- Rodriguez-Leon, J., Tomas, A.R., Johnson, A., Kawakami, Y.,** 2013. Recent advances in the study of limb development: the emergence and function of the apical ectodermal ridge. *J. Stem Cells* 8, 79–98. doi:jsc.2014.8.2.79
- Ros, M. A, López-Martínez, A, Simandl, B.K., Rodriguez, C., Izpisúa Belmonte, J.C., Dahn, R., Fallon, J.F.,** 1996. The limb field mesoderm determines initial limb bud anteroposterior asymmetry and budding independent of sonic hedgehog or apical ectodermal gene expressions. *Development* 122, 2319–2330.
- Rosello-Diez, A., Arques, C.G., Delgado, I., Giovinazzo, G., Torres, M.,** 2014. Diffusible signals and epigenetic timing cooperate in late proximo-distal limb patterning. *Development* 141, 1534–1543. doi:10.1242/dev.106831
- Rosello-Diez, A., Ros, M. A., Torres, M.,** 2011. Diffusible Signals, Not Autonomous Mechanisms, Determine the Main Proximodistal Limb Subdivision. *Science* (80-.). 332, 1086–1088. doi:10.1126/science.1199489
- Roux, P.P., Blenis, J.,** 2004. ERK and p38 MAPK-Activated Protein Kinases : a Family of Protein Kinases with Diverse Biological Functions ERK and p38 MAPK-Activated Protein Kinases : a Family of Protein Kinases with Diverse Biological Functions. *Microbiol. Mol. Biol. Rev.* 68, 320–344. doi:10.1128/MMBR.68.2.320
- Rowe, D.A., Cairns, J.M., Fallon, J.F.,** 1982. Spatial and temporal patterns of cell death in limb bud mesoderm after apical ectodermal ridge removal. *Dev. Biol.* 93, 83–91. doi:10.1016/0012-1606(82)90241-X
- Rubin, L., Saunders, J.W.,** 1972. Ectodermal-mesodermal interactions in the growth of limb buds in the chick embryo: Constancy and temporal limits of the ectodermal induction. *Dev. Biol.* 28, 94–112. doi:10.1016/0012-1606(72)90129-7
- Runko, A.P., Sagerström, C.G.,** 2003. Nlz belongs to a family of zinc-finger-containing repressors and controls segmental gene expression in the zebrafish hindbrain. *Dev. Biol.* 262, 254–67.
- Sahara, S., Kawakami, Y., Izpisua Belmonte, J., O’Leary, D.D.,** 2007a. Sp8 exhibits reciprocal induction with Fgf8 but has an opposing effect on anterior-posterior cortical area patterning. *Neural Dev.* 2, 10. doi:10.1186/1749-8104-2-10
- Saiz-Lopez, P., Chinnaiya, K., Campa, V.M., Delgado, I., Ros, M.A., Towers, M.,** 2015. An intrinsic timer specifies distal structures of the vertebrate limb. *Nat. Commun.* 6, 8108. doi:10.1038/ncomms9108
- Satokata, I., Maas, R.,** 1994. Msx1 deficient mice exhibit cleft palate and abnormalities of craniofacial and tooth development. *Nat. Genet.* 6, 348–356. doi:10.1038/ng0494-348
- Saunders, J.W.,** 1948. The proximo-distal sequence of origin of the parts of the chick wing and the role of the ectoderm. 1948. *J. Exp. Zool.* 282, 628–668.
- Saunders, J.W., Reuss, C.,** 1974. Inductive and axial properties of prospective wing-bud mesoderm in the chick embryo. *Dev. Biol.* 38, 41–50.
- Schaeper, N.D., Prpic, N.-M., Wimmer, E. A,** 2010. A clustered set of three Sp-family genes is ancestral in the Metazoa: evidence from sequence analysis, protein domain structure, developmental expression patterns and chromosomal location. *BMC Evol. Biol.* 10, 88. doi:10.1186/1471-2148-10-88

- Schatz, O., Langer, E., Ben-Arie, N.,** 2014. Gene dosage of the transcription factor *Fingerin* (*bHLHA9*) affects digit development and links syndactyly to ectrodactyly. *Hum. Mol. Genet.* 23, 5394–5401. doi:10.1093/hmg/ddu257
- Schatz, O., Langer, E., Ben-Arie, N.,** 2014. Gene dosage of the transcription factor *Fingerin* (*bHLHA9*) affects digit development and links syndactyly to ectrodactyly. *Hum. Mol. Genet.* 23, 5394–5401. doi:10.1093/hmg/ddu257
- Scherer, S.W., Poorkaj, P., Allen, T., Kim, J., Geshuri, D., Nunes, M., Soder, S., Stephens, K., Pagon, R.A., Patton, M.A.,** 1994. Fine mapping of the autosomal dominant split hand/split foot locus on chromosome 7, band q21.3-q22.1. *Am J Hum Genet* 55, 12–20.
- Scherz, P.J., McGlinn, E., Nissim, S., Tabin, C.J.,** 2007. Extended exposure to Sonic hedgehog is required for patterning the posterior digits of the vertebrate limb. *Dev. Biol.* 308, 343–354. doi:10.1016/j.ydbio.2007.05.030
- Schmidl, C., Rendeiro, A.F., Sheffield, N.C., Bock, C.,** 2015. ChIPmentation: fast, robust, low-input ChIP-seq for histones and transcription factors. *Nat. Methods* 12, 963–5. doi:10.1038/nmeth.3542
- Sekine, K., Ohuchi, H., Fujiwara, M., Yamasaki, M., Yoshizawa, T., Sato, T., Yagishita, N., Matsui, D., Koga, Y., Itoh, N., Kato, S.,** 1999. *Fgf10* is essential for limb and lung formation. *Nat. Genet.* 21, 138–41. doi:10.1038/5096
- Selever, J., Liu, W., Lu, M.F., Behringer, R.R., Martin, J.F.,** 2004. *Bmp4* in limb bud mesoderm regulates digit pattern by controlling AER development. *Dev. Biol.* 276, 268–279. doi:10.1016/j.ydbio.2004.08.024
- Seto, M.L., Nunes, M.E., MacArthur, C. a, Cunningham, M.L.,** 1997. Pathogenesis of ectrodactyly in the Dactylaplasia mouse: aberrant cell death of the apical ectodermal ridge. *Teratology* 56, 262–70. doi:10.1002/(SICI)1096-9926(199710)56:4<262::AID-TERA5>3.0.CO;2-0
- Shamseldin, H.E., Faden, M. a, Alashram, W., Alkuraya, F.S.,** 2012. Identification of a novel *DLX5* mutation in a family with autosomal recessive split hand and foot malformation. *J. Med. Genet.* 49, 16–20. doi:10.1136/jmedgenet-2011-100556
- Shen, Y., Yue, F., McCleary, D.F., Ye, Z., Edsall, L., Kuan, S., Wagner, U., Dixon, J., Lee, L., Lobanenko, V. V., Ren, B.,** 2012. A map of the cis-regulatory sequences in the mouse genome. *Nature* 488, 116–120. doi:10.1038/nature11243
- Sheth, R., Marcon, L., Bastida, M.F., Junco, M., Quintana, L., Dahn, R., Kmita, M., Sharpe, J., Ros, M.A.,** 2012. Hox genes regulate digit patterning by controlling the wavelength of a Turing-type mechanism. *Science* 338, 1476–80. doi:10.1126/science.1226804
- Sidow, A., Bulotsky, M.S., Kerrebrock, A.W., Bronson, R.T., Daly, M.J., Reeve, M.P., Hawkins, T.L., Birren, B.W., Jaenisch, R., Lander, E.S.,** 1997. *Serrate2* is disrupted in the mouse limb-development mutant syndactylism. *Nature* 389, 722–725. doi:10.1038/39587
- Sifakis, S., Basel, D., Ianakiev, P., Kilpatrick, M., Tsipouras, P.,** 2001. Distal limb malformations: underlying mechanisms and clinical associations. *Clin. Genet.* 60, 165–72.
- Simonazzi, G., Miccoli, S., Salfi, N., Bonasoni, M.P., Bocciardi, R., Ravazzolo, R., Seri, M., Curti, A., Pilu, G., Rizzo, N., Turchetti, D.,** 2012. A novel *p63* mutation in a fetus with ultrasound detection of split hand/foot malformation. *Prenat. Diagn.* 32, 296–298.

doi:10.1002/pd.2932

- Soshnikova, N., Zechner, D., Huelsken, J., Mishina, Y., Behringer, R.R., Taketo, M.M., Crenshaw, E.B., Birchmeier, W.**, 2003. Genetic interaction between Wnt/??-catenin and BMP receptor signaling during formation of the AER and the dorsal-ventral axis in the limb. *Genes Dev.* 17, 1963–1968. doi:10.1101/gad.263003
- Sowińska-Seidler, A., Socha, M., Jamsheer, A.**, 2014. Split-hand/foot malformation - molecular cause and implications in genetic counseling. *J. Appl. Genet.* 55, 105–15. doi:10.1007/s13353-013-0178-5
- Spielmann, M., Kakar, N., Tayebi, N., Leettola, C., Nürnberg, G., Sowada, N., Lupiáñez, D.G., Harabula, I., Flöttmann, R., Horn, D., Chan, W.L., Wittler, L., Yilmaz, R., Altmüller, J., Thiele, H., van Bokhoven, H., Schwartz, C.E., Nürnberg, P., Bowie, J.U., Ahmad, J., Kubisch, C., Mundlos, S., Borck, G.**, 2016. Exome sequencing and CRISPR/Cas genome editing identify mutations of ZAK as a cause of limb defects in humans and mice. *Genome Res.* 26, 183–91. doi:10.1101/gr.199430.115
- Spitz, F., Gonzalez, F., Peichel, C., Vogt, T.F., Duboule, D., Zákány, J.**, 2001. Large scale transgenic and cluster deletion analysis of the HoxD complex separate an ancestral regulatory module from evolutionary innovations. *Genes Dev.* 15, 2209–2214. doi:10.1101/gad.205701
- Summerbell, D., Lewis, J.H.**, 1975. Time, place and positional value in the chick limb-bud. *J. Embryol. Exp. Morphol.* 33, 621–643.
- Summerbell, D., Lewis, J.H., Wolpert, L.**, 1973. Positional information in chick limb morphogenesis. *Nature* 244, 492–496. doi:10.1038/244492a0
- Sun, X., Mariani, F. V., Martin, G.R.**, 2002. Functions of FGF signalling from the apical ectodermal ridge in limb development. *Nature* 418, 501–8. doi:10.1038/nature00902
- Suske, G.**, 1999. The Sp-family of transcription factors. *Gene.* doi:10.1016/S0378-1119(99)00357-1
- Suske, G., Bruford, E., Philipsen, S.**, 2005. Mammalian SP/KLF transcription factors: Bring in the family. *Genomics* 85, 551–556. doi:10.1016/j.ygeno.2005.01.005
- Suzuki, T., Hasso, S.M., Fallon, J.F.**, 2008. Unique SMAD1/5/8 activity at the phalanx-forming region determines digit identity. *Proc. Natl. Acad. Sci. U. S. A.* 105, 4185–90. doi:10.1073/pnas.0707899105
- Szenker-Ravi, E., Altunoglu, U., Leushacke, M., Bosso-Lefèvre, C., Khatoo, M., Thi Tran, H., Naert, T., Noelanders, R., Hajamohideen, A., Beneteau, C., de Sousa, S.B., Karaman, B., Latypova, X., Başaran, S., Yücel, E.B., Tan, T.T., Vlaeminck, L., Nayak, S.S., Shukla, A., Girisha, K.M., Le Caignec, C., Soshnikova, N., Uyguner, Z.O., Vleminckx, K., Barker, N., Kayserili, H., Reversade, B.**, 2018. RSPO2 inhibition of RNF43 and ZNRF3 governs limb development independently of LGR4/5/6. *Nature* 1. doi:10.1038/s41586-018-0118-
- Takeuchi, J.K.**, 2003. Tbx5 and Tbx4 trigger limb initiation through activation of the Wnt/Fgf signaling cascade. *Development* 130, 2729–2739. doi:10.1242/dev.00474
- Talamillo, A., Delgado, I., Nakamura, T., de-Vega, S., Yoshitomi, Y., Unda, F., Birchmeier, W., Yamada, Y., Ros, M. A.**, 2010. Role of Epiprofin, a zinc-finger transcription factor, in limb development. *Dev. Biol.* 337, 363–374. doi:10.1016/j.ydbio.2009.11.007

- Tanaka, M., Tamura, K., Noji, S., Nohno, T., Ide, H.,** 1997. Induction of additional limb at the dorsal-ventral boundary of a chick embryo. *Dev. Biol.* 182, 191–203. doi:10.1006/dbio.1996.8476
- Tarchini, B., Duboule, D.,** 2006. Control of Hoxd genes' collinearity during early limb development. *Dev. Cell* 10, 93–103. doi:10.1016/j.devcel.2005.11.014
- te Welscher, P., Fernandez-Teran, M., Ros, M.A., Zeller, R.,** 2002. Mutual genetic antagonism involving GLI3 and dHAND prepatterns the vertebrate limb bud mesenchyme prior to SHH signaling. *Genes Dev.* 16, 421–6. doi:10.1101/gad.219202
- Temtamy, S.A., McKusick, V.A.,** 1978. The genetics of hand malformations. *Birth Defects Orig. Artic. Ser.* 14, i–xviii, 1-619.
- Tickle, C.,** 1981. The number of polarizing region cells required to specify additional digits in the developing chick wing. *Nature* 289, 295–8.
- Tickle, C., Alberts, B., Wolpert, L., Lee, J.,** 1982. Local application of retinoic acid to the limb bond mimics the action of the polarizing region. *Nature* 296, 564–6.
- Tickle, C., Münsterberg, A.,** 2001. Vertebrate limb development--the early stages in chick and mouse. *Curr. Opin. Genet. Dev.* 11, 476–481. doi:S0959-437X(00)00220-3 [pii]
- Tickle, C., Summerbell, D., Wolpert, L.,** 1975. Positional signalling and specification of digits in chick limb morphogenesis. *Nature* 254, 199–202. doi:10.1038/254199a0
- Towers, M., Mahood, R., Yin, Y., Tickle, C.,** 2008. Integration of growth and specification in chick wing digit-patterning. *Nature* 452, 882–6. doi:10.1038/nature06718
- Trapnell, C., Williams, B. A., Pertea, G., Mortazavi, A., Kwan, G., van Baren, M.J., Salzberg, S.L., Wold, B.J., Pachter, L.,** 2010. Transcript assembly and abundance estimation from RNA-Seq reveals thousands of new transcripts and switching among isoforms. *Nat. Biotechnol.* 28, 511–515. doi:10.1038/nbt.1621.Transcript
- Treichel, D., Schöck, F., Jäckle, H., Gruss, P., Mansouri, A.,** 2003. mBtd is required to maintain signaling during murine limb development. *Genes Dev.* 17, 2630–5. doi:10.1101/gad.274103
- Truett, G.E., Heeger, P., Mynatt, R.L., Truett, A.A., Walker, J.A., Warman, M.L.,** 2000. Preparation of PCR-quality mouse genomic dna with hot sodium hydroxide and tris (HotSHOT). *Biotechniques* 29, 52–54. doi:10.1016/j.jacc.2014.05.073
- Ugur, S. a., Tolun, A.,** 2008. Homozygous WNT10b mutation and complex inheritance in Split-Hand/Foot Malformation. *Hum. Mol. Genet.* 17, 2644–2653. doi:10.1093/hmg/ddn164
- Ullah, A., Gul, A., Umair, M., Irfanullah, Ahmad, F., Aziz, A., Wali, A., Ahmad, W.,** 2018. Homozygous sequence variants in the WNT10B gene underlie split hand/foot malformation. *Genet. Mol. Biol.* 41, 1–8. doi:10.1590/1678-4685-gmb-2016-0162
- Ullah, A., Hammid, A., Umair, M., Ahmad, W.,** 2017. A Novel Heterozygous Intragenic Sequence Variant in DLX6 Probably Underlies First Case of Autosomal Dominant Split-Hand/Foot Malformation Type 1. *Mol. Syndromol.* 8, 79–84. doi:10.1159/000453350
- Ullah, A., Ullah, M.F., Khalid, Z.M., Ahmad, W.,** 2016. Novel heterozygous frameshift mutation in *distal-less homeobox 5* underlies isolated split hand/foot malformation type 1. *Pediatr. Int.* 58, 1348–1350. doi:10.1111/ped.13023

- Umair, M., Ullah, A., Abbas, S., Ahmad, F., Basit, S., Ahmad, W., 2018. First direct evidence of involvement of a homozygous loss-of-function variant in the EPS15L1 gene underlying split-hand/split-foot malformation. *Clin. Genet.* 93, 699–702. doi:10.1111/cge.13152
- V. Hamburger, H.L.H., 1951. A series of normal stages in the development of the chick embryo. *Dev. Dyn.* 88, 49–92. doi:10.1002/aja.1001950404
- van Bokhoven, H., Hamel, B.C.J., Bamshad, M., Sangiorgi, E., Gurrieri, F., Duijf, P.H.G., Vanmolkot, K.R.J., van Beusekom, E., van Beersum, S.E.C., Celli, J., Merkx, G.F.M., Tenconi, R., Fryns, J.P., Verloes, A., Newbury-Ecob, R.A., Raas-Rotschild, A., Majewski, F., Beemer, F.A., Janecke, A., Chitayat, D., Crisponi, G., Kayserili, H., Yates, J.R.W., Neri, G., Brunner, H.G., 2001. p63 Gene Mutations in EEC Syndrome, Limb-Mammary Syndrome, and Isolated Split Hand–Split Foot Malformation Suggest a Genotype-Phenotype Correlation. *Am. J. Hum. Genet.* 69, 481–492. doi:10.1086/323123
- Vaudin, P., Delanoue, R., Davidson, I., Silber, J., Zider, A., 1999. TONDU (TDU), a novel human protein related to the product of vestigial (vg) gene of *Drosophila melanogaster* interacts with vertebrate TEF factors and substitutes for Vg function in wing formation. *Development* 126, 4807–16.
- Velinov, M., Ahmad, A., Brown-Kipphut, B., Shafiq, M., Blau, J., Cooma, R., Roth, P., Iqbal, M.A., 2012. A 0.7 Mb *de novo* duplication at 7q21.3 including the genes *DLX5* and *DLX6* in a patient with split-hand/split-foot malformation. *Am. J. Med. Genet. Part A* 158A, 3201–3206. doi:10.1002/ajmg.a.35644
- Vera-Carbonell, A., Moya-Quiles, M.R., Ballesta-Martínez, M., López-González, V., Bafallú, J.A., Guillén-Navarro, E., López-Expósito, I., 2012. Rapp-Hodgkin syndrome and SHFM1 patients: delineating the p63-Dlx5/Dlx6 pathway. *Gene* 497, 292–7. doi:10.1016/j.gene.2012.01.088
- Verheyden, J.M., Sun, X., 2008. An Fgf/Gremlin inhibitory feedback loop triggers termination of limb bud outgrowth. *Nature* 454, 638–641. doi:10.1038/nature07085
- Villanueva, C., Jacobson-Dickman, E., Xu, C., Manouvrier, S., Dwyer, A.A., Sykiotis, G.P., Beenken, A., Liu, Y., Tommiska, J., Hu, Y., Tiosano, D., Gerard, M., Leger, J., Drouin-Garraud, V., Lefebvre, H., Polak, M., Carel, J.-C., Phan-Hug, F., Hauschild, M., Plummer, L., Rey, J.-P., Raivio, T., Bouloux, P., Sidis, Y., Mohammadi, M., de Roux, N., Pitteloud, N., 2015. Congenital hypogonadotropic hypogonadism with split hand/foot malformation: a clinical entity with a high frequency of FGFR1 mutations. *Genet. Med.* 17, 651–659. doi:10.1038/gim.2014.166
- Vogel, A., Rodriguez, C., Warnken, W., Izpissúa Belmonte, J.C., 1995. Dorsal cell fate specified by chick *Lmx1* during vertebrate limb development. *Nature* 378, 716–20. doi:10.1038/378716a0
- Vokes, S. a., Ji, H., Wong, W.H., McMahon, A. P., 2008. A genome-scale analysis of the cis-regulatory circuitry underlying sonic hedgehog-mediated patterning of the mammalian limb. *Genes Dev.* 22, 2651–2663. doi:10.1101/gad.1693008
- Wada, N., Ide, H., 1994. Sorting out of limb bud cells in monolayer culture. *Int. J. Dev. Biol.* 38, 351–6.
- Wagle, P., Nikolić, M., Frommolt, P., 2015. QuickNGS elevates Next-Generation Sequencing data analysis to a new level of automation. *BMC Genomics* 16, 487. doi:10.1186/s12864-015-1695-x

- Wanek, N., Muneoka, K., Holler-Dinsmore, G., Burton, R., Bryant, S. V., 1989.** A staging system for mouse limb development. *J. Exp. Zool.* 249, 41–9. doi:10.1002/jez.1402490109
- Wang, B., Fallon, J.F., Beachy, P.A., 2000.** Hedgehog-regulated processing of Gli3 produces an anterior/posterior repressor gradient in the developing vertebrate limb. *Cell* 100, 423–34.
- Wang, X., Xin, Q., Li, L., Li, J., Zhang, C., Qiu, R., Qian, C., Zhao, H., Liu, Y., Shan, S., Dang, J., Bian, X., Shao, C., Gong, Y., Liu, Q., 2014.** Exome sequencing reveals a heterozygous DLX5 mutation in a Chinese family with autosomal-dominant split-hand/foot malformation. *Eur. J. Hum. Genet.* 22, 1105–1110. doi:10.1038/ejhg.2014.7
- Wieland, I., Muschke, P., Jakubiczka, S., Volleth, M., Freigang, B., Wieacker, P.F., 2004.** Refinement of the deletion in 7q21.3 associated with split hand/foot malformation type 1 and Mondini dysplasia. *J. Med. Genet.* 41, e54. doi:10.1136/JMG.2003.010587
- Wolpert, L., 1969.** Positional information and the spatial pattern of cellular differentiation. *J. Theor. Biol.* 25, 1–47.
- Xiang, R., Du, R., Guo, S., Jin, J.-Y., Fan, L.-L., Tang, J.-Y., Zhou, Z.-B., 2017.** Microduplications of 10q24 Detected in Two Chinese Patients with Split-hand/foot Malformation Type 3. *Ann. Clin. Lab. Sci.* 47, 754–757.
- Xiao, J., Xu, M., Li, J., Chang Chan, H., Lin, M., Zhu, H., Zhang, W., Zhou, Z., Zhao, B., Sha, J., 2002.** NYD-SP6, a novel gene potentially involved in regulating testicular development/spermatogenesis. *Biochem. Biophys. Res. Commun.* 291, 101–10. doi:10.1006/bbrc.2002.6396
- Xu, B., Wellik, D.M., 2011.** Axial Hox9 activity establishes the posterior field in the developing forelimb. *Proc. Natl. Acad. Sci.* 108, 4888–4891. doi:10.1073/pnas.1018161108
- Xu, R., Rudd, T.R., Hughes, A.J., Siligardi, G., Fernig, D.G., Yates, E.A., 2013.** Analysis of the fibroblast growth factor receptor (FGFR) signalling network with heparin as coreceptor: Evidence for the expansion of the core FGFR signalling network. *FEBS J.* 280, 2260–2270. doi:10.1111/febs.12201
- Yang, Y., Drossopoulou, G., Chuang, P.T., Duprez, D., Marti, E., Bumcrot, D., Vargesson, N., Clarke, J., Niswander, L., McMahon, A., Tickle, C., 1997.** Relationship between dose, distance and time in Sonic Hedgehog-mediated regulation of anteroposterior polarity in the chick limb. *Development* 124, 4393–404.
- Yashiro, K., Zhao, X., Uehara, M., Yamashita, K., Nishijima, M., Nishino, J., Saijoh, Y., Sakai, Y., Hamada, H., 2004.** Regulation of retinoic acid distribution is required for proximodistal patterning and outgrowth of the developing mouse limb. *Dev. Cell* 6, 411–422. doi:10.1016/S1534-5807(04)00062-0
- Yu, M., Riva, L., Xie, H., Schindler, Y., Moran, T.B., Cheng, Y., Yu, D., Hardison, R., Weiss, M.J., Orkin, S.H., Bernstein, B.E., Fraenkel, E., Cantor, A.B., 2009.** Insights into GATA-1-Mediated Gene Activation versus Repression via Genome-wide Chromatin Occupancy Analysis. *Mol. Cell* 36, 682–695. doi:10.1016/j.molcel.2009.11.002
- Zakany, J., Zacchetti, G., Duboule, D., 2007.** Interactions between HOXD and Gli3 genes control the limb apical ectodermal ridge via Fgf10. *Dev. Biol.* 306, 883–893. doi:10.1016/j.ydbio.2007.03.517
- Zhang, X., Peterson, K.A., Liu, X.S., McMahon, A.P., Ohba, S., 2013.** Gene regulatory

networks mediating canonical wnt signal-directed control of pluripotency and differentiation in embryo stem cells. *Stem Cells* 31, 2667–2679. doi:10.1002/stem.1371

Zhao, X., Sirbu, I.O., Mic, F.A., Molotkova, N., Molotkov, A., Kumar, S., Duester, G., 2009. Retinoic Acid Promotes Limb Induction through Effects on Body Axis Extension but Is Unnecessary for Limb Patterning. *Curr. Biol.* 19, 1050–1057. doi:10.1016/j.cub.2009.04.059

Zhu, J., Nakamura, E., Nguyen, M.T., Bao, X., Akiyama, H., Mackem, S., 2008. Uncoupling Sonic Hedgehog Control of Pattern and Expansion of the Developing Limb Bud. *Dev. Cell* 14, 624–632. doi:10.1016/j.devcel.2008.01.008

Zúñiga, A., Haramis, A.P., McMahon, A.P., Zeller, R., 1999. Signal relay by BMP antagonism controls the SHH/FGF4 feedback loop in vertebrate limb buds. *Nature* 401, 598–602. doi:10.1038/44157

8. AGRADECIMIENTOS

AGRADECIMIENTOS

Este trabajo no hubiera sido posible sin mi tutora y directora de Tesis, la Dra. Marian Ros, quien me brindó esta gran oportunidad al acogerme en su laboratorio. Gracias por compartir tus conocimientos, por tu paciencia y por todos los comentarios críticos que me han permitido formarme y crecer como científica. Tu entusiasmo y dedicación por la ciencia son un modelo a seguir. Igualmente, agradecer también al Dr. Juan F. López Giménez, co-director de esta Tesis, por haberme enseñado con paciencia y constancia, especialmente en los primeros años.

A mis evaluadores, la Dra. Federica Bertocchini y el Dr. Juan García Porrero por seguir mi trayectoria en estos años y sus consejos.

A **todos** los miembros del IBBTEC, centro de investigación que en este tiempo se ha convertido en una segunda casa. A Mar y a Marta por su labor en el estabulario. A Víctor por su apoyo en microscopía y su gran disposición. A Sandra por su dedicación y palabras de ánimo. Al laboratorio de apoyo y a todos los laboratorios y sus miembros en general, especialmente a *los Piero*, siempre dispuestos a ayudar con una sonrisa.

Siguiendo con los miembros del laboratorio, quiero agradecer a las dos generaciones con las que he compartido muchos momentos. Aquella con la que empecé, con Patri, Paula, y Lucía. Y en especial a la actual, a mis *Ratopollos*, Marc, Cristina, Laura y Sara, por todos los momentos que hemos compartido, dentro y fuera del laboratorio. Es una lotería teneros como compañeros y más aún como amigos. A M^a Félix, el altruismo personificado y a Endika, mi evaluador en la sombra.

To Álvaro Rada-Iglesias, and to all the people from his group at the CMMC who received me with enthusiasm. Thanks for your support in my work.

A mis amig@s, aquí tenéis los frutos de algunos sacrificios, gracias por entenderme. A ti Marta, porque tanto en lo personal como en lo profesional, siempre estás ahí. Pasado, presente y seguro que futuro.

Y finalmente, pero no menos importante, a mi familia. Especialmente a mis padres, por vuestro apoyo incondicional y velar siempre por mis intereses. No hubiera llegado hasta aquí sin vosotros.

Rocío

=)

9. ANEX

9.1 SP8 bound regions

Chr	start	end	Chr	start	end
chr12	42972649	42973211	chr16	42699180	42699651
chr11	74648885	74649636	chr4	127365399	127365914
chr9	44084084	44085084	chr11	71512530	71512953
chr13	9329279	9329890	chr6	53314299	53314674
chr11	116334978	116335761	chr6	30957807	30958222
chr2	59403919	59404543	chr8	113845651	113846074
chr2	172789052	172789651	chr1	75124406	75125245
chr8	66486167	66486884	chr8	42348387	42348777
chr2	33641506	33643118	chr8	26961050	26961651
chr10	20474830	20475432	chr11	76666143	76666711
chr14	21991054	21991686	chr5	135484918	135485278
chr19	4988938	4989374	chr6	125876778	125877335
chr11	60913609	60914092	chr12	91589656	91590196
chr1	37429783	37430445	chr12	46635291	46635761
chr8	120755106	120755709	chr15	72568501	72568974
chr4	129406283	129406696	chr12	24425086	24425393
chr12	86726297	86726778	chr11	102040196	102040544
chr16	91610192	91610590	chr9	46152470	46152827
chr7	34313382	34313905	chr11	53706495	53706921
chr3	101963444	101963985	chr1	88847726	88848182
chr1	194637681	194638249	chr16	25690702	25691065
chr2	119997678	119998223	chr9	105272275	105272554
chr8	46152298	46152800	chr6	147177858	147178573
chr8	18595325	18595957	chr9	21950261	21950783
chr12	118847300	118850887	chr19	53338751	53339149
chr9	118705598	118706118	chr12	12763604	12764030
chr5	138160660	138161414	chr3	54696780	54697276
chr11	121698443	121699051	chr15	102326085	102326632
chr11	95645753	95646242	chr9	44498184	44499120
chr2	159149131	159150081	chr18	24361794	24362419
chr1	135069724	135070091	chr6	73014071	73014862
chr11	52000429	52000783	chr5	4685780	4686092
chr5	111298728	111299078	chr16	18248579	18248936
chr4	148229686	148230221	chr5	20843862	20844850
chr3	89430064	89430461	chr6	95059645	95059987
chr1	64087846	64088306	chr19	12795250	12795798
chr11	116669825	116670329	chr1	149546094	149546567
chr8	61591083	61591477	chr2	158402206	158402498
chr17	87532226	87532968	chr5	113310541	113311075
chr3	127745287	127745975	chr3	9711133	9711688
chr4	43492893	43493484	chr1	67038543	67039124
chr3	155577041	155577473	chr17	35076351	35076820
chr7	96672382	96672976	chr11	120378536	120379056
chr15	88393689	88394199	chr15	72689821	72690092
chr2	165275122	165275709	chr19	7482513	7482774

ANEX 8.1 SP8 bound regions

chr9	98508506	98509037	chr14	47298126	47298377
chr14	14702730	14703088	chr1	114710399	114710829
chr18	65559780	65560304	chr11	113107958	113108309
chr9	43863675	43864472	chr8	33933289	33933739
chr6	71632852	71633530	chr1	74808075	74808501
chr1	12875504	12876011	chr7	30534961	30535278
chr17	91013216	91013716	chr18	75697344	75697975
chr17	4778212	4778511	chr6	91323302	91325605
chr1	91494246	91494838	chr5	143758016	143758483
chr10	12636457	12636685	chr8	95137530	95138053
chr15	38473676	38474134	chr6	30720743	30721034
chr5	113164624	113165323	chr16	3884445	3884703
chr6	115774121	115774902	chr17	56830892	56831228
chr10	43666453	43666978	chr13	92645026	92645418
chr10	43578955	43579226	chr11	55607777	55608054
chr10	117985839	117986654	chr2	170709032	170709320
chr2	18056607	18057016	chr2	121044612	121045243
chr12	80115291	80115923	chr6	122485877	122486550
chr18	46198907	46199141	chr11	25099951	25100347
chr15	83640419	83641091	chr2	74825594	74825890
chr9	8004023	8004934	chr4	106091874	106092636
chr3	97227189	97228101	chr15	80318411	80318862
chr1	58197394	58197828	chr6	94453371	94453910
chr2	160730910	160731565	chr17	81400499	81400957
chr2	9577570	9578207	chr12	36247452	36248049
chr13	55100205	55100590	chr1	182250646	182250946
chr11	106788291	106788803	chr2	156839806	156840053
chr4	131115314	131115544	chr17	64559210	64559622
chr5	146794742	146795331	chr17	27555092	27555494
chr1	95294997	95295365	chr15	89174935	89175266
chr9	101356617	101357068	chr18	3566488	3567096
chr12	112885452	112885812	chr8	106935458	106935919
chr9	31840053	31840455	chr4	74464164	74464527
chr5	37828585	37829076	chr7	19309925	19310266
chr11	35572057	35572567	chr12	88579921	88580286
chr18	56189463	56189910	chr9	123021365	123021867
chr4	111200210	111200529	chr11	112795721	112796198
chr6	39725271	39725537	chr13	23390840	23391243
chr9	98423704	98424347	chr9	62608556	62608793
chr14	54575571	54575975	chr15	76521828	76522725
chr17	56722539	56722922	chr11	77467103	77467304
chr19	34091229	34092133	chr3	125228264	125228604
chr5	109558551	109559153	chr11	102604237	102604533
chr5	79499185	79499702	chr15	76947902	76948621
chr4	43669268	43669733	chr6	9022468	9022964
chr9	48985067	48985532	chr8	35020611	35020869
chr4	129500890	129501219	chr2	158595186	158595447
chr13	102142344	102142810	chr1	186455303	186455596

ANEX 8.1 SP8 bound regions

chr9	73209674	73210369	chr4	126600646	126600979
chr11	116306621	116306905	chr11	22990621	22991192
chr4	129742347	129742796	chr3	124770439	124770700
chr2	156726207	156726656	chr15	102998570	102999324
chr12	73859910	73860537	chr6	77000437	77000732
chr15	86952567	86953043	chr2	157058510	157058875
chr2	155011395	155011674	chr1	14718621	14718976
chr17	4626069	4626699	chr5	64230134	64230615
chr17	73048106	73048429	chr9	115310168	115310876
chr10	36093030	36093233	chr8	84200656	84200967
chr16	20098108	20098435	chr14	32165482	32165764
chr11	18266037	18266483	chr8	108804804	108805058
chr13	112196906	112197126	chr1	133363516	133363758
chr11	120236308	120239045	chr14	104336822	104337164
chr7	99534227	99534589	chr16	85803013	85803332
chr4	124526642	124527129	chr4	1470	1952
chr2	164540883	164541267	chr19	28690047	28690740
chr7	80031706	80032029	chr19	25353290	25353605
chr11	120098746	120098988	chr12	71429723	71430161
chr4	151604403	151605217	chr10	63243618	63243913
chr13	24173643	24173857	chr4	83623234	83623444
chr14	103939759	103939997	chr2	135140705	135141014
chr8	116790103	116790464	chr1	13081425	13081765
chr3	116808097	116808355	chr13	101902172	101902510
chr11	100206437	100206724	chr11	5416837	5417166
chr16	77005519	77005895	chr4	133969359	133969707
chr1	93272524	93272956	chr7	4777056	4777565
chr3	128379368	128379776	chr19	5447627	5448027
chr2	34090613	34090999	chr10	127324629	127324899
chr13	72219328	72219667	chr6	97318609	97318883
chr6	136470856	136471207	chr12	118836460	118836766
chr1	118891428	118891741	chr11	80476531	80476925
chr12	55600143	55600493	chr6	126184207	126184501
chr6	52012219	52012602	chr2	170534149	170534500
chr16	32930240	32930616	chr2	59820044	59820386
chr8	14072455	14072830	chr4	123311905	123312257
chr11	88626121	88626546	chr2	71719159	71719389
chrX	153139623	153139874	chr4	140258951	140259463
chr14	21983468	21985889	chr12	76881329	76881591
chr7	77005313	77005569	chr13	53196357	53196688
chr14	52014232	52014498	chr16	77013430	77013822
chr14	28089941	28090157	chr15	64202989	64203374
chr4	43443011	43443223	chr15	5116396	5116909
chr13	54693847	54694449	chr6	119307850	119308141
chr3	88769101	88769334	chr12	107686429	107686697
chr17	56199871	56200222	chr3	100495490	100495886
chr9	64017039	64017522	chr13	12494846	12495156
chr11	84707877	84708208	chr7	25249433	25249861

ANEX 8.1 SP8 bound regions

chr10	13641916	13642121	chr4	107434347	107434587
chr14	55721801	55722087	chr4	140420975	140421457
chr16	85625664	85625887	chr14	100890544	100890941
chr3	138489457	138489705	chr13	102842219	102842426
chr11	85139767	85140126	chr5	43233008	43233495
chr7	28597326	28598302	chr14	28484155	28484469
chr1	61387580	61387994	chr4	137142314	137142751
chr4	53440289	53440488	chr11	105126272	105126587
chr1	43147462	43147852	chr2	164879142	164879826
chr5	48747418	48747988	chr19	45742891	45743507
chr8	92910404	92910827	chr7	72150778	72151309
chr13	53472769	53473504	chr12	112172314	112172744
chr2	71371656	71371889	chr2	33370573	33371226
chr5	77265038	77265795	chr16	4594009	4594544
chr2	83723883	83724202	chr15	102406502	102406891
chr18	56707401	56707923	chr17	46751881	46752166
chr14	54426748	54427019	chr5	147726859	147727088
chr18	38211930	38212132	chr2	71541022	71541601
chr5	115007606	115008036	chr12	5506076	5506663
chr6	121057286	121057655	chr13	107831131	107831330
chr16	32643931	32644141	chr7	81762566	81763034
chr4	43058599	43058984	chr7	28311893	28312230
chr15	78436901	78437148	chr5	96376119	96376449
chr19	40894820	40895245	chr13	8948360	8948639
chr17	31564768	31565299	chr2	47184384	47184842
chr10	3839954	3840318	chr10	29981543	29981885
chr3	146520863	146521124	chr3	55539300	55539597
chr14	117048985	117049236	chr4	142251438	142251778
chr3	22076168	22076711	chr7	45052088	45053012
chr7	100678044	100678259	chr9	109095066	109095493
chr2	155473511	155474142	chr2	23291069	23291382
chr10	111506297	111506593	chr2	136485918	136486161
chr15	99094573	99095012	chr12	21111570	21111769
chr4	41055359	41055558	chr5	76744900	76745180
chr1	194295132	194295366	chr1	181853092	181853446
chr16	32246903	32247196	chr15	70971446	70972108
chr5	41764290	41764762	chr17	84049507	84049989
chr4	45499757	45499967	chr15	99294962	99295474
chr12	79755577	79756157	chr15	86166995	86167285
chr17	41936786	41937169	chr10	126680996	126681303
chr2	6075011	6075424	chr12	4417592	4417791
chr2	150909626	150909995	chr10	76963791	76964217
chr9	108826925	108827216	chr10	70871831	70872142
chr1	59481910	59482227	chr18	60624162	60624440
chr13	111489861	111490390	chr12	27996759	27997030
chr4	149426651	149426936	chr16	36828211	36828597
chr9	101546352	101546841	chr6	120665982	120666489
chr7	90475856	90476254	chr3	52101941	52102437

ANEX 8.1 SP8 bound regions

chr2	164830540	164830796	chr7	25395763	25396114
chr11	77093394	77093593	chr7	24628918	24629253
chr10	95848907	95849112	chr16	57606812	57607074
chr17	14960982	14961697	chr5	149247979	149248335
chr1	86434255	86434484	chr19	37717004	37717270
chr9	70875599	70875869	chr11	115164489	115164709
chr17	29438340	29438884	chr3	14071593	14071913
chr5	134555258	134555819	chr1	180813541	180813869
chr3	54692788	54692997	chr12	98745370	98745718
chr6	86438406	86438859	chr4	119539325	119539670
chr4	84876424	84876679	chr7	7080969	7081199
chr11	120673001	120673332	chr2	75704402	75704872
chr19	21271945	21272208	chr17	66436876	66437257
chr2	93517988	93518227	chr11	106612935	106613231
chr11	93995645	93996104	chr1	75479130	75479582
chr6	98555788	98556102	chr5	139639275	139639532
chr17	34850155	34850386	chr5	109557212	109557665
chr3	110341130	110341533	chr6	113077265	113077470
chr17	17294334	17294557	chr13	94596294	94596792
chr2	33017951	33018412	chr10	12528378	12529045
chr10	45495753	45496034	chr3	59200610	59201041
chr10	61273339	61273711	chr16	75960477	75960908
chr7	73391039	73391413	chr11	3114755	3115484
chr9	77544905	77545298	chr9	103431742	103432178
chr12	86891439	86891860	chr9	59750279	59750576
chr8	13200428	13200752	chr3	152617239	152617788
chr18	39488737	39488983	chr4	55316805	55317165
chr11	61952557	61953375	chr1	7777117	7778522
chr14	21995316	21995756	chr7	34654984	34655287
chr1	23383093	23383432	chr18	20624074	20626113
chr4	151057849	151058143	chr10	17948107	17948310
chr3	88829261	88829515	chr2	139112115	139112413
chr4	136924458	136924938	chr7	28283288	28283796
chr17	85872935	85873449	chr7	71746386	71746601
chr16	70314180	70314486	chr7	75761063	75761340
chr17	15259499	15259716	chr7	27765576	27765775
chr10	121498857	121499056	chr5	12498569	12498790
chr10	85386493	85386747	chr2	68383182	68383498
chr5	108694502	108694756	chr15	38300882	38301478
chr13	17694705	17695097	chr18	38380024	38380391
chr16	8829865	8830130	chr1	132315764	132316089
chr1	69591509	69591827	chr1	119048041	119048771
chr5	65763895	65764149	chr10	66897468	66897667
chr5	64802967	64803733	chr11	34123308	34123534
chr12	84883613	84883885	chr15	99457487	99457763
chr5	77242387	77242661	chr17	56516103	56516474
chr8	9494154	9494390	chr17	29398115	29398428
chr8	89057036	89057391	chr17	62882662	62883211

ANEX 8.1 SP8 bound regions

chr9	19575300	19575660	chr3	51341132	51341386
chr4	7917837	7918093	chr4	3938138	3938558
chr16	75919075	75919373	chr13	53230936	53231208
chr4	89644627	89644944	chr3	108283923	108284348
chr2	27972235	27972583	chr3	68493998	68494423
chr18	38789141	38789358	chr11	88439115	88439424
chr9	57765030	57765238	chr19	10017921	10018322
chr11	76659166	76659685	chr13	26747198	26747448
chr15	102692555	102693237	chr7	127512734	127513065
chr9	51103873	51104148	chr18	67205136	67205351
chr3	96450676	96451055	chr11	106920679	106920914
chr2	93014370	93015021	chr3	27710288	27711449
chr6	140623232	140623592	chr15	86034121	86034351
chr4	134287222	134287841	chr19	45017749	45018378
chr17	14203723	14204061	chr6	10186251	10186594
chr16	4586383	4586926	chr6	128437498	128438023
chr17	47629411	47629803	chr1	152902916	152903315
chr7	45623561	45623894	chr17	84185427	84187345
chr8	120113915	120114264	chr11	51650791	51651286
chr13	40642981	40643293	chr12	110850195	110850454
chr13	54970905	54971283	chr9	40873721	40873941
chr19	42280175	42280722	chr5	106560638	106560837
chr3	50443390	50443681	chr5	66618807	66619073
chr13	41220042	41220708	chr17	31705609	31705848
chr9	70806040	70806371	chr13	17061774	17062542
chr8	116227032	116227270	chr12	42793474	42793836
chr3	15113425	15113660	chr3	23409491	23409897
chr19	57119977	57120378	chr3	35027957	35028218
chr10	59221485	59222149	chr16	28805880	28806358
chr8	36094701	36094918	chr1	36939588	36940144
chr1	156303603	156303844	chr5	74645334	74645694
chr1	153332779	153333284	chr4	5644003	5644269
chr11	101798109	101798423	chr5	128565631	128566078
chr11	51855314	51856584	chr11	102296123	102296618
chr8	71392933	71393217	chr8	109693201	109693554
chr17	46862652	46862961	chr2	50005224	50005542
chr18	75367197	75367400	chr7	135537618	135537828
chr13	24045296	24045507	chr2	125247133	125247444
chr10	43467703	43467965	chr2	115860089	115860338
chr4	140702136	140702533	chr13	63430988	63431294
chrX	122831259	122831590	chr8	123753922	123754272
chr2	32713058	32713681	chr2	144010471	144010670
chr1	7398142	7398417	chr8	45726367	45726857
chr5	140062253	140062592	chr7	64839814	64840422
chr18	15084807	15085158	chr5	105495168	105495498
chr2	16682947	16683288	chr11	30268112	30268370
chr4	83024945	83025270	chr13	69534433	69534638
chr7	25686711	25687154	chr7	89404195	89404397

ANEX 8.1 SP8 bound regions

chr18	64339761	64340044	chr13	109512405	109512664
chr19	43949344	43949683	chr4	125319375	125319683
chr8	94601606	94602108	chr17	25920311	25920632
chr7	6706263	6706613	chr5	105860266	105860586
chr5	86069611	86069810	chr6	70862258	70862881
chr11	94311257	94311706	chr13	44210503	44210816
chr2	27009665	27009959	chr11	120185763	120188332
chr13	114152951	114153229	chr6	85431717	85432040
chr13	61317192	61317445	chr2	17900397	17900635
chr14	49172075	49172606	chr8	93810164	93810369
chr5	91603510	91603767	chr4	127619897	127620111
chr4	153526494	153526776	chr19	42255992	42256281
chr4	127077142	127077427	chr4	22488320	22488634
chr16	10307370	10307668	chr4	133671829	133672270
chr11	4135011	4135221	chr4	107674041	107674358
chr2	72471723	72472244	chr1	36068087	36068576
chr18	68942829	68943257	chr8	33599460	33599775
chr14	102329573	102329861	chr12	112146052	112146263
chr8	91561385	91561686	chr1	90156909	90157257
chr8	18799980	18800431	chr1	44951092	44951419
chr14	57998710	57999035	chr10	4386883	4387338
chr5	16082316	16082565	chr7	70331263	70331794
chr7	63112104	63112375	chr11	72607065	72608014
chr13	97305641	97305901	chr11	97021240	97023064
chr10	126978629	126978837	chr2	147132751	147133018
chr19	4756247	4756666	chr8	45674141	45674478
chr7	113193018	113193406	chr3	37639669	37640020
chr14	46661847	46662310	chr2	167503064	167503424
chr4	83500371	83500676	chr1	31051730	31051931
chr5	67223076	67223304	chr9	57262526	57262905
chrX	75674434	75674676	chr9	21320637	21320853
chr15	102470545	102471007	chr6	113795302	113795713
chr4	95744500	95744853	chr5	135790594	135790838
chr6	72755226	72755480	chrX	135885733	135885970
chr19	55743022	55743393	chr10	41450178	41450436
chr3	52138548	52139035	chr1	131910115	131910334
chr19	46499842	46501506	chr12	36135986	36136322
chr13	119790866	119791172	chr4	86911987	86912418
chr5	111701746	111702002	chr18	57354434	57354999
chr12	70227625	70227930	chr13	98523995	98524198
chr10	85538313	85538546	chr14	26669706	26670013
chr14	60868767	60868966	chr16	42875852	42876171
chr12	17881526	17881910	chr12	69041804	69042053
chr5	122157970	122158253	chr1	16533070	16533504
chr7	66238337	66238540	chr18	35403047	35403589
chrX	170676728	170677867	chr8	92408311	92408573
chr7	97147837	97148145	chr9	124422594	124423654
chr6	64605056	64605304	chr10	3740197	3740595

ANEX 8.1 SP8 bound regions

chr1	182020174	182020408	chr10	37263638	37263939
chr8	116434827	116435321	chr1	14010821	14011177
chr2	39806860	39807098	chr17	74294859	74295113
chr6	145865493	145865769	chr6	113483277	113483478
chr13	107955420	107955645	chr1	178748287	178748614
chr17	56233699	56233904	chr8	26892030	26892229
chr12	24974743	24975122	chr18	73762202	73762444
chr14	29203162	29203448	chr6	122339951	122340199
chr8	61623890	61624222	chr1	166736584	166736856
chr2	3713286	3713563	chr7	98900110	98900507
chr17	35837100	35837299	chr1	51478270	51478469
chr17	28952447	28952646	chr11	23665800	23665999
chr6	55108432	55108640	chr14	61556794	61557145
chr13	70347960	70348246	chr11	97400398	97400679
chr6	120038462	120038724	chr2	153032325	153032570
chr10	88222708	88223058	chr5	134552418	134552632
chr9	97018904	97019112	chr3	102674250	102674449
chr7	127026288	127027194	chr11	69758461	69758858
chr11	120189857	120190072	chr1	166003011	166003445
chr1	77233560	77234458	chr15	57662254	57662470
chr2	126147746	126148090	chr19	44606961	44607286
chr17	88065574	88066636	chr1	94278936	94279204
chr19	14693151	14693691	chr9	72662088	72662405
chr11	84870144	84870415	chr13	54520259	54520487
chr6	131420646	131420949	chr15	6708185	6708443
chr3	117186868	117187086	chr3	50845197	50845430
chr9	44881296	44882207	chr19	10403096	10403298
chr16	84773622	84774172	chr5	111417003	111417243
chr17	78256554	78256956	chr9	79792660	79793473
chr18	88647657	88648110	chr11	102407550	102407766
chr15	88862253	88862475	chr3	93520266	93520557
chr10	66853360	66853624	chr4	99267847	99268052
chr10	24737372	24737714	chr11	76365702	76365944
chr17	79739122	79739485	chr6	117907591	117908220
chr17	79744999	79745250	chr15	43388494	43388960
chr7	98489845	98490129	chr2	18318051	18318250
chr8	46617092	46617450	chr10	37495408	37495684
chr5	136393123	136393380	chr6	33935900	33936141
chr1	105663491	105663802	chr4	133125352	133125894
chr14	57890108	57890430	chr2	74752954	74753367
chr11	78197966	78198245	chr6	128438834	128439033
chr4	133754063	133754307	chr1	189921514	189922030
chr6	23292609	23292934	chr16	41888704	41889000
chr12	53988709	53989033	chr1	152808201	152808455
chr14	121379016	121379569	chr13	119409115	119409599
chr2	3283843	3284217	chr7	75743994	75744193
chr19	21628318	21628690	chr11	23895172	23895390
chr6	42349752	42349951	chr7	138909574	138909792

ANEX 8.1 SP8 bound regions

chr18	47703755	47704034	chr6	30896333	30896969
chr18	45882452	45882689	chr19	5272931	5273311
chr3	88208210	88208409	chr2	34249621	34249958
chr1	55087986	55088215	chr6	48488065	48488279
chr1	55803997	55804326	chr11	30288027	30288226
chr2	70564268	70564536	chr14	121035311	121035618
chr6	48444270	48444668	chr5	142814162	142815650
chr10	113946931	113947179	chr12	108792766	108793080
chr10	79956701	79956949	chr1	55887610	55887830
chr18	76241234	76241560	chr9	45906145	45906539
chr10	126005039	126005527	chr17	47924088	47924974
chr5	149051791	149052016	chr16	95093816	95094041
chr2	165848290	165848513	chr6	142345547	142345810
chr1	115463671	115463897	chr9	104063377	104063725
chr14	56811767	56812201	chr1	177257739	177258526
chr12	80113127	80113548	chr5	140788683	140788961
chr5	134081185	134081423	chr17	26716224	26716445
chr11	25026684	25026971	chr6	6597735	6597968
chr2	91649939	91650336	chr9	17226730	17226945
chr18	56678711	56679105	chr13	117931490	117931717
chr18	68157070	68157407	chr8	70792776	70793127
chr2	174329631	174330466	chr18	60789837	60790417
chr2	92401203	92401402	chr4	20004122	20004504
chr10	37136991	37137403	chrX	116287032	116287387
chr13	28958214	28958823	chr9	88553107	88553447
chr11	94327913	94328118	chr9	15071870	15072078
chr11	69416128	69416373	chr17	7870690	7870910
chr6	127453689	127454104	chr4	32950697	32950992
chr19	47937445	47937682	chr7	44662131	44662454
chr8	125910137	125910408	chr13	107096937	107097136
chr11	54866368	54866991	chr6	81148605	81148821
chr10	87929688	87930234	chr2	131352768	131352970
chr11	98794942	98795718	chr2	91963560	91963850
chr1	79858594	79858919	chr5	113908204	113908998
chr13	35188765	35189044	chr17	29965933	29966290
chr12	47234043	47234313	chr2	71532486	71532693
chr13	12384827	12385042	chr3	134235784	134236444
chr17	80206810	80207387	chr10	80657158	80657380
chr18	43984823	43985142	chr16	89944663	89944867
chr2	174324548	174324987	chr18	3509076	3509334
chr16	17619251	17619496	chr15	76009370	76009629
chr2	71535904	71536338	chr6	95718751	95719021
chr10	28211963	28212376	chr7	28069834	28070190
chr2	144270211	144270410	chr5	149228987	149229512
chr14	100284736	100285071	chr11	117101572	117101797
chr16	34426302	34426637	chr1	12644647	12644998
chr11	78536283	78536509	chr2	91976429	91976682
chr1	42714465	42714699	chr4	139338184	139338515

ANEX 8.1 SP8 bound regions

chr11	97661699	97662012	chr14	118021960	118022166
chr8	58313522	58313795	chr1	36558309	36558575
chr4	156197470	156198172	chr11	97883505	97884341
chr6	125008866	125009341	chr4	154170634	154170850
chr11	98863526	98864107	chr4	137913398	137913683
chr13	37873632	37873842	chr2	156789212	156789489
chr8	84104378	84104786	chr11	21370767	21371111
chr19	4121509	4121708	chr6	121473177	121473377
chr9	51875590	51875964	chr8	94012029	94012281
chr7	35554757	35555243	chr9	85394990	85395348
chr9	120884775	120885262	chr19	8252095	8252448
chr5	34949262	34949613	chr2	22744709	22745059
chr5	108461358	108461834	chr5	76974591	76974831
chr1	105885743	105886076	chr15	102983020	102983363
chr5	103412139	103412389	chr13	107045093	107045355
chr2	165833585	165833793	chr6	100287151	100287643
chr6	127659749	127660106	chr2	16490831	16491088
chr11	104105831	104106158	chr8	95434688	95435097
chr3	89391825	89392054	chr5	33438170	33438562
chr17	83215023	83215384	chr11	120492176	120492460
chr5	123524342	123524716	chr4	105347798	105348152
chr8	128685638	128686646	chr4	44024000	44024199
chr5	147565189	147565506	chr2	104027666	104027952
chr9	52047701	52048192	chr11	121203956	121204541
chr12	49383611	49383839	chr7	127345334	127345614
chr14	119952900	119953373	chr6	101260642	101260980
chr11	88313778	88313999	chr12	88620057	88620310
chr1	77220238	77220444	chr14	35270246	35270445
chr15	84829443	84829824	chr14	27227585	27228047
chr11	96352894	96353954	chr7	100582656	100583019
chr6	124809521	124809771	chr1	88919316	88919515
chr11	102624358	102624606	chr16	56867585	56867872
chr4	298	597	chr4	57282305	57282504
chr12	112828989	112829530	chr1	66816966	66817177
chr5	123676739	123677111	chr6	58831328	58831561
chr13	107970209	107970409	chr5	151185587	151186023
chr13	73070192	73070479	chr5	138992112	138993176
chr2	32768656	32768911	chr10	21588671	21588874
chr1	92831379	92831588	chr15	78529696	78529914
chr2	30982087	30982286	chr15	78119750	78120155
chr15	62465514	62465904	chr17	8856439	8856865
chr1	150919191	150919676	chr10	9557845	9558095
chr11	6647709	6648174	chr8	120550044	120550248
chr10	80577537	80578123	chr7	82868417	82868936
chr2	92182898	92183097	chr8	110726856	110727168
chr11	70026812	70027312	chr7	70350907	70351328
chr1	184033504	184033759	chr9	96478278	96478773
chr17	27909204	27909403	chr11	56871624	56872178

ANEX 8.1 SP8 bound regions

chr8	94214467	94214932	chr7	45215662	45216857
chr18	61952052	61952304	chr18	43878554	43878921
chr2	51147210	51147457	chr9	122419330	122419579
chr18	23954399	23954847	chr14	28505435	28505815
chr7	110122194	110122393	chr7	70359158	70360044
chr16	35207412	35207611	chr16	24600652	24601015
chr6	86525616	86525989	chr1	90028534	90028733
chr10	17656015	17656214	chr7	28448264	28448584
chr17	29490208	29490675	chr10	18194915	18195274
chr2	90940480	90940891	chr4	133212672	133213284
chr8	117684096	117684307	chr9	114528117	114528405
chr15	68258209	68258640	chr7	87395492	87395731
chr9	118469439	118469638	chr10	116473415	116473829
chr9	88482048	88482874	chrX	7899201	7899542
chr7	19271684	19272647	chr8	11009236	11009473
chr17	30004670	30005175	chr1	43098381	43098654
chr5	140829713	140830164	chr9	37508016	37508291
chr5	21055979	21056326	chr3	129705265	129705770
chr11	120235090	120235351	chr10	42277489	42277761
chr11	47459297	47459590	chr4	134019205	134019516
chr4	41108155	41108425	chr11	69996868	69997398
chr5	137032789	137033043	chr11	82989614	82989815
chr4	151044563	151045053	chr15	38078081	38078876
chr15	81857650	81858382	chr6	29735438	29735716
chr3	21793577	21793798	chr12	30099882	30100109
chr8	84947206	84947405	chr11	53493540	53493940
chr15	59066137	59066639	chr13	60737938	60738137
chr10	41810045	41810305	chr7	65693188	65693624
chr5	112718592	112719014	chr8	84976822	84977587
chr7	25282117	25282763	chr5	23675684	23676346
chr7	126007510	126007712	chr8	13974612	13975174
chrX	170674301	170675844	chr7	27487235	27487871
chr7	19131609	19131838	chr7	80026601	80026800
chr11	72411657	72412002	chr6	18514703	18515004
chr8	39005753	39006494	chr15	75921348	75921729
chr6	88974522	88974761	chr11	24643592	24644012
chr13	42051679	42052228	chr6	49073717	49073933
chr6	82783394	82784046	chr11	103809619	103810224
chr17	35046746	35047080	chr4	116150338	116150541
chr5	138999468	138999723	chr9	62122714	62122937
chr8	34807145	34807490	chr3	123890111	123890495
chr14	64568688	64568887	chr5	135078297	135078545
chr5	107437845	107438056	chr10	127380575	127380802
chr5	49996540	49996966	chr15	99702538	99702737
chr10	80172776	80173188	chr8	123253555	123253872
chr11	97744716	97745287	chr18	25668063	25668423
chr12	16894413	16894847	chr17	87446799	87447207
chr1	47572816	47573246	chr5	35759135	35759554

ANEX 8.1 SP8 bound regions

chr6	90988721	90988940	chr8	103376012	103376362
chr11	5255645	5255880	chr7	3694192	3694557
chr12	87388301	87388518	chr7	143829870	143830132
chr1	192855559	192855834	chr7	110059412	110059747
chr8	48843882	48844315	chr8	45622039	45622336
chr13	63272505	63272794	chr16	76319953	76320157
chr3	87970826	87971145	chr8	91532887	91533088
chr12	72325030	72325328	chr13	40697566	40697818
chr2	153649227	153650337	chr17	69224143	69224434
chr1	120621817	120622105	chr11	53769785	53769984
chr2	118745537	118745814	chr3	99148337	99148568
chr13	53519732	53520050	chr2	122702531	122702987
chr15	98609662	98610052	chr1	99772257	99772553
chr13	63566467	63566719	chr1	86188420	86188722
chr2	32951886	32952563	chr18	69346486	69346695
chr3	137623557	137623821	chr13	54766381	54766711
chr13	54750761	54751011	chr15	31224148	31224391
chr5	73793179	73793488	chr1	156474364	156474601
chr10	80148144	80151160	chr2	52072656	52073025
chr10	60794332	60794653	chr2	153345513	153346735
chr11	75190670	75191417	chr7	75863246	75863484
chr8	120449970	120450339	chr16	44564680	44564879
chr17	47611371	47611686	chr3	8667016	8667377
chr11	99230031	99230816	chr5	142821670	142822016
chr18	13929986	13930326	chr8	85700794	85701186
chr11	114973371	114973686	chr6	112678980	112679387
chr4	134020695	134020951	chr3	96696228	96697392
chr1	37299655	37299976	chr15	99972678	99972984
chr2	28916066	28916392	chr7	116032544	116032813
chr5	127241692	127241891	chr1	151571069	151571472
chr19	20806007	20806577	chr13	23756747	23757030
chr11	56012085	56012288	chr7	70505901	70506110
chr5	9161444	9161790	chr11	118248398	118248601
chr1	93478226	93478930	chr8	108918593	108918887
chr10	83137958	83138210	chr2	31141953	31142166
chr1	134837143	134837393	chr2	13544408	13544650
chr5	114823329	114823597	chr1	40857295	40857624
chr11	113614291	113614523	chr5	64441618	64441944
chr4	34895	36031	chr12	107669148	107669493
chr5	138441933	138442169	chr11	82677603	82677812
chr6	3133890	3134470	chr12	55491894	55492302
chr2	35942442	35942691	chr18	3507668	3507976
chr2	26503975	26504174	chr14	56320099	56320635
chr6	72899624	72899985	chr4	122992342	122992557
chr17	28179858	28180114	chr11	5261116	5261992
chr16	30063975	30064200	chr15	102920697	102921105
chr19	36111102	36111336	chr17	56276667	56277005
chr13	37638362	37638650	chr5	37009841	37010056

ANEX 8.1 SP8 bound regions

chr7	43465736	43466057	chr2	28446542	28446988
chr17	32389130	32389631	chr2	115581383	115581647
chr6	111842852	111843207	chr4	140813628	140814166
chr3	139074871	139075470	chr15	4027347	4027626
chr2	153291131	153291330	chr8	89046225	89046495
chr11	96345147	96346299	chr13	100650997	100651196
chr2	27475672	27476118	chr10	123196909	123197177
chr13	63562961	63563274	chr15	78877529	78877777
chr1	64737542	64738082	chr17	47749817	47750132
chr2	167349505	167349714	chr5	12651218	12651529
chr6	51178454	51178861	chr16	96081824	96082764
chr6	3139862	3140185	chr13	45142001	45142200
chr6	43265414	43265718	chr13	107890625	107890871
chr1	74797460	74797716	chr7	19094132	19094343
chr3	31094319	31094717	chr6	49215221	49215546
chr18	83023484	83023725	chr5	138994115	138995795
chr12	106322348	106322620	chr1	155742062	155742293
chr12	21784436	21784672	chr9	80066791	80067081
chr15	59279028	59279710	chr8	22858966	22859453
chr11	113565656	113565899	chr10	121476237	121476619
chr1	166409260	166409897	chr8	71485605	71486533
chr13	81046686	81047134	chr17	43963243	43963453
chr14	14346798	14348133	chr2	166249152	166249451
chr13	63693805	63694015	chr8	120535803	120536642
chr10	98914342	98914576	chr2	12145103	12145437
chrX	170021903	170022102	chr11	95991355	95991734
chrX	77433340	77433931	chr4	3180124	3180974
chr11	5444849	5445055	chr9	52035623	52036037
chr7	65370036	65371064	chr7	6410046	6410468
chr2	91931657	91932055	chr15	82244401	82244669
chrX	144392293	144392492	chr2	120563745	120564085
chr2	115402434	115402667	chr10	12868529	12869042
chr10	80159841	80160643	chr2	181147723	181148198
chr4	133813546	133814415	chr8	92355727	92356463
chr11	96884053	96884385	chr1	74770771	74771599
chr5	107868636	107869337	chr13	63156411	63157008
chr1	183798687	183798964	chr1	69687390	69687663
chr6	30547528	30547947	chr17	27204346	27204551
chr3	96459071	96459797	chr2	29776875	29777220
chr18	34777034	34777252	chr2	153444686	153444895
chr2	31152206	31152446	chr5	140606597	140607277
chr18	35118516	35118889	chr17	13760848	13761234
chr11	69417713	69418082	chr2	28153971	28154268
chr11	97187105	97187860	chr15	100074848	100075242
chr8	10859740	10859999	chr7	16048251	16048521
chr9	59656445	59657367	chr2	145486049	145486458
chr7	70367412	70367803	chr7	30956695	30956980
chr5	139200334	139200569	chr11	74837973	74838472

ANEX 8.1 SP8 bound regions

chr11	69411261	69411485	chr9	101251594	101251904
chr3	34207464	34207678	chr17	34121180	34121983
chr12	118301164	118302217	chr18	62923647	62924212
chr3	87150556	87150897	chr1	179445963	179446205
chr7	94541919	94542448	chr4	32238838	32239278
chr1	56971594	56971908	chr2	172856062	172856369
chr2	164953277	164953606	chr7	120835776	120835975
chr2	4881578	4882050	chr9	72374934	72375331
chr6	121069549	121069759	chr17	35980024	35980391
chr3	89164680	89164905	chr11	69369143	69369447
chr1	155083192	155083515	chr18	75309468	75309672
chr11	116852512	116852802	chr7	127876078	127876582
chr17	71259835	71260124	chrX	94917529	94917808
chr19	53944373	53944990	chr9	66974730	66975493
chr3	88531520	88532165	chr2	170319082	170319471
chr11	69980942	69981141	chr12	84193933	84194142
chr2	72979434	72979782	chr11	102026941	102027266
chr17	6978362	6979006	chr3	52662262	52662493
chr7	19322472	19322844	chr17	90639029	90639386
chr4	129513778	129514145	chr5	123137582	123138146
chr10	95940514	95941061	chr9	55546016	55546544
chr3	144202280	144202687	chr14	105417181	105417392
chr17	66449471	66449874	chr1	22755179	22755497
chr5	3596091	3596372	chr12	13043072	13043314
chr3	38484841	38485152	chr13	40722893	40723164
chr19	53314075	53314518	chr19	10688778	10689037
chr19	61226185	61227236	chr6	52190951	52191774
chr6	100823327	100823649	chr7	34630380	34630800
chr18	80104805	80105112	chr19	45058106	45058574
chr19	61224596	61225010	chr15	83100087	83100330
chr6	145746447	145746646	chr11	75572763	75573030
chr19	10525332	10525830	chr13	23318177	23318386
chr11	69560273	69560472	chr3	122334003	122334245
chr5	4555948	4556211	chr1	19981703	19981929
chr10	8807084	8807283	chr1	133696037	133696404
chr13	47105593	47106070	chr10	80131674	80132197
chr8	71087330	71087629	chr10	90692932	90693236
chr13	21161244	21161582	chr10	116276828	116277174
chr5	119682592	119683255	chr15	25413304	25413603
chr17	31386027	31386372	chr17	34898634	34899031
chr5	121837085	121837406	chr19	29805613	29806472
chr17	6693969	6694256	chr2	30066262	30067055
chr13	26030292	26030729	chr4	44167978	44168323
chr4	82506119	82506840	chr4	155491183	155491541
chr4	107253519	107254005	chr5	124425807	124426006
chr5	97110772	97111678	chr6	92092034	92092367
chr18	20627999	20628777	chr6	124755838	124756602
chr2	144101517	144101829	chr9	24593325	24593604

ANEX 8.1 SP8 bound regions

chr8	106721018	106721234	chr4	3175794	3177112
chr2	148532864	148533281	chr2	157913326	157913639
chr6	134826062	134826262	chr2	180024639	180024919
chr8	86623814	86624182	chr2	128125674	128125934
chr6	132463600	132463937	chr1	179586560	179587041
chr13	39104946	39105211	chr1	62599655	62599891
chr3	94757226	94758307	chr17	28247625	28247932
chr12	70825269	70825523	chr4	15657	15908
chr18	20619911	20620861	chr1	39678386	39678662
chr8	35826578	35826987	chr4	136247767	136248042
chr16	73245199	73245452	chr11	118584818	118585149
chr9	61434088	61434458	chr10	89446140	89446377
chr5	113937695	113938002	chr19	7143625	7143974
chr6	72763534	72764099	chr13	97341505	97341730
chr8	123332720	123332919	chr15	98775916	98776213
chr12	112928852	112929174	chr19	25273474	25273787
chr17	17828174	17828417	chr1	182686333	182686746
chr12	3891473	3891842	chr16	57241813	57242142
chr16	17531029	17531245	chr6	148896086	148896403
chr18	82914462	82914842	chr14	65343786	65343985
chr7	3644733	3645123	chr9	61853897	61854106
chr2	170552146	170552390	chr8	10713754	10713985
chr8	84980096	84980440	chr12	16615652	16615880
chr7	63937504	63939584	chr19	27116154	27116400
chr1	34714329	34714580	chr10	84287212	84287421
chr5	142962015	142962342	chr6	68011792	68012123
chr6	40471228	40471460	chr4	120589854	120590100
chr5	52655004	52655340	chr3	89394604	89395134
chr8	8109703	8110073	chr11	34544206	34544862
chrX	4136175	4136504	chr4	137282883	137283175
chr6	39515780	39516042	chr7	141123127	141123337
chr4	42999475	42999931	chr11	106720321	106720750
chr18	81054121	81054435	chr4	151996430	151996667
chr12	105685262	105685554	chr8	26984517	26984878
chr7	141279009	141279322	chr6	125096036	125096886
chr17	16951428	16951712	chr13	71270603	71270927
chr9	65580044	65580520	chr15	25983993	25984276
chr11	99138994	99139265	chr2	92024464	92024815
chr7	4164677	4164973	chr17	84188259	84188507
chr11	6444340	6444654	chr18	75380296	75380728
chr14	107075177	107075512	chr8	11555548	11556311
chr8	70698488	70699106	chr16	90742031	90742524
chr6	54967558	54967886	chr11	95210749	95211163
chr18	20622158	20622488	chr4	37388938	37389223
chr8	70659554	70660027	chr7	4690457	4690709
chr2	25551938	25552270	chr14	56693876	56694200
chr5	142936510	142936837	chr12	69361184	69361622
chr2	60402628	60402959	chr3	143985109	143985364

ANEX 8.1 SP8 bound regions

chr4	122455152	122455482
chr17	7952237	7952564
chr2	71543290	71543568
chr17	44777042	44777555
chr7	140902219	140902475
chr9	59486255	59486784
chr16	38088230	38088514
chr17	26244109	26244323
chr15	82961066	82961334
chr11	97365787	97366045
chr1	46075965	46076276
chr7	83921709	83922071
chr15	50963783	50964011
chr4	135570106	135570307
chr5	110074360	110074690
chr14	21988715	21989815
chr17	6390037	6391113

9.2 Differentially expressed genes

Up-regulated in *Sp8KO*

Symbol	FoldChange	pValue	KO_average; FPKM	WT_average; FPKM
Slc8a3	5,04	0	3,080683333	0,550077667
Pthlh	4,59	0	4,680046667	0,714395333
Smoc1	4,54	0	12,3106	1,894693333
Pex5l	4,1	0	1,319896667	0,295708667
Trpa1	3,62	0	0,635845	0,1024909
Ak5	3,58	0	2,894386667	0,620642667
Ptgfr	3,43	0	0,437131333	0,069493667
Kcnip1	3,26	0	1,132421333	0,1702026
Hdac9	3,19	0	8,66147	2,683563333
Irx2	3,18	0	38,15236667	11,6635
Foxb2	3,13	0	1,86483	0,395779333
Phactr3	3,13	0	4,2533	1,188395667
Flrt1	3,1	0	3,895493333	1,194434
Tmem200a	3,09	0	0,500626667	0,0960054
Ripply3	2,97	0	4,017103333	1,032919
Irx4	2,96	0	7,28398	2,264613333
Wnt10b	2,96	0	12,69993333	4,23355
Edn3	2,92	0	12,49786667	3,889523333
1700016K19Rik	2,84	0	2,352196667	0,535650333
Scube2	2,79	0	0,318859667	0,040689867
Mt2	2,78	0	207,5893333	55,73913333
Dab1	2,77	0	7,768133333	2,810276667
Cxcl14	2,72	0	64,69266667	23,50786667
Chdh	2,68	0	0,302842	0,055281267
Eddm3b	2,68	0	0,922087	0,1235004
Irx5	2,68	0	1,74818	0,544056
Mt1	2,68	0	56,21146667	20,2169
Enpp2	2,67	0	1,64087	0,482090333
Thsd7b	2,65	0	1,690263333	0,505930667
Ccdc162	2,52	0	1,564603333	0,502386333
Pou2af1	2,48	0	2,26394	0,368288667
Usp13	2,48	0	1,65918	0,930315667
Nptx2	2,45	0	0,831083333	0,241176667
Klf14	2,42	0	0,394347667	0,078642433
Rgl3	2,39	0	2,04589	0,800286
Acss3	2,38	0	0,825959667	0,216785667
Irx1	2,38	0	1,407216667	0,496658667
Smoc2	2,37	0	6,17372	2,447563333

ANEX 8.2 DEG

Hpgd	2,36	0	2,323656667	0,756288
Nos2	2,35	0	0,237086	0,137556503
Postn	2,35	0	3,49235	1,369088333
Asprv1	2,34	0	7,721783333	3,168513333
Adamts17	2,32	0	12,3372	4,428936667
Megf10	2,3	0	0,228657667	0,065186
Ramp3	2,3	0	1,992936667	0,631133667
Cdh13	2,27	0	5,81127	2,286816667
Bnc2	2,23	0	8,968366667	3,065916667
Fam214a	2,23	0	2,18008	1,050597333
Abca13	2,22	0	0,273507333	0,060593367
Arhgap24	2,22	0	4,240893333	1,874013333
Kcnd3	2,22	0,000002	0,402083333	0,030054697
Tmem132c	2,22	0,000002	8,11483	2,040416667
Xpnpep2	2,21	0,000001	0,150134667	0,002679747
Zfp703	2,21	0	18,4999	8,63253
Crabp1	2,2	0	145,1463333	60,85866667
Rsph4a	2,2	0,000001	0,367603667	0,100151233
Hmcn1	2,19	0	7,401163333	3,375543333
Mettl21c	2,19	0	0,925457333	0,233124
Sox9	2,19	0	14,29383333	6,4999
Map1b	2,17	0	24,67716667	11,3072
Ntng1	2,17	0	1,249380667	0,447732667
Mylk	2,15	0	6,5536	2,92571
Kcnb2	2,11	0	0,872106667	0,359056333
Podn	2,11	0,000008	0,224981	0,072456333
Barx2	2,1	0	4,015766667	1,806573333
Clstn2	2,09	0	1,30936	0,585628333
Grasp	2,08	0	2,378213333	0,981072
Txlnb	2,08	0,000001	0,468143333	0,199654
Cd248	2,07	0	1,500903333	0,600519667
Pappa2	2,07	0,000011	0,169964833	0,037554527
Psemb9	2,07	0,000013	0,955724333	0,255869667
Snhg11	2,07	0	0,574744333	0,201351
Itm2a	2,06	0	13,954	6,4414
Mal	2,06	0	1,364803333	0,571703
Kctd12	2,04	0	8,88747	3,78929
Ngfr	2,04	0	8,51311	3,424173333
Phyhip	2,04	0	2,192943333	0,959183
Vgll3	2,04	0	6,7334	3,26127
Sgpp2	2,03	0	2,104593333	0,912117667
Rab30	2,02	0	2,747813333	1,338136667
Lmx1b	2	0	13,70633333	5,952666667
Cd74	1,99	0,000033	1,019902333	0,207113667

Dock8	1,99	0	1,677366667	0,843718333
Esrrg	1,99	0,000035	0,1987919	0,082192033
Adamts15	1,98	0,000001	0,482813333	0,208547
Capn11	1,98	0,000007	0,1479754	0
Nfkbie	1,98	0,00001	0,660660667	0,216868
Hs3st3a1	1,97	0,000024	0,436812333	0,158430467
Mfap4	1,96	0,000003	42,4789	17,43253333
Al464131	1,95	0,000016	0,408275333	0,157272667
Ankrd45	1,95	0	3,9146	2,096946667
Drd5	1,95	0,000016	0,236071667	0,01965541
Lrrtm3	1,95	0,000046	0,902778667	0,068234233
Sdk2	1,95	0	0,821088333	0,415598667
Shd	1,95	0,000062	0,507228667	0,151724633
Btg2	1,94	0	6,549443333	3,343546667
Gata2	1,94	0,000034	0,491944	0,169356333
Pacsin1	1,94	0	1,912726667	0,787819333
Gsap	1,93	0,000009	0,669623667	0,310419333
Rec8	1,93	0	4,114806667	1,84496
Sh2d3c	1,93	0,000031	0,818750333	0,275421667
Akap12	1,92	0	14,0945	7,298506667
Dkk4	1,92	0,000025	2,2843	0,867011
Hgf	1,92	0	8,35747	4,295233333
Nptx1	1,91	0,00011	1,099541667	0,286792667
Slitrk5	1,91	0,000001	0,892158333	0,404205333
Gpr153	1,9	0	1,06533	0,50238
Thsd7a	1,89	0	1,83267	0,882346333
Col6a1	1,88	0,000045	0,377783	0,153892333
Fos	1,88	0,000146	0,475505667	0,175915333
Mlxipl	1,88	0,000026	0,488486333	0,257925667
Ntng2	1,88	0,000109	0,774348	0,267414233
Prlr	1,88	0	0,722455333	0,378975333
Dnajc1	1,87	0	21,9592	12,5229
Nlgn1	1,87	0,000128	0,386359333	0,149358367
Oprk1	1,87	0,000002	0,973123667	0,439793
Fam227a	1,86	0,000007	0,780649	0,346272333
Myrip	1,86	0,000186	0,351154667	0,1141592
Rras	1,86	0,000002	4,521663333	2,160266667
Shisa7	1,86	0	1,128241667	0,522954667
Tcerg1l	1,85	0,000096	0,776737	0,269921
Nrros	1,84	0,000027	0,923505	0,758828667
Umodl1	1,84	0,000238	0,122265667	0,031840767
Cacng7	1,83	0,000001	3,25426	1,591497667
Chn2	1,83	0	3,793583333	1,84883
Cmklr1	1,83	0	4,84077	2,36689

ANEX 8.2 DEG

Cxcr4	1,83	0,000053	1,372066667	0,640287333
Edil3	1,83	0	1,86401	0,932528333
Fcer1g	1,83	0,000163	0,839304667	0,1558038
Kcnq4	1,83	0,000001	1,1649	0,553214667
Ncan	1,83	0,000121	0,215868333	0,0883716
Tekt2	1,83	0,000262	0,750618	0,216114333
Adcy1	1,82	0	2,028323333	1,168316667
Cbr2	1,82	0	51,6558	27,99506667
Lrrc9	1,81	0,000131	0,587926333	0,141810667
Map1a	1,81	0,00004	0,366794333	0,1057023
Igtp	1,8	0,000051	1,377676667	0,629526
Ampd3	1,79	0,000364	0,566702333	0,1200582
Cldn23	1,79	0	4,971743333	2,657856667
Rspo1	1,79	0,000047	2,010546667	0,920659333
Vsnl1	1,79	0,000462	0,759095667	0,275399
Fas	1,78	0,000584	0,720733	0,181987
Negr1	1,78	0	3,11063	1,478687
Ppp1r3b	1,78	0	2,327643333	1,239686667
St8sia2	1,78	0,000045	3,49683	1,68103
Adamts1	1,77	0,000373	0,83144	0,379208667
Clmp	1,77	0,000114	6,898946667	3,98882
Adgrv1	1,76	0,000173	0,453909	0,1752036
Ebf2	1,76	0,00054	0,2600814	0,054734767
Ckb	1,75	0	5,63227	3,106946667
Tfap2b	1,75	0	98,60483333	56,46926667
Tnc	1,75	0,000493	0,278267	0,120471967
Cacna1h	1,74	0,000335	0,347071667	0,287550333
Col8a2	1,74	0,000859	0,171240667	0,211924967
Fam131a	1,74	0,000615	0,224980667	0,066345767
Krt9	1,74	0	10,96207333	6,189036667
Mxd1	1,74	0	3,840846667	2,15847
Egfem1	1,73	0,000502	0,969695667	0,491871667
Itgb7	1,73	0,000112	0,6713	0,358385
Klhl31	1,73	0,00032	0,268426	0,125613467
Slc25a48	1,73	0,000668	0,423820667	0,182939667
Slc4a8	1,73	0,000024	0,772291667	0,462464
Susd2	1,73	0,000269	0,706216333	0,344947
Tmem151b	1,73	0	2,60217	1,483386667
Tnfrsf11a	1,73	0,000857	0,242047333	0,133327467
Ttc28	1,73	0	4,838196667	2,62285
Adamts16	1,72	0,000356	0,617088	0,253064667
Grik1	1,72	0,001189	0,208559667	0,0761104
Lcp1	1,72	0,000646	0,570571	0,246064
Olfml2b	1,72	0,000397	0,620355667	0,292915667

Trpm6	1,72	0,001077	0,122262333	0,042063267
A830018L16Rik	1,71	0,001343	0,258694333	0,119480033
Efhc2	1,71	0,000004	1,893656667	0,994199333
Fam43a	1,71	0,000057	0,888895333	0,462248
Gjb6	1,71	0	15,23443333	8,920613333
H2-K1	1,71	0,000001	3,674953333	2,188646667
Ntf3	1,71	0,000424	1,678793333	0,802129333
Adgrf2	1,7	0,001423	0,208308667	0,0753691
Cyyr1	1,7	0,000078	0,802923333	0,414138667
Irx3	1,7	0,000483	0,631359333	0,283802
B230118H07Rik	1,69	0	21,3641	13,623
Capsl	1,69	0,000015	6,698443333	3,733453333
Chrn4	1,69	0,001639	0,194323	0,0409857
Gstt3	1,69	0	4,138736667	2,418193333
Ifitm1	1,69	0,000115	7,127636667	3,836543333
Pirb	1,69	0,000876	0,245206667	0,097136633
Pou6f1	1,69	0,000248	0,564634333	0,387042
Rnf213	1,69	0	1,77169	0,931227667
Vav3	1,69	0	2,179186667	1,106898
Dact3	1,68	0,000709	1,073794667	0,537005333
Dnah7b	1,68	0	1,130633667	0,361910333
Galnt18	1,68	0	13,8654	8,396546667
Hoxa1	1,68	0,00001	2,757243333	1,583633333
Kif27	1,68	0,000209	0,514947	0,261768667
Psd2	1,68	0,000589	0,393073333	0,197279
Tmem200b	1,68	0,000869	0,2013573	0,0264145
Hoxb1	1,67	0,002037	0,669610667	0,268327667
Ncf1	1,67	0,001742	0,312305333	0,0476196
Rarres2	1,67	0,002234	3,544393333	3,178186667
Rgs9	1,67	0	2,620726667	1,46292
Sncaip	1,67	0,000114	1,458323333	0,810496333
Spo11	1,67	0,000629	0,710181667	0,355658667
Cend1	1,66	0,002213	0,914869	0,339256667
Nid2	1,66	0,002068	2,611356667	1,101789
Plekhb1	1,66	0,000309	1,49803	0,62998
Rgag1	1,66	0,001497	0,1400962	0,0309455
Ror1	1,66	0,000006	8,820773333	5,050376667
Astn2	1,65	0,002091	1,524953333	0,706945667
Eda	1,65	0,000018	1,20106	0,638022
Efha	1,65	0,001392	0,134509333	0,025886033
Exph5	1,65	0	7,84285	4,898863333
Rasl11b	1,65	0	17,23206667	10,18061
Rnase4	1,65	0,000037	4,58519	2,579586667
Syt17	1,65	0,000156	1,199162667	0,660931667

ANEX 8.2 DEG

Cntn4	1,64	0,001916	0,300456	0,085772367
Dcxr	1,64	0,000023	6,32681	3,80229
Dnah2	1,64	0,001142	0,195733667	0,142885667
Kremen2	1,64	0	18,94193333	11,712
Lrrc32	1,64	0,002339	0,332742667	0,146524
Maf	1,64	0,002799	0,200401333	0,0750356
Prune2	1,64	0	0,533521	0,316781667
Sipa1l2	1,64	0	2,50851	1,50266
Slc35d1	1,64	0	13,46106667	8,366803333
Tll1	1,64	0,002751	0,319568333	0,135247867
Ttc30b	1,64	0,000197	1,250768667	0,694537667
Cttnbp2	1,63	0	2,52628	1,611313333
Cx3cl1	1,63	0,00287	0,367931	0,273598733
Dnajc6	1,63	0	5,088103333	3,23591
Gprc5a	1,63	0,002409	0,253228	0,062659533
Impg2	1,63	0,002622	0,197542333	0,134344667
Lgr4	1,63	0	10,91663333	6,964403333
Pde3a	1,63	0,000173	0,658159667	0,371527667
Rab11fip2	1,63	0	11,91186667	7,317336667
Relb	1,63	0,003409	0,373952333	0,113713467
Zfp36l2	1,63	0	16,9627	10,46578333
Art4	1,62	0	7,324116667	4,4495
Entpd1	1,62	0,002436	0,368702	0,039771653
Oit1	1,62	0,003757	0,490783	0,175633467
Rgma	1,62	0	12,34589	9,50357
Skap2	1,62	0	39,7481	25,93243333
Slc2a9	1,62	0,000247	1,195853	0,735979667
Snx13	1,62	0	13,30413333	8,09582
Sytl2	1,62	0,000006	3,029026667	1,774383333
Acbd4	1,61	0,000907	2,864593333	1,88629
Ecm2	1,61	0,001388	0,413353333	0,208678667
Ednrb	1,61	0,001783	0,399042667	0,206394
Gas1	1,61	0	43,47316667	27,34496667
Hoxa5	1,61	0,002948	0,652372667	0,315512667
Runx1t1	1,61	0,001742	5,735816667	2,936653333
Spag17	1,61	0,003396	0,1652162	0,0587736
Tjp3	1,61	0,000001	2,69162	1,603326667
Dcn	1,6	0,004736	0,386193333	0,138637567
Dpf3	1,6	0,003873	0,484716667	0,209293667
Emilin1	1,6	0,000085	4,29169	2,791376667
Lmod1	1,6	0,003304	0,320227667	0,159652333
Moxd1	1,6	0	13,78556667	8,707446667
Pcdh11x	1,6	0,004759	0,187718567	0,0810773
Rffl	1,6	0	11,0786	10,6496

Sema3e	1,6	0	1,931596667	1,257573333
Sfmbt2	1,6	0,000027	0,837118	0,563947333
Adamtsl5	1,59	0,000719	0,694961667	0,393876
Clip3	1,59	0	92,16736667	56,4451
Cpeb2	1,59	0,000001	1,89387	1,085625667
Itga9	1,59	0	8,779336667	5,328646667
Lpar3	1,59	0,001718	0,886593	0,479827667
Lpar4	1,59	0,000001	2,876626667	1,760446667
Mturn	1,59	0,000005	1,561373333	0,963356333
Penk	1,59	0,000002	5,983193333	3,67269
Plat	1,59	0,004968	0,468456	0,221510967
Rgmb	1,59	0,000001	4,957386667	3,028586667
Trp53inp1	1,59	0	17,07776667	10,96103333
Actn3	1,58	0,006026	0,2176	0,1374339
Bmf	1,58	0	12,35096667	7,692386667
Cabyr	1,58	0,005075	0,759432333	0,320246367
Cthrc1	1,58	0	10,10618333	6,4677
Lrrc17	1,58	0,005348	0,809172	0,388377
Mlf1	1,58	0,004632	1,151942667	0,570856
Prickle2	1,58	0,000012	0,936541667	0,580927
Sdk1	1,58	0	4,268856667	2,562886667
Unc5a	1,58	0,004019	1,259705	0,416360333
Aifm2	1,57	0,006342	0,471111667	0,270974
Cyp4v3	1,57	0,006841	0,255499	0,1018777
D7Erttd443e	1,57	0,006543	0,466193333	0,237872667
Dnm1	1,57	0,006393	6,736093333	2,790046667
Dzank1	1,57	0,000403	0,470343	0,388654
Gjb2	1,57	0,000083	96,96413333	58,94676667
Gm3558	1,57	0,006621	0,376737333	0,168123333
Hhip	1,57	0,000088	0,625119	0,368048333
Lrig1	1,57	0	11,15700667	8,574503333
Necab1	1,57	0,004068	0,434300333	0,266208
Ptges3l	1,57	0,006475	1,304728	0,482316667
Ptk2b	1,57	0,006104	0,275183333	0,138561433
Tgfbr3	1,57	0,001747	4,030003333	2,400063333
Abcc2	1,56	0,005051	0,1263966	0,041016733
Col23a1	1,56	0,005907	1,165256333	0,342182
Crtac1	1,56	0,003001	0,605751333	0,343982
Dpysl3	1,56	0	7,052766667	4,573303333
Efcab1	1,56	0	8,923846667	5,776623333
Glp1r	1,56	0,000718	0,138236	0
Kcnd1	1,56	0,000002	2,471536667	1,65154
Lrrc4	1,56	0,000103	1,85451	1,225224333
Oacyl	1,56	0,000569	0,825251333	0,474109

ANEX 8.2 DEG

Rbms3	1,56	0	6,26612	3,981276667
Adamtsl2	1,55	0,002191	1,305796667	0,741307
BC051142	1,55	0,003357	0,203084	0,03945
C2cd4d	1,55	0,00866	0,902803	0,303000667
Cfap53	1,55	0,007289	0,706402333	0,386149333
Ddx4	1,55	0,00754	0,205102333	0,067478207
Dnm3	1,55	0,000021	2,75901	1,37504
Efnb3	1,55	0	5,528946667	3,534456667
Enpp4	1,55	0,000101	0,975773	0,596144667
Exoc3l4	1,55	0,007585	0,421878	0,178964
Fli1	1,55	0,00829	8,07206	3,27656
Lima1	1,55	0	23,27253333	15,04946667
Mas1	1,55	0,004245	0,894119667	0,474151
Nap1l3	1,55	0,000769	0,996461	0,592462333
Npc1l1	1,55	0,0086	0,117837333	0,044293933
Pdk4	1,55	0,00481	0,914425333	0,597177667
Rel	1,55	0,00004	1,485496667	0,922299333
Serpina3i	1,55	0,003448	0,156990167	0,012618267
Sh3bp5	1,55	0	12,3342	7,80359
Spock2	1,55	0	2,103893333	1,380426667
C1ql3	1,54	0,003939	0,151871033	0,048079633
Ces1d	1,54	0,004621	0,917501333	0,529698
Fam228b	1,54	0,00967	0,160958	0,0626186
Gata3	1,54	0,000001	5,283353333	3,594243333
Gpr20	1,54	0,000026	5,401223333	3,298193333
Hmgn3	1,54	0,000001	20,6045	12,88206667
Ifitm3	1,54	0,000041	245,3126667	154,8986667
Klk12	1,54	0,009123	0,148316333	0,0375898
Myrf	1,54	0,000199	1,202976667	0,695642333
Pgm5	1,54	0,004705	0,285551767	0,054284133
Ppp1r14c	1,54	0,000004	7,59266	4,79301
Rdh12	1,54	0,007899	0,769743	0,370934333
Sostdc1	1,54	0	20,3893	13,28206667
Aass	1,53	0,000373	1,020484333	0,672899667
Alpk1	1,53	0,004958	0,38117	0,164774333
Capn1	1,53	0,000293	1,367813333	0,810381333
Cox6b2	1,53	0,000027	16,90176667	10,54427333
Eepd1	1,53	0,006952	0,712306667	0,380151
Has2	1,53	0,009734	1,87422	0,708442667
Mxd4	1,53	0	7,37151	4,635963333
Myo5b	1,53	0,000001	4,371416667	2,967776667
Papolb	1,53	0,009624	0,185456333	0,0690207
Phactr1	1,53	0,004912	0,996765	0,285675667
Rab20	1,53	0,009202	0,716535	0,351261

Rbm24	1,53	0,007393	0,405105	0,220504333
Slit3	1,53	0	10,38927	6,632056667
Col6a2	1,52	0,008758	0,368415667	0,198215667
Cyp2u1	1,52	0,006494	0,132742167	0,051169133
Dmrt2	1,52	0,001962	0,115507633	0
Gprc5c	1,52	0	78,4535	47,2313
Mapk13	1,52	0,00033	3,579913333	2,185303333
Nkain4	1,52	0,00844	1,768666667	0,831438
Rac3	1,52	0,000076	5,727316667	3,789223333
Rhoq	1,52	0	6,58906	4,367526667
Smad1	1,52	0	15,26846667	10,19539
Tril	1,52	0	15,04046667	9,916696667
Ankrd44	1,51	0,005071	6,655766667	3,96904
Anxa8	1,51	0,000495	2,943896667	1,900273333
Cap2	1,51	0,00168	0,995674667	0,548511
Ggt1	1,51	0,005998	1,588233333	1,124367333
Pkdcc	1,51	0,008738	1,609684667	0,447438667
Plekha6	1,51	0	3,00547	2,099863333
Podxl2	1,51	0,009047	1,033129333	0,469095
Rdh10	1,51	0	11,99656667	8,030433333
Selenop	1,51	0,000015	67,80976667	29,19573333
Tyrobp	1,51	0,004961	0,602655	0,105130333
Arhgap8	1,5	0	16,89973333	11,3818
Cldn8	1,5	0	7,224446667	4,827156667
Csrp2	1,5	0,000326	7,275323333	4,705826667
Dtx4	1,5	0,000177	0,809248	0,526093667
Lmtk3	1,5	0,003567	2,040816667	1,203638
Nbl1	1,5	0,007732	1,151504667	0,278270667
Pcdhb22	1,5	0,002478	0,527315333	0,296488667
Pik3c2g	1,5	0,006286	1,062530333	0,647166
Podxl	1,5	0	22,7377	15,21036667
Rnasel	1,5	0,00032	1,82829	1,156457
Sgip1	1,5	0	8,054406667	5,557363333
Slc24a3	1,5	0,00681	0,588937	0,354875

Down-regulated in Sp8KO

Symbol	FoldChange	pValue	KO_average; FPKM	WT_average; FPKM
Fam46a	-70,39	0	0,1130871	14,0692
Rspo2	-36,16	0	0,227233333	13,9666
Fgf4	-31,91	0	0,0359366	10,22486333
Vwde	-21,77	0	0,118330667	11,39416667
Slc35d3	-19,79	0	0,012607267	2,94962
Itga4	-16,08	0	0,516149333	9,867636667
St6galnac5	-13,89	0	0,151237	3,24053
Tmem229a	-13,25	0	0,278443	5,480223333
Rgs5	-13,17	0	0,443287333	11,32343333
Bambi	-12,32	0	0,587457333	8,424433333
Gpx2	-11,2	0	0,293212	22,02033333
Smpd3	-11,1	0	0,127725233	2,232896667
Slc16a10	-10,93	0	1,241793333	14,4957
Fgf9	-9,84	0	0,846250333	10,68130333
Pou6f2	-9,49	0	0,202987667	2,604323333
Slc41a2	-9,29	0	0,014239433	0,850937333
Slitrk4	-9,03	0	0,381942333	3,761966667
Sorbs2	-8,49	0	2,533456667	26,98593333
Slc6a2	-8,39	0	0,138220433	1,71377
Ube2ql1	-8,3	0	0,045320767	1,419526667
Nrxn3	-8,23	0	0,018090713	0,892135667
Srms	-7,94	0	0,031879797	1,294793333
Fgf3	-6,81	0	0,0036767	1,079854
Adamts20	-6,59	0	0,404698	2,906153333
Sct	-6,37	0	0,313379667	10,10406
Sp9	-6,18	0	0,0224519	0,638465
Cd44	-5,72	0	1,310871	27,73086667
Vat1l	-5,31	0	0,429907	2,954036667
Tulp2	-5,24	0	0,550712667	3,414676667
Rcan2	-5,18	0	0,453854667	3,47334
Kirrel3	-5,02	0	0,570330333	3,10451
Gad2	-4,73	0	0,020311467	0,441251
Fgf8	-4,72	0	0,645113	32,50576667
Bhlha9	-4,67	0	2,209666667	34,33073333
Scn3a	-4,65	0	0,170863333	0,937333
Lmo7	-4,64	0	3,82254	18,24943333
Wnt5a	-4,6	0	13,34343333	64,68016667
Igfbpl1	-4,53	0	0,026592	0,664732
Gprin3	-4,47	0	0,0451535	0,437341
Slc27a6	-4,47	0	0,576655333	3,55987
D930020B18Rik	-4,43	0	0,007775233	0,58126
Lrrtm1	-4,41	0	0,492834	2,79445
Plcx3	-4,39	0	0,583109	3,7042
Enpp1	-4,36	0	0,833230333	3,856073333

Dio2	-4,22	0	0,012261067	0,420086667
Fam20c	-4,19	0	0,225835333	1,59932
Sp8	-4,16	0	0,787067333	10,92922333
Rab11fip5	-4,12	0	0,681591667	3,18105
Fzd1	-4,09	0	11,75496667	51,2285
Fam19a2	-4,08	0	0,100420133	0,763074
Vldlr	-4,03	0	0,825576333	3,581623333
Galnt6	-4	0	0,036838533	0,542155333
Slc39a14	-3,91	0	1,8722	7,63486
Col19a1	-3,89	0	0,111817	0,769403
D430041D05Rik	-3,89	0	0,243856667	1,141653333
Spon1	-3,88	0	0,276326	1,523723333
Creb3l1	-3,82	0	0,078089867	0,768058
Gcg	-3,81	0	0,020253067	1,262925
Isl2	-3,78	0	0,078568033	0,988847333
Pou4f1	-3,74	0	0,1737463	1,410093333
Sall1	-3,73	0	1,677583333	6,78539
Cyp26a1	-3,7	0	1,131361667	5,140893333
Lrrk2	-3,68	0	0,438952	1,853526667
Lmo2	-3,67	0	0,333829667	2,343243333
Satb2	-3,63	0	0,958798	3,40618
Adamts3	-3,49	0	0,460883	5,54744
Sstr2	-3,46	0	0,337198	1,87714
Adamts18	-3,36	0	5,376846667	19,38793333
C1qtnf3	-3,36	0	1,397443333	8,060143333
Thbs1	-3,36	0	3,81984	15,6704
Grm8	-3,35	0	0,252506133	1,19007
Msx2	-3,33	0	13,4642	46,8229
Sptlc3	-3,33	0	2,445526667	9,23311
Kcne1l	-3,31	0	0,380248	2,061796667
Sema6d	-3,31	0	1,641253333	7,73586
Abca4	-3,27	0	1,045229333	3,374163333
Itgb8	-3,26	0	0,827199667	2,51848
Pgbd5	-3,21	0	0,259008667	2,459396667
Tcf7	-3,19	0	9,049796667	30,9325
Lbh	-3,18	0	17,10533333	63,62763333
Bmp4	-3,17	0	37,66223333	125,4873333
Prkd1	-3,17	0	0,868275333	3,18921
Dpp4	-3,14	0	0,105359233	0,429577667
Lrrn1	-3,13	0	1,103857333	8,665813333
Colec12	-3,09	0	2,542466667	9,114
Plekha2	-3,08	0	0,663436333	2,797903333
C430049E01Rik	-3,07	0	0,0151403	0,545345333
Relt	-3,07	0	0,210681667	0,961634
Spry1	-3,07	0	5,772086667	18,82953333
Gad1	-3,05	0	0,0093016	0,275118667
Gpnmb	-3,02	0	0,1017022	0,700854
Scara3	-3,01	0	0,671827	2,494923333

ANEX 8.2 DEG

Il1rap	-3	0	0,341132	1,33781
Gpr68	-2,97	0	0,014290967	0,336793667
Col17a1	-2,96	0	0,616402	2,08696
Cybrd1	-2,96	0	0,067722333	0,434700333
Map2	-2,93	0	4,77111	16,38943333
Dlx1	-2,92	0	2,55305	10,69123333
Rassf9	-2,92	0	1,152365333	4,207126667
Slc13a5	-2,92	0	0,0222873	0,341099333
Frem1	-2,89	0	3,469363333	10,81820667
Pcolce2	-2,89	0	0,1166581	1,172832
Fat3	-2,87	0	5,397876667	15,71566667
Hao	-2,87	0	0,130764933	1,050041333
Snap91	-2,87	0	0,945704	5,52032
Id1	-2,84	0	3,28574	10,90881667
Proser2	-2,83	0	1,056225333	3,390253333
Pcsk6	-2,81	0	0,380384667	1,48715
Cacna1i	-2,8	0	0,045229143	0,227433333
Epha2	-2,8	0	0,751885333	2,49105
Abcc3	-2,78	0	0,190289033	0,466188
Arfgef3	-2,77	0	0,400551333	1,265026667
Dlx2	-2,76	0	1,92285	10,05765333
Acpp	-2,75	0	4,8876	15,58086667
Adgrg6	-2,74	0	0,656672333	2,1177
Cd36	-2,72	0	0,516114667	2,285073333
Mgst3	-2,71	0	3,235686667	10,05194
Otx1	-2,71	0	0,0604467	0,438026667
Efhd1	-2,7	0	0,0688524	0,661602
Sp7	-2,69	0	0,0387259	0,346777333
Fam89a	-2,68	0	1,316703667	4,70842
Nedd9	-2,68	0	1,856216667	5,350796667
Slc7a1	-2,68	0	3,397096667	11,8091
Cox4i2	-2,67	0	3,267646667	10,40303333
Eogt	-2,67	0	8,568716667	24,92786667
Itm2b	-2,67	0	32,85776667	92,0631
Bach2	-2,64	0	5,727333333	14,83353333
Fgf17	-2,64	0	0,1083614	0,918139667
Dkk1	-2,62	0	0,68166	2,288016667
Eva1a	-2,62	0	0,1054006	0,751263
Hoxc9	-2,62	0	0,621238667	2,037216667
Hoxc10	-2,61	0	0,207413667	3,53469
Unc5c	-2,61	0	4,617996667	12,4683
Dlx4	-2,59	0	0,793906	2,512216667
Fam81a	-2,59	0	0,1363181	0,656722
Tmem200c	-2,59	0	0,06479478	0,457825333
Luzp2	-2,57	0	0,0086213	0,184844
Msx1	-2,56	0	2,66531	7,63007
Ambn	-2,54	0	0	0,332857333
Gpr87	-2,54	0	0,425412	1,794916667

Tnni1	-2,54	0	0,126767667	0,931234667
Abcg5	-2,51	0	0,240317333	0,870118333
Syt2	-2,51	0	0,1670918	0,392685333
Tnfaip8l3	-2,49	0	0,015773717	0,178560667
Enc1	-2,47	0	2,522516667	6,538753333
Gpr85	-2,46	0	0,45651	1,53754
Tgfb1	-2,46	0	0,376672667	1,378273333
Gja1	-2,45	0	39,3664	100,9780333
Raly1	-2,45	0	0,007342067	0,808779667
Tmtc1	-2,44	0	1,19982	3,198706667
Agpat9	-2,41	0	0,148654233	0,575399333
Dcbld1	-2,41	0	5,568873333	14,82256667
Hrk	-2,4	0	0,0255296	0,183919333
Gldn	-2,38	0	0,0137623	0,159908667
Trhde	-2,37	0	0,022080253	0,625176667
N4bp3	-2,36	0	0,681562333	1,874153333
Lad1	-2,35	0	3,600803333	13,33813333
Nsg2	-2,35	0	0,453315667	1,409713333
S100a6	-2,35	0	5,533173333	15,8735
Fjx1	-2,34	0	8,13314	20,3483
Palld	-2,33	0	3,359466667	8,357913333
Fgf15	-2,32	0	0,0189782	0,389445333
S1pr1	-2,32	0	0,186628333	0,721221667
Pof1b	-2,31	0	0,182526667	0,660019
Diras2	-2,3	0	1,580163333	3,972343333
Gabrb2	-2,3	0,000001	0,090295033	0,561717667
Hk2	-2,29	0	37,38116667	107,1712333
En1	-2,27	0	2,825166667	11,21795667
Gria1	-2,27	0	0,158226333	0,409379
Khdrbs3	-2,27	0	6,65815	16,2882
Serpinb6c	-2,26	0,000001	0,070820267	0,664903
Adam9	-2,25	0	3,175196667	7,623886667
Eya2	-2,25	0	2,40968	6,366716667
Ablim2	-2,24	0	0	0,2168239
Dok5	-2,24	0	0,501707667	1,528786667
Itga2	-2,24	0	0,170580667	0,554688333
Slc30a4	-2,23	0	3,93634	9,35328
Arhgef3	-2,22	0	1,243611333	3,232413333
Fmn1	-2,22	0	3,02826	6,356556667
Grm4	-2,22	0,000002	0,0795126	0,351333
Prickle1	-2,22	0	2,018403333	4,901083333
Slc16a12	-2,22	0	0,37848	0,97232
Adam19	-2,21	0	1,449193333	4,997093333
Dsg3	-2,21	0,000001	0,0734617	0,292486
Man2a1	-2,21	0	12,8564	30,6964
Smad9	-2,21	0,000002	0,021714267	0,132994333
Atoh8	-2,2	0	0,760831333	2,073286667
Stc2	-2,2	0,000001	0,120819333	0,467571

ANEX 8.2 DEG

Hoxc13	-2,19	0	0,0644606	2,49458
Tiam2	-2,19	0	0,517636333	1,446336667
C130074G19Rik	-2,18	0,000002	0,1053041	0,448365667
Adcyap1r1	-2,17	0,000003	0,026313833	0,131515933
Grhl1	-2,17	0	0,337765333	0,950205667
Atxn1	-2,16	0	1,62408	3,676566667
Pcdh19	-2,16	0,000004	0,796735	4,046803333
Zfp322a	-2,16	0	24,68716667	52,7568
Ttc9	-2,15	0	0,389488	1,158246667
Wipf3	-2,15	0	1,266066667	2,971946667
Wnt7a	-2,15	0	16,1559	32,49006667
Fam196b	-2,13	0	0,669818333	1,57828
St14	-2,13	0	11,08816	25,38343333
Gsg1	-2,12	0,000004	0,263597	1,232284
Slc16a7	-2,12	0	3,542133333	5,756503333
Adamts5	-2,11	0	0,579968	1,326536667
Id4	-2,11	0,000001	0,473256667	1,372316667
Plpp3	-2,11	0	8,372663333	18,65233333
Tbc1d4	-2,11	0	1,844133333	4,130796667
Plxnc1	-2,1	0	0,792741333	1,893483333
Rxfp3	-2,1	0,000008	0,027993867	0,180676333
Chrna7	-2,09	0	0,437573667	1,15608
Fam189a2	-2,09	0,00001	0,0583458	0,291639333
Ust	-2,09	0	0,755358	1,77937
Id3	-2,08	0	13,7309	34,80326667
Pdzd2	-2,07	0	0,542365667	1,203980667
Bmp5	-2,06	0	0,618557333	1,703836667
Egln3	-2,06	0,000001	0,501383333	1,351719
Pcsk1	-2,06	0,000015	0,077969567	0,281510333
Cdh10	-2,05	0,000015	0,089957133	0,364551333
Cntnap4	-2,05	0,000016	0,185792667	0,329888
Chst8	-2,04	0,000006	0,392950667	0,949053333
Crhr1	-2,04	0	0,732024	1,890706667
Fam19a4	-2,04	0,000012	0,175576667	0,538357667
Kcnj15	-2,03	0	2,726293333	5,906573333
Mycn	-2,03	0	10,39479	22,2418
Ptprz1	-2,03	0	0,33887	0,905102333
Tnnt2	-2,02	0,000009	0,00784	0,256251667
Capg	-2	0	5,075616667	11,1895
Clu	-2	0,000004	0,546526333	1,503216667
Nrxn1	-2	0	1,457094	2,291866667
Cntn5	-1,99	0,000015	0,051379337	0,131693
Hspa2	-1,99	0	1,165376667	2,587096667
Maff	-1,99	0,000003	0,487685	1,513796667
Pdlim5	-1,98	0	5,383233333	10,69766333
Stac	-1,98	0,000044	0,098046767	0,527012667
Fam19a1	-1,97	0,000031	0,026414833	0,338872667
Nrg1	-1,97	0,000037	0,161011467	0,413143667

Ntm	-1,97	0,000021	1,90574	6,007593333
Prdm1	-1,97	0,000045	1,464878667	4,704803333
Qrfpr	-1,96	0,000009	0,011693233	0,304795
Unc5b	-1,96	0	10,89654333	23,7929
Olfm2	-1,95	0,000062	0,0808039	0,387958667
Sgms2	-1,95	0	0,822176333	1,90464
Lnx1	-1,94	0	1,026547667	2,918043333
Tle4	-1,94	0	6,941526667	14,00206667
Etv4	-1,93	0,000069	1,717783333	5,3708
Calcr	-1,92	0,000038	0,178692	0,575235667
Cpxm1	-1,91	0	3,946066667	8,570286667
Igfbp3	-1,91	0	3,348823333	6,924773333
Myo6	-1,91	0	0,526613667	1,050851667
Itgb4	-1,9	0	0,749207333	1,66747
Nuak1	-1,9	0	0,940935667	2,200733333
Pkp1	-1,9	0	1,524553333	3,10534
St8sia3	-1,9	0,000011	0,1793	0,795461333
Hs3st1	-1,89	0,000098	0,397527333	1,140347667
Myc	-1,89	0	1,992243333	4,276913333
Nfia	-1,89	0	2,4054	5,994923333
Plcb1	-1,89	0	1,38159	2,16272
Timp3	-1,89	0	4,110523333	8,09322
Tmem100	-1,89	0,000144	0,137585167	0,504018
Trpc5	-1,89	0,000021	0,024802467	0,551350667
Clca2	-1,88	0,000146	0,0520504	0,236235667
Tuba8	-1,88	0,000052	0,022429133	0,250575
AF529169	-1,87	0,000188	0,031749467	0,155714667
Ankrd6	-1,87	0	4,41303	8,602776667
Btbd3	-1,87	0	5,345043333	10,41998667
Dlx6	-1,87	0,000059	0,906473	2,747836667
Etv5	-1,87	0,00008	11,24933	30,2235
Lrrc15	-1,87	0,000001	0,545468667	1,178743333
Tbx3	-1,87	0	5,47249	10,34328667
Bmp8a	-1,86	0,000119	0,018734433	0,226056667
Emp1	-1,86	0	47,83003333	91,85706667
Fgf1	-1,86	0,000126	0,953306	2,502716667
Ofcc1	-1,86	0,000182	0,124300567	0,379440667
Pik3r1	-1,86	0	12,3975	22,99263333
Serinc5	-1,86	0	4,8298	9,376443333
Abhd3	-1,85	0,000086	0,413326	1,152170667
Epha4	-1,85	0,000003	8,072006667	17,66566667
Shh	-1,85	0,000199	0,065240633	0,291071
Tubb6	-1,85	0,000001	20,6737	44,30983333
Celsr2	-1,84	0	6,24427	11,49186667
Lmx1a	-1,84	0,000217	0,0928049	0,278626
Mamld1	-1,83	0,000143	0,142314133	0,413585667
Selenbp1	-1,83	0,000046	0,474450667	1,101503333
Slc39a11	-1,83	0,000001	0,903323333	2,024136667

ANEX 8.2 DEG

1700024P16Rik	-1,82	0,00026	0,122580233	0,368321
Gas7	-1,82	0	0,632849333	1,14048
Pcsk5	-1,82	0	3,85148	7,503733333
Abcg8	-1,81	0,000388	0,079295533	0,243659333
Ackr3	-1,81	0,000004	6,46739	13,44576667
Arntl	-1,81	0	1,922336667	3,954406667
Dlx5	-1,81	0,000012	8,203183333	17,7475
E130012A19Rik	-1,81	0	1,30784	2,62352
Sox8	-1,81	0,000245	0,288308333	0,555439
Tox	-1,81	0,000001	0,915194667	1,859233333
Alcam	-1,8	0,000241	3,543566667	8,659756667
Dgkk	-1,8	0	2,017173333	3,892286667
Ina	-1,8	0,000421	0,0874743	0,263997333
Mapkbp1	-1,8	0	2,43966	4,941956667
Megf11	-1,8	0	0,350429667	0,898571333
Aox3	-1,79	0,000037	0,01399484	1,759219667
Dusp8	-1,79	0,000489	0,036745267	0,1694386
Has3	-1,79	0	0,962412	1,894113333
Nr4a1	-1,79	0,000122	0,331478667	0,747292667
Utf1	-1,79	0,000481	0,143643867	0,678589
Zim1	-1,79	0	12,18613333	23,6267
Egfr	-1,78	0	6,306313333	11,867
Kremen1	-1,78	0	6,0653	10,9046
Rnaset2a	-1,78	0,000417	0,248052	0,736576333
Angpt1	-1,77	0,000274	0,324852333	0,708564667
Ccdc85a	-1,77	0,000383	0,0279169	0,179040333
Dusp4	-1,77	0	2,782693333	5,32642
Fap	-1,77	0,000537	0,299112333	0,550158
Lrrc4c	-1,77	0,000064	0	0,120465233
Prr5	-1,77	0	10,89332	20,4358
Cpne2	-1,76	0	1,810536667	3,99132
Mid2	-1,76	0,000002	4,51312	8,764793333
Clca1	-1,75	0,000099	0,21188367	1,47126
Dync1i1	-1,75	0,000711	0,285715	0,609263667
Egr1	-1,75	0,00031	0,30302	0,684794333
Emx1	-1,75	0,000174	0,854315	1,986896667
Gna15	-1,75	0,000777	0,206741667	0,520845667
Hpca	-1,75	0,000142	1,151724	2,55359
Ica1	-1,75	0,000031	0,917794333	2,346226667
P4ha1	-1,75	0	9,780213333	18,74703333
P4ha2	-1,75	0	3,133	6,160646667
Sox2	-1,75	0,000367	0,033139633	0,234186333
Crmp1	-1,74	0	2,09583	3,73428
Pcdh9	-1,74	0,000001	1,268043333	2,0462
Ptn	-1,74	0,000004	92,172	181,5113333
4930427A07Rik	-1,73	0,000073	3,286553333	5,616506667
Sp6	-1,73	0,001027	8,203136667	25,12256667
Fgf5	-1,73	0,000141	0,747104333	1,553016667

Sox13	-1,73	0	6,69083	12,30133333
Spry4	-1,73	0,000673	11,46816	27,94606667
Tusc5	-1,73	0,000852	0,113488467	0,291887667
Acsl4	-1,72	0,000195	6,305203333	13,5845
Cdh2	-1,72	0,000851	1,907827667	8,59523
Chst3	-1,72	0	1,029673667	1,87695
Dlx3	-1,72	0	9,49502	16,97836667
Kcnt2	-1,72	0,000013	0,67313	1,37065
Bhlhe40	-1,71	0,000039	0,551414	1,105997333
Fam134b	-1,71	0	1,337913333	2,525626667
Glt1d1	-1,71	0,000103	0,519266333	0,900736667
Il17d	-1,71	0,000985	0,0422606	0,182174
P3h2	-1,71	0	2,933846667	5,17763
Pon2	-1,71	0	9,97588	18,22816667
Rassf10	-1,71	0	2,915343333	5,179856667
Slc25a33	-1,71	0,000002	1,478623333	2,732123333
Smpd3b	-1,71	0,001162	0,104237233	0,417928667
Steap1	-1,71	0,001267	0,269382667	0,745245333
Timm10	-1,71	0	15,47763333	27,95516667
1810041L15Rik	-1,7	0,000234	0,210461333	0,478374667
Klf4	-1,7	0,000465	0,266134667	0,630577667
Mtss1	-1,7	0	2,274023333	4,13089
Rgs4	-1,7	0,00018	0,003249207	0,1339004
Slc7a11	-1,7	0,000003	5,93825	11,36643333
Cemip	-1,69	0,001386	0,0907727	0,249004667
Krt17	-1,69	0,000084	0,871515667	1,730133333
Prcp	-1,69	0	5,2713	9,522606667
Txndc17	-1,69	0	70,8348	124,3493333
5031439G07Rik	-1,68	0	4,265113333	7,398653333
Atp2a3	-1,68	0,000378	0,005386973	0,105533167
Cyp26b1	-1,68	0,001434	6,45234	25,40436667
Jun	-1,68	0	1,261013333	2,264183333
Rbm43	-1,68	0	2,211563333	3,83697
S100a16	-1,68	0,000003	3,29116	6,106676667
Slc25a13	-1,68	0	6,415106667	10,92096667
Sptb	-1,68	0,000024	0,652982	1,619636667
Cobl	-1,67	0,000003	0,648217	0,967616
Cst3	-1,67	0	32,52736667	56,662
Parp8	-1,67	0	13,4891	23,53333333
Sh3tc1	-1,67	0,002155	0,136333033	0,187541667
Slc12a2	-1,67	0	4,104883333	7,163613333
Ttc39b	-1,67	0,000091	0,226089667	0,652201333
Arrdc4	-1,66	0	4,646406667	8,156196667
Fndc3a	-1,66	0	40,34343333	74,7753
Nr3c1	-1,66	0	1,28246	2,133893333
Psd4	-1,66	0,001133	0,269740567	0,473141
Slc52a3	-1,66	0,002304	0,1665357	0,45973
Tmem59l	-1,66	0,000014	2,636576667	4,92703

ANEX 8.2 DEG

Kcnf1	-1,65	0,002728	0,0654232	0,179481
Npm3	-1,65	0,000453	1,38666	2,83585
Plppr1	-1,65	0,001302	0,238723	0,523043333
Txnrd1	-1,65	0	415,4656667	601,156
Vegfd	-1,65	0,002636	0,400822333	0,839221333
Bgn	-1,64	0	5,651893333	9,551313333
Chl1	-1,64	0,002974	1,002137667	2,399063333
Evpl	-1,64	0,000003	0,525064667	0,944283
Fxyd3	-1,64	0,000268	14,69436667	29,4331
Gclm	-1,64	0	5,00468	7,855543333
Il20ra	-1,64	0,000284	0	0,102494267
Pxdc1	-1,64	0,001669	0,2493306	1,314692667
Sil1	-1,64	0,000008	1,82033	3,368563333
Coro6	-1,63	0,003526	0,0779617	0,245191333
Dusp6	-1,63	0	6,68029	11,43423333
Esyt3	-1,63	0,000828	0,62416	0,846018667
Fbxo40	-1,63	0,000347	0,503367333	0,948081667
Lclat1	-1,63	0	12,66636667	21,9893
Ppp2r2c	-1,63	0,002036	0,614440333	2,754293333
Pusl1	-1,63	0,001569	3,520006667	4,706626667
Rragd	-1,63	0	6,35591	10,22597333
Styk1	-1,63	0,002334	0,551389333	0,831680333
Zfyve28	-1,63	0,00311	0,0551499	0,173200667
Cited4	-1,62	0,002698	0,691167333	1,562543333
Eif4ebp1	-1,62	0,000001	5,478746667	9,449566667
Flt1	-1,62	0,003841	0,072822633	0,175835333
Gpm6b	-1,62	0,000269	0,525250667	1,109462
Gpr35	-1,62	0,003276	0,033619467	0,163085133
Id2	-1,62	0	14,24913333	24,20933333
Meox1	-1,62	0,003561	2,617056667	6,381396667
Mesdc2	-1,62	0	24,33646667	40,36876667
Tmeff2	-1,62	0,002959	0,178545333	0,408878333
Vipr2	-1,62	0,00363	0,275636667	0,304379
Adarb2	-1,61	0,0016	0,188802	0,352995333
Asphd2	-1,61	0,000901	1,194210333	2,45179
Atp2b3	-1,61	0,000453	0,345419333	0,662885
Galnt7	-1,61	0	9,00437	13,6343
Igsf11	-1,61	0,004101	0,1408344	0,258823
Nav3	-1,61	0,000388	0,406813	0,536482667
Sall3	-1,61	0,004181	0,515661	1,668663333
Smim3	-1,61	0,000027	1,62022	2,885443333
Tgfb2	-1,61	0,001261	2,933476667	4,959946667
Vwa1	-1,61	0	1,795113333	2,963766667
Car12	-1,6	0	3,245216667	5,57192
Ccdc149	-1,6	0,00303	0,252331333	0,540798667
Filip1	-1,6	0,002692	0,054727047	0,137559967
Galnt14	-1,6	0,001178	0,586323667	1,163263333
Hs3st3b1	-1,6	0	2,706446667	4,545613333

Itpr3	-1,6	0	1,20655	2,101866667
Map3k8	-1,6	0,000709	0,496809667	1,122355333
Nhp2	-1,6	0	26,95263333	45,77093333
Pdia6	-1,6	0	54,46133333	88,76143333
Pla2g12a	-1,6	0,000002	3,332763333	5,700996667
Rexo2	-1,6	0	22,33656667	37,64903333
Alpl	-1,59	0,003906	3,604776667	7,47787
Apcdd1	-1,59	0	12,28846667	20,2257
AW551984	-1,59	0,001436	0,300362333	0,563609333
Cpne8	-1,59	0,000054	10,01446667	13,8161
Etv3	-1,59	0	4,547543333	7,204223333
Fam3c	-1,59	0	18,61486667	31,59443333
Lrrfip1	-1,59	0	10,89865667	18,63583333
Pax8	-1,59	0,005771	0,1089344	0,343970333
Serpinh1	-1,59	0	59,81873333	97,44103333
Sgk3	-1,59	0	8,919406667	14,92106667
Srm	-1,59	0	14,31853333	24,2799
Ace2	-1,58	0,005235	0,164593333	0,298893333
Adamts12	-1,58	0,000522	0,256637333	0,441773667
Heyl	-1,58	0	3,19594	4,85071
Ifih1	-1,58	0,004709	0,352929667	0,388661667
Igfbp5	-1,58	0	182,6643333	297,896
Mogs	-1,58	0	5,268526667	8,631153333
Ptprd	-1,58	0	25,0558	40,5605
Slnf9	-1,58	0	3,781146667	6,39721
Tec	-1,58	0,001417	0,414611667	0,794058
Cmah	-1,57	0	10,19052667	16,70556667
Fut4	-1,57	0,000004	1,246303333	2,090703333
Papss2	-1,57	0,000518	0,40325	0,741461667
Rrp12	-1,57	0	1,821183333	2,916853333
Rrp9	-1,57	0,000002	3,954186667	6,5547
Spns2	-1,57	0,003559	0,391560333	0,794497333
Aox4	-1,56	0,003706	0,01583139	0,119472867
Arhgap26	-1,56	0,000001	4,41578	6,45065
Ccser1	-1,56	0,000478	1,672506667	3,39573
Gab2	-1,56	0,000004	1,642973333	2,38129
Mboat1	-1,56	0,001251	0,541296333	1,11242
Ncf2	-1,56	0,000806	0,382927333	0,872925333
Smad6	-1,56	0,000091	0,866865667	1,485313333
Ttpa	-1,56	0	2,357076667	3,995396667
Ccnd1	-1,55	0	31,14346667	50,96236667
Crat	-1,55	0	2,77048	4,334363333
Fam49a	-1,55	0	5,626266667	9,10715
Fut8	-1,55	0	2,89421	4,953083333
Gm14137	-1,55	0,008388	0,151367667	0,330657333
Gnai1	-1,55	0	5,91249	9,589863333
Hapln3	-1,55	0,00443	0,266880667	0,620290333
Rab15	-1,55	0,000082	12,34906667	20,55916667

ANEX 8.2 DEG

Tdrd7	-1,55	0,005602	0,280371333	0,45025
Adrb1	-1,54	0,005781	0,040947167	0,151584333
Aebp1	-1,54	0,00005	1,313726667	2,072723333
Aen	-1,54	0	11,76081	17,65833333
Cables1	-1,54	0,000447	0,683987333	1,241626667
Cerk	-1,54	0,000029	1,243823333	2,04525
Col13a1	-1,54	0,008483	0,110485733	0,278581
Col9a3	-1,54	0,005476	0,513698333	0,839674333
Grik4	-1,54	0,00108	0,661295667	1,192473333
Immp2l	-1,54	0,009879	0,408275667	1,038184333
Ltbr	-1,54	0,00032	1,447436667	2,89127
Mgat4a	-1,54	0	5,043526667	8,25903
Naaa	-1,54	0,00698	0,423666	0,755125667
Prdx4	-1,54	0	18,28076667	29,34333333
Rnf125	-1,54	0,00622	0,681597	1,360897333
Tln2	-1,54	0	35,15706667	60,5036
Carmil1	-1,53	0	11,09512333	29,21696667
Gpr179	-1,53	0,005624	0,075145333	0,148739667
Hacd1	-1,53	0,000581	2,3768	4,32281
Hgh1	-1,53	0,000592	1,201058667	2,014323333
Kif21a	-1,53	0	4,55484	7,23629
Mapre2	-1,53	0	21,78943333	34,37253333
Nefl	-1,53	0,001151	0,82877	1,446826667
Nr4a3	-1,53	0,003033	0,009514867	0,108758267
Psmb10	-1,53	0,002205	3,17449	5,46481
Pwp2	-1,53	0	4,079573333	6,47278
Rhov	-1,53	0,000078	2,56237	4,211833333
Tfcp2l1	-1,53	0,000397	0,356263333	0,610406333
Cav2	-1,52	0,002198	0,784797	1,30334
Cdx1	-1,52	0,004251	0,019865033	0,195621
Gpr27	-1,52	0,002205	0,872985	1,513136667
Hps6	-1,52	0,009906	0,205705667	0,420995667
Inf2	-1,52	0,001014	0,393410333	0,688000667
Inpp1	-1,52	0,000001	1,512653333	2,690283333
Nop2	-1,52	0	9,856453333	15,39603333
Odc1	-1,52	0,000181	110,6653333	184,338
Ppp1r12b	-1,52	0,000001	1,077421333	1,713386667
Ptk6	-1,52	0,004974	0,022361543	0,106417633
Tnfrsf21	-1,52	0	2,702253333	4,343403333
Cdk18	-1,51	0,000042	1,397113333	2,19186
Cdkn1a	-1,51	0,000521	39,31606667	66,0059
Fam163b	-1,51	0,000369	1,394538	2,30124
Klf13	-1,51	0	2,652066667	4,09016
Krtap17-1	-1,51	0,007565	0,156202333	0,684331333
Nomo1	-1,51	0	5,060573333	7,929323333
Tmem238	-1,51	0,001991	1,001379667	1,624056667
Ybx3	-1,51	0	72,75723333	111,294
Alox12	-1,5	0,001073	1,269884333	2,142913333

Anxa1	-1,5	0,004981	1,192853333	2,547806667
Chpf	-1,5	0,001644	0,827948667	1,310736667
Cib2	-1,5	0,000927	2,41003	3,99651
Dscaml1	-1,5	0,007045	0,046076533	0,202310967
Itgav	-1,5	0	13,68056667	21,32713333
Klhl21	-1,5	0	4,772606667	7,42354
Ndufaf4	-1,5	0	12,50702667	19,60116667
Ogfod3	-1,5	0,000359	4,525013333	7,529793333

9.3 SP8 direct targets

Ablim2	Enpp1	Lrrtm1	Skap2
Adamts18	Epha4	Maf	Slc24a3
Ak5	Etv4	Mapkbp1	Slc30a4
Alpk1	Eya2	Meox1	Slc39a11
Ankrd6	Fam196b	Mesdc2	Slc41a2
Aox3	Fam46a	Msx1	Slc6a2
Aox4	Fam49a	Msx2	Slc7a11
Apcdd1	Fgf1	Mt1	Slfn9
Arhgap26	Fgf8	Mtss1	Slit3
Arhgap8	Flrt1	Myc	Smad6
Arhgef3	Flt1	Mycn	Snhg11
Arntl	Frem1	N4bp3	Sorbs2
Bach2	Fzd1	Nap1l3	Sostdc1
Bambi	Gab2	Ncf2	Sox2
Barx2	Gad1	Negr1	Sox9
Bhlha9	Gad2	Ngfr	Sp6
Bmp4	Gata3	Nr3c1	Sp8
Bnc2	Gpr87	Nrxn3	Spry1
Btbd3	Gria1	Ntf3	Sptlc3
Cacna1i	Hao	Nuak1	Sstr2
Cd74	Has3	Ofcc1	Syt2
Cerk	Hgf	Ogfod3	Tbx3
Chpf	Hk2	Palld	Tfap2b
Chrna7	Hmcn1	Pcsk6	Tfcp2l1
Cited4	Hoxb1	Pik3r1	Tgfb1
Cldn23	Hoxc13	Pkdcc	Tgfb2
Coro6	Hoxc9	Plcb1	Tle4
Cpeb2	Irx1	Plcx3	Tmem132c
Creb3l1	Irx2	Plekhb1	Tnfrsf11a
Crhr1	Irx3	Pou4f1	Tox
Crtac1	Irx4	Ppp1r12b	Trhde
Cttnbp2	Irx5	Ppp1r3b	Trpc5
Cyp26a1	Isl2	Proser2	Ttc28
Cypr1	Itga9	Pthlh	Ttpa
Dlx1	Itgav	Raly1	Unc5a
Dlx2	Kcnj15	Ramp3	Unc5b
Dlx4	Klf13	Rcan2	Ust
Dlx6	Klf14	Rgma	Vldlr
Dnajc1	Kremen1	Rnaset2a	Wnt10b
Dok5	Lbh	Rragd	Wnt5a
Dusp4	Lclat1	Sall1	Wnt7a
Ednrb	Lmo7	Sall3	Ybx3
Efnb3	Lmx1b	Satb2	Zfp322a
Egln3	Lnx1	Sct	Zfp36l2
En1	Lrig1	Serinc5	Zfp703
Enc1	Lrrc32	Sil1	Zim1

